OPTIMIZATION OF CHARGING STRATEGIES UNDER THE CONSIDERATION OF ERROR-PRONE TRAFFIC INFORMATION

Gerhard Huber

Vollständiger Abdruck der von der Fakultät für Bauingenieurwesen und Umweltwissenschaften der Universität der Bundeswehr München zur Erlangung des akademischen Grades eines

Doktors der Ingenieurwissenschaften (Dr.-Ing.)

genehmigten Dissertation.

Gutachter/Gutachterin:

1. Univ.-Prof. Dr.-Ing. Klaus Bogenberger
2. Prof. Dr. Ir. J.W.C. van Lint

Die Dissertation wurde am 30.11.2016 bei der Universität der Bundeswehr München eingereicht und durch die Fakultät fr Bauingenieurwesen und Umweltwissenschaften am 11.07.2017 angenommen. Die mündliche Prüfung fand am 02.08.2017 statt.

Kurzfassung

Elektroautomobile bieten eine Vielzahl an Vorteilen gegenüber konventionellen, mit fossilen Brennstoffen betriebenen Kraftfahrzeugen. Insbesondere die Möglichkeit, lokale Schadstoffemissionen zu vermeiden, wird oftmals als ihr größter Vorteil angesehen. Nichtsdestotrotz sind die Verkaufszahlen in vielen Ländern äußerst gering. Hohe Anschaffungskosten und eine typischerweise geringe Reichweite werden häufig als die Kernursachen hierfür angesehen. Geringe Reichweiten führen zur sogenannten „Reichweitenangst“. Dieser Begriff beschreibt die Angst davor, dass während der Fahrt die in der Batterie gespeicherte Energie vollständig aufgebraucht wird und das Fahrzeug stehen bleibt. Die vorliegende Doktorarbeit wurde durch die Annahme motiviert, dass Fahrern von Elektroautomobilen ihre Reichweitenangst genommen werden kann, indem ihnen präzise und zuverlässige Navigationsinformationen zur Verfügung gestellt werden. Solche Navigationsinformationen beschreiben hierbei nicht nur Routen, sondern auch, an welchen Ladesäulen und bis zu welchem Ladezustand das Elektroautomobil wieder aufgeladen werden soll. Diese Art der Information wird hier als „Ladestrategie“ bezeichnet und kann als eine Art Boxenstopp-Strategie für Elektroautomobile interpretiert werden. Dabei ist entscheidend, dass die Anweisungen, aus denen eine solche Ladestrategie besteht, ein Erreichen des Ziels sicherstellen, was bedeutet, das Risiko stehen zu bleiben muss sehr gering gehalten werden. Zugleich sollen aber auch unnötige und unnötig lange Ladestopps vermieden werden.

Um solche Ladestrategien berechnen zu können, wird innerhalb der ersten Kapitel der Arbeit ein geeignetes mathematisches Optimierungsmodell entwickelt. Zunächst werden zu diesem Zweck bereits existierende wissenschaftliche Arbeiten im Bereich der Navigationsanwendungen für Elektroautomobile näher beleuchtet. Dabei stellt sich heraus, dass das Problem des Findens optimaler Ladestrategien zwar bereits einige Male untersucht wurde, dass aber die vorgeschlagenen Problemformulierungen häufig starke Vereinfachungen realer Situationen darstellten. Insbesondere wird die Existenz von Unsicherheiten innerhalb der für die Berechnungen notwendigen Prognosen (z.B. hinsichtlich des für den Fahrtvorgang notwendigen Energieverbrauchs) nicht oder nur unzureichend berücksichtigt. Um diese Forschungslücke zu schließen, wird eine generische Formulierung als sogenanntes Multistage Decision Problem vorgeschlagen. Diese Formulierung ist sehr flexibel und erlaubt das Miteinbeziehen praktisch beliebiger Faktoren. Allerdings ist das Finden einer Lösung auf numerischem Wege kaum mehr möglich.

Daher wird, basierend auf diesem ersten Vorschlag, eine zweite, deutlich anwendungsorientiertere Problemformulierung vorgeschlagen. Hierbei wird das Problem, optimale Ladestrategien zu finden, als deterministisches kürzeste Wege Problem modelliert. Ladestrategien werden in diesem Zuge hinsichtlich der erwarteten Reisezeit optimiert. Das vollständige Entleeren der Batterie wird über eine Nebenbedingung verhindert. Diese Formulierung als kürzeste Wege Problem stellt einen Kompromiss zwischen der notwendigen Realitätsnähe und numerischer Lösbarkeit dar. Eine Analyse der Eigenschaften dieser Problemformulierung weist nach, dass das Berechnen einer Lösung trotz der erheblichen Vereinfachungen im Vergleich zur ersten Formulierung immer noch sehr aufwändig ist. Es werden zwei auf Dijkstra's Algorithmus basierende Optimierungsansätze vorgestellt. Der erste erlaubt es, optimale Lösungen für das entwickelte Modell zu berechnen. Der zweite Algorithmus kann dies nicht mehr garantieren, aber er ermöglicht es, Berechnungszeiten auf ein für praktische Anwendungen realistisches Maß zu reduzieren.

Auch diese zweite Formulierung als deterministisches kürzeste Wege Problem stellt nur einen weiteren Zwischenschritt dar. Ihre zentrale Schwäche ist, dass es – wie bereits in früheren wissenschaftlichen Arbeiten – nicht möglich ist, Unsicherheiten explizit zu berücksichtigen. Liegen nämlich prognostizierte Energieverbräuche unter den real auftretenden, so kann es passieren, dass ein Fahrzeug, welches einer auf diesem Modell basierenden Ladestrategie folgt, mangels Energie auf der Strecke liegen bleibt. Um derartige Situationen zu vermeiden, wird die zuvor erwähnte Nebenbedingung erweitert. Nun werden nicht nur solche Ladestrategien in der Betrachtung ausgeschlossen, für die prognostiziert wird, dass der Ladezustand während der Fahrt auf null sinkt, sondern es wird darüber hinaus ein Teil der Batteriekapazität als Energie-Puffer reserviert. Dieser dient ausschließlich dazu, unerwartet hohe Energieverbräuche kompensieren zu können. Das bedeutet, dass eine Ladestrategie nur dann empfohlen wird, wenn diese ohne den als Puffer definierten Teil der Batterie auskommt. Entscheidend ist in diesem Zusammenhang, dass kein zu großer Teil der Batteriekapazität als Puffer veranschlagt wird, da man durch diesen letztendlich die für die Ladestrategieoptimierung verfügbare Energie reduziert. Große Energie-Puffer machen es daher notwendig, häufiger zu laden, beziehungsweise es kann vermehrt zu Situationen kommen, in denen überhaupt keine Ladestrategie, die einen solchen Puffer unberührt lässt, empfohlen werden kann. Anderseits darf der Puffer auch nicht zu klein gewählt werden, da er sonst nicht ausreicht, um die auftretenden Unterschiede zwischen realem und prognostiziertem Energieverbrauch zu kompensieren. Im Rahmen dieser Arbeit werden verschiedene Ansätze zur Bestimmung der Größe des Energie-Puffers vorgestellt. Ihnen allen ist gemein, dass sich die vorgeschlagene Größe des Puffers im Laufe einer Fahrt ständig verändert. So wächst der Puffer beispielsweise für Streckenabschnitte, die besonders hohe Unsicherheitsfaktoren aufweisen, und er schrumpft, falls es unwahrscheinlich ist, dass der reale Energieverbrauch deutlich über den prognostizierten steigt. Das so resultierende kürzeste

Wege Problem erlaubt es, mit Unsicherheiten umzugehen, und kann weiterhin durch die zuvor erwähnten Modifikationen von Dijkstra's Algorithmus gelöst werden. Hierdurch wird ein weiteres Anwachsen von Rechenzeiten bei der Problemlösung verhindert.

In einem nächsten Schritt wird mittels Simulation getestet, inwieweit das Konzept des Energie-Puffers tatsächlich fähig ist, mit auftretenden Unsicherheiten umzugehen. Zu diesem Zweck wird das bisher noch weitestgehend abstrakte Modell dahingehend konkretisiert, dass der Einfluss von Verkehrszuständen entlang der Streckenabschnitte einer Route auf Energieverbrauch und Reisezeit abgebildet wird. Darüber hinaus wird im Rahmen der Simulation davon ausgegangen, dass zu dem Zeitpunkt, zu welchem eine Ladestrategie berechnet und empfohlen wird, lediglich fehlerbehaftete Verkehrsprognosen zur Verfügung stehen. Ein einzelner Simulationslauf ist dann wie folgt aufgebaut: Grundsätzlich soll die Fahrt eines Elektroautomobils entlang einer langen Strecke simuliert werden. Zunächst wird eine Ladestrategie für ein gegebenes Szenario an dieser Strecke berechnet. Ein solches Szenario ist definiert durch die sich entlang der betrachteten Strecken befindende Ladeinfrastruktur, den Ladezustand des Elektroautomobils zu Beginn der Fahrt sowie durch weitere Aspekte, die im Kontext der Ladestrategieoptimierung von Relevanz sind. Während des eigentlichen Simulationslaufes folgt das Elektroautomobil der berechneten Ladestrategie. Dabei trifft es, wie bereits angedeutet, auf Verkehrssituationen, die teilweise von der für die Berechnung der Ladestrategie prognostizierten Verkehrssituation abweichen. Entsprechend weichen auch Fahrgeschwindigkeiten, Reisezeiten, Energieverbräuche und die Entwicklung des Ladezustands von der Prognose ab. Allerdings wird das Elektroautomobil während der Fahrt ständig mit neuen Ladestrategien versorgt. Diese Updates beziehen die bis zum Zeitpunkt der Berechnung tatsächlich eingetretenen Energieverbräuche und Reisezeiten mit ein und basieren zudem auf aktualisierten Verkehrsprognosen. Falls nun, im Rahmen der Simulation, das Elektroautomobil in der Lage ist, das Ende des vorgegebenen Streckenabschnitts zu erreichen, so wird der Simulationslauf als Erfolg gewertet. Falls die Abweichungen zwischen Realität und Prognose dazu führen, dass das Fahrzeug mangels Energie auf der Strecke liegen bleibt, wird der Simulationslauf als Versagen gewertet.
Um nun den Einfluss unterschiedlicher Arten von Verkehrsprognosen (z.B. das Verwenden von auf historischen Daten basierender Durchschnittsgeschwindigkeiten oder die Anwendung sogenannter instantaner Fahrgeschwindigkeiten) und unterschiedlicher Ansätze zur Bestimmung der Größe des Energie-Puffers auf die Qualität der resultierenden Ladestrategien zu bestimmen, wird eine Vielzahl von Simulationsläufen durchgeführt. Dabei werden unterschiedlichste Szenarien betrachtet, um möglichst robuste, das heißt allgemeingültige Ergebnisse zu erhalten. Folglich ist es notwendig, die Rechenzeiten für einen einzelnen Simulationslauf sehr kurz zu halten. Dies wird dadurch erreicht, dass – wie bereits zuvor erwähnt – lediglich eine einzelne, lange Strecke (ca. 360 Kilometer) betrachtet wird statt eines gesamten Verkehrsnetzes, welches

dann auch eine Alternativroutenwahl erlauben würde. Durchschnittliche Reisezeiten und Erfolgsraten werden verwendet, um die Qualität der berechneten Ladestrategien in Abhängigkeit der verwendeten Verkehrsprognose und der angewandten Methode zur Bestimmung der Größe des Energie-Puffers zu bestimmen.
Eine Analyse der Simulationsergebnisse zeigt, dass sowohl die Art der Verkehrsprognose als auch die Methode zur Bestimmung der Größe des Energie-Puffers erheblichen Einfluss auf die Erfolgsrate haben. Allerdings stellt sich deren Einfluss auf Reisezeiten als eher gering heraus. Darüber hinaus zeigt sich ebenfalls, dass die Beziehung zwischen der Qualität der Ladestrategien und der Güte der Verkehrsprognosen äußerst komplex ist. Die Ergebnisse belegen, dass die Wahrscheinlichkeit, auf der Strecke liegen zu bleiben, nicht nur davon abhängt, wie zutreffend die Verkehrsprognose, auf der die verwendete Ladestrategie basierte, war – obwohl der Unterschied zwischen Verkehrsprognose und realer Verkehrssituation die einzige Unsicherheitsquelle innerhalb der Simulation darstellt. Zudem wird durch die Simulationsergebnisse deutlich, dass akkuratere Verkehrsprognosen nicht zwingend zu besseren Ladestrategien führen. Am wichtigsten ist aber die Beobachtung, dass die Wahl eines geeigneten Energie-Puffers stets ein Qualitätslevel der Ladestrategien sicherstellt, welches auch eine Anwendung in der Realität erlauben sollte. So kann ein Liegenbleiben in praktisch allen simulierten Situationen verhindert werden. Zugleich wird aber auch ein übervorsichtiges Verhalten in der Regel vermieden, das heißt es ist (fast immer) möglich, eine Ladestrategieempfehlung abzugeben.

Im letzten inhaltlichen Kapitel der Arbeit werden reale Testläufe auf Basis des entwickelten Modells durchgeführt. Ein Elektroautomobil mit einer offiziellen Reichweite von 170 Kilometern wird hierbei dazu genutzt, eine mit ausreichend Ladeinfrastruktur ausgestattete Strecke von über 400 Kilometern zurückzulegen. Den Testfahrern wird eine prototypische Software zur Verfügung gestellt, die diesen während der Fahrt – auf Basis des aktuellen Ladezustands, der aktuellen Position sowie aktueller Verkehrsinformationen – optimierte Ladestrategien empfiehlt. Eine Auswertung der resultierenden Fahrtverläufe ergibt, dass Energie-Puffer grundsätzlich auch für reale Anwendungen geeignet sind. Allerdings zeigen die Testfahrten auch einen Schwachpunkt der vorgeschlagenen Modellierung auf: Ausfälle von Ladeinfrastruktur sind zum Zeitpunkt der Testfahrten vergleichsweise häufig aufgetreten. Das entwickelte Modell erlaubt es aber nicht, diese Art von Unsicherheiten zu berücksichtigen. Entsprechend muss für eine Anwendung der entwickelten Konzepte entweder solange gewartet werden, bis Fehlfunktionen von Ladestationen weitestgehend ausgeschlossen werden können, oder das Modell muss noch einmal grundlegend angepasst werden.

Executive Summary

Battery electric vehicles (BEVs) provide many advantages in comparison to conventional, internal combustion engine vehicles. Especially their ability to avoid local exhaust emissions is often understood as a possible solution for cities which suffer from air pollution. Still, in many countries BEV selling numbers are low. It is assumed that this is primarily caused by high acquisition costs and their limited driving range. The latter leads to the so-called „range anxiety“, i.e., the fear of running out of energy during a trip. This limits application possibilities. For instance, it seems to be commonly accepted that BEVs cannot be used for long-distance trips. The main motivation of this thesis is to reduce or, in the best case, to eliminate range anxiety (particularly for long-distance trips) by providing accurate and reliable navigation information to BEV drivers. In this context, a navigation system is not only intended to recommend routes, but also to suggest where the BEV should be charged and how much energy should be charged. This kind of information is here denoted as „charging strategy“. A charging strategy can be understood similarly to a pit strategy in Formula One. For its construction, basically two objectives are pursued: First and foremost, the given instructions have to ensure a reliable arrival, i.e., the risk of running out of energy has to be kept very low. Second, the total travel time and along with it the number and duration of charging stops has to be kept low.

To be able to compute such charging strategies, a suitable mathematical framework is developed in the first chapters of the thesis. A literature review, where the focus is set on prior works about navigation applications that are primarily intended for BEVs, forms the fundament. It turns out that the problem of finding „optimal“ (different interpretations of optimality exist) charging strategies has already been addressed several times. However, the corresponding problem formulations lack realism, since several potentially relevant aspects are not taken into account or not considered in a realistic way. To fill this research gap, a generic formulation as a multistage decision problem is suggested. This formulation surpasses prior approaches in terms of generality and flexibility. On the other hand, this optimization problem can hardly be handled numerically. Hence, a second, more practical problem formulation is provided, where the problem of finding optimal charging strategies is interpreted as a deterministic shortest path problem (SPP). This reformulation is intended as a compromise between ensuring realism and

achieving numerical computability. Minimizing total travel times is applied as the optimization criterion and avoiding empty batteries is ensured via a side constraint. An analysis of the properties of this SPP is conducted. It shows that, despite the simplifications that result from reducing the originally suggested multistage decision problem to a deterministic SPP, computing optimal solutions is still quite expensive. Two different modifications of Dijkstra's algorithm are introduced to solve the problem efficiently. The first one is able to compute optimal charging strategies for the described setting. The second one leads to in general very good, though suboptimal solutions. At the same time, the second approach is able to reduce computation times down to a level which should be sufficient for practical applications.

Also this formulation as a deterministic SPP is just another intermediate step. The issue is that charging strategies, particularly if they are intended for long-distance trips, need to take information about future events into account to achieve a high level of quality. Such predictions, on the other hand, are often not absolutely correct. The suggested deterministic SPP is at this point of the thesis unable to handle uncertainties caused by imperfect predictions about, for instance, energy consumption. The consequence is that following recommended charging strategies would often lead to an empty battery, at least under realistic conditions. To solve this issue, the side constraint which is intended to ensure that running out of energy is avoided is adjusted. Instead of only demanding that the battery's state of charge has to always be above zero during a trip, a certain percentage of the battery's maximal energy capacity is reserved to compensate for unexpectedly high energy consumption. Such „energy buffers" need to be kept as small as possible. Otherwise significant parts of the battery capacity would remain unused. This would cause additional charging stops and, along with that, increased travel times. On the other hand, the buffers need to be big enough to be able to compensate for prediction errors. Several different approaches for quantifying the size of this energy buffer are introduced. The motivation for all of these approaches is to adjust the size of the energy buffer dynamically during a trip depending on the level of uncertainty which exits in the respective situation. The resulting problem formulation is more robust against uncertainties and can again be solved by the aforementioned modifications of Dijkstra's algorithm. Thus, no significant increase of computation times needs to be expected.

In a next step, it is tested via simulation how well the concept of energy buffers allows handling uncertainties. For this purpose, some preparatory steps are necessary. The yet very general problem formulation is concretized in such a way that the impact of traffic conditions on energy consumption and travel times is included into the problem formulation. Furthermore, it is assumed that at the time at which a charging strategy is requested, computed and recommended, only imperfect information about the future development of traffic is available. Based on these preparatory steps, a single simulation run is structured as follows: First, a charging strategy is

computed for a given scenario. A scenario is defined by the available charging infrastructure, the state of charge at the beginning of the trip, and by other aspects which are of relevance in the context of charging strategy optimization. Then, a simulated BEV starts following the recommended charging strategy while facing a traffic situation that is possibly different to the one which was presumed during the computation of the charging strategy. Hence, experienced driving speeds and states of charge differ from the predicted values. During the simulated trip, steadily new charging strategies are computed. These computations take updated traffic predictions and updated information about the BEV's state of charge into account and provide guidance for the remaining part of the trip. The BEV always follows the latest charging strategy. If the simulated BEV is finally able to reach the destination, it is counted as a success. If the experienced situation makes it run out of energy, then the simulation run is counted as a failure.

To test the influence of different traffic prediction methods (for example, using average driving speeds based on historical data or applying instantaneous driving speeds as a best guess for the future) and different approaches for quantifying the size of the applied energy buffers, many simulation runs are carried out. Robustness of the results is ensured by considering many different scenarios. This makes it necessary to keep the computation time which is necessary for a single simulation run reasonably low. For this purpose, charging strategies are always computed for a single, predetermined (long-distance) route, i.e., the simulated BEV is unable to take alternative routes to reach its destination. Success rates and total travel times are used to measure the quality of charging strategies in dependency of traffic prediction approaches and energy buffer methods.

An analysis of the simulation results shows that both traffic prediction approaches and energy buffer methods have significant influence on success rates. Their impact on travel times, however, is comparably small. It can also be observed that the relation between traffic prediction quality and charging strategy quality is not trivial. The findings prove that the risk of running out of energy does not only depend on the traffic prediction quality, even though it represents the only source of uncertainty. Furthermore, it turns out that better traffic predictions not necessarily lead to better charging strategies. On the other hand, it can at least be stated that sufficiently accurate traffic predictions ensure charging strategies of high quality. Moreover, the results of the simulation study also indicate that the concept of energy buffers is well-suited to handle uncertainties, at least if these uncertainties are caused by error-prone traffic predictions. For most of the tested scenarios, the risk to run out of energy can almost be eliminated. At the same time, an over-cautious behavior can be avoided.

Finally, in order to gain a different and more practical perspective on the problem of finding optimal charging strategies, a few field tests are conducted. An electric vehicle with an official

electrical driving range of 170 kilometers is used to cover a distance of more than 400 kilometers. A prototypic implementation of a software tool for computing charging strategies is provided to the test drivers in order to support them during their trips. The gathered experiences indicate that the proposed framework is basically suited to provide reasonable charging strategies also for practical applications. However, the gathered experiences also show that, currently, one cannot rely on the existing charging infrastructure. This is a major thread to the proposed framework, since the concept of energy buffers, the way it is described in this thesis, is hardly able to compensate charging station failures. Hence, either the reliability of the charging stations has to be improved or the developed framework needs further adjustments.

In conclusion, there are two main contributions of this research: The first one is the formulation of the problem of finding optimal charging strategies as an optimization problem which

- provides the possibility to take those aspects in realistic way into account which show the highest influence on charging strategies
- optimizes charging strategies with regard to reliability and total travel time
- is able to handle the existence of uncertainties
- can be solved rather efficiently.

Particularly the ability to handle uncertainties represents a significant enhancement in comparison to existing approaches for charging strategy optimization. Moreover, a detailed analysis of the properties of the developed problem formulation as a deterministic SPP is conducted and, based on the findings of this analysis, two solution algorithms are suggested.
The second important contribution of this work is the intensive analysis of the ability of the developed problem formulation to handle uncertainties. The simulation study provides detailed insights into the complex relation between existing uncertainties and the quality of charging strategies. Moreover, the findings of this study show that the concept of energy buffers allows handling uncertainties for a huge variety of scenarios. The conducted field tests complement the simulation study and indicate that, even though some issues need to be solved before, the developed framework can also be applied in practice.

Acknowledgements

First and foremost, I wish to thank my primary supervisor Professor Klaus Bogenberger. The scope of this work is based on an idea that originally came from him. Moreover, it was Professor Bogenberger who gave me four years ago the possibility to work on the topic of navigation applications for battery electric vehicles. Throughout all this time, he provided guidance and advice to me. Without him, this thesis would not exist.

I also want to express my gratitude to Professor Hans van Lint. We met only a few times, but each time he asked the right questions and brought in many ideas and new perspectives. It was a great gain to win him as my second supervisor. Besides Professor Bogenberger and myself, he was the one who had the biggest impact on this thesis.

My sincere thanks also go to all colleagues at the Department of Traffic Engineering. They were a great team and it was a privilege to work in such a pleasant atmosphere. Furthermore, I want to acknowledge those who proofread this work, especially Martin Weingärtner, Stefan Schmöller, and Williams Ackaah. Special thanks also goes to my co-drivers, Florian Dandl, Benedikt Bracher and Svenja Reiss, who were „brave“ enough to accompany me on the 400 kilometers long test drives with an electric vehicle.

Next, I want to thank the Federal Ministry for Transport, Innovation and Technology (Germany), which funds the project „DC-Charging at the Olympia-Park“, in which the described research took place. Furthermore, I want to thank the South Bavarian Autobahn Authority for providing detector data. Special thanks go to Mr. Johannes Grötsch for his aid and advice.

Finally, I want to thank Rita for all her support, understanding and patience. Moreover, I want to thank my parents. I owe them all that I am and all that I have achieved. Hence, I would like to dedicate this thesis to them.

Publications

Some ideas, figures and tables presented in this dissertation have appeared previously in the publications listed below:

Journal Papers

- Williams Ackaah, **Gerhard Huber**, Klaus Bogenberger, and Robert L Bertini. Assessing the harmonization potential of variable speed limit systems. Accepted for publication in *Transportation Research Record: Journal of the Transportation Research Board*, 2016.

- **Gerhard Huber**, Klaus Bogenberger. Long-Trip Optimization of Charging Strategies for Battery Electric Vehicles. *Transportation Research Record: Journal of the Transportation Research Board*, (2736):45-53, 2015.

- Williams Ackaah, **Gerhard Huber**, and Klaus Bogenberger. Quality evaluation method for variable speed limit systems: Incident detection and warning potential. *Transportation Research Record: Journal of the Transportation Research Board*, (2484):80-89, 2015.

Conference Publications, Full Papers Refereed

- Lisa Kessler, **Gerhard Huber**, Arne Kesting, and Klaus Bogenberger. Comparison of Floating-Car Based Speed Data With Stationary Detector Data. Submitted for the *19th IFAC 2017 World Congress*, Toulouse, France, 2016.

- Felix Rempe, **Gerhard Huber**, and Klaus Bogenberger. Travel Time Prediction in Partitioned Road Networks based on Commuting Patterns. In *19th International IEEE Conference on Intelligent Transport Systems*, Rio de Janeiro, Brazil, 1982-1987, 2016.

- Williams Ackaah, Klaus Bogenberger, Robert L Bertini, and **Gerhard Huber**. Comparative analysis of real-time traffc information for navigation and the variable speed limit system. In *14th IFAC Symposium on Control in Transportation Systems Compendium of Papers*, Istanbul, Turkey, 2016.

- Felix Rempe, **Gerhard Huber**, and Klaus Bogenberger. Macroscopic Urban Traffic Congestion Prediction based on Spatio-Temporal Patterns. *International Symposium on Enhancing Highway Performance, Berlin*, 2016.

- **Gerhard Huber**, Klaus Bogenberger, and Hans van Lint. Concept for Estimating Energy Buffer Size for Battery Electric Vehicles to Account for Error-prone Traffic Predictions. *Transportation Research Board, 95th Annual Meeting, Compendium of Papers, Washington DC*, 2016.

- Williams Ackaah, **Gerhard Huber**, Klaus Bogenberger, and Robert L Bertini. Assessing the harmonization potential of variable speed limit systems. *Transportation Research Board, 95th Annual Meeting, Compendium of Papers, Washington DC*, 2016.

- **Gerhard Huber**, Klaus Bogenberger. Long-Trip Optimization of Charging Strategies for Battery Electric Vehicles. *Transportation Research Board, 94th Annual Meeting, Compendium of Papers, Washington DC*, 2015.

- Williams Ackaah, **Gerhard Huber**, and Klaus Bogenberger. Quality evaluation method for variable speed limit systems. *Transportation Research Board, 94th Annual Meeting, Compendium of Papers, Washington DC*, 2015.

- **Gerhard Huber**, Klaus Bogenberger, and Robert L Bertini. New Methods for Quality Assessment of Real Time Traffic Information. *Transportation Research Board, 93th Annual Meeting, Compendium of Papers, Washington DC*, 2014.

- **Gerhard Huber**, Klaus Bogenberger. Eine Bewertungs- und Optimierungsmethode für dynamische Verkehrslagedarstellungen. *HEUREKA 2014, Stuttgart*, 2014.

- **Gerhard Huber**, Klaus Bogenberger. Optimal Charging Strategies for Electric Cars on Long Trips. *3rd Conference on Future Automotive Technology, Munich*, 2014.

- **Gerhard Huber**, Klaus Bogenberger. A Quality Evaluation Model for Real-Time Traffic Information. *16th International IEEE Conference on Intelligent Transport Systems, The Hague*, 2126-2131, 2013.

Contents

Chapter 1

Introduction

In this chapter, the conducted research is motivated, followed by an introduction of desired research objectives. At the end, an outline of the thesis is provided.

1.1 Research Context

In 2011, the German government stated the goal of bringing one million battery electric vehicles (BEV) onto the roads by the year 2020. This goal is motivated by a variety of advantages that BEVs show in comparison to internal combustion engine vehicles (ICEV): No local emission of pollutants, less noise emissions, less dependency on oil imports, and even the possibility to use car batteries as a dynamic energy storage to compensate for irregular electricity supply caused by renewable energies (*6*). Unfortunately, with each passing day, it becomes more obvious that this goal won't be reached. High acquisition costs and the deeply rooted fear of potential customers to run out of energy while driving a BEV, the so-called „range-anxiety", are often assumed to be the main reasons for the limited demand for BEVs (see p. 10 in (*104*)). To counter the former, the German government recently followed the example of other countries, such as Norway, and started offering monetary incentives to people who buy a BEV (*24*). To counter the latter, a closer look at the topic of BEVs is necessary.

The maximum driving range of BEVs, i.e., the distance that can be covered without recharging, is very small compared to ICEVs. At the moment, the official maximal driving range lies only for a few models above 250 kilometers (*98*) (*155*). Furthermore, low outdoor temperatures or high driving speeds may reduce this in most cases too optimistic estimation drastically (*66*). ICEVs, by contrast, achieve driving ranges of several hundred and some even of more than one thousand kilometers. Thus, thinking about driving ranges usually has not been necessary. Another relevant aspect is that the publicly accessible charging infrastructure is in many countries, including Germany, sparsely distributed over the road network, at least when being compared to the coverage with gas stations. According to (*27*), currently there exist about 4,800 charging stations in Germany. The number of gas stations is three times as high (*3*) and due to charging

durations of up to several hours, a charging station is not able to serve the same number of vehicles that can be served by a gas station. The comparably low number of publicly available charging infrastructure along with the significantly lower driving ranges are the main reasons for the fear that driving BEVs leads to situations in which it is impossible to reach the next charging station (*120*).

Based on these considerations, two obvious approaches to counter range-anxiety can be derived: Additional charging stations could be built or the driving range of BEVs could be increased. Currently, both approaches are realized. Between July 2015 and June 2016 alone, the number of charging stations was raised by 1,200 in Germany (*27*). Furthermore, many car manufacturers launched improved versions of their first generation BEVs, which provide enhanced battery capacities (*98*). Unfortunately, both approaches lead to drawbacks. Infrastructure measures, for instance, are expensive. According to (*104*), average costs for building a publicly accessible charging station ranged in 2013, depending on the energy throughput of the charging station, between 10,000 and 27,000 Euros. Operating costs between 1,700 and 3,000 Euros per year and charging station need to be added. The critical point is that these costs are too high. Making profit by selling electricity is, at least at the moment, not realistic (p. 35 in (*106*)). Hence, often the public is left with building up or subsidizing charging infrastructure. Increasing battery capacities, unfortunately, also hides some drawbacks. Costs for research in the area of battery technologies are included into the acquisition costs of BEVs and keep them high. A side-effect of this is that low-budget BEVs will be offered in the near future, which ensure lower acquisition costs by using less-efficient or comparably small batteries (*40*). The possibility to make trade-offs between acquisition costs and battery capacity already exists today, since for more and more BEV models the option of including an enlarged (*16*) (or reduced (*144*), respectively) battery is available. Hence, the topic of limited driving ranges probably remains relevant during the next years, even though ranges of BEVs in general will improve.

In this thesis, a third approach to tackle range-anxiety is pursued. The central goal is to reduce range-anxiety via advanced navigation applications which are particularly developed for BEVs. This is motivated by the fact that a well-informed driver, i.e., a driver who is aware that she/he receives reliable information about remaining driving ranges and trustworthy instructions concerning future charging processes, is less vulnerable to range-anxiety (*120*). To illustrate the idea, let the situation that is described in the left part of Figure 1.1 be considered: A person wants to use a BEV to drive from her/his current location to a certain destination. The battery's state of charge (SOC) is at about 50 percent, which is not enough to reach the destination. There exist several different routes leading from the BEV's current position to the destination. Along each route several charging stations can be found. The driver wants to reach the destination reliably, i.e., she/he has to prevent the BEV from running out of energy during

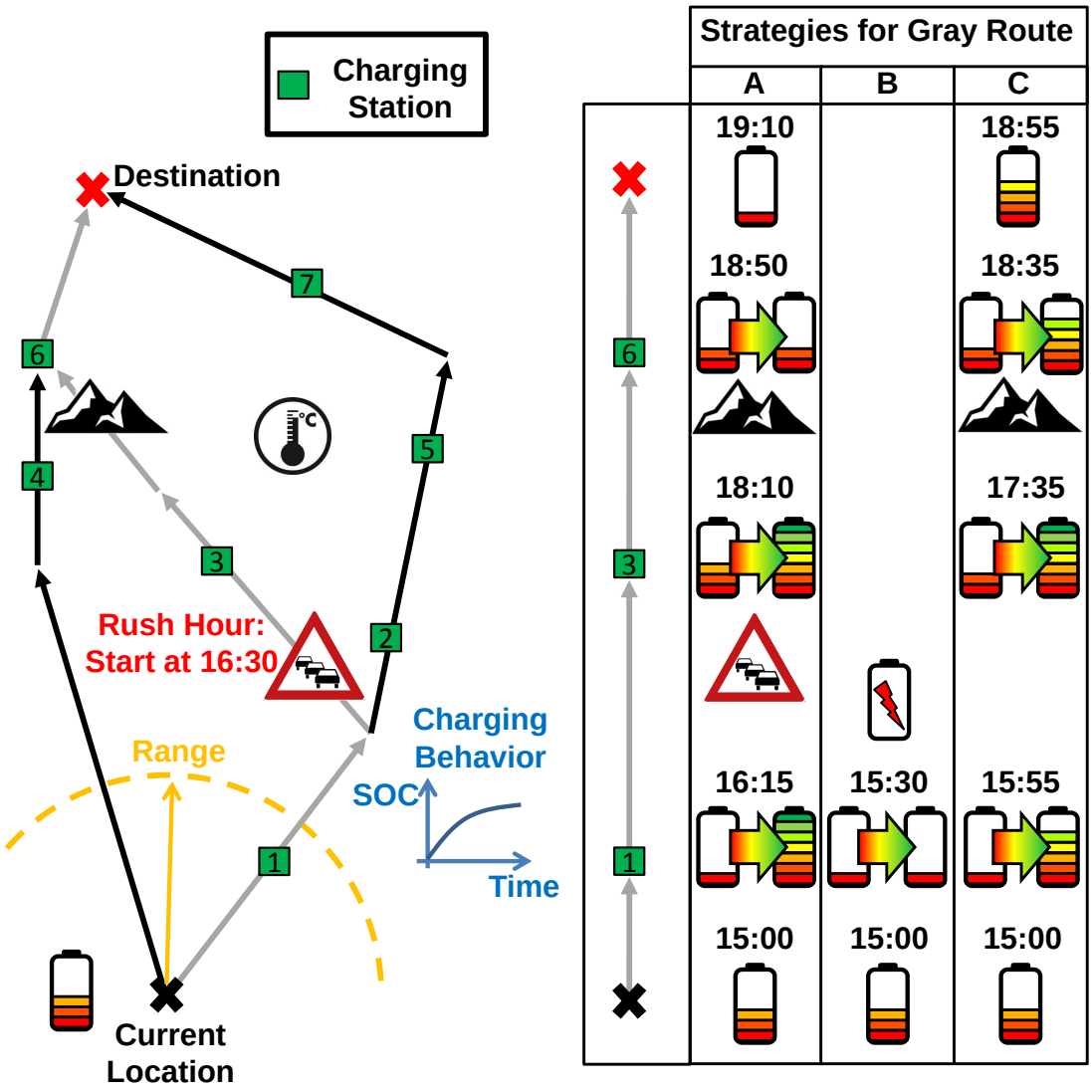

Figure 1.1: The problem of finding charging strategies.

the trip. At the same time, the trip should be conducted efficiently, i.e., the number of charging stops and their duration should be kept low. The following questions arise in this context:

- Which route should be taken?
- At which charging stations along this route should be charged?
- How much energy should be charged?

First experience reports about people using BEVs for trips of several hundred kilometers show that answers to these questions are very important for drivers (*2*) (*39*). The main problem is that there are many aspects which have influence on energy consumption and thus should be taken into account. Some of these potentially relevant aspects are indicated in Figure 1.1, such

as outdoor temperature, traffic conditions, charging durations, and road steepness. For a single person, however, it is hard to gather and consider all this information. Hence, it seems reasonable to let these questions be answered by the navigation system of the BEV. This means that, similar to current navigation systems, the driver requests a route describing the way from his current position to a certain destination. The navigation system, on the other hand, not only provides route guidance, but also information defining at which charging stations the BEV has to be recharged and up to which state of charge it has to be recharged. Such a type of information, which consists of route and charging instructions, is from here on denoted as **charging strategy**. Note that a necessary condition for the existence of reasonable charging strategies is the availability of fast-charging stations. Such stations allow recharging large parts of the battery of current BEVs in less than half an hour (*17*). This represents a huge improvement in comparison to „conventional“ charging which causes, depending on the charging technology, charging durations of up to several hours. Without the possibility to quickly charge energy, recharging during a trip was not practicable.

Three examples of charging strategies are shown in the right part of Figure 1.1. They refer to the situation in the left part of Figure 1.1. The conditions at the start of the trip are the same for all three charging strategies: The state of charge is equal to about 40 percent and the trip is started at 15:00. All three strategies suggest taking the gray route, i.e., charging stations one, three and six can be visited during the trip. A BEV following the first strategy, which is denoted as strategy A, drives to charging station one and then completely recharges its battery. This consumes lots of time and thus it is already 16:15 when the BEV again proceeds with driving. The BEV experiences a traffic jam shortly before reaching charging station three. This causes some delay. At charging station three, it is again fully recharged until 18:10. As a consequence, the BEV has enough energy stored to get over the mountains, which can be found shortly before charging station six, and to skip charging at station six. It arrives at the destination at 19:10 with a very low state of charge. Charging strategy B represents an extreme case. To avoid the rush hour traffic between charging stations one and three, which is for the sake of the example assumed to emerge at around 16:30, no charging at station one is suggested. Unfortunately, the available energy is not enough to reach station three and the BEV runs out of energy shortly after passing charging station one. The last charging strategy suggests charging up to a state of charge of about 80 percent at charging station one. This allows leaving station one twenty minutes earlier than when following charging strategy A, but the charged energy is still enough to reach station three. Hence, the rush hour traffic between stations one and three can be avoided as the corresponding road stretch is passed earlier. Analogously to strategy A, strategy C also specifies to fully recharge the battery at station three. In contrast to strategy A, however, an additional charging process is suggested at station six.

The consequence is that the destination is reached with a higher state of charge than when following strategy A. Additionally, the destination is even reached earlier. In conclusion, it can be assumed that strategy C takes a prediction about a probably occurring congestion into account to keep travel times low. This travel time reduction is afterwards used to avoid low states of charge, which are critical if the real energy consumption exceeds the predicted consumption.

It is important to mention that the example which is described by Figure 1.1 is artificially generated and not based on real data. Nevertheless, the example and the described charging strategies express the idea to achieve reliable and efficient trips through a smart planning of charging stops. For the purpose of reducing range-anxiety, a navigation system which is able to provide such high quality instructions represents an attractive supplement to the aforementioned approaches (more charging infrastructure and bigger batteries). It is attractive, because it can be expected that developing a charging strategy optimization (CSO) functionality and implementing it into existing navigation devices is significantly cheaper than expensive infrastructure measures. Moreover, long-distance trips with BEVs would become much more convenient, since no trip planning was necessary. Hence, it would also be more likely that long-distance trips are conducted with BEVs. Furthermore, CSO should be able to ensure that unnecessary charging stops, which are often the consequence of an over-cautious charging behavior due to range anxiety (*50*), are avoided. Along with this, an efficient usage of available battery capacities could be encouraged. In the long run, this may even allow reducing battery capacities, which again could lead to lower acquisition costs and less weight of BEVs.

1.2 Research Objectives

The primary intention of the described research is providing a first basis for a later inclusion of CSO functionalities into real world navigation systems. Achieving this objective requires the development of a mathematical framework which allows deriving practicable charging strategies. This leads to the first central research objective (RO) of this work:

RO 1: Formulate a mathematical optimization problem that allows computing reliable and efficient charging strategies.

Note that several such ROs are stated in the following. This will make it easier to motivate and explain the structure of the thesis.

The formulation of the first RO is not very specific. To make the idea of RO 1 more concrete, three additional and more specific subobjectives regarding the problem formulation are introduced. The first of these subobjectives, denoted by RO 1a, can be found below:

RO 1a: The suggested problem formulation has to be able to realistically represent those aspects which are relevant for a practical application of CSO.

All kinds of factors that have influence on the energy consumption of the BEV or on travel time may be understood as relevant aspects, such as traffic conditions or vehicle specific parameters. Also the driver's level of risk aversion may be seen as a relevant aspect. However, it is very likely that a unique list of aspects that have to be included into the problem formulation does not exist. This is also a consequence of an often limited data availability. For example, the driver's mood may have influence on his driving style and, along with that, on the energy that the BEV consumes when passing a certain road segment. Thus, the driver's mood also impacts the amount of energy that is necessary to be able to pass a certain road segment. If no information about her/his mood (or about the influence it has on her/his driving style) is available, then this aspect can hardly be taken into account within the formulation of a mathematical optimization problem. In order to make it possible to flexibly integrate different sets of aspects into the developed model, it should be formulated generically.
A further important component of RO 1a is the requirement of realism. Those aspects which are represented within the optimization model need to be represented in a realistic way. Otherwise, computed solutions may not be applicable in reality. Realism can easily be lost during the construction of optimization problems. One of the main reasons for this is that often simplifications are necessary for the formulation of certain types of optimization problems. An example of such simplifications are discretizations of decision variables whenever a problem is modeled as an integer program. Another widely applied simplification is the deterministic representation of in fact stochastic problem components.

To introduce the second subobjective, RO 1b, it is necessary to describe how „efficiency“ and „reliability“ are interpreted in the context of charging strategies (these interpretations have been mentioned in section 1.1): A charging strategy is denoted as efficient if the number and duration of charging stops is kept low. A charging strategy is denoted as reliable if the probability that a BEV which follows this charging strategy runs out of energy is very low[1]. These interpretations are again not very concrete. Finding adequate mathematical definitions for both terms is understood here as a part of the model development process and thus will be done later on. Though, already these vague interpretations show the contrast between both criteria. This makes it clear that it won't be possible to construct charging strategies which are optimal with regard to both criteria. At the same time, it is not reasonable to compute charging strategies which are only efficient or only reliable. The result would be that either no charging stops are

[1]The interpretations of the terms „efficiency“ and „reliability“ which exist in literature differ significantly – even if only contributions in the area of routing are considered: Efficiency often refers to travel time or fuel/energy consumption minimization (*125*) (*128*). A whole set of possibilities to define and measure reliability in the context of routing can be found in (*77*). The fundamental idea of both terms, however, remains basically the same in all of these works.

suggested or that charging stops are recommended whenever a charging station is passed. The former leads to a high risk of being stranded, the latter to unbearably long travel times. These considerations lead directly to RO 1b:

RO 1b: The suggested problem formulation has to ensure that charging strategies are optimized with regard to both efficiency and reliability.

Note that the described interpretation of reliability is particularly intended for situations in which uncertainty exists. If any current and future aspect which has influence on the BEV's condition (state of charge, arrival times, etc.) was known with absolute precision at the time at which a charging strategy is computed, then it actually would not be necessary to speak of reliability. The reason for this is that it could be decided with absolute certainty whether a specific charging strategy leads to an empty battery or not. As a consequence, it would be more reasonable to speak of „feasible" charging strategies instead of „reliable" charging strategies. However, presuming absolute certainty lacks realism in the context of CSO. Future energy consumption or arrival times can solely be estimated. Note that imperfect predictions represent not the only source of uncertainty. Missing data (recall the aforementioned example about the unknown mood of the driver), incorrect data, or inappropriate models may lead to issues, too.

The third subobjective concerns the solution process and not, which is the case for ROs 1a and 1b, the problem formulation itself:

RO 1c: The suggested problem formulation has to make a practical computation of solutions possible.

Here, practicability primarily means that computing problem solutions must be possible in reasonable time. In the context of navigation applications, computation times of a few seconds or, at most, of half a minute can be understood to be reasonable. Computation times depend on the computational effort and the available hardware. The computational effort that is necessary to solve a mathematical optimization problem depends again on the problem itself, i.e., on the problem structure and the amount of input data, and on the applied optimization algorithm, i.e., on the applied method and its implementation. Trade-offs between computational effort and solution qualities are usually possible. In the end, the suggested problem formulation is intended to make the computation of near-optimal solutions, within a few seconds, on the basis of the hardware limitations of navigation systems possible.

In the following, RO 2 is formulated. The motivation for RO 2 is the assumption that it is not sufficient, which is postulated by RO 1b, to simply consider efficiency and reliability in parallel

when computing charging strategies. Instead, charging strategies need to show a certain level of efficiency and reliability. Otherwise, an application in practice is not reasonable. This means particularly that a high level of reliability has to be achieved without causing unbearable travel times. As a consequence, it appears to be reasonable to demand within the second RO that it has to be shown that the developed framework leads to charging strategies which show a level of reliability and efficiency that makes an application in practice possible. Unfortunately, the quality of charging strategies is not only a consequence of the applied optimization framework. In some situations, a reliable charging strategy does not even exist. This is the case, for instance, if a trip is started with a state of charge that is not sufficient to reach the next charging station. Due to these considerations, RO 2 is formulated less strongly:

RO 2: Test the suggested problem formulation under the existence of uncertainties and evaluate its ability to ensure charging strategies of practicable quality.

The „quality“ of charging strategies is here understood to describe both their level of efficiency and their level of reliability. RO 2 basically consists of two tasks: First, a framework which allows conducting adequate tests has to be developed. Second, the corresponding results have to be evaluated in order to decide whether the achieved charging strategy qualities can be said to be practicable. Note that RO 2 can be interpreted as a preliminary step. Eventually, the goal has to be to identify the conditions under which a specific framework is able to ensure practicable charging strategies. However, this will not be in the scope of the described research.

1.3 Outline of the Dissertation

The design of the described research and, along with it, the structure of the thesis are the result of the attempt to achieve the introduced ROs. An overview of the chapters and their content can be found in Figure 1.2. The thesis starts with a description of the state of the art in chapter 2. It forms the basis of all further considerations. Its purpose is to gain an overview of work in potentially relevant areas of research, such as estimating energy consumption of BEVs or modeling uncertainty within routing applications. The focus of the review, however, is set on existing studies concerning CSO. It is discussed up to which degree these prior works allow achieving the stated ROs.

This discussion reveals several aspects which are particularly necessary for RO 1a and RO 1b, but have not been addressed sufficiently by existing models. To make up for these shortcomings, the problem of finding optimal charging strategies is formulated as a multistage decision problem in chapter 3. This initial model marks the start of an iterative process, which is illustrated in Figure 1.3. During this process, a potential problem formulation is analyzed with regard to its ability to fulfill ROs 1a, 1b and 1c. Depending on whether a considered problem formulation satisfies these requirements, it is either extended, simplified or, at the end of the

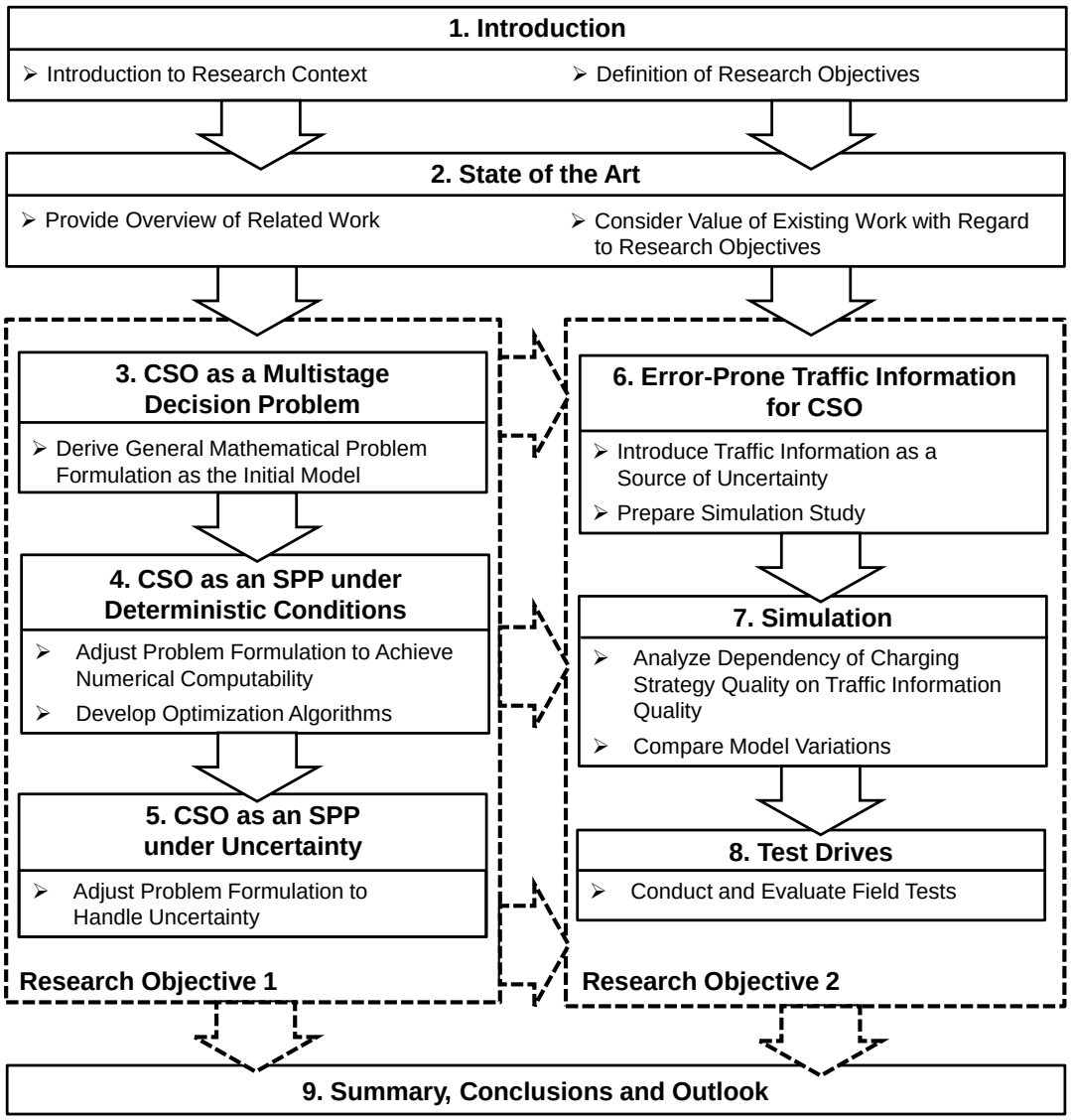

Figure 1.2: Structure of thesis.

whole process, accepted. During this iterative process, the initial formulation as a multistage decision problem is at first reduced in chapter 4 to a deterministic shortest path problem (SPP) and afterwards, in chapter 5, extended again. The reduction is necessary for the development of optimization algorithms which allow computing solutions in reasonable time, the extension in order to address the potential existence of uncertainties. The final result, at the end of chapter 5, is a problem formulation that fulfills all criteria defined by the subobjectives belonging to RO 1.

In order to achieve the second RO, an extensive simulation study is conducted. For this purpose, some preparations are necessary to be able to provide charging strategies to simulated BEVs. During these preparations, it is defined which input data (weather, steepness, etc.) are

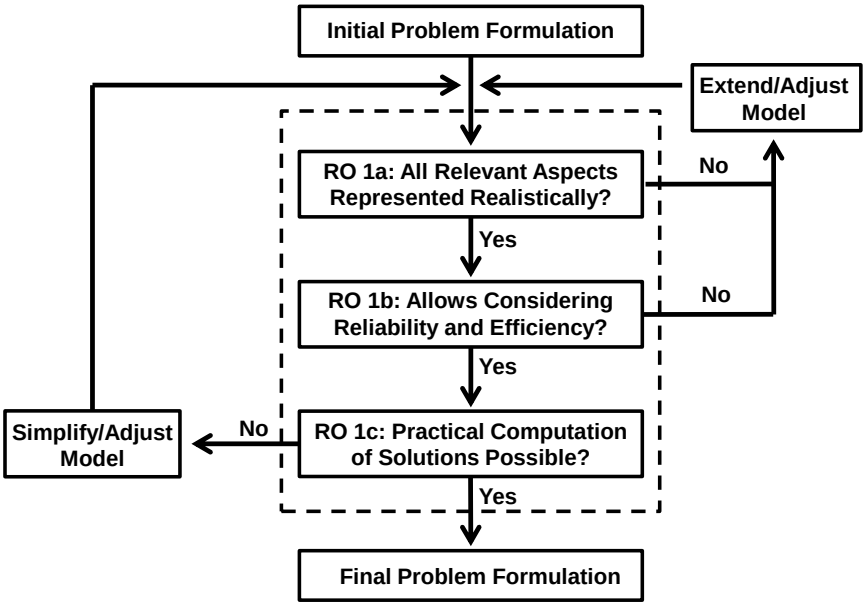

Figure 1.3: Iterative process leading to final problem formulation.

considered and how they affect energy consumption and arrival times. Moreover, error-prone traffic information is introduced as source of uncertainty, i.e., the traffic information that is considered during the computation of charging strategies may not mirror the simulated reality perfectly. These preparatory steps are primarily conducted in chapter 6. The simulation itself is described in chapter 7. A BEV driving from its starting location to a destination is simulated. During this trip, the BEV follows charging strategies which are provided to it. These charging strategies are based on partly incorrect information about current and future traffic states. Thus, the BEV may face a simulated reality that differs from the situation which was presumed during the computation of the charging strategy it follows. The quality of charging strategies resulting from different types of traffic prediction approaches, which show different levels of similarity to the simulated reality, is analyzed. These analyses allow drawing conclusions on the ability of the suggested mathematical framework to handle uncertainty, at least for the case of error-prone traffic information.

As a supplement to the simulation study, the execution of a small number of field tests is finally described in chapter 8. An electric vehicle is used to cover a distance of several hundred kilometers. To support the test drivers, a prototypic implementation of a software tool for computing charging strategies is provided to them. The purpose of the field tests is to test the developed framework under realistic conditions. Moreover, it allows identifying aspects which may be relevant from a practical perspective, but which have not been considered up to this point.

Chapter 2

State of the Art

The purpose of the following chapter is to provide an overview of prior works in areas that are related to the problem of finding optimal charging strategies. At the beginning, in section 2.1, the estimation of the energy consumption of BEVs is thematized. Based on this, different types of navigation services for BEVs are considered. The focus is set on literature about CSO. It is discussed up to which degree existing models are able to fulfill the requirements defined by the stated ROs. The result of this discussion is that particularly the topic of handling uncertainty is not addressed sufficiently. Due to this, the focus of the literature review is shifted in section 2.2 from CSO to modeling uncertainty in routing problems. Finally, in section 2.3, an overview of existing studies on traffic information services that are used in practice is provided. This excursus is motivated by the fact that, as mentioned in the outline of the thesis in section 1.3, imperfect traffic information represents the only source of uncertainty within the simulation study in chapter 7. In order to be able to ensure a high level of realism of the simulation runs in chapter 7, it seems helpful to gain an understanding of the features of traffic information which is provided by professional traffic content providers.

2.1 Battery Electric Vehicles

The main objective of the described research is to provide a basis for an inclusion of CSO functionalities into navigation systems. This makes it necessary to be able to estimate the amount of energy a BEV consumes when passing a certain road segment. Section 2.1.2 addresses this topic. In section 2.1.3, prior works regarding navigation services which are particularly intended for BEVs are considered. But at first, a general introduction to electric vehicles is given.

2.1.1 Introduction to Battery Electric Vehicles

In the context of cars, electric engines are used for propulsion in various ways. Besides purely electrically driven vehicles (which are denoted as BEVs), also so-called hybrid electric vehicles

(HEV) exist. This type of electric cars combine electric with combustion engines[2]. Depending on the architecture of the power train, it can be differentiated between three different types of HEVs (*96*): Serial, parallel, and combined HEVs[3].

Serial HEVs The internal combustion engine of a serial HEV does not work as a propulsion device. It is just used to generate electricity, which is either used to recharge the battery or directly for propulsion. In contrast to parallel or combined HEVs, serial HEVs show the advantage that the size of the internal combustion engine typically can be kept rather small. Furthermore, the complexity of the whole power train is comparably low. It is also simpler than the power train of a conventional ICEV, since, for instance, only a simplified gearbox needs to be integrated. On the downside, the serial structure of the power train tends to reduce energy efficiency (*26*).

Parallel HEVs For parallel HEVs, the internal combustion engine is no longer used as a generator for electricity (see Figure 2 in (*26*)). Instead, both the internal combustion engine and the electric motor have the possibility to propel the vehicle. It is possible that both engines work in parallel, but also that only the internal combustion engine or only the electric motor is activated. It depends on the driving situation, which of these possibilities is applied. The most important advantage of parallel HEVs is that the torque generated by the electric engine and the torque generated by the combustion engine add up. Hence, in comparison to the serial HEVs, a smaller electric motor can be used without loosing performance. On the contrary, the whole system becomes more complex. See (*51*) for more detailed explanations.

Combined HEVs For combined HEVs, the internal combustion engine can work as a generator, but it is in addition able to directly propel the vehicle. This allows combining the the advantages of the serial and the parallel HEVs – up to some degree. On the other hand, the power train of combined HEVs are even more complex than those of parallel HEVs and, along with this, also their costs tend to be higher (*26*).

In general, there exist three ways for recharging the battery of an HEV (or BEV, respectively): First, the battery can be charged via „recuperation“ or „regenerative braking“, respectively. This is a mechanism that allows converting kinetic energy into electricity. To achieve this, the electric motor is used in reverse function, i.e., it is used as a generator. Electricity is generated

[2]The term „hybrid electric vehicle“ basically refers to a car which has (at least) a second type of energy storage – besides its battery. In this work, the term solely refers to cars which are equipped with an internal combustion engine and an electric engine.

[3]Depending on the literature which is considered, several different classification schemes can be found. These schemes in most cases distinguish between three (*51*) (*96*) or four (*26*) (*85*) types of HEVs. Furthermore, also the way the classification is done varies.

and stored in the vehicle's battery while the vehicle's speed is reduced. Using the internal combustion engine as an electricity generator represents the second possibility to charge the battery of an HEV. This is not possible for parallel HEVs and obviously not for BEVs. The third method is to make use of an external source of electric power. At the moment, the transmission of energy from an external source to the battery of a BEV or an HEV is usually done via a cable and a plug. Corresponding HEVs are denoted as plug-in hybrid electric vehicle (PHEV) (*85*) (*163*). Depending on the available charging technology, the energy throughput varies between 3.7 kilowatt and almost 50 kilowatt (*56*). Assuming typical battery capacities (see Table 2.1), these values lead to charging durations between less than one hour and almost a whole day. The highest charging throughput is at the moment achieved via direct current (DC) charging. However, building up infrastructure which enables DC charging is expensive. Moreover, it

Table 2.1: Most sold electric vehicles in Germany in 2015

Model	**Type**	**Battery Capacity**	**Pure Electrical Range (NEDC)**	**DC-Charging Standard**
Kia Soul EV (*54*)	BEV	27 kWh	212 km	CHAdeMO
BMW i3 (*18*)	BEV	19.8 kWh (27.2kWh)	190 km (300 km)	CCS
Mitsubishi Outlander PHEV (*55*)	PHEV	12 kWh	52 km	CHAdeMO
Volkswagen Golf GTE (*150*)	PHEV	8.7 kWh	50 km	-
Audi A3 e-tron (*4*)	PHEV	8.8 kWh	48 km	-
Renault Zoe (*124*)	BEV	22 kWh (41 kWh)	240 km (400 km)	-
Tesla Model S (*83*) (*142*)	BEV	70 kWh (85 kWh)	442 km (502 km)	Supercharger

should be mentioned that a further drawback of DC charging is the fact that several different standards were established. The CHAdeMo standard (derived from „CHArge de MOve“), the combined charging system (CCS), and Tesla Motor's „supercharger“. These standards are not compatible.

Besides the approach to directly connect to the electricity grid, there exist two alternative approaches which allow making use of external power sources: It is possible to completely switch the battery or to transfer electric energy wirelessly via electromagnetic induction. Switching batteries can be done rather quickly and thus saves time, but it also requires a high level of standardization and such systems show currently no relevant market share (*56*). Recharging car batteries via electromagnetic induction possibly will be of importance in the future, but at the moment it is realized only on a prototypic level, mainly within research projects (*56*) (*158*).

Until today, a huge variety of electric vehicles (BEVs and HEVs) has been released. See (*114*) or (*155*) for corresponding lists of vehicle models. Table 2.1 provides a tiny excerpt from these lists. It shows the seven electric vehicles which were sold most often in Germany in 2015 (*23*). This short list is intended to give an idea of currently achieved driving ranges. It is worth mentioning in this context that the driving ranges which the BEVs that can be found in Table 2.1 achieve are upon the highest of all available BEVs. Furthermore, note that the driving ranges are based on the „New European Driving Cycle“ (NEDC). These official driving ranges tend to lie significantly above the driving ranges which can be experienced in practice (*66*). If two different values for battery capacity or driving range are stated in Table 2.1, then this means that the vehicle can be equipped with batteries of different size. The two given values represent the lowest and the highest (in brackets) of all possible battery capacities.

2.1.2 Energy Consumption of Battery Electric Vehicles

First, factors influencing the energy consumption of BEVs are considered. Second, it is sketched how energy consumption estimations are typically conducted.

Factors Influencing Energy Consumption of BEVs The comparably small amount of energy currently available car batteries are able to provide leads to the need of highly accurate energy consumption models. To achieve such a high level of precision, all factors which significantly influence the energy consumption of BEVs have to be identified. In literature, factors known to influence the fuel consumption of ICEVs, such as driving behavior (*44*), traffic conditions (*148*) (*164*) and vehicle parameters (*49*), are often initially considered. For BEVs, the importance of traffic conditions on energy consumption is confirmed in (*86*) and (*123*). The dependency of energy consumption on the characteristics of the considered BEV is emphasized in (*57*) and (*123*) and the impact of individual driving style is included in the energy consumption model in (*57*). However, in recent studies, it has been shown that road steepness (*92*) and weather conditions (*66*) also have significant impact on the range of BEVs. Note that road steepness (due to increased driving resistance) and weather conditions (primarily if the air conditioning or the heating are activated) influence the fuel consumption of ICEVs, too. The difference is, as mentioned, that the battery of BEVs in most cases cannot provide the same amount of energy which the fuel in the tank of an ICEV provides. Thus, more detailed models are applied to get a more precise estimation of the remaining driving range. Another reason for the consideration of road steepness in the context of BEVs is their ability of regaining energy via recuperation. This implies that by driving downhill, the BEV's battery may even be recharged. Furthermore, the effect of weather conditions is stronger on BEVs than on ICEVs: Battery capacity reduces at low temperatures (*66*). This effect does not increase energy consumption, but achievable driving ranges still get reduced. Furthermore, ICEVs automatically generate a lot of warmth while driving. This warmth can be used for heating. BEVs, on the other hand, have to operate an electric heating and thus need additional energy for heating.

Energy Consumption Estimation To get from factors influencing energy consumption to specific energy consumption values, energy consumption models are necessary. In principle, energy consumption models for BEVs are based on the same ideas as fuel consumption models for ICEVs. In (*161*), for example, a regression model is suggested to estimate energy consumption. This model describes the dependency of energy consumption on a set of explanatory variables which are primarily based on instantaneous driving speeds and instantaneous accelerations. Alternatively, physical consumption models are applied (*86*). Such models include a variety of vehicle parameters (frontal area, vehicle mass, etc.) to determine driving resistance[4] in dependency of driving speed, acceleration and road steepness. Based on the driving resistance, the BEV's mass, and the energy conversion efficiency of the electric motor, the energy which is necessary to move and accelerate the BEV can be derived. Besides the energy consumption caused by movement, which is also denoted as primary energy consumption, additional energy is necessary for operating the so-called secondary consumers, such as the radio or the air conditioning system.

To predict the energy or fuel that is necessary to pass a certain road segment, typically a two-step proceeding is executed in literature: First, a speed profile is estimated, i.e., the temporal development of the speed with which the considered vehicle passes the relevant road segment is estimated. These estimations are usually based on historical traffic data, current traffic information or road categories (highway, freeway, etc.). In a second step, an energy consumption model is applied to the estimated speed profile. In (*57*), for instance, real speed profiles were recorded. Then, these profiles are used to predict driving characteristics (such as the number of stops, average speeds along road segments, etc.) depending on road class. The energy consumption model is afterwards fed with these characteristics to estimate energy consumption necessary for passing road segments. In (*123*), recent information on the current (macroscopic) traffic state is taken into account for simulating potential future speed profiles. These profiles are again used as input for energy consumption models and the resulting energy consumption values are applied to find routes that keep energy consumption as low as possible. Such routes are denoted as energy efficient routes. Comparable approaches can also be found in (*74*), (*86*) or (*90*). This already leads to the topic of navigation services for BEVs.

2.1.3 Navigation Services for Battery Electric Vehicles

Scientific work on three different types of navigation services, which are relevant for BEVs, are considered in the following: The provision of energy efficient routes, the recommendation of refueling or recharging stops, and the coordination of fleets of BEVs. In order to be able to follow the subsequent statements, it is important to know that, within optimization problems in

[4] Driving resistance consists of rolling resistance, climbing resistance, aerodynamic resistance, and inertial resistance.

the context of navigation applications, road networks are usually represented by mathematical graphs. The edges of the graph represent road segments and the nodes represent intersections. Furthermore, costs are assigned to edges. These costs can be interpreted, for instance, as the time that is necessary for passing the road segment which is represented by the edge to which the costs are assigned. Alternatively, these costs can also be interpreted as the length of the corresponding road segment or as the fuel/energy that is necessary to pass it.

Energy Efficient Routing In literature, the problem of finding energy efficient routes (i.e., to minimize energy consumption) is typically modeled as an SPP. In this context, some of the characteristics of BEVs need to be explicitly taken into account. In (*7*), (*12*) and (*42*), for instance, it is shown how it can be included into the formulation of SPPs that the battery of a BEV is not charged up to more than 100 percent due to recuperation. Moreover, routing algorithms known from travel time and travel distance minimization are modified in such a way that paths leading to an empty battery are not considered within the route search process. Another frequently discussed issue is the possible existence of negative edge costs (*12*) (*42*) (*74*) (*128*), which is also caused by the recuperation ability of BEVs. This has significant influence on the applicability of many established routing algorithms. A detailed discussion on the topic of negative edge costs will be provided later on in section 4.2.

Vehicle Refueling Problem Charging strategies consist of two components: Route recommendations and charging recommendations. Route recommendations are important for both BEVs and ICEVs. Instructions where a vehicle has to be recharged or refueled, respectively, and how much energy/fuel has to be charged/fueled appear to be less important for ICEVs than for BEVs. Nevertheless, there exist some articles about the so-called vehicle refueling problem: Let it be assumed that a road network and a set of gas stations spread across this network are given. Furthermore, the ICEV's current position and a destination are specified. Moreover, the prices for fuel differ between the gas stations. The goal is to provide a refueling strategy which minimizes fuel costs and assures a reliable arrival at the destination. This problem was discussed for the first time in (*93*). In this study, it is assumed for simplicity that the considered ICEV can only take a single, pre-determined route. In (*140*), the vehicle refueling problem is extended to the network level, i.e., alternative routes are possible. Furthermore, long detours, which are a possible result when minimizing total fuel costs, are penalized to achieve more practicable route recommendations. In (*127*), a real-world case study is described. The money savings, which a trucking company obtained after introducing a software-tool for refueling optimization, are analyzed. In (*82*), refueling issues are even included into the context of traveling salesman problems. In this work also a fuel-buffer, i.e., a minimal amount of fuel that has to remain in the tank to be able to compensate for unexpectedly high fuel consumption, is suggested to keep the risk of running out of fuel low.

Charging Strategy Optimization for Single Vehicles During the last years, along with an increasing interest in BEVs, the basic idea of the refueling problem has been transferred to BEVs, i.e., the task of finding optimal charging strategies emerged. Probably one of the first publications about charging strategies for BEVs is (*87*) (published in 2011). There, a formulation as an SPP[5] is proposed. A graph is considered which represents a road network and a few nodes are selected which mark the positions of charging stations. A shortest path between a start node and a destination node has to be computed. Shortest paths are associated with charging strategies by assuming that a BEV following such a path is fully recharged at each visited node that marks the position of a charging station. The paths or charging strategies, respectively, are optimized in (*87*) either with regard to the total distance traveled or the total travel time. „Total“ travel time refers to the time for driving plus the time for charging. Furthermore, it is assumed that the energy consumption of a BEV solely depends on the traveled distance. This implies that energy consumption costs are assumed to be static, i.e., the energy consumption costs for passing an edge remain the same under all circumstances. Also time costs are assumed to be static in (*87*). For travel times and energy consumption, this represents a significant simplification, since dynamic impacts, such as changing traffic conditions, cannot be taken into account. On the other hand, presuming static edge costs facilitates the application of so-called preprocessing methods. Such approaches are applied a priori, i.e., before the first route search is carried out, to generate auxiliary data for a given graph and given edge cost functions. These data are afterwards taken into account by (conventional) route search algorithms to prune their search space.

In (*87*), such additional data are generated a priori. Time and distance costs between pairs of charging stations are calculated. Based on this information, an additional graph consisting only of those nodes which represent charging stations and edges between pairs of charging stations is constructed. The edges, however, are left out if the distance between a pair of charging stations is very high. Let this graph be denoted as auxiliary graph. The route search is then conducted as follows: First, the set of all nodes which can be reached from the start node based on the currently available energy is computed. Dijkstra's algorithm (*36*) is used for this purpose. Second, all nodes are identified from which the destination can be reached under the assumption of a fully recharged battery. This is again done via Dijkstra. It is checked whether in both nodes sets at least one charging station is available. If this is not the case and if the destination cannot be reached directly from the start node, then no appropriate charging strategy exists. Otherwise, all routes from charging stations, which can be reached from the start node, to charging stations, which allow reaching the destination, are computed. This route search is done on the auxiliary graph (again by applying Dijkstra's algorithm). The result of this proceeding are three types of routes or paths, respectively: The first type leads from the start node

[5] SPPs are typically interpreted as dynamic programs, even though there exist also formulations of SPP as, for example, integer linear programs. If not stated differently, SPPs are in this work always interpreted as dynamic programs.

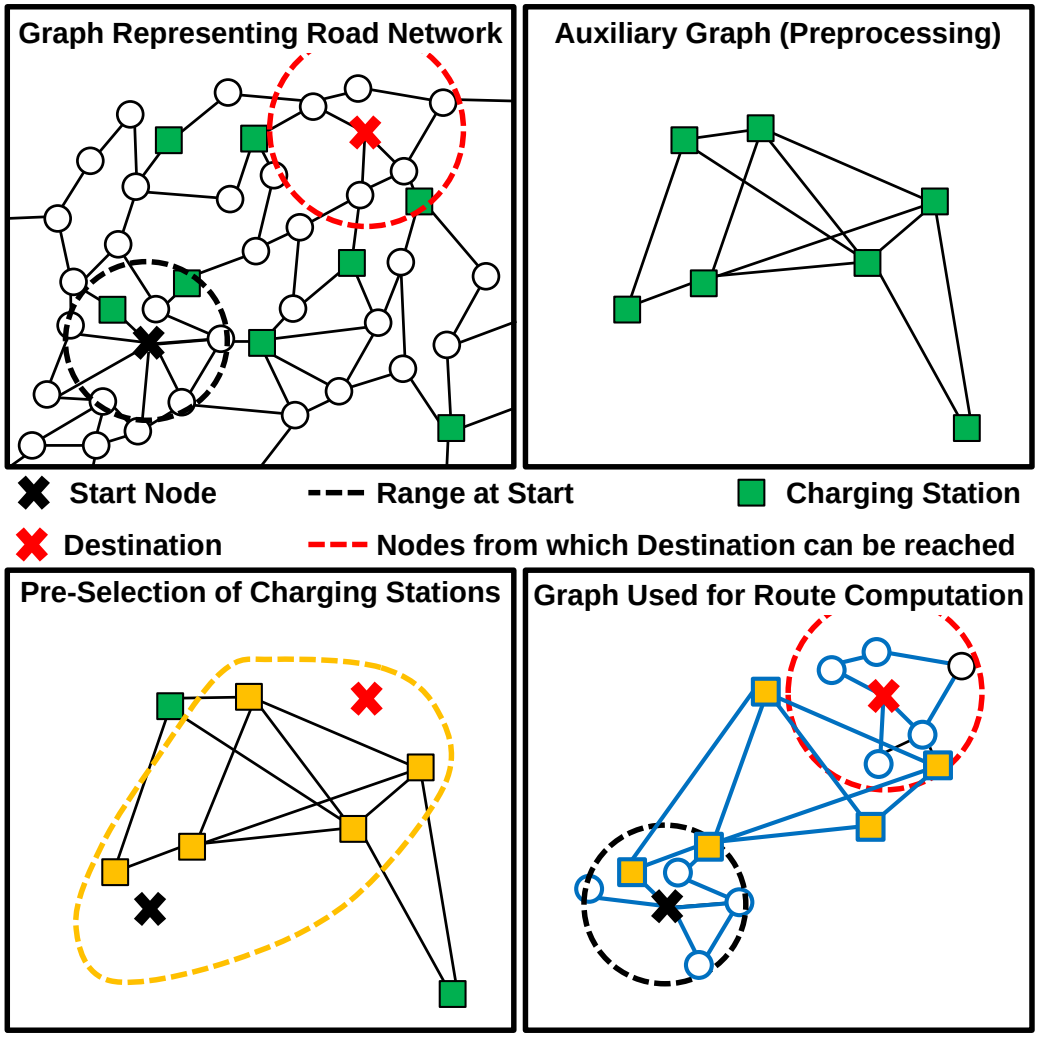

Figure 2.1: Computation of charging strategies according to the methodology described in (87).

to a nearby charging station on the original graph, paths of the second type are part of the auxiliary graph and describe a sequence of charging stations leading from a possible first charging station (near the start) to a possible last charging station (near the destination), and paths of the third type describe routes on the original graph from one of the possible last charging stations to the destination. To receive a complete charging strategy, the concatenation of paths needs to be found which leads from the start to the destination and, in parallel, minimizes the overall travel time or traveled distance, respectively. This is again achieved on the basis of Dijkstra's algorithm.

Besides the described preprocessing, another speed-up technique is applied in (87) in order to reduce computation times. At the time at which a request for a charging strategy is stated, a set of relevant charging stations is identified in a first step. For this purpose, an approach is proposed in (87) which selects only charging stations (from the set of all charging stations) which

are located (more or less) between the start and the destination. No detailed description of this approach is provided here. Then, the auxiliary graph is reduced correspondingly, i.e., only those nodes and edges remain in the auxiliary graph, which represent either one of the selected charging stations or a route between two of these charging stations. In total, it is proceeded as follows (compare also Figure 2.1): A priori, costs to get from one charging station to another are calculated. As soon as a charging strategy is requested, a set of reasonable charging stations is selected. An auxiliary graph consisting of the corresponding set of nodes is generated. Edge costs for this graph are based on the preprocessed data. Finally, the route search is first conducted on the original graph to identify reachable charging stations, then on the auxiliary graph in order to get close to the destination, and finally again on the original graph to reach the destination. Note that the preprocessing step and the two-steps process (identify reasonable charging stations, afterwards compute a charging strategy by considering only these charging stations) during the route search are explained here in detail, since several studies concerning CSO propose similar approaches.

In (*138*), a mathematical framework is described that allows deciding whether a certain destination can be reached without charging (given a starting location and a starting state of charge), whether it is possible to reach this destination on the basis of the existing charging infrastructure, and how the number of necessary charging stops can be minimized. All these problems are formulated as SPPs and modified versions of Dijkstra's algorithm are used for the computation of solutions[6]. In contrast to (*87*), energy consumption costs are the only type of edge costs which are considered in (*138*). These costs are again assumed to be static. Furthermore, a preprocessing step is conducted in (*138*), too. However, not only costs to get from one charging station to another are computed. Instead, the amount of energy that is necessary to get from one node to another is calculated and stored for pairs of nodes where at least one of both nodes represents a charging station. It is shown how these additional data can be exploited by dynamic programming approaches. A conducted case study confirmed that the suggested procedure allows solving the described problems very quickly, even for huge road networks consisting of millions of road segments and intersections. Another relevant aspect is the fact that the described framework is developed for so-called battery switch stations. This means that the considered BEVs are actually not assumed to charge energy. Instead, the whole battery is switched. As a consequence, similar to (*87*), a state of charge of 100 percent is obtained after each „charging“ process. Hence, a driver cannot decide how much energy she/he wants to recharge. Charging strategies as, for example, strategy 3 from Figure 1.1, where the BEV is charged up to a state of charge less than 100 percent, cannot be represented.
In (*137*), the framework from (*138*) is extended. Now, multicriteria SPPs related to BEVs are investigated. The considered problem formulations are intended to represent the wish to find

[6]The original version of Dijkstra's algorithm cannot be applied here, since it is taken into account that energy consumption costs may be negative.

compromises between consumed energy, travel time, and traveled distance. This is motivated by the conjecture that even very eco-friendly drivers are not willing to accept extremely long detours or drastically increased travel times just to save some energy. Similar to (*138*), the need to recharge and, along with that, times for charging processes are taken into account. Problem formulations, such as „Find the fastest path with at most two charging stops“ are investigated. All problems are formulated as SPPs and modified versions of Dijkstra's algorithm are applied for the computation of solutions. Again, all edge cost functions (energy consumption, distance, travel time) are assumed to be static, which allows keeping computation times low. Furthermore, it is again solely possible to fully recharge the battery.

In (*141*), the problem of finding optimal charging strategies is modeled as a dynamic program, where total travel time is minimized. For the proposed optimization framework, some simplifying assumptions are made: First, it is assumed that a possibility to charge exists at each node of the graph. Second, time and energy costs are again assumed to be static. Third, energy consumption for passing edges is assumed to be non-negative, i.e., the possibility of BEVs to recuperate energy is up to some degree ignored. In contrast to these simplifications, the set of possible charging actions is modeled flexibly. Instead of providing solely the option to fully recharge the battery whenever a charging process is started (compare the aforementioned papers (*137*) and (*138*)), any state of charge between the BEVs initial state of charge and a fully recharged battery can be obtained within the proposed formulation as a dynamic program. Such a continuous set of decision possibilities is very uncommon for dynamic programming approaches. Usually, all aspects of a dynamic program need to be discretized. Otherwise, typical solutions approaches for dynamic programs are unable to guarantee optimality of the computed solutions. In (*141*), however, a backward recursion algorithm is suggested, which is able to ensure optimality of the calculated solutions under some mild assumptions. Besides the backward recursion algorithm, an approximate dynamic programming algorithm is described, which is able to find at least good solutions even if these mild conditions are not fulfilled. However, this second algorithm discretizes the set of possible charging actions. Discretizing the set of possible charging actions means that the recommended state of charge, i.e., the state of charge which has to be reached at the end of a charging process, can solely be equal to one of a few, a priori defined values. For example, all suggested charging processes end with a state of charge that is a multiple of five percent ($5\%, 10\%, ..., 95\%, 100\%$). Since not all possible charging options are considered by the approximate dynamic programming algorithm, optimization potential is lost up to some degree and consequently, optimality of computed solutions cannot be guaranteed.

The most remarkable aspect of (*141*) is that the condition that ensures that a suggested charging strategy does not lead to an empty battery is designed in a more flexible way than in other contributions about CSO. A (static) positive value is defined as the minimal necessary state of

charge. If a charging strategy leads to a state of charge during the trip which is lower than the minimal state of charge, then the corresponding charging strategy is not accepted. The idea is the same as for the case of the vehicle refueling problem in (*82*), where a fuel buffer is suggested to be able to compensate for unexpectedly high fuel consumption.

In (*152*), the problem of finding optimal charging strategies is again modeled as an SPP. In contrast to previously mentioned studies, energy consumption costs are here interpreted as time-dependent quantities and thus are no longer static. Furthermore, similar to (*141*) for the case of the approximate dynamic programming approach, the set of possible charging actions is discretized. Charging strategies are optimized with regard to two different objectives: Travel time minimization and, as an alternative, a combination of travel time and energy consumption minimization. In addition, two different solution approaches are suggested. The first one is a modified version of the so-called A^*-algorithm (*62*) (*63*). The A^*-algorithm can be interpreted as an extension of Dijkstra's algorithm. It uses additional information, for instance information about geographical coordinates, to direct the route search to the destination. The second approach is an approximate dynamic programming approach. It uses basically again the A^*-algorithm to compute routes. The difference to the first approach is that a heuristic is applied to determine the sequence of charging stations that are visited. This means that the heuristic proposes which charging station has to be visited next and then a route to this charging station is computed. If this is not possible, then the corresponding charging station is excluded from further consideration and another charging station is selected. One proceeds until either the destination is reached or no more charging stations are left. A traffic simulation tool is used at the end of (*152*) to compare the two solution approaches with regard to the total travel time and the total energy consumption that result from the corresponding charging strategies.

In (*10*), a similar approach as in (*87*), (*137*) and (*138*) is pursued. A formulation of the problem of finding optimal charging strategies as an SPP is suggested. Again, a preprocessing step is executed, in which the energy consumption that is necessary to get from one charging station to another is computed for any pair of charging stations. The corresponding energy consumption values are computed using the dynamic programming approach which is applied in (*7*) for the generation of energy efficient routes for BEVs. Though, in (*7*) the possibility to recharge is not considered. Note that again static edge costs are presumed in (*10*). The route search itself is executed analogously to (*87*), but no pre-selection of charging stations is proposed. Optimality is interpreted as a combination of minimizing total travel time and minimizing energy consumption. Even though it is not explicitly stated, it seems that the described framework allows only full rechargings. At the end of (*10*), a case study is mentioned shortly, which showed that low computation times (less than one second on average) are achieved on rather big graphs.

In (*25*) and (*151*)[7], a mixed integer nonlinear program is formulated to compute optimal charging strategies for single BEVs. Total travel times are considered as the optimization criterion and a constraint is added to the problem formulation in order to avoid an empty battery. Energy consumption and travel time costs are again modeled as static quantities. Analogously to (*141*), solutions of the described optimization problem may recommend arbitrary recharging amounts. To solve the mixed integer nonlinear program, it is separated into two subproblems. Both of these are linear programs. Solving the first subproblem leads to a route. Based on this route, the second subproblem is formulated. Solving the second problem leads to recommendations concerning the amount of energy that has to be charged at the charging stations which are available along the already computed route. It is shown that the separation into two subproblems still ensures optimality of the computed solution for the described setting. Furthermore, because both subproblems are linear programs, low computation times even for big problem instances can be expected.

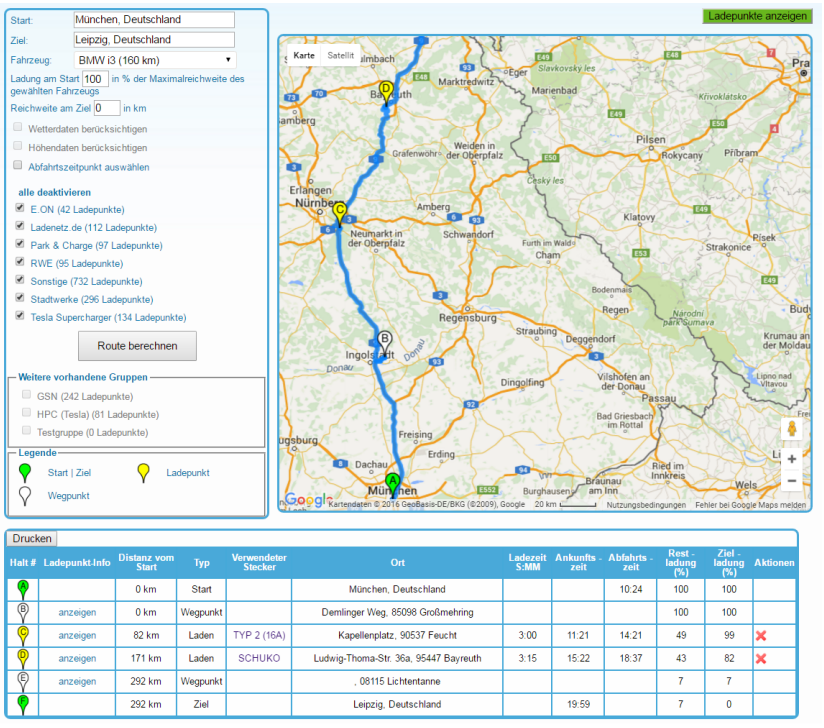

Halt #	Ladepunkt-Info	Distanz vom Start	Typ	Verwendeter Stecker	Ort	Ladezeit S:MM	Ankunfts-zeit	Abfahrts-zeit	Rest-ladung (%)	Ziel-ladung (%)	Aktionen
		0 km	Start		München, Deutschland			10:24	100	100	
B	anzeigen	0 km	Wegpunkt		Demlinger Weg, 85098 Großmehring				100	100	
C	anzeigen	82 km	Laden	TYP 2 (16A)	Kapellenplatz, 90537 Feucht	3:00	11:21	14:21	49	99	✖
D	anzeigen	171 km	Laden	SCHUKO	Ludwig-Thoma-Str. 36a, 95447 Bayreuth	3:15	15:22	18:37	43	82	✖
E	anzeigen	292 km	Wegpunkt		, 08115 Lichtentanne				7	7	
		292 km	Ziel		Leipzig, Deutschland		19:59		7	0	

Figure 2.2: Screenshot taken from www.erouting.net (*45*). The output information of an existing web-service for charging strategy computation is shown.

First approaches to provide charging strategies also emerged in practice. The eridea AG, a small engineering company, launched a non-profit project allowing users to request charging strategies via a website (*45*). It is possible to choose from a range of BEV models and to define

[7](*25*) is a more detailed, but unpublished version of (*151*).

at which charging stations the customer who requests the charging strategy is able to charge[8]. After a, compared to typical routing applications, long computation time, the user receives a route, a list of charging recommendations, and information about the time at which the charging stations are reached and with which state of charge they are reached (see Figure 2.2). A similar web-service can be found in (*60*). In 2015, with Tesla Motors, the first car manufacturer started providing charging strategies (*143*). The corresponding tool is denoted as „Trip Planner“ and it is embedded in the in-dash navigation system.

Table 2.2 summarizes the central aspects of the above described literature about CSO. Note that no contributions from practice are listed here, since not much information concerning the underlying optimization problems and algorithms is available. It is remarkable that almost all listed contributions suffer from two significant simplifications: First, except for (*152*), edge costs are always modeled as static values. This makes it impossible to take the influence of dynamic aspects into account. For example, the impact of changing traffic situations on energy consumption or travel time cannot be represented. As a consequence, the accuracy of the whole model and, along with this, the quality of the resulting charging strategies is limited. Second, the topic of reliability is only addressed in a very basic form. A constraint which ensures that the considered BEV does not run out of energy is part of each of the listed problem formulations. However, the possibility that energy consumption values that are considered within the models may not mirror real energy consumption absolutely correctly cannot be taken into account by the suggested problem formulations. This is extremely critical, since without the ability to handle unexpected developments, reliability cannot be ensured in practice. The only exception is the model described in (*141*), where a static part of the battery capacity can be used as an energy buffer. This concept is rather simple. Its main limitation is that the minimal state of charge remains the same, independently of the intended trip. If five percent of the battery capacity are reserved to account for unexpectedly high energy consumption, then this is probably a rather big buffer if the destination is one kilometer away. On the other hand, the buffer may be too small if the destination is 100 kilometers away. Considering the importance of reliability for drivers, it is surprising that not more attention is drawn to this topic. On the other hand, keeping the models simpler reduces the computational effort which is necessary for solving the corresponding optimization problems. Some of the listed studies prove this (*10*) (*137*) (*138*) .

[8]It is not possible to charge BEVs at arbitrary charging stations. It was already mentioned that different technical standards exist. Furthermore, specific user accounts are often necessary. These accounts allow recharging BEVs at charging stations of a certain charging station operator and only of this operator.

Table 2.2: Existing studies on CSO for single BEVs

Study Reference	Problem Formulation	Optimization Criteria	Solution Approach	Model Characteristics
Kobayashi & et al. (*87*)	SPP (dynamic program)	- minimize trip distance - minimize total travel time	- Dijkstra's algorithm - preprocessing costs between charging stations - ex ante reduction of considered charging stations	- only full recharging possible - static edge costs - energy costs assumed to be directly proportional to distance traveled
Storandt (*138*)	SPP (dynamic program)	- minimize number of rechargings	- modified Dijkstra - preprocessing costs between charging stations and nodes	- only full recharging possible - static edge costs - case study proved low computation times for huge graphs
Storandt & Funke (*137*)	SPP (dynamic program)	- different compromises between consumed energy, travel time and traveled distance	- modified Dijkstra	- only full recharging possible - static edge costs - case study proved low computation times for huge graphs
Sweda (*141*)	dynamic program	minimize total travel time	- backward recursion - approximate dynamic programmig approach	- arbitrary recharging amounts possible - static edge costs - recharging possible at each node - energy buffer to account for uncertainty

Table continuation on next page

Table 2.2 – Existing studies on CSO for single BEVs *continued*

Study Reference	Problem Formulation	Optimization Criteria	Solution Approach	Model Characteristics
Wang & et al. (*152*)	SPP (dynamic program)	minimize energy costs along total travel time	- modified A^*-algorithm - heuristic selection of charging station order for speed-up	- discretized set of possible recharging amounts - time-dependent edge costs
Baouche, et al. (*10*)	SPP (dynamic program)	minimize energy costs along total travel time	- dynamic programming approach from (*7*) - preprocessing costs between charging stations	- static edge costs - (probably) only full recharging possible - case study showed reasonably low computation times
Wang & Cassandras (*25*) (*151*)	mixed integer nonlinear program	minimize total travel time	- linear programming approaches	- arbitrary recharging amounts possible - static edge costs - reduction to linear programs ensures low computation times

In conclusion, it seems that most existing models for CSO were primarily developed to achieve good computation times. If necessary, unrealistic simplifications were accepted. Hence, the requirements which are defined by ROs 1a and 1b cannot be fulfilled on the basis of prior work. Especially the question of how uncertainty can be handled is not or not sufficiently answered. To construct a problem formulation for CSO that is able to adequately include the possible existence of uncertainties, it seems reasonable to shift the focus of the literature review. In the following, scientific works about taking uncertainty within routing applications into account is considered. But before this is done, existing work about providing charging strategies to whole fleets of BEVs is described.

Coordination of Electric Fleets Besides situations in which solely one BEV has to be led to a destination, situations in which a whole fleet of BEVs needs to be managed are also treated in research. Given a road network and limited charging infrastructure, the goal for this type of problem is to provide route guidance to each of the BEVs of the considered fleet. For this purpose, charging processes need to be scheduled to ensure that each BEV can reach its destination. There exist many different formulations of this type of problem, each of them focusing on different aspects: In (*101*), a rather simple approach is described. A framework is sketched in which for each BEV the route which leads to the lowest energy consumption is computed. The BEVs are routed to free charging stations during their trips if this is necessary to reach the destination. In (*126*), BEVs are modeled as agents intending to minimize their travel times and monetary costs for charging energy. One of the goals of this research is to achieve an equal distribution of charging demand over the available charging stations and over time. For this purpose, several pricing strategies, which define the price of electricity in dependency of, for example, the expected utilization of the corresponding charging stations, are suggested. The effects of the described pricing strategies are compared via simulation. In (*11*) and (*131*) , a fleet of BEVs is assumed to visit a set of customers. It is assumed that each customer can only be visited during a limited time period. The problem is formulated as a so-called vehicle routing problem with time-windows, which is a frequently studied type of a (mixed) integer linear program. The route planning includes an assignment of customers to vehicles to ensure that each customer is visited at least once. In (*73*), an approach to manage a fleet of electric taxis is described. In contrast to the approaches which were mentioned up to this point, the problem formulation which is suggested in (*73*) also includes the possibility that charging stations are occupied by „external“ BEVs, i.e., by BEVs which are not part of the managed fleet. The charging demand caused by these BEVs is modeled as a random variable. Recently, also contributions considering the management of fleets of autonomous BEVs appeared (*29*) (*76*). The most significant difference to managing fleets of conventional BEVs is the ability of the vehicles to drive on their own. This can be used to conduct necessary charging processes without any human intervention.

Providing charging strategies to a single BEV is obviously easier than managing a whole fleet of BEVs. This fact has influence on the structure and complexity of the resulting optimization problems and, along with this, also on the applied solution approaches. If fleets are coordinated, then quickly rising computation times often make it impossible to apply optimization algorithms to big problem instances or necessitate keeping problem formulations very simple, which in most cases leads to unrealistic assumptions. These drawbacks represent a contrast to ROs 1a to 1c. Hence, the focus for the described research is set on the single-vehicle case. The fundamental idea is that as long as this situation cannot be handled in such a way that ROs 1a to 1c are achieved, it is not reasonable to attempt more complex scenarios.

2.2 Routing under Uncertainty

In this thesis, uncertainty refers to situations in which a decision has to be made or a computation has to be carried out, but there exists no or possibly incorrect information about one or several aspects that are relevant for the decision or computation, respectively. Within mathematical models, uncertain aspects (predictions are a typical source of uncertainty) are in most cases represented via random variables – if uncertainty is represented at all. In the context of traffic and especially in the context of navigation applications, a wide range of literature about uncertainty exists, particularly about uncertainty of travel time predictions.

Travel Times and Uncertainty Initial research showed that trip travel times are not static and usually follow a skewed distribution with a long tail (*153*). The consequence is that predicting travel times is not trivial. Hence, real travel times often differ from predicted travel times. In (*112*), it is distinguished between two reasons for potentially incorrect travel time predictions: Forecasting errors of (macroscopic) traffic state predictions and uncertainty due to individual driving style. Other studies attempt to disaggregate the random aspects of travel time into regular components (depends primarily on demand), irregular components (depends primarily on capacity), and real random aspects (*157*). In (*91*) and (*121*), based on conducted surveys, it is concluded that not only expected or mean travel times, but also travel time uncertainty has significant influence on route choice and thus is important for drivers. These findings motivated further, more application related contributions. In (*15*), for instance, it is argued that traffic management operations need to improve travel time reliability. Building on these considerations, a methodology for rating managed lane operations based on their influence on travel time reliability is suggested. In the context of routing applications, so-called risk-averse or robust routing approaches are often thematized when it comes to taking uncertainty into account. In (*80*) and (*81*) a neural networks approach for predicting travel times is described which forecasts lower and upper travel time bounds instead of specific values. Most important for the described research, however, are studies describing how uncertainty of travel time predictions can be integrated into problem formulations that are related to navigation applications, such as SPPs.

Modelling Uncertainty in Shortest Path Problems Uncertainty is typically addressed in SPPs by considering random instead of deterministic edge costs. From literature, basically two different types of SPPs resulting from this are known (*77*): Stochastic SPPs and robust SPPs. For stochastic SPPs, it is necessary to know for each edge of the considered graph the probability distribution of the corresponding edge costs. Based on this information, different types of optimality criteria can be considered. The most common criterion is to minimize expected paths costs (*53*) (*160*). Other approaches suggest maximizing the probability that the costs for reaching the destination do not exceed a certain, a priori given cost budget (*129*) (*136*). Alternatively, the goal is to determine a cost budget, which is, on the one hand, as small as possible, on the other hand, it needs to be big enough to ensure that the probability that this budget is exceeded is not higher than a given maximal probability (*28*) (*159*).
Similar to stochastic SPPs, it is additionally assumed for robust SPPs that edge costs are randomly distributed. The main difference to stochastic SPP is that not the probability distributions are known, but only a continuous interval in which possible realizations of the random edge costs must lie, i.e., a lower and an upper bound are known for each edge. The path is denoted as optimal which fulfills the „minmax regret criterion“ (also denoted as „minmax robust deviation criterion“ (*77*)). This means that the path has to be found which is able to keep the maximal difference to the best solution as small as possible, independently of the realizations of the random edge costs (*89*). This can be interpreted in the context of game theory: Player A intends to choose a path that leads to costs that are not much higher than the costs of the best possible path. It is important in this context that player A does not know the realizations of the random edge costs. After player A has selected a path, player B, who is the opponent of player A, constructs a scenario, i.e., a combination of realizations of random edge costs, which makes the selected path as expensive as possible and, at the same time, generates another, extremely cheap path. The goal of the opponent is to achieve a large difference between the costs of the selected path and the costs of the path which leads for the constructed scenario to the lowest possible costs. Solving a robust SPP is the same as finding an optimal solution for player A.

Solving both stochastic SPPs and robust SPPs is computationally expensive (*102*) (*165*). In order to reduce computational effort, some works propose deterministic frameworks. In (*30*) and (*78*), for example, travel times are considered to be the optimization criterion. The goal is to compute paths which lead to low travel times and, simultaneously, achieve a high level of travel time reliability. This means that edges which often lead to significantly higher travel times than the expected travel time[9] should be avoided. However, instead of explicitly considering travel time distributions on an edge level, unreliable edges are simply penalized by increasing their deterministic edge costs in dependency of the variability of the corresponding travel time distribution. Hence, unreliable edges can be avoided, even though edge costs are modeled in a

[9]The travel time distributions of such edges show long tails.

deterministic way. Note that the already mentioned idea of applying fuel/energy buffers in the context of vehicle refueling problems (*82*) or CSO (*141*) can also be understood as a possibility to handle uncertainty of edge costs within a deterministic framework.

Energy Consumption and Uncertainty There are probably some parallels between energy consumption uncertainty and travel time uncertainty. The dependency of energy consumption on driving speeds and accelerations, for example, indicates that forecasting errors of traffic state predictions and uncertainty due to individual driving style are likely to cause not only uncertainty of travel time predictions (*112*), but are a potential reason for uncertainty of energy consumption predictions, too. However, only few scientific contributions seem to exist which address the uncertainty of energy consumption predictions. This is surprising, since it can be expected that it is more important for a driver of a BEV to take the uncertainty of energy consumption predictions into account than it is important for a driver of an ICEV to take uncertainty of travel time predictions into account. An example of such a contribution is (*47*). There, a robust optimization approach is described that allows computing solutions for SPPs where stochastic energy consumption costs have to be minimized. In (*107*), a framework to interpret remaining driving ranges for BEVs as stochastic variables is explained. Uncertainty of future driving profiles is modeled via a discrete-time Markov chain.

2.3 Real-time Traffic Information

As mentioned, the simulation study in chapter 7, where the impact of uncertainty on the quality of charging strategies[10] is analyzed, takes imperfect traffic information as the only source of uncertainty into account. Note that in this thesis, a differentiation is made between traffic information, traffic state estimations, and traffic predictions. Traffic state estimations are intended to describe the current traffic situation, traffic predictions try to describe the future development of traffic conditions, and traffic information denotes both traffic state estimations and traffic predictions. In order to gain a comprehensive understanding of the dependency of charging strategy quality on the quality of the available traffic information, different approaches to generate traffic information are considered during the simulation study. Depending on the generation approach, the resulting traffic information shows different levels of quality[11]. It is important that, besides artificially produced traffic information, actual traffic information which is used within market-ready tools, such as navigation devices, is also considered. Otherwise, the risk exists that some aspects, which are relevant for bringing CSO into practice, are ignored within the simulation study. These considerations motivate taking a closer look into commercially provided traffic information.

[10] Recall that the quality of charging strategies consists of reliability and efficiency.

[11] Quality in the context of traffic information is in this work interpreted as the level of similarity between the considered traffic information and the real traffic situation.

Introduction to Traffic Information in Practice Modern navigation systems, but also other types of traffic related services that can be found in practice, typically base their route recommendations on so-called real-time traffic information (RTTI). For the remainder of this work, RTTI denotes information which fulfills the following properties:

1. The information is primarily based on recently collected, traffic related data.
2. The information is frequently updated.
3. The information either intends to describe current traffic states or to predict future traffic states.

Thus, such navigation systems not only suggest routes which depend on static factors like historical speed averages or the road network, but also include recent incidents. In practice, the

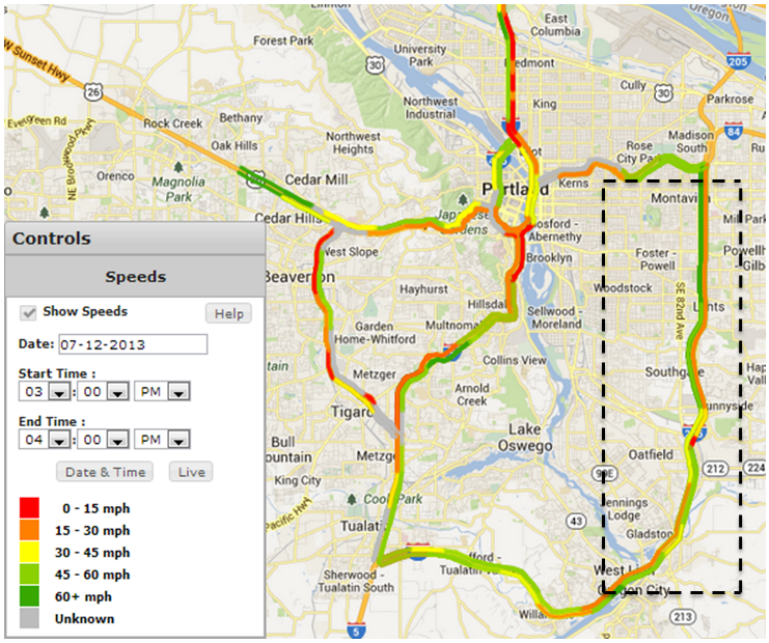

Figure 2.3: Map of Portland (United States of America) visualizing real-time traffic information (*115*)

considered RTTI is usually not generated by the manufacturers of the navigation systems themselves. Instead, traffic predictions and traffic state estimations are received from private traffic content providers, such as TomTom or INRIX. These companies have access to a wide range of traffic related data, for example, speed and flow data gathered by inductive loop detectors or so-called journalistic data (information about road works, events, etc.; see (*71*) for an overview of data sources). Their main data source, however, are probe data. This kind of data is gathered via mobile devices that are located within vehicles, for example navigation systems or smart phones. These devices regularly report their current location and possibly further information.

All available data are fused by the traffic content providers. The primarily purpose is to estimate the current traffic situation. Recently, traffic content providers also started to compute and broadcast traffic predictions in real-time.
In many cases, average driving speeds are used to describe traffic situations, i.e., RTTI is information about speeds. If nothing else is stated, in this work RTTI is considered to be information about speeds, too. To be able to associate speed information with specific locations, usually standardized digital maps are applied. These maps separate the road network into road segments and denote each road segment with a unique identification key. Traffic content providers regularly send speed information along with an identification key to their customers, who use this information for the provision of their own traffic related services. Examples for such services are routing apps or illustrations of road networks, where each road segment is colored according to the estimated current average driving speed. An example of such a map is displayed in Figure 2.3[12]. Note that the identification key is necessary in order to be able to associate a broadcasted speed value with a road segment.

RTTI provided by professional traffic content providers shows some important features. This type of information covers road networks comprehensively. For the case of CSO, which is particularly relevant if longer distances have to be covered with BEVs, the availability of regularly updated traffic information along the whole distance is essential, at least if one intends to take the impact of traffic on energy consumption and travel times into account. Commercial RTTI is probably the only possibility to ensure this. Another benefit is that professional traffic content providers have lots of data available. It was impossible for most companies to gain and handle comparably huge amounts of traffic related data. More data provides, in principle, the possibility to obtain more accurate estimations of current and future traffic states. Though, it cannot be expected that recent data are always (24 hours a day, seven days a week) available for each part of the whole road network. To detect congestion, for instance, there needs to be either some kind of stationary detector at the corresponding position or a vehicle equipped with a mobile device which experiences the congestion. Hence, the detection of traffic related incidents may take some time or is not achieved at all. Moreover, gathered data need to be aggregated, interpreted, and a corresponding traffic information has to be broadcasted. Each of these steps consumes time and may cause errors (misinterpretations, transmission errors, etc.). The consequence is that even traffic state estimations provided by professional traffic content providers often are unable to mirror the real traffic situation accurately (*19*) (*21*). This raises the question about the quality of RTTI and how it can be measured.

Assessment of Real-time Traffic Information An important task, which is frequently addressed in literature, is the assessment of the quality of commercial RTTI. For the intended

[12]The dashed rectangle in Figure 2.3 will be relevant later on.

simulation study in chapter 7, where the dependency of the quality of charging strategies on the quality of the available traffic information is analyzed, it is also important to be able to measure the quality of RTTI quantitatively. Before this can be done, however, the term „quality“ needs to be defined in the context of RTTI.
There exist very detailed considerations about the definition of information quality in general. In (*156*), for instance, seven different facets of information quality are listed (accuracy, consistency, completeness, availability, recentness, metric precision and semantic precision). Even though this contribution has a traffic related background, the suggested concept for defining information quality differs significantly from the interpretation of quality which can be found in studies that particularly deal with the assessment of commercial RTTI[13]. In these studies, it is always proposed to generate at first a numerical representation of the real traffic situation, and then define quality as the level of similarity between broadcasted RTTI and the generated representation.

Basically, it can be distinguished between two different types of methods for generating numerical representations of traffic situations (*21*). One possibility is the execution of test drivings where the global positioning system (GPS)-traces of the test vehicles are recorded. Such traces consist of data about the vehicle's position in dependency of time. This makes it possible to derive driving speeds, which again allows drawing conclusions on prevailing traffic conditions. Methods for rating the quality of RTTI compare the trace-data or probe-data, respectively, with the RTTI. In (*20*), for example, road segments where congestion was experienced by the drivers during the tests drive are identified based on the probe-data. For this purpose, a speed threshold is defined. If the average driving speed along a road segments fell below this threshold, it is assumed that the considered vehicle encountered congestion. Afterwards, the times and segments for which congestion was experienced during the test drivings are compared to the times and segments for which congestion should have been experienced according to the analyzed RTTI. A false alarm rate and a hit rate are derived to assess the quality of the RTTI. In (*95*), a similar procedure is suggested. However, the RTTI is rated according to the amount of additional travel time which a routing recommendation on the basis of the broadcasted RTTI may cause in comparison to the situation of having perfect RTTI available. The term „perfect“ means in this context that RTTI meets exactly the situation described by the recorded GPS-traces.
The other possibility for generating numerical representations of traffic situations is the construction of spatio-temporal descriptions of the development of traffic. Such descriptions show, for example, average driving speeds in dependency of space and time (usually for a certain road corridor during a specific time period). Methods for generating such spatio-temporal traffic state reconstructions are the ASDA/FOTO (automatische Staudynamikanalyse/forecasting of traffic objects) models, which are based on Kerner's three phase traffic theory (chapters 2

[13]Whenever rating commercial RTTI is addressed in studies, then solely traffic state estimations and no traffic predictions are considered. The described ideas, certainly, can in most cases be directly transferred to the latter, too.

and 9 in (*79*)), and the adaptive smoothing method (ASM) proposed in (*146*). More details about macroscopic traffic state reconstructions will be provided later on in section 6.2. Methods for rating the quality of RTTI compare the spatio-temporal traffic state reconstructions with the RTTI. In (*19*), spatio-temporal regions of congestion are identified on the basis of a traffic state reconstruction which is computed according to the ASM. These regions are compared to broadcasted congestion warnings (according to the analyzed RTTI) and, similar to (*20*), a false alarm rate and a hit rate are derived to assess the quality of the RTTI. In (*122*), the ASDA/FOTO-models are used to produce spatio-temporal traffic state reconstructions for a certain road corridor. Then, (instantaneous) travel times resulting from this reconstruction are compared to (instantaneous) travel times resulting from the considered RTTI. The RTTI is rated depending on the differences between both types of travel times.

Data Availability and Real-time Traffic Information Quality Instead of assessing traffic information quality, it is often analyzed in literature which level of quality can be achieved given a certain level of data availability. In (*22*), a pure statistical analysis is carried out to derive a relation between traffic volume, percentage of vehicles that constantly send their driving speeds to a traffic content provider, and the time that is necessary to detect congestion after its occurrence. Another approach for analyzing the relation between data availability and the possible traffic information quality is stated in (*110*). In this study, a freeway corridor is simulated using a microscopic traffic simulation tool. Hence, the movements of all vehicles and along with them the „real“ (real refers to the reality within the simulation) traffic situation are fully available. In a next step, a certain percentage of the vehicles is randomly selected and, based on the data belonging to the selected vehicles, a traffic state reconstruction is executed. This traffic state reconstruction resulting from considering only a reduced data set is compared to the real traffic situation. This allows deriving a relation between penetration rate (number of tracked vehicles divided by the number of total vehicles) and achievable traffic estimation accuracy. In (*105*) the procedure is almost the same. Other works do not rely on traffic simulation to get a close idea of the real traffic situation. In (*65*) and (*100*), the traffic situation on a freeway corridor during a period of a few hours was comprehensively captured by organizing hundreds of test drives. Each of the corresponding vehicles sent its current position and driving speed every few seconds. With having a set of traces that is big enough to describe the real traffic situation adequately, the procedure itself is then the same as in (*110*). In (*5*), so-called next generation simulation (NGSIM) data are analyzed in an urban scenario. For the generation of the NGSIM data, the movement of all vehicles within a small part of a road network was fully recorded via cameras for a short time period. Based on the resulting videos, the exact movement of each vehicle is derived, providing an almost perfect picture of the whole traffic situation. Again, data from different percentages of randomly selected vehicles are used for traffic state estimations and the result is compared to the real traffic states, i.e., to traffic state reconstructions that are based on the whole data set.

2.4 Summary

In chapter 2, literature in areas that are related to the problem of finding optimal charging strategies has been described. It started in section 2.1 with a general introduction to the topic of electric vehicles. Studies were discussed, which describe which factors have influence on the energy consumption of BEVs and how energy consumption can be estimated or predicted, respectively. Next, different topics in the context of navigation applications for BEVs were considered. Besides contributions about energy efficient routing, the vehicle refueling problem, and fleet management approaches for BEVs, also prior works on CSO were described. It turned out that existing problem formulations are too simple as if they were able to fulfill the requirements defined by ROs 1a and 1b. Particularly the uncertainty of future energy consumption has not yet been addressed sufficiently. As a consequence, the focus was shifted in section 2.2 to modeling uncertainty within routing applications. Finally, in section 2.3, traffic information which is available in practice was described. It was sketched how traffic information is generated and why errors occur. Moreover, an overview of existing approaches to measure the quality of such information was provided. Section 2.3 was intended as a preparation for the simulation study in chapter 7, where error-prone traffic information is considered to be the only source of uncertainty.

Chapter 3

Charging Strategy Optimization as a Multistage Decision Problem

From the literature review in chapter 2, it can be observed that prior work on CSO primarily focuses on achieving low computation times. To obtain this, the suggested models are kept rather simple. It is assumed, for example, that all charging stops lead to a fully recharged battery or that time and energy necessary for passing road segments are static values. The most crucial simplification, however, is that the possibility of incorrectly predicted energy consumption is not taken into account at all. Due to this, it is concluded in chapter 2 that existing approaches are inappropriate for achieving ROs 1a and 1b. The goal of chapter 3 is to start closing existing research gaps. For this purpose, the problem of finding optimal charging strategies will be modeled as a multistage decision problem (MDP). This problem formulation will be primarily designed to lead to a realistic modeling and to be able to include all relevant problem aspects. This will ensure that particularly RO 1a can be achieved. Moreover, the formulation as an MDP will form the basis for further models, which will finally be able to fulfill all subobjectives of RO 1.

Chapter 3 is structured as follows: At the beginning, fundamentals in decision theory are explained and the essential components of sequential MDPs are described. In a next step, it is motivated why the problem of finding optimal charging strategies is formulated as an MDP. The meaning of each of the components of MDPs in the context of CSO is discussed and appropriate adjustments of their definitions are provided. It is finally analyzed up to which degree the resulting problem formulation as an MDP is sufficient to achieve RO 1a to RO 1c.

3.1 Fundamentals of Decision Theory

Consider the following situation: With her/his actions a decision maker has the possibility to influence the behavior of a (probabilistic) system as it evolves through time. She/he can only

act at specific points in time (so-called decision stages) and there exists a number of action possibilities from which she/he can choose at each of these points in time. Her/his goal is to influence the system in such a way that it behaves optimally with regard to some criteria. Then, an MDP can be formulated in a non-formal way as follows: Find a sequence of actions (one action at each decision stage) which optimizes the system's development with respect to the given criteria (formulation is taken from p. 17 in (*117*)).

For a mathematical formulation of MDPs, the subsequent notations are used. Similar definitions can be found in section 2.3 in (*34*):

1. A finite set of **decision stages** $t_1, t_2, ..., t_K$ with $K \in \mathbb{N}$, a starting time t_0 and an ending time t_{K+1}.
2. A set of **decision spaces** $\mathcal{U}_k$ with $k \in \{1, 2, ..., K\}$.
3. A sequence of real-valued random variables ξ_k with $k \in \{0, 1, ..., K+1\}$. The corresponding realizations are denoted by $\bar{\xi}_k \in \mathbb{R}^m$ with $m \in \mathbb{N} \setminus \{0\}$.
4. A real-valued **performance measure** f.
5. A **decision policy** π consisting of **decision rules** π_k with $k \in \{1, 2, ..., K\}$.

Decision stages $t_1, t_2, ..., t_K$ represent points in time at which the decision maker is able to act. Decision spaces $\mathcal{U}_k$ describe the set of feasible actions at time t_k, from which the decision maker can choose. The development of the system over time is represented by random variables ξ_k and performance measure f represents the criteria according to which the system behavior shall be optimized. Performance measure f returns a penalty (or revenue, respectively) depending on the chosen decisions $u_k \in \mathcal{U}_k$ and the system's development $\bar{\xi}_k$ (recall that $\bar{\xi}_k \in \mathbb{R}^m$ for all $k \in \{0, 1, ..., K+1\}$):

$$f : \mathbb{R}^{(K+2)*m} \times \mathcal{U}_1 \times \mathcal{U}_2 \times ... \times \mathcal{U}_K \longrightarrow \mathbb{R}. \tag{3.1}$$

Finally, a decision rule π_k describes which decision is recommended at decision stage t_k according to decision policy π.

Figure 3.1 illustrates a sequential multistage decision process. In this context „sequential" means that the decision stages are ordered, i.e., $t_k \leq t_{k+1}\ \forall k \in \{0, 1, ..., K\}$, and that when reaching decision stage t_k, all previous decision stages t_{k^*} with $k^* < k$ have been visited before. The whole process starts at time t_0. $\bar{\xi}_0$ represents the system's initial state[14]. Variable ξ_0 (and all further ξ_k) usually consists not only of one single number, but of a whole vector of

[14]The initial state is usually understood as a given set of values and not as a random variable. Nevertheless, it is distinguished between the vector $\bar{\xi}_0 \in \mathbb{R}^m$ and the deterministic variable ξ_0

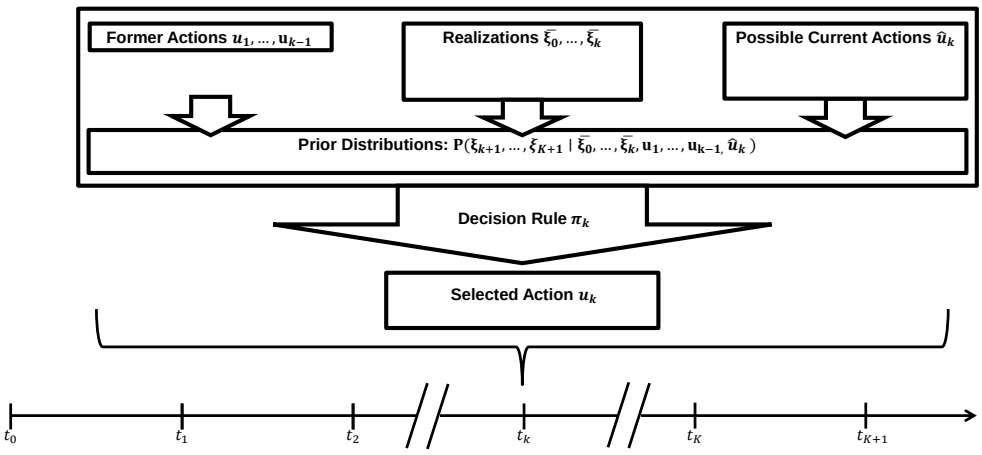

Figure 3.1: Overview of information which is available at the time at which an action needs to be chosen (for the case of a sequential MDP).

quantities which are relevant for the decision maker. Quantities are relevant if they are considered directly by the performance measure f, if they have influence on the available actions or if they allow deriving a more accurate prediction of the future development of relevant quantities. After the start, the system evolves between times t_0 and t_1. The results of this development (and possibly also the development itself) are represented by $\bar{\xi}_1$. Then, the decision maker is allowed to choose her/his first action from decision space $\mathcal{U}_1$, since the first decision stage is reached at time t_1. All information that is available at time t_1 can be taken into account for this first decision. As shown in Figure 3.1, it is assumed that the realized system states $\bar{\xi}_0$ and $\bar{\xi}_1$ are known at that time. For all following decision stages t_k with $k \in \{2, 3, ..., K\}$, all former decisions $u_1, ..., u_{k-1}$ are assumed to be known, too. However, it is also assumed that some kind of knowledge about the system's future behavior is given. This is an essential assumption in decision theory. It means that some information about random variables ξ_k for $k \in \{2, 3, ..., K+1\}$ and about their dependency on the current action has to be available. If this was not the case, then the future impact of current actions could not be estimated. At decision stage t_k, this knowledge of the system's future behavior typically is represented by conditional probability distributions. These distributions depend on former realizations, on former decisions, and on the action that will be executed at the current decision stage:

$$\mathbb{P}(\xi_{k+1}, \xi_{k+2}, ..., \xi_{K+1} \mid \bar{\xi}_0, \bar{\xi}_1, ..., \bar{\xi}_k, u_1, u_2, ..., u_{k-1}, \hat{u}_k). \tag{3.2}$$

These distributions are often referred to as **prior probability distributions** or **priors**. In equation 3.2, variables $u_1, u_2, ..., u_{k-1}$ denote actions which have already been executed at previously reached decisions stages. The $\hat{}$-symbol, on the other hand, is intended to emphasize that the corresponding action $\hat{u}_k$ is now (i.e., at time t_k) available, but it has not been executed yet.

This means that, depending on the current decision, the probabilities of future system developments change. Now, return to the situation where decision stage t_1 has just been reached. The decision maker selects one feasible action from decision space $\mathcal{U}_1$ based on her/his current knowledge. It is assumed that for any feasible actions $\hat{u}_1 \in \mathcal{U}_1$ the corresponding prior distribution is known. The procedure or methodology according to which the action is selected by the decision maker at a specific decision stage t_k is denoted as decision rule π_k. π_k is a function which returns, depending on former actions and realizations of random variables, an action from the current decision space:

$$\begin{aligned} &\pi_k : \mathbb{R}^{m\cdot(k+1)} \times \mathcal{U}_1 \times ... \times \mathcal{U}_{k-1} \to \mathcal{U}_k \\ &\pi_k(\bar{\xi}_0, ..., \bar{\xi}_k, u_1, ..., u_{k-1}) = u_k \end{aligned} \tag{3.3}$$

Here, it is used that each random variable ξ_k obtains values in $\mathbb{R}^m$. Any function of the form described by equation 3.3 can be applied as a decision rule. Certainly, solving a decision problem means to find a decision policy $\pi = (\pi_1, ..., \pi_K)$, which optimizes the value that is returned by f. For formulating a decision problem mathematically, it is important to stress that π_k can solely depend on information that is available at time t_k. A decision policy consisting only of decision rules which fulfill this property is denoted as **non-anticipative** (p. 11 in (*34*)). This notion allows giving a general formulation of (sequential) MDPs:

$$\begin{aligned} \text{minimize} \quad & \mathbb{E}[f(\xi, \pi(\xi))] \\ \text{subject to} \quad & \pi_k \in \mathcal{F}(\mathbb{R}^{m\cdot(k+1)} \times \mathcal{U}_1 \times ... \times \mathcal{U}_{k-1}, \mathcal{U}_k) \\ & \pi \text{ non-anticipative} \end{aligned} \tag{3.4}$$

Here, variable ξ is defined as the vector $(\xi_0, ..., \xi_{K+1})$ and furthermore

$$\mathcal{F}(\mathbb{R}^{m\cdot(k+2)} \times \mathcal{U}_1 \times ... \times \mathcal{U}_{k-1}, \mathcal{U}_k) \tag{3.5}$$

as the space of all functions mapping from $\mathbb{R}^{m*(k+1)} \times \mathcal{U}_1 \times ... \times \mathcal{U}_{k-1}$ to $\mathcal{U}_k$. So far, a general mathematical formulation of decision problems is derived, but it seems necessary to state some additional remarks:

Even though ξ_k is considered to be a random variable, the processes which are described by ξ_k not necessarily need to be understood to be random processes. The randomness may just be a way to represent uncertainty or missing knowledge.

Formulating the optimization problem as a minimization problem does not limit its generality, since (in the case of maximization problems, i.e., if f is a utility function and not a penalty function) there is no difference between maximizing $\mathbb{E}[f(\xi, \pi(\xi))]$ or minimizing $\mathbb{E}[-f(\xi, \pi(\xi))]$.

Optimizing the expected value $\mathbb{E}[f(\xi, \pi(\xi))]$, on the other hand, can be understood as a minor limitation of generality (see p. 11 in (*34*)). Nevertheless, it is the typical way of handling random variables within objective functions of optimization problems. In this context, $\mathbb{E}[f(\xi, \pi(\xi))]$ is from here on denoted as objective function, whereas f is denoted as performance measure. This distinction will keep further statements clearer.

In the formulation of problem 3.4, it could be expected that the decision policy π within the objective function does not only depend on ξ. It should also depend on chosen actions $u_1, ..., u_K$, since the decision rules π_k depend on them (see equation 3.3). However, it is not necessary to explicitly state this within the problem formulation, since all made decisions directly result from the decision policy itself and the realizations of random variables ξ_k.

The suggested formulation of the decision problem can be generalized further, for instance, by making random variables ξ_k, actions spaces $\mathcal{U}_k$ or decision stages t_k dependent on previously made decisions and realizations. For this purpose, it can be written

$$\xi_k(\bar{\xi}_0, ..., \bar{\xi}_{k-1}, u_1, ..., u_{k-1}) \text{ instead of } \xi_k, \tag{3.6}$$

$$\mathcal{U}_k(\bar{\xi}_0, ..., \bar{\xi}_k, u_1, ..., u_{k-1}) \text{ instead of } \mathcal{U}_k, \tag{3.7}$$

$$t_k(\bar{\xi}_0, ..., \bar{\xi}_k, u_1, ..., u_{k-1}) \text{ instead of } t_k. \tag{3.8}$$

Some of these additional dependencies are necessary to adequately formulate the problem of finding optimal charging strategies as an MDP. In order to reduce notational complexity, it is still written ξ_k – even though these realizations may also depend on former actions or the system's former development. For any other component of the decision model, i.e., for decision stages, decision policies and rules, decision spaces and the performance measure, all dependencies are explicitly formulated.

3.2 Decision Problem Components for Charging Strategies

There are three main reasons suggesting to formulate the problem of finding optimal charging strategies as an MDP: First, a person who wants to use a BEV to reach a specific destination needs to make decisions: Should she/he turn left or stay on the current road, should she/he charge at the next charging station up to 40 or 50 percent? Consequently, applying considerations from decision theory to compute charging strategies appears to be reasonable. A further important aspect is that the driver of the BEV can only take actions when certain locations are reached, such as intersections and charging stations. Many other real world problems, for instance problems known from control theory, usually allow taking actions continuously. This suggests to model the problem of finding optimal charging strategies as a „multistage“ decision problem, since this special version of decision problems represents the idea of having solely a limited number of stages at which the considered system can be influenced. To explain the

third reason for favoring a formulation as an MDP, let it be considered that different types of mathematical optimization problems (linear programs, dynamic programs, etc.) typically lead to different types of restrictions during the modeling process. For instance, linear programs, as the name implies, allow only representing relations which can be described by linear models. Integer programs make the discretization of problem components necessary. Such restrictions are in most cases intended to enable an efficient computation of solutions, but they are not necessary to represent the properties of the considered real world problem. The main restriction caused by formulating a problem as an MDP is the aforementioned limitation to be only able to take action when a decision stage is reached. However, it has already been explained that this is actually no restriction in the context of CSO. Later on, other potential formulations of the problem of finding optimal charging strategies will be discussed, which do, in contrast to the formulation as an MDP, lead to unnatural model properties and limitations, respectively.

To formulate the problem of finding optimal charging strategies as an MDP, the meaning of all components of MDPs (decision stages, actions spaces, the system's development, performance measure, and decision policy) needs to be explained for this specific context. Partly, the definitions of these components are also adjusted. Two preparatory steps are necessary for this purpose.
First, basic notions in the context of graph theory have to be introduced: A directed graph $\vec{G}$ is a tuple of nodes V and edges $\vec{E}$, i.e., $\vec{G} = (V, \vec{E})$. Each edge is a directed connection between two nodes, i.e., $\vec{E} \subseteq V \times V$. Here, only finite graphs, i.e., $|V| < \infty$, are considered. A path P on a graph $\vec{G}$ is defined as a finite sequence of nodes $P = [v_1, v_2, ..., v_Q]$, with $Q \in \mathbb{N} \setminus \{0\}$ and $(v_i, v_{i+1}) \in \vec{E}$ for all $1 \leq i < Q$. The subpath of P which consists only of nodes $[v_i, v_{i+1}, ..., v_j]$ with $1 \leq i \leq j \leq Q$ is denoted by $P_{i:j}$. Given two nodes $s, d \in V$, any path starting at s and ending at d is called an s-d-path and the corresponding set of all paths on $\vec{G}$ leading from s to d is denoted by $\mathcal{P}(\vec{G}, s, d)$. A cycle is an s-d-path with $s = d$.

The second preparatory step is the construction of a graph representing the spatial situation, i.e., the graph has to represent the starting location of the driver, her/his destination location, the relevant parts of the road network, and the available charging stations. This can be achieved by using a graph representing the considered part of the road network and adding one additional node for each location at which a charging station is available. Moreover, one further node is added for the starting location. The resulting graph is from here on denoted as **decision graph** $\vec{G}_D = (V_D, \vec{E}_D)$. Figure 3.2 visualizes an example. Here, it is assumed that a person located at node v_0 wants to use a BEV to get to node v_7 when starting at a specific starting time t_S with a specific starting state of charge SOC_S. Charging stations can be found between nodes v_1 and v_3, nodes v_1 and v_5, and nodes v_5 and v_7. Note that nodes v_0, v_2, v_4 and v_6 possibly are not part of the original graph, which just represents the road network. Moreover, it can be

assumed that v_0 and v_1 are located at the same spatial position, i.e., the driver actually starts at node v_1. Node v_0 is just added as a dummy node. In the following, this allows avoiding that

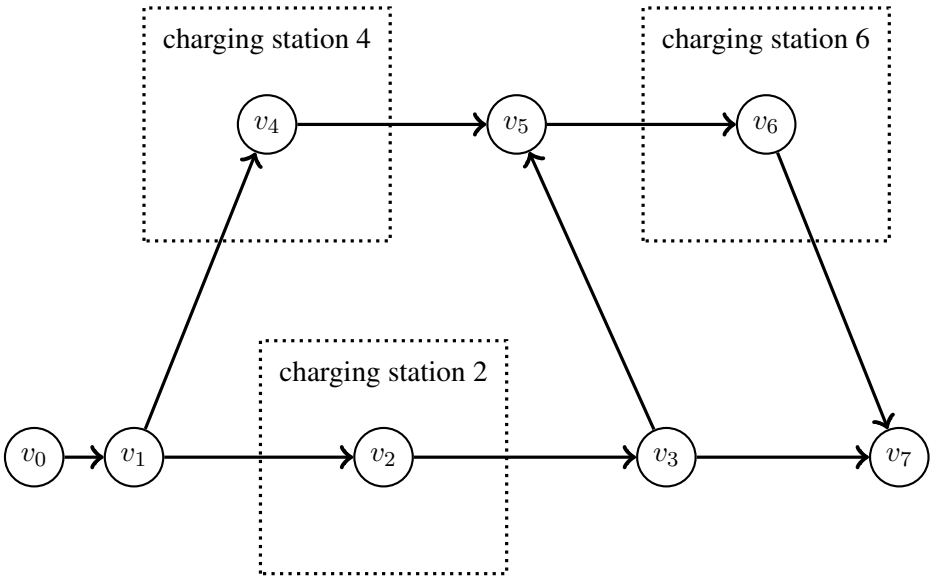

Figure 3.2: Example of a graph used to model the problem of finding optimal charging strategies as a non-sequential MDP.

already at the starting node a decision has to be made. Otherwise, it would not be possible to keep notation consistent with section 3.1. There, no decision can be made at starting time t_0.

Decision Stages According to section 3.1, decision stages are points in time at which a choice has to be made by the decision maker. In the situation described by Figure 3.2, the decision maker has the possibility to choose from two different routes at nodes v_1 and v_3. At nodes v_2, v_4 and v_6, she/he can decide whether to charge at the corresponding charging station or not and, in the case that her/his decision is positive, she/he additionally has to decide how much energy she/he wants to charge. Therefore, decision stage t_k is defined as the the time at which node v_k is reached by the BEV. To keep notation consistent with section 3.1, there is one decision stage for each node of the graph, except for the starting node and for the destination node[15]. Thus, there is also a decision stage t_5 when reaching node v_5 in the graph of Figure 3.2, although there exists neither a routing nor a charging choice at this location.

The central difference between the situation in Figure 3.2 and the decision model described in section 3.1 is the fact that the sequential structure of the decision problem is lost. This means that the sequence of decision stages is not fixed. It depends on the executed actions. Some of the decision stages may not even be reached before the destination node. Consequently,

[15] According to section 3.1, t_0 and t_{K+1} are no decision stages!

they are actually not part of the decision process. The sequential structure is lost as soon as route choices can be made. For the example in Figure 3.2, node v_4 (and along with it decision stage t_4) cannot be reached if the driver decides at stage t_1 to take the road segment leading to node v_2. Note that, for the sake of simplicity, it is assumed that decision graphs do not include cycles. Otherwise, it would be possible to visit nodes multiple times, which again would make notational adjustments necessary. From a practical perspective, this is actually no significant restriction, since visiting a location twice is not meaningful when trying to get from a location A to a location B.

Decision Spaces For each decision stage t_k, a decision space $\mathcal{U}_k$ has to exist. Here, the definition of $\mathcal{U}_k$ depends on the type of node v_k. If v_k represents a charging possibility, then $\mathcal{U}_k$ is defined as the set of all possible states of charge that can be obtained. As the state of charge is measured in percent, it holds:

$$\mathcal{U}_k := [0\%, 100\%] = [0.0, 1.0] \quad \forall v_k \in V_D^{cs}, \tag{3.9}$$

where V_D^{cs} denotes the set of all nodes which represent locations of charging stations. It is important in this context that the decision model is able to handle infeasible charging actions. For example, if a vehicle arrives at a certain node with a state of charge of 80 percent, then it makes no sense that the driver decides to recharge the battery up to a state of charge less than 80 percent. Later on in this section, it will be shown how the model can be adjusted to avoid such decisions.
If v_k does not indicate the position of a charging station (for example, if v_k embodies an intersection), then $\mathcal{U}_k$ is defined as the set of all edges leaving this node:

$$\mathcal{U}_k := \{(v_i, v_j) \in \vec{E}_D \mid v_i = v_k\} \quad \forall v_k \in V_D \setminus \{V_D^{cs} \cup \{v_0, v_{K+1}\}\}. \tag{3.10}$$

The System's Development Random variable ξ_k represents the development of the „system“ until time t_k. Keep in mind that each random variable ξ_k actually is a vector of random variables and thus can theoretically store an arbitrary amount of information. Any aspect which has a direct or indirect influence on the planned trip may be part of ξ_k. In this context, „indirect“ means that some quantities may only be considered as they allow making more precise predictions of other (directly influencing) aspects which are considered by performance measure f, i.e., they contribute solely to prior distributions. Here, the description of ξ_k is kept very general. The intention is to keep also the resulting decision model general, despite the fact that the problem of finding optimal charging strategies is modeled. However, it is assumed that ξ_k contains at least two specific quantities, namely the arrival time $t_k^A \geq 0$ of the considered vehicle at node v_k and the vehicle's state of charge $SOC_k \in [0.0, 1.0]$ when arriving at node v_k, i.e,. $\xi_k = (t_k^A, SOC_k, ...)$. The dots indicate that ξ_k may contain additional random variables.

Correspondingly, t_0^A is equal to the starting time t_S and SOC_0 is equal to the state of charge at the beginning, which is denoted by SOC_S.

Information about the state of charge of the vehicle is crucial for estimating whether or not a sequence of actions leads to an empty battery. Furthermore, SOC_k allows adjusting decision space $\mathcal{U}_k$ to avoid the aforementioned infeasible charging actions. This is done by making the definition of decision spaces which represent charging possibilities (compare definition 3.9) dependent on the realized state of charge:

$$\mathcal{U}_k(\overline{SOC}_k) := [\overline{SOC}_k, 1.0] \quad \forall v_k \in V_D^{cs} \tag{3.11}$$

The realizations of t_k^A, i.e., the actual arrival times, are necessary in order to be able to define decision stages t_k mathematically:

$$t_k(\bar{\xi}_k) = t_k(\bar{t}_k^A, \overline{SOC}_k, ...) := \bar{t}_k^A. \tag{3.12}$$

Here, $\bar{t}_k^A$ denotes the realized[16] arrival time at node v_k and is set equal to ∞ if v_k is not reached during the decision process. If t_k^A was not part of ξ_k, there would be no part of the decision model which provides the possibility to compute arrival times. This would make adjustments of the definition of decision stages necessary, since they could no longer be understood to be points in time. Furthermore, knowing realized and estimating future arrival times is essential to predict the influence of dynamic factors (such as traffic or outdoor temperature) on the BEV's future experiences (such as energy consumption).

Performance Measure There are many reasonable ways for defining the performance measure f in the area of CSO. Measures which are typically applied within routing applications, such as the total travel time or the total energy consumption, could be used. According to the described formulation of general decision problems, f depends on the realizations of ξ and on the executed actions. Since the decision model for the case of CSO is, in general, not sequential and thus not all decision stages may be reached, the performance measure may simply ignore the corresponding ξ_k and u_k. To emphasize that f does not depend on any decision model component belonging to such decision stages, it is written $f(\bar{\xi}_{\leq K+1}, \pi(\bar{\xi}_{\leq K+1}))$ instead of $f(\bar{\xi}, \pi(\bar{\xi}))$ (compare the definition of general MDPs in equation 3.4). The vector $\bar{\xi}_{\leq K+1}$ consists of all $\bar{\xi}_k$ with $\bar{t}_k^A \leq \bar{t}_{K+1}^A$, i.e., of all realizations of random variables which belong to decision stages that are visited until the destination is reached. The corresponding sequence of decisions is represented by $\pi(\bar{\xi}_{\leq K+1})$.

[16] Random variable t_k^A is part of random process ξ_k. Its realizations are denoted by $\bar{t}_k^A$, even though the arrival time typically depends on former decisions. It has already been mentioned that this is done to reduce notational complexity.

Another aspect which can be handled by f is the penalization of executed sequences of actions $\pi(\bar{\xi}_{\leq K+1})$ that lead to an empty battery. If the available energy, which results from the executed decision policy and the realizations of the random variables, at some point is not enough to pass a certain road segment, then none of the following decision stages can be reached anymore. Consequently, destination v_{K+1} is also never reached. The realized arrival time $\bar{t}^A_{K+1}$ is set to infinity according to equation 3.12. To penalize such situations, any performance measure f could be modified as stated below:

$$f(\bar{\xi}, \pi(\bar{\xi})) := \infty \quad \text{if } \bar{t}^A_{K+1} = \infty \tag{3.13}$$

Alternatively, instead of using f to exclude unreliable sequences of actions from consideration, the definition of decision spaces could be adjusted. However, no details are shown here. It is worth mentioning that assigning a value of ∞ to certain sequences of actions is problematic for computing the expected value $E[f(\bar{\xi}, \pi(\bar{\xi}))]$, since it is possibly not well-defined. To avoid this, the infinity sign in equation 3.13 could be replaced with a large positive number $M \in \mathbb{R}_{>0}$.

Decision Policy According to section 3.1, a decision policy π consists of decision rules π_k. These decision rules π_k are functions mapping from the space of all possible system developments and all possible combinations of former actions to the set of available actions $\mathcal{U}_k$. This implies that in the context of CSO, a decision rule π_k for $v_k \notin V_D^{cs}$ suggests which road segment should be taken next. If $v_k \in V_D^{cs}$, then the decision rule states whether the BEV should be charged at the charging station represented by node v_k and, if this statement is positive, up to which state of charge it should be charged.

In section 2.1.5 in (*117*), it is mentioned that in decision theory often the term „strategy“ is used as a synonym for the term „policy“. For the described research, it is distinguished between these two terms to be notationally consistent with the idea of charging strategies which was mentioned in chapter 1:

A **decision strategy** is defined as the sequence of actions $\pi(\bar{\xi})$ (or $\pi(\bar{\xi}_{\leq K+1})$, respectively), which results from the applied decision policy and the realizations of the random variables which describe the system's development.

In contrast to a decision policy, a decision strategy consists of actions or instructions, respectively, and not of decision rules, which themselves return instructions. This means that a decision policy π can be interpreted as a function which returns, depending on the considered system's development $\bar{\xi}$, a specific decision strategy $\pi(\bar{\xi})$. Table 3.1 lists the differences between a decision strategy and a decision policy. An interesting aspect is that, even though π itself is a deterministic function, $\pi(\xi)$ (or $\pi(\xi_{\leq K+1})$, respectively) can be interpreted as a

Table 3.1: Difference between decision policy and charging strategy.

Mathematical Formula	**Verbal Explanation**	**Verbal Term**	**Mathematical Interpretation**
$\pi(\bar{\xi})$	sequence of actions/instructions	decision strategy	realizations of random variable $\pi(\xi)$
π	(deterministic) scheme defining how to react to realizations of ξ	decision policy	deterministic function

random variable. The reason for this is that deterministic functions applied to random variables again can be interpreted as random variables. Note that in the context of CSO, the terms „charging policies“ and „charging strategies“ are used as alternatives for „decision policies“ and „decision strategies“.

To clarify the difference between charging strategies and charging policies and to illustrate the meaning of some of the components of the suggested multistage decision model in the context of CSO, an example based on the graph displayed in Figure 3.3 is discussed in the following. This graph is basically the same as shown in Figure 3.2. For the moment, let it be assumed that a driver located at node v_0 wants to drive (now, at time $t_S = t_0$) to node v_7 with a BEV. Furthermore, the performance measure f is defined as the total travel time, i.e., the goal is to minimize the expected travel time $\mathbb{E}[t_7^A - t_S]$ for the given starting time t_S. Moreover, it is

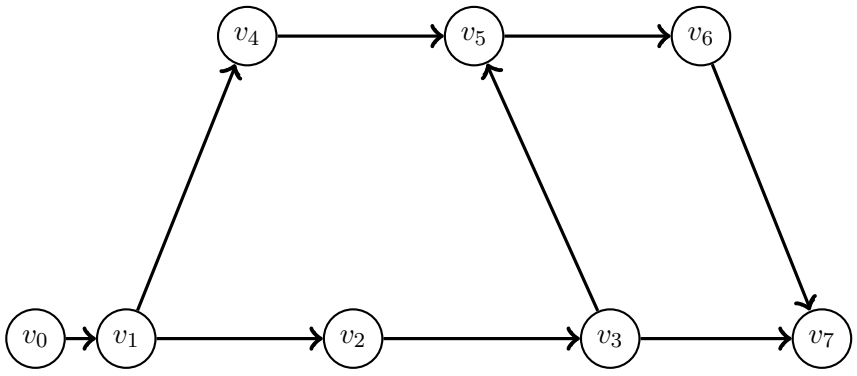

Edge Costs [min]	Probability	(v_2, v_3)	(v_3, v_7)	other edges
Scenario 1	90%	1	1	1
Scenario 2	10%	2	11	1

Figure 3.3: Example Graph: Difference between charging policies and charging strategies.

assumed that the initial state of charge SOC_S, for any realization of ξ and independently of the

chosen route, is sufficient to reliably reach v_7. Correspondingly, it is not necessary to consider any charging stops in this example. The travel time for any of the edges of the graph is equal to one minute, except for the edges (v_2, v_3) and (v_3, v_7). For them, random travel times are assumed: With a probability of ten percent, the travel time for passing edge (v_2, v_3) is equal to two minutes, with a probability of ninety percent, it is also equal to one minute:

$$\begin{aligned} c_T(v_2, v_3) &:= t_3^A - t_2^A \\ \mathbb{P}(c_T(v_2, v_3) = 1 \text{ minute}) &= 0.9 \\ \mathbb{P}(c_T(v_2, v_3) = 2 \text{ minutes}) &= 0.1 \end{aligned} \tag{3.14}$$

In equation 3.14, $c_T(v_2, v_3)$ denotes the travel time necessary for passing edge (v_2, v_3). The travel times for edge (v_3, v_7) are distributed as follows:

$$\begin{aligned} c_T(v_3, v_7) &:= t_7^A - t_3^A \\ \mathbb{P}(c_T(v_3, v_7) = 1 \text{ minute}) &= 0.9 \\ \mathbb{P}(c_T(v_3, v_7) = 11 \text{ minutes}) &= 0.1 \end{aligned} \tag{3.15}$$

Finally, it is assumed that if $c_T(v_2, v_3)$ is equal to two minutes, then $c_T(v_3, v_7)$ is always equal to eleven minutes. Consequently, if $c_T(v_2, v_3)$ is equal to one minute, then the probability that $c_T(v_3, v_7)$ is equal to eleven minutes is zero. All resulting conditional prior distributions can be found below:

$$\begin{aligned} \mathbb{P}\left(c_T(v_3, v_7) = 1 \text{ minute} \mid \bar{c}_T(v_2, v_3) = 1 \text{ minute}\right) &= 1.0 \\ \mathbb{P}\left(c_T(v_3, v_7) = 11 \text{ minutes} \mid \bar{c}_T(v_2, v_3) = 1 \text{ minute}\right) &= 0 \\ \mathbb{P}\left(c_T(v_3, v_7) = 1 \text{ minute} \mid \bar{c}_T(v_2, v_3) = 2 \text{ minutes}\right) &= 0 \\ \mathbb{P}\left(c_T(v_3, v_7) = 11 \text{ minutes} \mid \bar{c}_T(v_2, v_3) = 2 \text{ minutes}\right) &= 1.0 \end{aligned} \tag{3.16}$$

Random variable $c_T(v_2, v_3)$ is here interpreted as a part of ξ_3 and $\bar{c}_T(v_2, v_3)$ denotes the corresponding realization. To simplify the following explanations concerning charging policies and charging strategies, the subsequently described notations are introduced:

$$\begin{aligned} &\text{Route A} := [v_0, v_1, v_2, v_3, v_7] \\ &\text{Route B} := [v_0, v_1, v_4, v_5, v_6, v_7] \\ &\text{Route C} := [v_0, v_1, v_2, v_3, v_5, v_6, v_7] \end{aligned} \tag{3.17}$$

The distributions of travel times resulting from following these routes are stated below:

$$\begin{aligned} \mathbb{P}(c_T(A) = 4) &= 0.9 \\ \mathbb{P}(c_T(A) = 15) &= 0.1 \\ c_T(B) &= 5 \\ \mathbb{P}(c_T(C) = 6) &= 0.9 \\ \mathbb{P}(c_T(C) = 7) &= 0.1 \end{aligned} \tag{3.18}$$

Expected travel times result as follows:

$$\begin{aligned} \mathbb{E}[c_T(A)] &= 5.1 \\ \mathbb{E}[c_T(B)] &= 5 \\ \mathbb{E}[c_T(C)] &= 6.1 \end{aligned} \tag{3.19}$$

Based on the stated travel time expectations, it seems reasonable to assume that an optimal charging policy recommends taking route B. However, this is not the case. It can be verified easily that the best policy is to follow paths A and C at decision stage t_1 and to make the decision at stage t_3 dependent on the realization of $c_T(v_2, v_3)$. Formally, this can be expressed by defining the sequence of decision rules as subsequently described:

$$\pi_1 := (v_1, v_2) \tag{3.20}$$

$$\pi_2(\overline{SOC}_2) := \overline{SOC}_2 \tag{3.21}$$

$$\pi_3(\bar{c}_T(v_2, v_3)) := \begin{cases} (v_3, v_5) & \text{if } \bar{c}_T(v_2, v_3) = 2 \text{ minutes} \\ (v_3, v_7) & \text{else} \end{cases} \tag{3.22}$$

$$\pi_4(\overline{SOC}_4) := \overline{SOC}_4 \tag{3.23}$$

$$\pi_5 := (v_5, v_6) \tag{3.24}$$

$$\pi_6(\overline{SOC}_6) := \overline{SOC}_6 \tag{3.25}$$

Decision rule π_4 is never applied, since node v_4 cannot be reached when following the recommendations of charging policy π. Decision rules π_2, π_4 and π_6 are a consequence of the fact that the BEV does not need to be recharged. The expected travel time resulting from this charging policy is equal to 4.3 minutes, since for the case of increased travel time at edge (e_2, e_3) route C is chosen, otherwise route A (90 percent probability to choose path A with costs of 4 minutes, 10 percent probability to choose path C with costs of 7 minutes). This means that the suggested charging policy leads to one of two possible charging strategies. The first charging strategy consists of instructions that can be represented by route A, the second one of instructions leading to route C. Note that, independently of the system's development, the charging policy π itself does not change during the trip. Only the resulting charging strategies change.

Model Extension: Decisions during Charging Processes The suggested definitions of the components of an MDP in the context of CSO hide one minor restriction: In the current version of the model, the state of charge that needs to be reached at the end of a charging process is determined when the BEV arrives at the corresponding decision stage, i.e., it is determined at the beginning of the charging process. Instead, it could be suggested to simply start charging and then it could continuously be asked whether or not the charging process has to be continued. The advantage of this idea is that the charging policy could react to changes of the system that occur during the charging process. Let it be assumed, for example, that a BEV is currently charged at a charging station. Furthermore, it is assumed that a traffic accident causes the blockage of one lane of a two-lane freeway a few kilometers downstream of the BEV's current position. In this case, it may be beneficial to stop charging and continue the trip in order to pass the accident before a long queue is formed. In order to allow charging policies considering such options, adjustments concerning the definition of decision stages and decision spaces are necessary. Decision stages t_k for nodes $v_k \in V_D^{cs}$ need to be understood as time periods and not as points in time, i.e.:

$$t_k := [t_k^{start}, t_k^{end}] \subset \mathbb{R}_{\geq 0} \tag{3.26}$$

Here, t_k^{start} simply represents the arrival time at the charging station and t_k^{end} the end of the charging process. Decision spaces belonging to charging stations, on the other hand, are no longer defined as continuous intervals, but as a discrete set of options:

$$\mathcal{U}_t(\overline{SOC}_t) := \begin{cases} \{0,1\} & \text{if } \overline{SOC}_t < 100\% \\ \{0\} & \text{else} \end{cases} \qquad \forall v_k \in V_D^{cs},\ \forall t \geq t_k^{start} \tag{3.27}$$

Variable $\overline{SOC}_t$ describes the state of charge at time t. Moreover, let u_t denote the action that is executed at time t. If decision $u_t \in \mathcal{U}_t(\overline{SOC}_t)$ is set equal to zero, then it means that the charging process is stopped at time t. Setting $u_t = 1$ means that the process is continued at time t. If $u_{t_k^{start}} = 0$, then it is decided that the BEV is not charged when it arrives at the charging station. Based on these considerations, the end of the charging process t_k^{end} is a result of a continuous sequence of decisions u_t:

$$t_k^{end} := min\{t \geq t_k^{start} \mid u_t = 0\} \tag{3.28}$$

Besides the definition of decision stages and decision spaces, some further modifications of the formulation as an MDP are necessary when it is allowed to make decisions during charging processes. For instance, due to a possibly infinite number of decision stages, the set of random variables ξ_k may no longer be finite. However, these modifications primarily a question of notation and do not affect the underlying ideas. Thus, no further details are mentioned – except for one aspect: The new problem formulation should no longer be denoted as a „multistage" decision problem, since the concept of discrete stages represents the essential feature of MDPs.

For the remainder of this work, the basic MDP is considered and not its extended version. The main reason for this is that, when returning to a practical perspective, it seems unrealistic that a driver constantly waits during charging processes for new instructions of her/his navigation device. Furthermore, it will turn out that the original formulation can be used as the fundament for an adjusted model formulation for the problem of finding optimal charging strategies. This will be relevant in chapter 4.

3.3 Model Assessment with Regard to Research Objectives

In the following, based on the considerations made in chapter 3, the suggested formulation of the problem of finding optimal charging strategies as an MDP is analyzed with regard to ROs 1a to 1c.

RO 1a: This RO consists of two main parts: The developed problem formulation has to be able to include all relevant aspects (whatever aspects are considered to be relevant) and the problem formulation needs to achieve a high level of realism.

The generic form of the introduced MDP (recall the problem formulation in equation 3.4) provides lots of flexibility. This is especially a consequence of the fact that random variables ξ_k and performance measure f have not been concretized. Thus, it can be expected that almost any factor which is considered to be relevant can be represented.

Regarding the topic of realism, it needs to be considered if the applied type of optimization problem shows unnatural model properties. In this context, it has already been argued that MDPs are particularly suitable to model the problem of finding optimal charging strategies. The main limitation, to which MDPs are bound, is the idea of discrete decision stages. It was argued at the beginning of section 3.2 that this represents no significant restriction in the context of CSO, since decisions primarily can be made when the BEV reaches certain locations (intersections or charging stations). The only restriction is that the option to adjust recommended instructions during charging processes is not given. As a consequence, some optimization potential is lost. From a practical perspective, however, being unable to adjust recommended instructions while charging seems irrelevant.
When considering prior models for CSO, it has already been mentioned that several unrealistic assumptions are made in order to simplify the resulting optimization problem. Particularly the missing possibility to represent uncertainty and the interpretation of travel times and energy consumption as static factors appear to be critical. The suggested MDP does not suffer from these limitations. The possible dependency of random variables ξ_k on former system developments (compare equation 3.6) provides the possibility to model the energy consumption and

the travel times which are necessary for passing road segments dynamically. Moreover, random variables ξ_k are, due to their random nature, able to represent randomness or uncertainty, respectively. However, as long as no concrete definitions for performance measure f and random variables ξ_k are made, it is not possible to decide whether or not the suggested problem formulation obtains a high level of realism. On the other hand, it can at least be stated that it provides the possibilities to ensure this.

RO 1b: For RO 1b, the same holds as for RO 1a: Up to which degree RO 1b can be achieved on the basis of the suggested MDP depends on how the problem components are specified. The model basically provides enough flexibility to ensure that resulting charging strategies (or charging policies, respectively) are efficient and reliable. In the end, performance measure f needs to be defined appropriately. Note in this context that f already penalizes charging policies that are likely to lead to an empty battery (compare equation 3.13).

RO 1c: Considering RO 1c, one pays for setting the focus on constructing a formulation that shows almost no unnatural properties and does not suffer from model inherent restrictions. Numerical optimization methods cannot directly handle the suggested MDP, since its formulation in equation 3.4 can hardly be specified with a finite number of optimization variables and constraints (p. 12 in (*34*)). The critical aspect is the space of functions $\mathcal{F}$, which is in general an infinite-dimensional space. As a consequence, the suggested problem formulation does not allow achieving RO 1c.

Conclusions: Summarizing the findings of section 3.3, it can be stated that the introduced MDP offers enough freedom to fulfill the requirements described by ROs 1a and 1b. On the other hand, RO 1c cannot be achieved. An adjustment of the model is necessary, primarily to make a numerically treatable representation of the function space $\mathcal{F}$ possible[17]. Such adjustments are typically based on some kind of discretization. For instance, discretizing the space of possible realizations of any random aspect of the MDP allows interpreting MDPs as stochastic programs (p. 12 in (*34*)). Hence, algorithms which are able to solve stochastic programs become applicable. If all decision spaces are discretized, then MDPs can be transformed into dynamic programs, for which again various numerical solution approaches exist. Developing an appropriate adjustment of the suggested MDP represents the main purpose of the following chapters. The MDP will in this context not only be used as a theoretical fundament, on which further problem formulations can be based. It will also be considered as a reference model. Other problem formulations, which are intended to fulfill the requirements of all subobjectives of RO 1, will be compared to it in order to identify model immanent restrictions.

[17] MDPs offer lots of flexibility, but it is often necessary to adjust them in such a way that they fit into a numerically treatable framework. (*34*)

3.4 Summary

This chapter provided a framework for modeling the problem of finding optimal charging strategies as an MDP. For this purpose, in section 3.1, a short description of the five components (decision stages, decision spaces, system development, performance measure, charging policy) of a sequential MDP was given. In section 3.2, these components and their meaning were interpreted in the context of CSO. The descriptions of the adjusted components were kept on a rather abstract level to achieve a very general and flexible problem formulation. The resulting problem formulation differed structurally from the original MDP from section 3.1, as the sequential nature of traditional MDPs is lost. This is a consequence of representing the possibility to make route choices, which causes the order according to which decision stages are reached to be dependent on previously chosen actions. Finally, in section 3.3, the developed MDP is analyzed with regard to ROs 1a to 1c. It turns out, as already expected, that the generic formulation allows achieving RO 1a and RO 1b. On the other hand, the problem cannot be addressed numerically. Thus, an alternative formulation needs to be found.

Chapter 4

Charging Strategy Optimization as a Shortest Path Problem under Deterministic Conditions

In chapter 3, the problem of finding optimal charging strategies was modeled as a multistage decision problem. This allowed representing the problem's characteristics in a very natural and generic way, but leads to issues concerning numerical solvability. Now, in chapter 4, the goal is to derive, based on these former considerations, an alternative problem formulation, which allows applying efficient (numerical) optimization algorithms and, along with that, to achieve RO 1c. For this purpose, the introduced formulation as an MDP is reduced to a deterministic SPP. Several simplifications come along with this reduction. Moreover, some of the components of the described deterministic SPP are concretized causing a less generic problem formulation. The concretization is necessary, since for the design of efficient shortest path algorithms, specific information about certain components of the considered SPP is required. The resulting problem formulation, however, again forms just an intermediate step towards the final problem formulation provided in chapter 5.

Chapter 4 is structured as follows: In section 4.1, reasons for reducing the MDP to an SPP are stated. Next, an intuitive scheme for constructing graphs representing road networks and charging stations is presented, which allows associating paths with charging strategies. Afterwards, two deterministic edge cost functions are derived, which are assumed to be relevant in the context of CSO. These cost functions are used as ingredients for the definition of the performance measure f and eventually for providing the final problem formulation as a deterministic SPP. In section 4.2, properties of the two considered edge cost functions and their influence on the solvability of the SPP are analyzed. Based on these considerations, in section 4.3, two different shortest path algorithms are described. One guarantees optimal solutions, the

other one promises improved computation times. The chapter finishes with a comparison of the deterministic SPP and the MDP, and a discussion concerning the SPP's abilities to satisfy the requirements postulated by ROs 1a to 1c.

4.1 Representation as a Deterministic Shortest Path Problem

The formulation of the problem of finding optimal charging strategies as an MDP, which was introduced in chapter 3, can hardly be solved numerically. This is, in fact, not uncommon for MDPs. Usually, they are modified in such a way that they fit into an optimization framework which allows applying efficient optimization algorithms. Among others, the most popular ideas are the reformulation as a linear program (*64*) or their interpretation as a dynamic program (section 4.2 in (*117*)). Which approaches work well and which do not depend on the problem's structure and often it is hardly possible to find out which approaches work best without testing them. However, all of them lead in some sense to inaccuracies during the solution process. For example, to transform a problem like problem 3.4 into a linear program, it is necessary to postulate that the number of possible realizations of ξ is finite. Otherwise, the linear programming reformulation of problem 3.4 can not be specified by a finite number of optimization variables and constraints (section 2.5 in (*34*)). From a practical perspective, the impact of this postulation on the resulting solutions might not be critical. Nevertheless, such adjustments lead to problem and solution properties which are, in fact, unnatural.

For the remainder of this work, the problem of finding optimal charging strategies is tackled via dynamic programming approaches. This also leads to some drawbacks, which will be discussed later on in this chapter. On the other hand, there are also some reasons for favoring using ideas from dynamic programming. For example, within navigation applications, in most cases optimal routes are computed via algorithms known from dynamic programming – often variations of Dijkstra's algorithm. Hence, to reduce potential barriers for a future implementation into market-ready navigation tools, it seems reasonable to rely on optimization approaches which are widely applied in this area. This may even allow making use of existing software infrastructure. Moreover, considering the literature review in chapter 2, there exists lots of work about dynamic programming approaches in the context of navigation applications for BEVs. Especially dynamic programming approaches for solving SPPs are well studied. This makes it possible to build on a broad fundament of existing knowledge. Note that in a preparatory step, the problem of finding optimal charging strategies will also here be reformulated to an SPP in order to make dynamic programming approaches applicable.

4.1.1 Graph Construction

One central component of an SPP is the graph on which shortest paths are computed. Here, the decision graph $\vec{G}_D$ is used as template. Road segments are again represented by edges, intersections by nodes. The only thing missing in $\vec{G}_D$ is the explicit representation of charging

stations via nodes and edges. In general, it holds that graphs are discrete objects. Hence, it is hardly possible to represent continuous decision spaces like those which have been introduced in section 3.2. This makes it necessary to discretize the decision spaces $\mathcal{U}_k$ with $v_k \in V_D^{cs}$ (V_D^{cs} is the set of nodes which represent locations of charging stations). This can be achieved by letting the charging strategies solely suggest states of charges which are a multiple of, for instance, five or ten percent. This has already been proposed in (*141*) and (*152*). From a practical perspective, this reduction appears to be insignificant. A driver at a charging station probably won't concentrate on charging exactly up to a state of charge of "86.45" percent. Supposedly, an instruction "Please charge up to 90 percent." is sufficient for him. Correspondingly, the decision space $\mathcal{U}_k^{\Delta}$ for some node $v_k \in V_D^{cs}$ and a step length $\Delta \in \mathbb{R}_{>0}$ can be defined for a given realized state of charge $\overline{SOC}_k$ as shown below:

$$\mathcal{U}_k^{\Delta}(\overline{SOC}_k) := \{x \ \in [\overline{SOC}_k, 1.0] \mid \exists l \ \in \mathbb{N} \text{ with } x = l \cdot \Delta\} \tag{4.1}$$

To give an example, let it be considered that Δ is equal to 0.05 (i.e., five percent) and that $\overline{SOC}_k$ is equal to 68 percent, i.e., the BEV arrives at the considered charging station with a state of charge of 68 percent. This results in the subsequently described decision space:

$$\mathcal{U}_k^{0.05}(0.68) := \{0.7, 0.75, 0.8, 0.85, 0.9, 0.95, 1.0\} \tag{4.2}$$

The described discretization of the decision spaces can be represented by an appropriate adjustment of the decision graph. For the decision graph $\vec{G}_D$ which is illustrated in Figure 3.2, the resulting adjusted decision graph $\vec{G}_D^{\Delta} = (V_D^{\Delta}, \vec{E}_D^{\Delta})$, which represents discretized decision stages, can be found in Figure 4.1. Basically, the new graph consists of the same parts as the original one. The only difference is that each node representing the location of a charging station is now replaced by a whole set of nodes and edges (compare those graph components in Figure 3.2 and 4.1 which are bordered by dashed rectangles). This replacement is achieved as follows: First of all, it is considered that charging stations may not be located directly at the considered part of the road network. This assumption makes it possible that not each tiny back road that may be used to get to one of the charging stations has to be represented explicitly. Instead, is can be assumed that the original graph $\vec{G}_D$ represents only major roads, i.e., roads which are typically used for covering longer distances. The set of these major roads is from now on denoted as „main road network". The idea is to introduce for each node $v_k \in V_D^{cs}$, which is part of the original graph $\vec{G}_D$, a new node v_k^a marking the position at which the major road network can be left in order to get to the corresponding charging station. Analogously, a node v_k^b is introduced at which one can return to the main road network. Hence, v_k^a and v_k^b can be understood as the positions of exit and entrance ramps. The charging station itself and all possible charging actions are represented by nodes v_k^i, v_k^o, $v_k^{l \cdot \Delta}$ and edges $(v_k^i, v_k^{l \cdot \Delta})$, $(v_k^{l \cdot \Delta}, v_k^o)$ with $\Delta \leq l \cdot \Delta \leq 100\%$ and $l \in \mathbb{N}$. Furthermore, an edge (v_k^a, v_k^i) is used to embody the way

from the main road network to the charging station and an edge (v_k^o, v_k^b) for the way back.

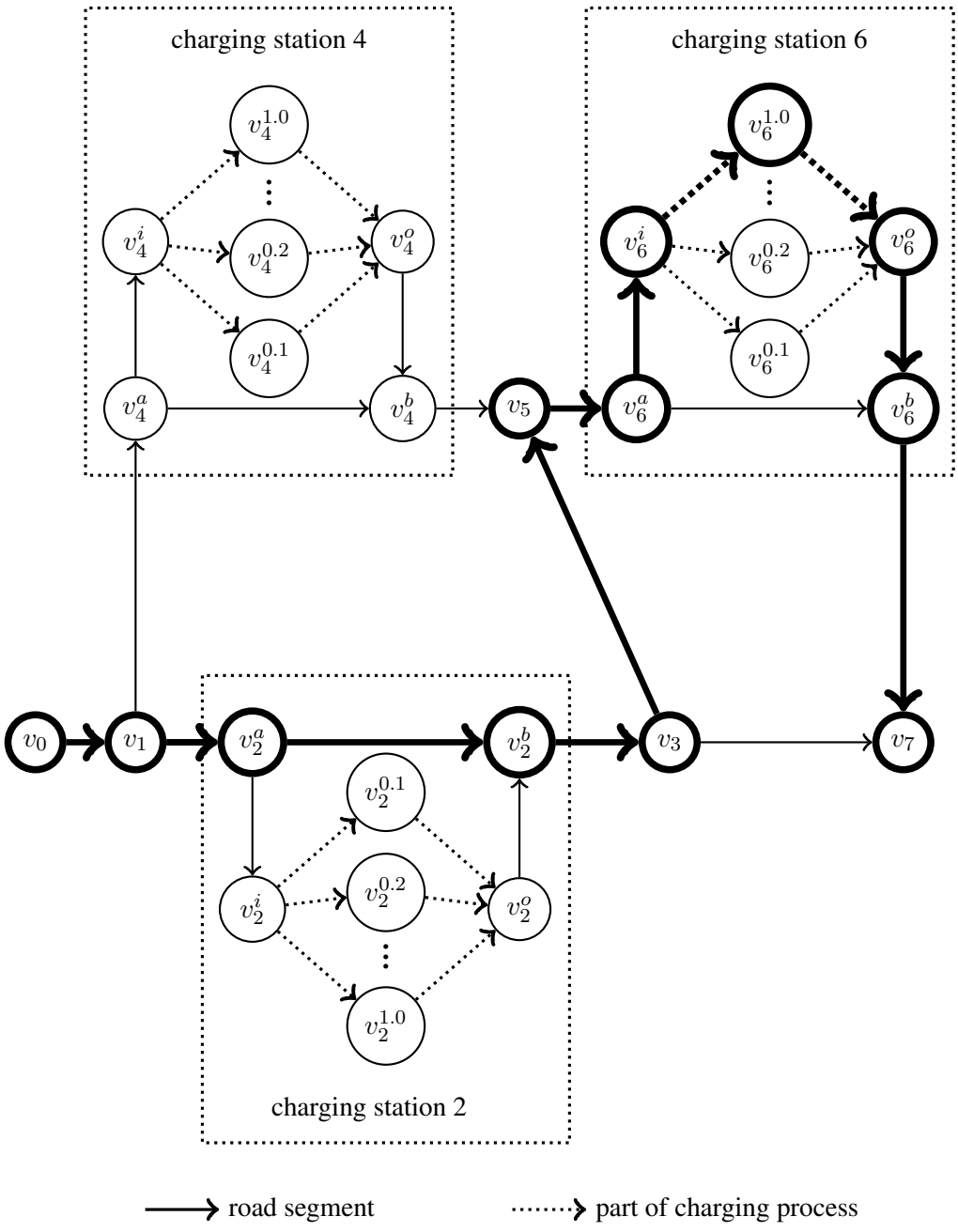

Figure 4.1: Graph-based model of charging possibilities

The goal is to associate charging policies with v_0-v_{K+1}-paths on $\vec{G}_D^{\Delta}$, i.e., with paths leading from the starting position to the destination. In this context, a node $v_k^{l \cdot \Delta}$ represents a charging process leading to a state of charge of $l \cdot \Delta$, i.e., any v_0-v_{K+1}-path on $\vec{G}_D^{\Delta}$ which covers the

node $v_k^{l\cdot\Delta}$ can be associated with a charging policy that suggests charging at charging station k up to a state of charge of $l \cdot \Delta$. By allowing a whole set of different target states at each charging station, various charging policies can be represented by paths on $\vec{G}_D^{\Delta}$. In Figure 4.1, steps of ten percent between the different charging states are used, i.e., $\Delta := 10\% = 0.1$. Clearly, a smaller step length allows considering a wider range of charging policies. Edges $(v_k^i, v_k^{l\cdot\Delta})$ and $(v_k^{l\cdot\Delta}, v_k^o)$ are parts of the charging process itself and are not used to model road segments. More details on these edges will be given later on. To support understanding, with path $[v_0, v_1, v_2^a, v_2^b, v_3, v_5, v_6^a, v_6^i, v_6^{1.0}, v_6^o, v_6^b, v_7]$, an example path is visualized in Figure 4.1 (bold nodes and edges). The corresponding charging policy suggests at decision stage t_1, i.e., at node v_1, to follow edge (v_1, v_2^a). Then, charging station 2 is ignored and at node v_3, it is recommended to drive to node v_5. From there on, no more „real“ route choices are possible. It is worth mentioning that in this context decisions, including charging decisions, are reduced to a route choice on $\vec{G}_D^{\Delta}$. For example, at charging station 6, charging is recommended as at node v_6^a the edge (v_6^a, v_6^i) is selected and not edge (v_6^a, v_6^b). The suggested target state of charge is defined by node $v_6^{1.0}$, i.e., charging up to a state of charge of 100 percent is recommended before proceeding with the travel to destination node v_7.

According to the construction of graph $\vec{G}_D^{\Delta}$, all decision spaces can be understood as sets of edges, since charging decisions are also modeled via route choices:

$$\mathcal{U}_k := \{(v_i, v_j) \in \vec{E}_D^{\Delta} \mid v_i = v_k\} \quad \forall v_k \in V_D^{\Delta} \setminus \{v_0, v_{K+1}\}. \tag{4.3}$$

Nodes v_0 and v_{K+1} are again excluded here to maintain consistency with section 3.1, i.e., t_0 and t_{K+1} are not considered to be decision stages. Note that graph $\vec{G}_D^{\Delta}$ is static, i.e., it is defined independently from the realizations of ξ. Hence, this graph still represents non-reasonable charging possibilities, i.e., target states of charge which are lower than the current state of charge. In contrast to section 3.2, where an adaption of the definition of decision spaces has been introduced in equation 3.11 to exclude such non-reasonable charging possibilities, here performance measure f is modified to handle such issues. For this purpose, performance measure f, independently of its concrete definition, assigns a value of infinity to any charging policy which is represented by a v_0-v_{K+1}-path P on $\vec{G}_D^{\Delta}$ that contains such edges, i.e. $f(P, \bar{\xi}) := \infty$ if path P contains at least one edge $(v_k^i, v_k^{l\cdot\Delta})$ which violates the following condition:

$$l \cdot \Delta > \overline{SOC}(v_k^i) \tag{4.4}$$

Here, variable $\overline{SOC}(v_k^i)$ denotes the state of charge which is realized when reaching node v_k^i. Algorithmically, this adjustment of f can be handled very efficiently. Edges with a value of infinity can be ignored, i.e., as soon as such an edge is reached during the route search, it is simply not considered.

To define point-to-point[18] SPPs uniquely, a graph, a starting node, a destination node, and an objective function have to be specified. Depending on the properties of the objective function, further information may be necessary. If, for instance, the objective function is time-dependent, then a starting time needs to be known in addition. All paths leading from the start to the destination node are potential solutions for this type of problem. For the case of CSO, the considered graph is already given by $\vec{G}_D^{\Delta}$. Also v_0 as starting node and v_{K+1} as destination node are defined. The objective function $\mathbb{E}[\xi, f(\xi)]$ is not yet specified. Nevertheless, a generic version of an SPP for the case of CSO can already be formulated:

$$\begin{aligned} \min \quad & \mathbb{E}[f(\xi, P(\bar{\xi_0}))] \\ \text{subject to} \quad & P \text{ is a } v_0\text{-}v_{K+1}\text{-path on } \vec{G}_D^{\Delta} \end{aligned} \tag{4.5}$$

When comparing the original multistage decision problem 3.4 and the SPP 4.5, two main differences can be observed: First, the set of possible charging policies is now represented by the set of v_0-v_{K+1}-paths on $\vec{G}_D^{\Delta}$. The idea is to associate a path, which solves the SPP, with a charging policy. It has already been shown how this can be done. Unfortunately, a path P^* which solves the stated SPP remains the same independently of the system's development $\bar{\xi_1}, ..., \bar{\xi}_{K+1}$. This means that the route and charging instructions which are associated with path P^* stay the same, too. Therefore, it can be concluded that paths on $\vec{G}_D^{\Delta}$ can be associated with charging strategies, i.e., with sequences of charging and route instructions. They cannot be associated with arbitrary charging policies. Charging policies which recommend different actions depending on the realizations of random variables $\xi_1, ..., \xi_{K+1}$, like the one that was described in chapter 3 for the problem illustrated in Figure 3.3, cannot be represented by a path on graph $\vec{G}_D^{\Delta}$. To emphasize this restriction, the objective function $\mathbb{E}[f(\xi, \pi(\xi))]$ is now replaced by $\mathbb{E}[f(\xi, P(\bar{\xi_0}))]$. This is the second difference between the suggested MDP and the SPP in its current form. Information that is available at the time when the SPP is solved[19], i.e., prior distributions or the system's initial state $\bar{\xi_0}$, can be taken into account for the computation of P^*. This does not hold for realizations of random variables $\xi_1, ..., \xi_{K+1}$.

In the following, these considerations are illustrated on the basis of the aforementioned example from chapter 3. Figure 4.2 shows the same graph as Figure 3.3. It is again assumed that all edges, except for (v_2, v_3) and (v_3, v_7), lead to time costs of one minute. Furthermore, it is again assumed that the state of charge at the start (at node v_0) is high enough to reach destination node v_7 without any charging stop and the goal is to minimize the total travel time. Since no charging

[18] A point-to-point SPP is a problem where the shortest path between a single starting point and a single destination needs to be found. Its counterparts are one-to-many, many-to-one or many-to-many SPPs.

[19] In chapter 3, the time at which the decision process starts is denoted with t_0. The start of the decision process typically also marks the time at which computations are started. Now, in chapter 4, the time at which the BEV starts to get from v_0 to v_{K+1} is typically denoted with t_S. In general, it does not hold that $t_0 = t_S$. For instance, if the introduced SPP is solved at time t_0 to prepare a trip with a planned start at $t_S > t_0$.

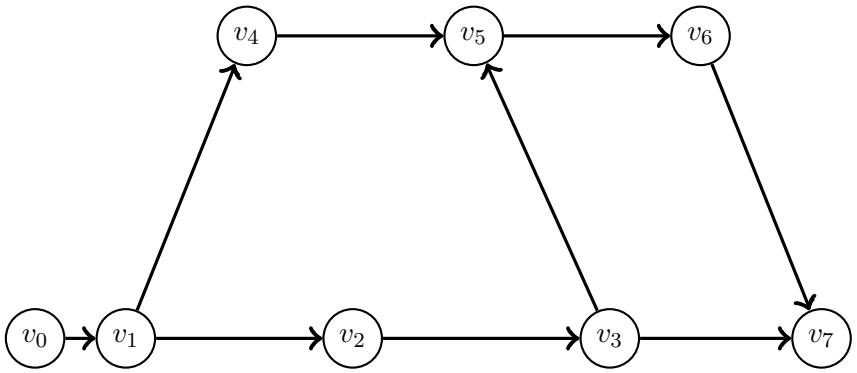

Edge Costs [min]	Probability	(v_2, v_3)	(v_3, v_7)	other edges
Scenario 1	90%	1	1	1
Scenario 2	10%	2	11	1

Figure 4.2: Example Graph: Difference between charging policies and charging strategies.

stations have to be considered, graph $\vec{G}_D^{\Delta}$ is equal to graph $\vec{G}_D$. Thus, the best charging policy is the same as in chapter 3: Drive to node v_2 and make the route decision at node v_3 dependent on the experienced travel time for passing edge (v_2, v_3). The issue is that there exist exactly three different v_0-v_{K+1}-paths on $\vec{G}_D^{\Delta}$:

$$\begin{aligned} &\text{Path A} := [v_0, v_1, v_2, v_3, v_7] \\ &\text{Path B} := [v_0, v_1, v_4, v_5, v_6, v_7] \\ &\text{Path C} := [v_0, v_1, v_2, v_3, v_5, v_6, v_7] \end{aligned} \tag{4.6}$$

The optimal solution of the SPP that results from the situation in Figure 4.2 is equal to one of these three paths. As a consequence, the charging policy that is received by solving the SPP is associated with one of these paths. However, none of these paths is able to represent the optimal charging policy. They are solely able to describe one of three different routes or charging strategies, respectively.

4.1.2 Derivation of Edge Cost Functions

In the context of SPPs, the considered objective function is typically based on edge cost functions, i.e., on functions that assign costs to edges of a graph. To be able to derive efficient shortest path algorithms, the properties of the objective function and thus of the considered edge cost functions are essential. This makes it necessary to state which edge cost functions are taken into account in this work and also to concretize them up to some degree. Otherwise, no statements on the properties of the objective function are possible.

In section 3.2, the meanings of the components of an MDP in the context of CSO have been discussed. It was postulated that at least information about arrival times and energy consumption has to be taken into account to handle CSO reasonably. Correspondingly, edge cost function c_T, describing time costs, and edge cost function c_E, describing energy costs, are considered in the following. It is again distinguished between edges representing road segments and edges representing parts of the charging process. In either case, travel times and energy consumption depend on various factors, such as traffic conditions, the state of charge when arriving at a charging station, vehicle parameters or individual driving style. As already discussed in chapter 2, some of these factors are hardly predictable. Consequently, in order to mirror the resulting uncertainty, it is probably more realistic to assume randomly distributed travel times and energy consumption than to assume deterministic values. However, for the moment c_T and c_E are assumed to be deterministic. Later on, in chapter 5, the non-deterministic case will be discussed. Besides a simplified notation, deterministic edge costs allow computing shortest paths on larger graphs than non-deterministic edge costs, since non-deterministic edge costs typically increase computation times for SPPs drastically (see also section 5.2). Unfortunately, it will turn out that even for deterministic edge costs, solving the resulting SPP becomes computationally very expensive.

Edge Costs for Road Segments In this section, it is not explained how cost functions c_T and $\grave{c}_E$[20], which assign time and energy costs, respectively, to edges representing road segments, can be constructed. It is simply assumed that such cost functions are given. They may depend on many factors, such as prevailing traffic conditions, the driver's mood, outdoor temperature, and so on. One possible way to represent these dependencies is to introduce objects ω_T and ω_E. Variable ω_T is intended to abstractly describe all available information about factors which influence travel time, ω_E correspondingly all information which is relevant for computing energy consumption. Based on these considerations, $c_T(e, \omega_T)$ describes the travel time which is necessary for passing edge e under the conditions defined by ω_T. Analogously, $\grave{c}_E(e, \omega_E)$ describes the energy consumption which is necessary for passing edge e under the conditions defined by ω_E. To simplify the following notations, objects ω_T and ω_E are left out in most situations. Instead, only those parts of ω_T and ω_E, which are explicitly relevant in the corresponding context, are listed. The most important example of such a quantity is arrival time. It depends directly on cost function c_T and typically has influence on c_T and $\grave{c}_E$. In the following, it will turn out to be expedient to explicitly list arrival time $t \in \mathbb{R}_{\geq 0}$[21], whenever edge costs are

[20] The reasons for writing $\grave{c}_E$ instead of c_E will be explained later on.

[21] In order to associate arrival times with real-valued numbers, an arrival time t could be defined as the number of seconds which elapsed since t_R, i.e., since the time at which the charging strategy was requested.

considered. This leads to the following terms for edge cost functions c_T and $\grave{c}_E$:

$$c_T: \quad \vec{E}_D^{\Delta} \setminus \vec{E}_{cs}^{\Delta} \times \mathbb{R}_{\geq 0} \longrightarrow \mathbb{R}_{\geq 0} \tag{4.7}$$

$$\grave{c}_E: \quad \vec{E}_D^{\Delta} \setminus \vec{E}_{cs}^{\Delta} \times \mathbb{R}_{\geq 0} \longrightarrow \mathbb{R} \tag{4.8}$$

Here, $\vec{E}_{cs}^{\Delta}$ denotes the set of all edges in $\vec{E}_D^{\Delta}$ which represent parts of a charging process. Cost functions $c_T(e,t)$ and $\grave{c}_E(e,t)$ describe the travel time or energy, respectively, which is necessary for passing edge $e = (v_i, v_j)$, when starting at time t at node v_i. Energy consumption is here measured in percent with regard to the maximal energy capacity of the BEV's battery. The idea is to compute the state of charge after passing an edge e at time t by subtracting $\grave{c}_E(e,t)$ from the original state of charge. One problem which occurs in this context is that either states of charge below zero percent or above 100 percent may be reached. The first case results if energy consumption exceeds the available energy, the latter may result if passing an edge leads to a gain of energy due to recuperation. To counter this issue, modified edge costs c_E are introduced. This cost function is based on $\grave{c}_E$, but depends on three quantities:

$$c_E: \quad \vec{E}_D^{\Delta} \setminus \vec{E}_{cs}^{\Delta} \times \mathbb{R}_{\geq 0} \times [0,1] \longrightarrow [-1,1] \tag{4.9}$$

$$c_E(e,t,SOC) := \begin{cases} SOC - 1 & \text{if } SOC - \grave{c}_E(e,t) > 1 \\ SOC & \text{if } SOC - \grave{c}_E(e,t) < 0 \\ \grave{c}_E(e,t) & \text{else} \end{cases} \tag{4.10}$$

This ensures that for any $e \in \vec{E}_D^{\Delta}$, any $t > 0$ and any $SOC \in [0,1]$, the following condition holds:

$$0 \leq SOC - c_E(e,t,SOC) \leq 1 \tag{4.11}$$

Condition 4.11 guarantees that neither recuperation nor charging can lead to a state of charge above 100 percent. Furthermore, if more energy than the battery can provide is necessary to pass a specific edge, then the resulting state of charge does not become negative, but simply is set to zero. This definition of c_E allows computing energy consumption costs for paths by summing up the costs of the corresponding edges and it allows representing the case of running out of energy. Similar proceedings for achieving reasonable states of charge have been suggested in (*12*), (*42*) and (*74*).

To illustrate the definitions of c_T and c_E and especially the dependency of c_E on $\grave{c}_E$, consider the example shown in Figure 4.3. Here, the costs for all edges but for (b,c) are time-independent. If the trip is started with a starting state of charge of 0.5 from node a to node c, then the energy costs c_E for edge (a,c) are equal to 0.4. However, starting with a state of charge of 0.3 leads to energy consumption costs $c_E(a,c)$ of 0.3 according to the definition in equation 4.10.

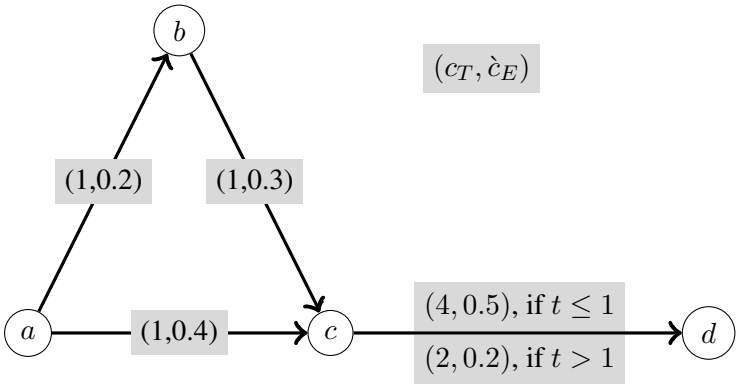

starting	destination	t_S	SOC_S
a	d	0	$0.9 = 90\%$

Figure 4.3: Edge costs depending on time and the current state of charge

Now, consider a starting time t_S which is equal to zero and a starting state of charge SOC_S of 0.9. Then the costs for the path $[a, c, d]$ can be computed as the sum of the costs of its edges. Here, the so-called frozen link model (*108*) is used to describe the dependency of costs on time and the current state of charge. According to this very intuitive model, the computation of time-dependent costs for a specific edge is done on the basis of the time at which the edge is reached. For the case of path $[a, c, d]$, for example, time costs for (c, d) can be calculated as soon as the arrival time at node c is known. This arrival time is the sum of starting time t_S and the time costs for passing edge (a, c). It can be proceeded similarly to take the dependency of c_T and c_E on the current state of charge into account, i.e., the state of charge when arriving at node c is given as the starting state of charge SOC_S minus the energy consumption costs assigned to edge (a, c). Consequently, in order to be able to compute the costs of a path, it has to be started with computing the costs of its first edge:

$$c_T((a, c), t_S) = c_T((a, c), 0) = 1 \tag{4.12}$$

$$c_E((a, c), t_S, SOC_S) = c_E((a, c), 0, 0.9) = 0.4 \tag{4.13}$$

Hence, the time when reaching (c, d) along path $[a, c, d]$ is given by $t_S + 1 = 1$ and the corresponding state of charge by $SOC_S - 0.4 = 0.5$. This leads to costs for edge (c, d) as subsequently shown:

$$c_T((c, d), t_S + c_T((a, c), t_S)) = 4 \tag{4.14}$$

$$c_E((c, d), t_S + c_T((a, c), t_S), SOC_S - c_E((a, c), t_S, SOC_S)) = 0.5 \tag{4.15}$$

Finally, time costs of five and consumption costs of 0.9 result for path $[a, c, d]$.

Edge Costs for Charging Processes Up to this point, only the case of edges representing road segments has been discussed. In the following, the focus is set on edges representing parts of charging processes. Considering the graph-based model described in section 4.1.1 (see Figure 4.1), charging processes are represented by edges $(v_k^i, v_k^{l\cdot\Delta})$ and edges $(v_k^{l\cdot\Delta}, v_k^o)$. Variable k is the index referring to the visited charging station and $l \cdot \Delta$ denotes the state of charge up to which the vehicle is charged at station k according to a strategy which is associated with a path that covers node $v_k^{l\cdot\Delta}$. The sum of the time costs of edges $(v_k^i, v_k^{l\cdot\Delta})$ and $(v_k^{l\cdot\Delta}, v_k^o)$ has to represent the time which is needed for the whole charging process. Analogously, the sum of the energy consumption „costs“ of these two edges has to be equal to „minus one multiplied by the amount of gained energy“[22].
Anything that happens at the charging station is understood to be part of the charging process. This may imply waiting times c_T^W caused by an occupied charging station, time c_T^A („A“ for „additional“) which is necessary, for example, to leave and get back into the car and for paying, the time c_T^C for charging the car, and the resulting energy gain represented by c_E^C. To predict waiting times, the time of arrival at the charging station, i.e., the time at which node v_k^i is reached, is essential, since charging demand typically changes throughout the day (9). Thus, predicted waiting times should be assigned to edges $(v_k^i, v_k^{l\cdot\Delta})$ and not to $(v_k^{l\cdot\Delta}, v_k^o)$. The time which is necessary for paying, leaving the car, and getting back into the car is throughout this work assumed to be independent of time and independent of the charging station. Due to this, it can be assigned to any of the two possible types of charging process edges. Assuming time independence is also reasonable for costs c_T^C and c_E^C, since charging durations and the amount of charged energy should not depend on the time at which the actual recharging is started. Based on these considerations, cost functions c_T and c_E for edges $(v_k^i, v_k^{l\cdot\Delta})$ and $(v_k^{l\cdot\Delta}, v_k^o)$ can be defined as follows:

$$c_T : \quad \vec{E}_{cs}^{\Delta} \times \mathbb{R}_{\geq 0} \times [0,1] \longrightarrow \mathbb{R}_{\geq 0} \tag{4.16}$$

$$c_E : \quad \vec{E}_{cs}^{\Delta} \times \mathbb{R}_{\geq 0} \times [0,1] \longrightarrow [-1,0] \tag{4.17}$$

$$c_T((v_k^i, v_k^{l\cdot\Delta}), t, SOC) := c_T^W((v_k^i, v_k^{l\cdot\Delta}), t) + c_T^C((i_k, v_k^{l\cdot\Delta}), SOC) \tag{4.18}$$

$$c_T((v_k^{l\cdot\Delta}, v_k^o), t, SOC) := c_T^A \tag{4.19}$$

$$c_E((v_k^i, v_k^{l\cdot\Delta}), t, SOC) := c_E^C((v_k^i, v_k^{l\cdot\Delta}), SOC) \tag{4.20}$$

$$c_E((v_k^{l\cdot\Delta}, v_k^o), t, SOC) := 0 \tag{4.21}$$

Note that, even though c_E is not time-dependent for edges in $\vec{E}_{cs}^{\Delta}$, it is written $c_E(e, t, SOC)$ instead of $c_E(e, SOC)$. This is done to keep the notation consistent with the definition of c_E for edges representing road segments.

The energy consumption „costs“ (actually energy is gained and thus the costs are negative) for

[22] Gaining energy is here represented by assigning negative edge costs to the corresponding edges

edges $(v_k^i, v_k^{l\cdot\Delta})$, i.e., for an intended target state of charge $l \cdot \Delta$, are given as follows:

$$c_E^C((v_k^i, v_k^{l\cdot\Delta}), SOC) := \begin{cases} SOC - l \cdot \Delta & \text{if } l \cdot \Delta > SOC \\ SOC & \text{else} \end{cases} \tag{4.22}$$

The formula is rather intuitive as long as $l \cdot \Delta > SOC$. It is just the difference between the current state of charge and the target state of charge. If $l \cdot \Delta$ is not bigger than SOC, then the corresponding charging process is not meaningful, since the state of charge when arriving at the charging station would be at least as high as the one after charging. To guarantee that such edges are not considered by any route search algorithm, energy costs leading to an empty battery are assigned to them. The computation of time costs for charging, i.e., the duration which is necessary to achieve a state of charge equal to $l \cdot \Delta$, is more complicated. A model describing the relation between charging duration and the resulting energy gain is necessary. Here, a rather simple model is applied. It is assumed that a function S is available with

$$S : \mathbb{R}_{\geq 0} \longrightarrow [0, 1]. \tag{4.23}$$

S returns for a specific charging duration $d \geq 0$ the resulting state of charge if an initial state of charge of zero is assumed. Such functions clearly vary depending on the technical features of the vehicle battery and the charging station. However, their shapes are always similar: The longer the charging process, the more energy is gained in total. Thus, S is strictly monotonically increasing up to a state of charge of 1.0 and a maximal charging duration $d_{max} > 0$, i.e., d_{max} is equal to the time that is necessary to fully recharge a completely empty vehicle battery. This property allows inverting S on $[0, d_{max}]$, leading to

$$S^{-1} : [0, 1] \longrightarrow [0, d_{max}]. \tag{4.24}$$

The inverse function returns for a given state of charge SOC the duration that is required to charge an empty battery up to this state of charge. For all durations higher than d_{max}, the battery is already completely recharged and consequently

$$S(d) \equiv 1 \quad \forall d \geq d_{max}. \tag{4.25}$$

It is worth mentioning that if a battery is almost fully recharged, the energy throughput is usually reduced to prolong the battery's lifespan. Due to this nonlinear charging behavior, S is concave. Figure 4.4 exemplarily illustrates how a function S could look like. Moreover, for a given initial state of charge SOC_{init} (the state of charge at the beginning of the charging process), a given process starting time t_{init}, and a target state of charge $l \cdot \Delta$, the cost computation for $(v_k^i, v_k^{l\cdot\Delta})$ is displayed. The energy consumption costs $c_E^C((v_k^i, v_k^{l\cdot\Delta}), SOC_{init})$ are calculated according to equation 4.22. The time costs $c_T^C((v_k^i, v_k^{l\cdot\Delta}), SOC_{init})$ are assumed to

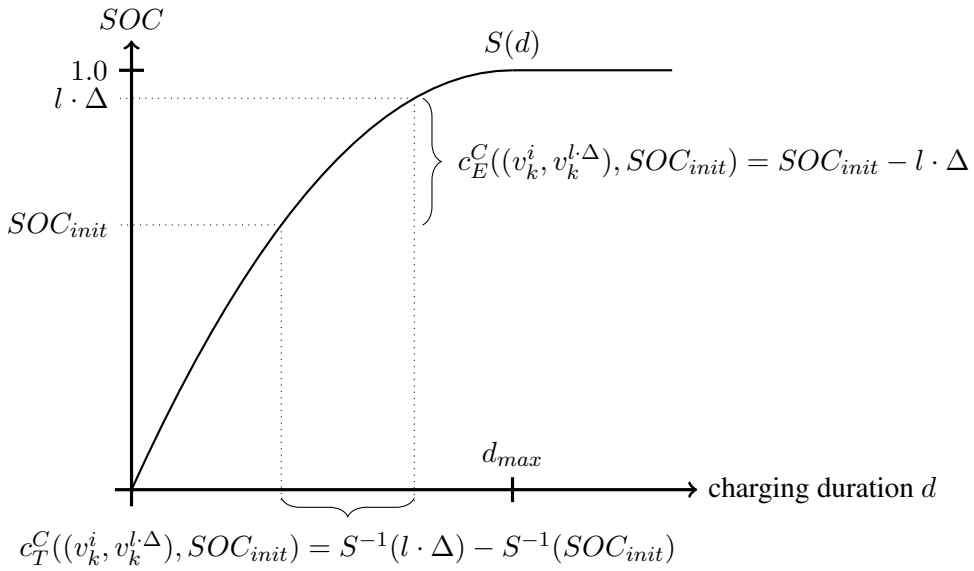

Figure 4.4: Relation between charging duration and state of charge.

result from the difference between the charging duration which is required to charge an empty battery up to $l \cdot \Delta$ and the charging duration which is necessary to charge up to SOC_{init}:

$$c_T^C((v_k^i, v_k^{l\cdot\Delta}), SOC_{init}) := S^{-1}(l \cdot \Delta) - S^{-1}(SOC_{init}). \tag{4.26}$$

4.1.3 Definition of Shortest Path Problems

Having described graph and edge cost functions, performance measure f is defined next. This is the only missing part to fully describe the problem of finding optimal charging strategies as an SPP. The performance measure is intended to rate and thus compare different paths on graph $\vec{G}_D^{\Delta}$ and it eventually defines what an „optimal“ charging strategy is. For the introduced setting, there are two criteria according to which this can be done: Charging strategies could be rated on the basis of energy consumption costs c_E, as shown in (*141*), or on the basis of the time costs c_T, as proposed in (*151*). In the case of considering c_E as rating criterion, as a first approach, it could simply be stated for two given paths P_1, $P_2 \in \mathcal{P}(\vec{G}_D^{\Delta}, v_0, v_{K+1})$, a given starting state of charge SOC_S, and a given starting time t_S that P_1 is „better“ than P_2 if and only if

$$c_E(P_1, t_S, SOC_S) < c_E(P_2, t_S, SOC_S) \tag{4.27}$$

Note that it is assumed that the costs assigned to a path result from the sum of the costs of all edges of which this path consists. However, the rating criterion described by inequality 4.27 leads to a non-intuitive rating behavior, since c_E also includes negative energy consumption costs caused by charging. Thus, fully recharging the vehicle battery at each charging station represents a possible way to construct an optimal charging strategy. To avoid this, charging

strategies could be rated depending on the energy consumption without considering the energy gain due to charging, i.e., P_1 is superior to P_2 if and only if

$$c_E(P_1, t_S, SOC_S) - c_E^C(P_1, t_S, SOC_S) < c_E(P_2, t_S, SOC_S) - c_E^C(P_2, t_S, SOC_S). \quad (4.28)$$

Here, c_E^C denotes the cumulative negative energy consumption costs caused by all charging processes which are represented by a path (see also equation 4.22). Correspondingly, charging strategies are characterized as good charging strategies if the resulting energy consumption caused by driving is low. Also this idea leads to an issue: Approaching charging stations, i.e., leaving the main road network to get to the charging station (and vice versa), leads to energy consumption costs. Consequently, by following solely the idea of inequality 4.28, charging strategies which suggest no stops for charging would receive comparably good ratings. On the other hand, it would not be considered whether the suggested charging strategy leads to an empty battery or not. Since leaving the main road network causes additional travel time, the same issue occurs if charging strategies are solely rated according to the resulting total travel time, i.e., if a path P_1 is superior to P_2 if and only if

$$c_T(P_1, t_S, SOC_S) < c_T(P_2, t_S, SOC_S). \quad (4.29)$$

Certainly, the minimum requirement for a charging strategy has to be that the destination is reached. Other charging strategies should not be considered or should be rated very badly. The subsequent definition is motivated by this consideration:

Let a path $P = [v_1^P, v_2^P, ..., v_Q^P]$ on $\vec{G}_D^{\Delta}$ be given. Furthermore, let a starting time t_S, a starting state of charge SOC_S, and deterministic edge cost functions c_T and c_E (as described before) be given. Then, path P is called **feasible** if and only if

$$SOC_S - c_E(P_{1:i}, t_S, SOC_S) > 0 \quad \forall i \in \{2, 3, ..., Q\} \quad (4.30)$$

This means that a path is feasible unless there exists at least one edge along this path, for which the energy costs for passing this edge are equal to or higher than the energy which is available when reaching the start of this edge. A similar definition of feasibility in the context of CSO can be found, for instance, in (*137*).

Finally, based on the definition of feasibility, the following definition of a performance measure is suggested:

$$f(P, t_S, SOC_S) := \begin{cases} c_T(P, t_S, SOC_S) & \text{if } P \text{ is feasible} \\ \infty & \text{else} \end{cases} \quad (4.31)$$

Time costs c_T are used as the primary rating criterion. In contrast to minimizing the energy

consumption costs, which would still be a reasonable optimization criterion[23], minimizing time costs has the advantage that optimized charging strategies avoid congestion. If c_E was used instead of c_T and if it is assumed that high driving speeds cause high energy consumption[24], then free-flow traffic conditions could be less desirable than, for example, minor congestion. Hence, a charging strategy leading a car driver into minor congestion could be rated better than a charging strategy which allows avoiding any kind of traffic jam. This probably does not mirror the will of drivers. By using performance measure f as the objective function[25], the corresponding SPP results directly:

$$\begin{aligned} \min \quad & f(P, t_S, SOC_S) \\ \text{subject to} \quad & P \text{ is a } v_0\text{-}v_{K+1}\text{-path on } \vec{G}_D^{\Delta} \end{aligned} \tag{4.32}$$

Alternatively, by replacing performance measure f with cost function c_T, the feasibility condition can be removed from the objective function and, instead, be represented by an additional constraint:

$$\begin{aligned} \min \quad & c_T(P, t_S, SOC_S) \\ \text{subject to} \quad & P \text{ is a } v_0\text{-}v_{K+1}\text{-path on } \vec{G}_D^{\Delta} \\ & P \text{ is feasible} \end{aligned} \tag{4.33}$$

Such types of SPPs are denoted as constrained shortest path problem (*7*) (*47*). During the next sections, problem formulation 4.33 is usually preferred.

4.2 Analysis of Cost Function Properties

Up to this point, the problem of finding optimal charging strategies is formulated as an SPP. As a next step, it is necessary to identify existing or develop new algorithms that can be used to find optimal or at least good solutions for problem 4.33 in reasonable time. For this purpose, the problem's properties are analyzed, allowing an evaluation of the applicability of known optimization algorithms and concepts.

There exists already a huge number of optimization algorithms for solving a variety of different types of SPPs in literature (overviews can be found for example in (*33*), (*109*) or (*139*)). In this section, the focus is set on modifications of Dijkstra's algorithm (*36*). Problem 4.33 will be solved by an algorithm which is an extended version of Dijkstra's algorithm. In Figure 4.5,

[23] It would also be reasonable to consider travel times and energy consumption simultaneously within the objective function as done in (*137*).

[24] In section 7.1, recorded consumption data of real BEVs confirm that BEVs show such an energy consumption behavior.

[25] Note that in a deterministic context, i.e., if f represents a deterministic function, it is not necessary to differentiate between the notion „performance measure“ and the notion „objective function“, since the expected value operator $\mathbb{E}[]$ applied to a deterministic function f does not show any impact.

Dijkstra's Algorithm

Input: A directed graph $\vec{G} = (V, \vec{E})$, a starting node v_0, a destination node v_{K+1} and a non-negative cost function c which assigns costs to edges

Initialization: Create label $L = (0, \emptyset, v_0)$ for node v_0. Define the set of temporal labels $\mathcal{L}_{temp} := \{L\}$ and the set of permanent labels $\mathcal{L}_{perm} := \emptyset$

1 While $\mathcal{L}_{temp} \neq \emptyset$ and no label belonging to v_{K+1} was added to $\mathcal{L}_{perm}$, do:
2 $L^{cur} = (c^{cur}, v^{pre}, v^{cur})$:= the label in $\mathcal{L}_{temp}$ with the lowest cost value.
3 Remove L^{cur} from $\mathcal{L}_{temp}$ and add it to $\mathcal{L}_{perm}$.
4 For all $v^{new} \in V$ such that $e := (v^{cur}, v^{new}) \in \vec{E}$ do:
5 Compute $c^{new} := c^{cur} + c(e)$
6 Create $L^{new} := (c^{new}, v^{cur}, v^{new})$
7 If there is no label in $\mathcal{L}_{perm}$ that belongs to node v^{new}
8 If there is no label belonging to v^{new} in $\mathcal{L}_{temp}$ then:
9 Add L^{new} to $\mathcal{L}_{temp}$.
10 Else (i.e., it already exists a label $L^{old} = (c^{old}, v^{pre}_{old}, v^{new}) \in \mathcal{L}_{temp}$):
11 If $c^{old} > c^{new}$
12 Delete L^{old} from $\mathcal{L}_{temp}$ and add L^{new} instead.
13 End if.
14 End if.
15 End if.
16 End for.
17 End while.
18 If possible, return the label $\bar{L} \in \mathcal{L}_{perm}$ that belongs to node v_{K+1},
19 otherwise return „No feasible solution found“.

Figure 4.5: Pseudo-code of Dijkstra's algorithm for solving point-to-point SPPs.

a possible pseudo-code for implementing Dijkstra's algorithm can be found. The reader is assumed to be familiar with Dijkstra's algorithm. Hence, no explanations on the procedure itself are provided here, but one difference between the pseudo-code in Figure 4.5 and the original version of Dijkstra's algorithm from (*36*) shall be pointed out: In line 1 of the pseudo-code, it is postulated that the algorithm leaves the while-loop (and hence terminates) as soon as a label belonging to the destination node is found. The original version of Dijkstra's algorithm did not have this condition. However, the possibility of including this additional condition into the shortest path algorithm is one reason for favoring algorithms which are derived from Dijkstra's algorithm in the context of CSO: Problem 4.33 is a so-called point-to-point SPP, i.e., the shortest path from one starting node to one destination node has to be computed. For such problems, so-called label-setting algorithms, like Dijkstra's algorithm, in most cases outperform other types of shortest path algorithms. Label-setting algorithms typically start their route-search at the starting node and expand from there on (more or less) circularly into all directions, while steadily assigning costs to the considered nodes. Such a behavior can also be observed for the pseudo-code in Figure 4.5. Examples of how the resulting search spaces look

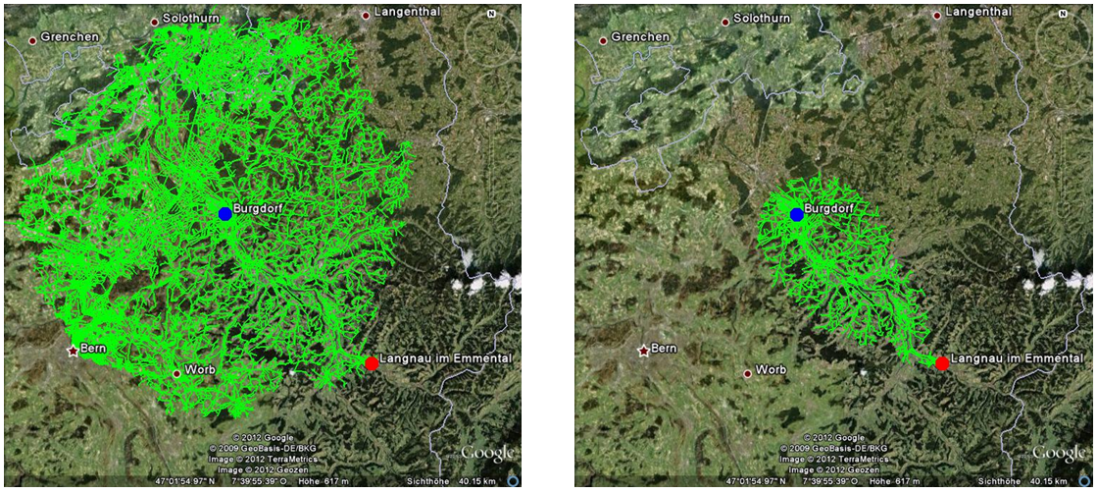

Figure 4.6: Visualization of typical search spaces of label-setting algorithms in Google Earth.

like can be found in Figure 4.6. There, the starting point is shown in blue, the destination in red and all edges which were added to the set of temporal labels $\mathcal{L}_{temp}$ or to the set of permanent labels $\mathcal{L}_{perm}$ during the route search are marked green[26]. On the left, Dijkstra's algorithm is applied and on the right, a version of the A^*-algorithm (*62*) (*63*) is used. The latter approach can be assigned to the family of the label-setting approaches, too. The graphics are taken from (*67*). If the considered cost function obtains no negative values, the circular expansion of label-setting approaches makes it possible to guarantee optimality of the computed path even if the route search is stopped as soon as a label belonging to the destination node is added to $\mathcal{L}_{perm}$. Other types of shortest path algorithms, like for example label-correcting algorithms[27], which are the most common algorithms for solving SPPs besides label-setting algorithms, do not show this advantage. If a label-correcting algorithm is terminated prematurely, i.e., before each edge of the whole graph has been considered during the route search, then optimality of the computed solution cannot be guaranteed (*52*). Thus, at least for point-to-point SPPs, label-correcting algorithms typically suffer from higher running time complexities and consequently also from higher computation times than label-setting algorithms (*7*) (*42*).

Unfortunately, there are several aspects of the suggested deterministic SPP[28], which the described version of Dijkstra's algorithm cannot handle: Two different cost functions have to be considered in parallel. Both of them depend on time and on the state of charge. The energy consumption costs even assume negative values. Any of these aspects not only impedes the applicability of Dijkstra's algorithm, but of most shortest path algorithms. In the following,

[26] In the context of dynamic SPP algorithms, the sets of temporal and permanent labels are often also denoted as the sets of opened and closed nodes.

[27] Both label-setting and label-correcting algorithms are types of dynamic programming approaches.

[28] If one speaks of problem properties in the context of routing algorithms, then one typically refers to the properties of the considered edge cost functions.

each of the mentioned cost function properties and its impact on potential solution approaches are analyzed in detail. Afterwards, these analyzes are used to derive appropriate optimization algorithms.

4.2.1 Negative Edge Costs

When optimizing paths with regard to a cost function which can attain negative values, the critical scenario for label-setting algorithms is that the optimal path $P^* = [v_1^*, v_2^*, ..., v_M^*]$ is very expensive at the beginning, i.e., the costs $c(P^*_{1:m})$ for $m < M$ are huge, but its last edges lead to negative costs, i.e., $c(P^*_{m+1:M}) < 0$. If a suboptimal solution $\bar{P}$ with $c(P^*) < c(\bar{P}) < c(P^*_{1:m})$ exists, then a label-setting algorithm typically terminates with returning $\bar{P}$ before finding P^*. In contrast, label-correcting algorithms, like the Moore-Bellman-Ford algorithm (*14*) (*48*) (*103*) or the algorithm of Floyd and Warshall (*46*), ensure optimality of their solutions even under the presence negative edge costs.

Nevertheless, in order to reduce computation times, label-setting algorithms are often applied even if negative edge costs exist. This can be done, for example, by following the method of Johnson (*72*). For this approach, so-called potential functions are computed to transform within a pre-processing step the relevant edge cost function in such a way that negative edge costs no longer occur. The essential property of such potential functions is that the shortest paths between any pair of nodes remain the same, even though the edge costs are changed. In (*74*), a potential function is generated on the basis of elevation data. In (*12*) and (*42*), preliminary route computations are carried out during the pre-processing step to construct an adequate potential function. The only restriction to Johnson's method is that no cycles leading to negative edge costs are allowed to exist in the given graph. Due to the law of conservation of energy, this is always fulfilled for traditional energy-efficient routing (*7*) – at least as long as charging stops are not considered[29].

An alternative to Johnson's method, which is frequently used in the context of energy-efficient routing, is to exclude energy consumption costs from the objective function and optimize according to another rating criterion (*116*) (*137*). To still be able to ensure feasibility of the computed paths, an additional constraint can be introduced as has been done for the formulation of problem 4.33 (which is the formulation as a constrained SPP). Hence, the potential negativity of c_E is no knock-out criterion for applying label-setting algorithms for CSO.

[29]The law of conservation of energy implies that, despite recuperation, driving in a circle can never lead to an increase of the state of charge.

4.2.2 Multicriteria Shortest Path Problems

Multicriteria SPPs for $Z \in \mathbb{N}_{>1}$ different criteria c_1, c_2, ..., c_Z, a starting node s, a destination node d, and a directed graph $\vec{G}$ can be formulated as subsequently stated:

$$\begin{aligned} \min \quad & \Big(c_1(P), c_2(P), ..., c_Z(P)\Big) \\ \text{subject to} \quad & P \text{ is an } s\text{-}d\text{-path on } \vec{G} \end{aligned} \tag{4.34}$$

If several objective functions are considered in parallel, then it is in general not trivial to compare different solutions and decide which one is the best. An example illustrating this statement can be found in Figure 4.7. Here, a shortest path from node a to node e has to be computed by minimizing the two criteria c_1 and c_2 at the same time. With P_A, P_B, P_C and P_D, one of four different paths can be chosen. Obviously, it can be concluded that P_A is better than P_D (and also better than P_C), since it is in both criteria at least as good as P_D and if c_1 is considered, it is even superior to P_D. Such a trivial statement is not possible when comparing P_A to P_B.

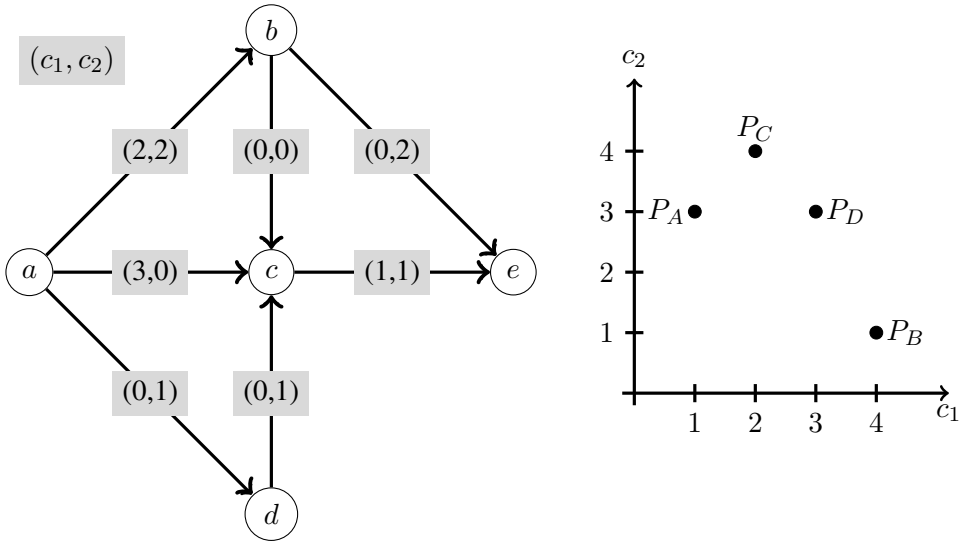

$$P_A := [a, d, c, e] \qquad P_B := [a, c, e] \qquad P_C := [a, b, e] \qquad P_D := [a, b, c, e]$$

Figure 4.7: Multicriteria SPP and resulting objective function values

Fortunately, the so-called Pareto optimality (*111*) provides a clear interpretation of optimality for multicriteria optimization problems: A solution is called **Pareto optimal** if there exists no other feasible solution which is for all considered criteria at least as good as the original solution and additionally for at least one criterion better than the original solution. All solutions that are not Pareto optimal are denoted as **dominated** solutions. This means that P_A and P_B are Pareto optimal solutions for the optimization problem described by Figure 4.7. Verbally, this is expressed by stating that „paths P_C and P_D are dominated by P_A“.

In literature, many different algorithms for solving multicriteria SPPs are suggested (see (*31*) (*35*) (*99*) (*119*) (*134*); for an overview, see section 9.1 in (*41*)). In most cases, these algorithms are intended to generate the whole set of Pareto optimal paths. However, computing the whole set of Pareto optimal solutions is, from a practical perspective, often not necessary. For the case of CSO, for instance, suggesting a low number of charging strategy recommendations seems sufficient. This is particularly important since the number of Pareto optimal solutions for multicriteria SPPs can grow exponentially with the number of nodes of the considered graph (*61*). Thus, simply listing up all solutions can lead to high computational efforts. In terms of complexity theory, multicriteria SPPs are proven to be $\mathcal{NP}$-complete (*133*), i.e., the computational effort for solving such a problem typically rise very quickly with the size of the graph. When applying dynamic programming approaches to multicriteria SPPs, all Pareto optimal paths from the starting node to any node which is visited during the route search are computed. Typically, this cannot be avoided even if it is not intended to compute the whole set of Pareto optimal paths. As label-setting (as well as label-correcting) algorithms encode paths via labels, dynamic programming algorithms applied to multicriteria SPPs have to be able to assign several labels to the same node. Otherwise, the parallel existence of several Pareto optimal paths leading from the starting node to another node could not be represented. This makes it necessary to generate and manage a huge number of labels. High computation times are the result. More details will be provided later on.

Clearly, the problem of finding optimal charging strategies, the way it is formulated in 4.33, differs from traditional multicriteria SPP. The main difference is that the energy consumption costs are (at least in the version stated in 4.33) removed from the objective function and, instead, represented within an additional constraint. Unfortunately, this does not simplify the problem. The resulting constrained SPPs is, in fact, a special version of a multicriteria SPP, since still both cost functions need to be considered simultaneously. As a consequence, the problem's complexity remains high[30].

4.2.3 Time Dependency of Edge Costs

To model time-dependent edge costs, the possibility to compute the time at which an edge is reached has to be given. Hence, a starting time and a function assigning time costs to edges are necessary. Furthermore, it has to be distinguished between minimizing time-costs, i.e., find a „fastest“ path, and minimizing general time-dependent costs, such as the energy consumption costs c_E which have been introduced in section 4.1.2. For the case of finding fastest paths, which was considered for the first time in (*32*), time dependency not necessarily increases the SPP's complexity. If the so-called FIFO-property (first-in first-out) holds, even an almost unchanged version of Dijktra's algorithm can be applied for finding fastest paths (*38*). A (directed) network $\vec{G} = (V, \vec{E})$ (or a directed graph, respectively) is denoted as a **FIFO-network**

[30] Constrained SPPs are $\mathcal{NP}$-complete according to section 3.1 in (*47*).

if and only if the time-costs, which are here again denoted with c_T, fulfill the following condition for arbitrary times $t_1 \leq t_2$:

$$t_1 + c_T(e, t_1) \leq t_2 + c_T(e, t_2) \quad \forall e \in \vec{E} \tag{4.35}$$

This can be understood as „overtaking is not allowed“. If a vehicle starts passing an edge before another vehicle, then it will also arrive at the end of this edge before the other one. In the context of routing, it is common to assume the FIFO-property to be true, even though overtaking is actually possible in reality. The same is assumed for CSO. Be aware that the FIFO-property may be violated if the time-dependent costs c_T^W for waiting at a highly frequented charging station are modeled inappropriately, i.e., if situations within the model exist in which a car driver is able to finish her/his charging process earlier if she/he arrives later at the charging station. This is not reasonable from a practical perspective, nor is it reasonable according to queuing theory. Note that a car driver facing such a situation would achieve a time-advantage if she/he simply waits at the charging station for an appropriate time period before she/he starts charging.

For the case of minimizing general time-dependent path costs, the situation becomes more complicated. The problem is that **Bellman's optimality principle** may no longer hold. In the context of SPPs, i.e., for finding a shortest path between two nodes v_0 and v_{K+1}, this principle postulates that any subpath $P^*_{m:n}$ of an optimal path $P^* = [v_0, ..., v_{K+1}]$ with $0 \leq m < n \leq K+1$ again is an optimal solution for the problem of finding a shortest path between v_m and v_n (*13*). General optimization problems which fulfill Bellman's optimality principle have the property that optimal solutions can always be constructed by stringing together solutions of subproblems.

Bellman's optimality principle represents the fundamental idea of any dynamic programming approach and ensures an efficient implementation of corresponding algorithms. For example, when applying Dijkstra's algorithm (or a modified version of it), then labels are constructed during the route search and assigned to nodes. These labels contain three types of information (see also the pseudo-code of Figure 4.5): First, the costs of a path which leads from the starting node to the node to which the considered label belongs. Actually, this path is the shortest path to this node which Dijkstra's algorithm has found up to the time at which the label is generated. Second, the preceding node on this path. The third information stored within labels is the node to which the label belongs. This is necessary to have a link between labels and nodes. The information about the preceding node is used to reconstruct the path which leads to the cost value stored by the label by successively following the predecessors until the starting node is reached. Thus, each label encodes a path from the starting node to the node to which the label belongs. The information about the costs is used to eliminate „bad“ subpaths. This is the point

where dynamic programming approaches, such as Dijkstra's algorithm, exploit Bellman's optimality principle: Let it be assumed that a path has been found during the route search leading from the starting node to another node. Furthermore, assume that, as the dynamic programming algorithm proceeds, a second path leading to this node is found. Dynamic programming algorithms check whether the new path leads to lower costs than the old one. If this is the case, then the old label is overwritten with a new one that encodes the new path. If the old label leads to lower costs, then it remains and the new label is dropped. This means for the multicriteria case, that labels or paths, respectively, are deleted as soon as they are identified to be dominated. Unfortunately, for time-dependent edge costs, this is no longer possible. In (*59*), it has been shown that even under strong assumptions concerning the properties of the considered time-dependent cost function, subpaths of optimal paths can be suboptimal. This is a contradiction to Bellman's optimality principle and makes it impossible to delete „bad" subpaths if general time-dependent edge cost function are considered and if optimality of the computed solutions has to be guaranteed. This is an important observation. It shows that during a route search, the search space cannot be pruned for the case of general time-dependent edge costs unless possibly suboptimal solutions are accepted. Instead, any possible sequence of edges has to be considered until the destination is reached. A side-effect of this is that, similar to the multicriteria case, applied algorithms need to be able to maintain several labels belonging to the same node during the route search[31].

Now, when returning to CSO, it is assumed that the FIFO-property holds for c_T. Furthermore, not general time-dependent costs, but time costs have to be optimized. Thus, it could be expected that Bellman's optimality principle still holds. Unfortunately, the example displayed in Figure 4.8 proves that this is not the case. Here, a time optimal route from v_0 to v_6 has to be found. It is assumed that there are altogether five charging stations along a fixed route, i.e., no route choices can be made. To keep the graphic clear, the first part of the graph between nodes v_0 and v_5^a is reduced to two edges. These edges represent alternative paths P_A and P_B between v_0 and v_5^a and the displayed costs are equal to the accumulated costs of these paths. The starting state of charge and the starting time are provided in the table below the figure. Because of edge (v_5^b, v_6), cost functions c_T and $\grave{c}_E$ are time-dependent. Edge costs for charging can be computed according to section 4.1. Target states of charge are given in steps of one percent, i.e., $\Delta = 0.01$. Furthermore, it can be observed that path P_B is dominated by P_A since it leads to higher time and higher energy consumption costs. To get from v_0 to v_6 on path P_A, it is necessary to charge at charging station 5. Otherwise, consumption costs would exceed the

[31] For the multicriteria case, this is necessary, since several non-dominated paths leading from the starting node to the currently considered node may exist in parallel (see, for instance, the example in Figure 4.7).

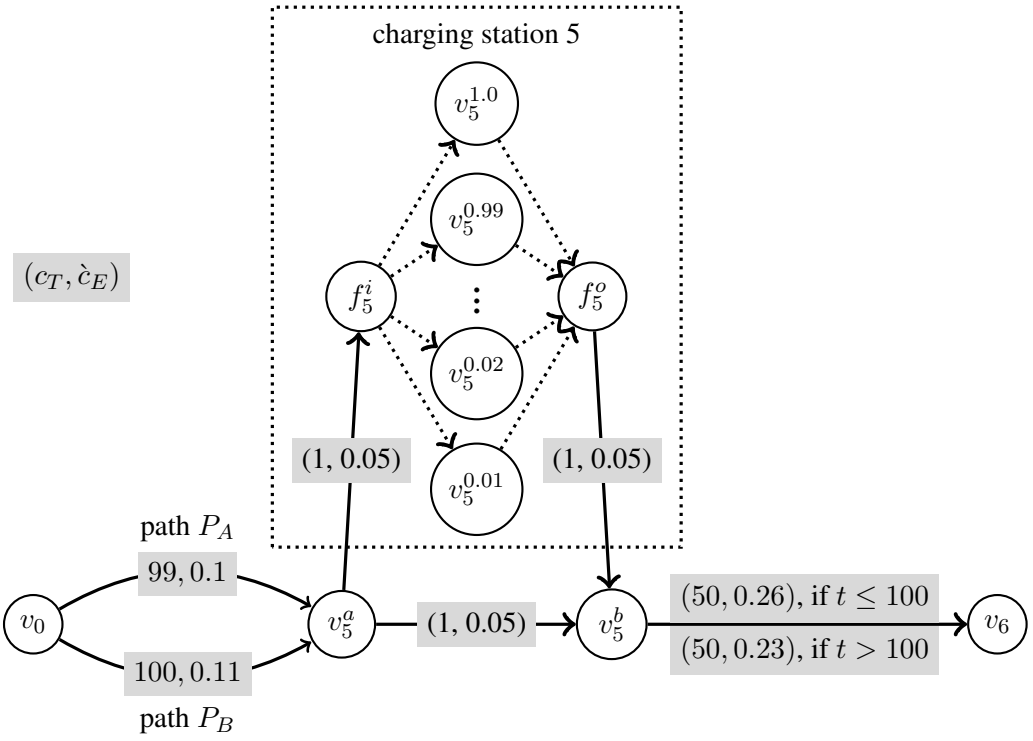

starting node	destination	SOC_S	t_S
s	d	40%	0

Figure 4.8: Example showing that subpaths of time optimal paths may be dominated for the problem of finding time optimal and feasible charging strategies

starting state of charge before node v_6 is reached:

$$\begin{aligned} &SOC_S - c_E(P_A, 0, 0.4) - c_E\Big(\big(v_5^a, v_5^b\big), 99, 0.3\Big) - c_E\Big(\big(v_5^b, v_6\big), 100, 0.25\Big) = \\ &= 0.4 - 0.1 - 0.05 - 0.26 = -0.01 \end{aligned} \tag{4.36}$$

The state of charge when reaching the charging station is equal to 25 percent. For the remaining route, i.e., for returning to the main route and finally getting to v_6, the state of charge is reduced by 28 percent, since node v_5^b cannot be reached before time $t = 101$. Therefore, the fastest possible and feasible charging strategy which is based on path P_A is to charge up to state of charge of 29 percent. Assuming that the charging duration for this charging process is given by a parameter $\hat{d} > 0$, the resulting total travel time is equal to $151 + \hat{d}$ and v_6 is reached with a state of charge of one percent. On the other hand, when using path P_B to get to v_5^a, then it is not necessary to charge at station 5, since node v_5^b is reached at time $t = 101$ with a state of charge of 24 percent. A total travel time of 151 and a final state of charge of one percent are the result. Hence, this second strategy is optimal for the described setting, even though its subpath P_B is dominated by another subpath.

Note that Bellman's optimality principle for CSO, under the assumption that travel times are minimized, could have been obtained if the energy consumption costs satisfied the so-called **cost consistency assumption** (*109*). The cost-consistency assumption is a generalization of the FIFO-property from time-dependent time costs to arbitrary time-dependent edge costs. A time-dependent cost function c fulfills the cost consistency assumption if leaving a node earlier does not lead to higher costs than leaving it later, i.e., it has to hold for arbitrary times $t_1 \leq t_2$ that:

$$c(e, t_1) \leq c(e, t_2) \quad \forall e \in \vec{E}. \tag{4.37}$$

In Figure 4.8, condition 4.37 is violated by edge (v_5^b, v_6), since arriving later at v_5^b reduces the energy consumption costs from 26 to 23 percent. It has to be remarked that the cost consistency assumption does not make sense if the energy consumption of a BEV is considered, since passing a road segment earlier not necessarily reduces the expected energy consumption. This implies that it cannot be expected that c_E fulfills the cost consistency condition.

4.2.4 Dependency of Edge Costs on the State of Charge

According to section 4.1.2, time costs c_T and energy consumption costs c_E depend for the case of CSO (at least according to the way the problem is modeled here) not only on time, but on the state of charge, too. For the dependency of the two considered cost functions c_T and c_E on the state of charge, similar statements as given in section 4.2.3 for their dependency on arrival times can be made. A generalization of the cost consistency assumption could be applied in this context. However, such a generalization would lead to unrealistic assumptions such as „If one car starts passing an edge with a lower state of charge than another car, then it also reaches the end of the edge with a lower state of charge.“ Another issue is that, besides the dependency on the state of charge, the dependency on time still remains for both cost functions c_E and c_T. According to the author's knowledge, there exists no literature treating comparable scenarios. However, for problem 4.33, it has already been reasoned that even without considering the dependency on the state of charge, Bellman's optimality principle does not hold. Thus, it could be stated that, at least from an algorithmic perspective, anything one could make use of is already lost. Hence, it seems to be a reasonable assumption that the dependency of edge cost functions c_E and c_T on the state of charge won't complicate the optimization problem. Later on, this conjecture will be confirmed implicitly in theorem 1. This theorem will actually prove the correctness of a shortest path algorithm proposed for solving the problem of finding optimal charging strategies.

4.3 Solution Approaches

Figure 4.9 summarizes the findings of section 4.2. Several different cost function properties, which are relevant in the context of shortest path computations, were discussed: The existence of negative edge costs, the coexistence of several optimization criteria, and the dependency of

these criteria on time and the state of charge. By removing energy consumption costs from the objective function, their potential negativity is supposed to have minor influence on potential solution approaches. Furthermore, the non-negativity of c_T ensures that applied label-setting algorithms can be stopped as soon as the destination node is reached. Taking two criteria into account, on the other hand, makes it necessary to consider not only time optimal subpaths during the route search. Thus, several labels belonging to the same node may exist in parallel. The time dependency of c_T has no influence, since c_T is assumed to fulfill the FIFO-property. In contrast, the time dependency of cost function c_E, along with its missing cost consistency, even destroys Bellman's optimality principle. Due to this, dominated subpaths cannot be ignored. With losing Bellman's optimality principle, any existing sequence of edges has to be pursued during the route search, i.e., any possible charging strategy has to be tested to guarantee optimality. This is the most intuitive and, at the same time, the most trivial approach that can be

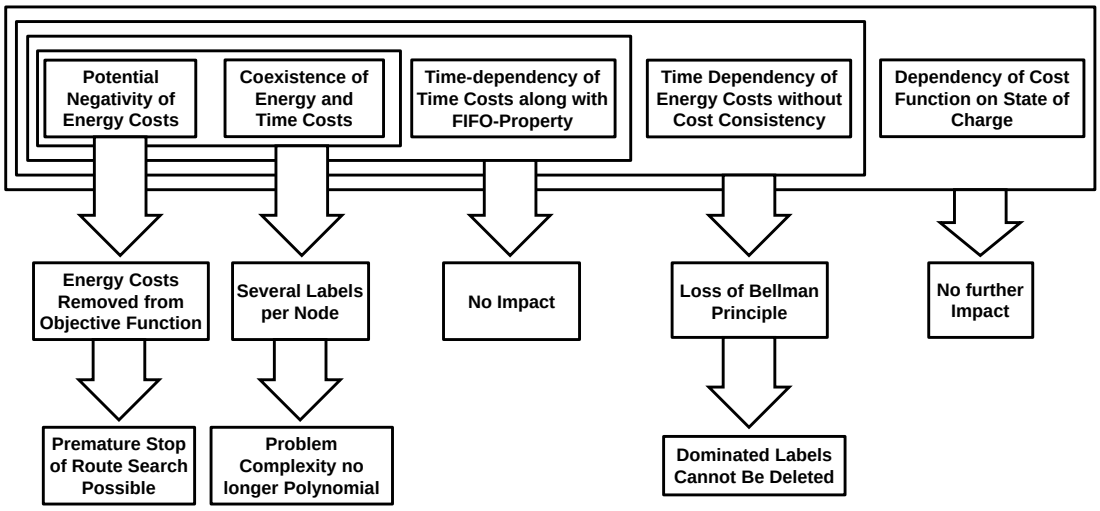

Figure 4.9: Cost function properties and their influence on solution approaches

applied. In this section, it will be argued that the resulting computational effort is extremely high, but also that this approach allows handling the dependency of functions c_T and c_E on the state of charge.

As shown in the previous section, approaches for handling most of the cost function properties can be found in literature, at least for handling them separately. Recent works also concerns combinations of the listed aspects. In (*88*) and (*37*), for example, algorithms for solving time-dependent multicriteria SPPs are provided. In (*59*), additionally the potential negativity of edge costs is addressed. Though, it seems that none of the existing shortest path algorithm is suitable for handling problem 4.33 with all its characteristics. As a consequence, an appropriate algorithm has to be derived. Here, this is done based on analyses conducted in section 4.2.

Algorithm A: Finding Optimal Charging Strategies
Input: A directed graph $\vec{G}_D^{\Delta} = (V_D^{\Delta}, \vec{E}_D^{\Delta})$, a starting node v_0, a destination node v_{K+1}, a starting time $t_S := 0$, cost functions c_T and $\grave{c}_E$ as described above, a starting state of charge SOC_S

Initialization: Create label $L = (0, 0\%, \emptyset, 0, v_0, 1)$ for node v_0. Define set of temporal labels $\mathcal{L}_{temp} := \{L\}$ and set of permanent labels $\mathcal{L}_{perm} := \emptyset$; define the for each node the highest existing index: $n^{max}(v_0) := 1$, $n^{max}(v) := 0 \qquad \forall v \neq v_0$

While $\mathcal{L}_{temp} \neq \emptyset$ and no label belonging to v_{K+1} was added to $\mathcal{L}_{perm}$, do:
  $L^{cur} = (c_T^{cur}, c_E^{cur}, v^{pre}, n^{pre}, v^{cur}, n^{cur})$:= the lexicographically
  smallest label in $\mathcal{L}_{temp}$.
  Remove L^{cur} from $\mathcal{L}_{temp}$ and add it to $\mathcal{L}_{perm}$.
  For all $v^{new} \in V$ such that $e := (v^{cur}, v^{new}) \in \vec{E}$ do:
    Compute $SOC^{cur} := SOC_S - c_E^{cur}$
    Compute $c_T^{new} := c_T^{cur} + c_T(e, t_S + c_T^{cur}, SOC^{cur})$
    Compute $c_E(e, t_S + c_T^{cur}, SOC^{cur})$ according to equation 4.10
    Compute $c_E^{new} := c_E^{cur} + c_E(e, t_S + c_T^{cur}, SOC^{cur})$
    Compute $n^{max}(v^{new}) := n^{max}(v^{new}) + 1$
    Compute $n^{new} := n^{max}(v^{new})$
    Create $L^{new} := (c_T^{new}, c_E^{new}, v^{cur}, n^{cur}, v^{new}, n^{new})$
    If $SOC_S - c_E^{new} > 0$, then:
      add L^{new} to $\mathcal{L}_{temp}$
    End if.
  End for.
End while.
If possible, return a label $\bar{L} \in \mathcal{L}_{perm}$ that belongs to node v_{K+1},
otherwise return „No feasible solution found“.

Figure 4.10: Pseudo-code of algorithm A

The result of these considerations is described by the pseudo-code which can be found in Figure 4.10. Algorithm A is based on „algorithm 1“ from (*99*), which can be understood as the straight-forward extension of Dijkstra's algorithm for the time-independent multicriteria case. From here on, this original algorithm is denoted as „Martins' algorithm“ (named after its inventor). The essential idea taken from Martins' algorithm is to use an extended type of labels. When applying Dijkstra's algorithm, labels contain information about the node to which they belong, the preceding node, and the costs for reaching the node to which the label belongs. At most one label is assigned to each node. It was stated in section 4.2 that for multicriteria SPPs, any non-dominated path can be a subpath of a time optimal path. Hence, several paths leading to the same node (which is not the destination node) may be relevant for finding eventually a time optimal solution. As each label can only encode one path, it is necessary to have the possibility to maintain several labels for each node. Martins' algorithm achieves this by assigning

indices to labels. All labels belonging to the same node are numbered consecutively by these indices („index 1“ is assigned to the first label, „index 2“ to the second, and so on). However, the existence of several labels per node and, along with that, the existence of several relevant paths leading to the same node, makes it insufficient to save only the information about the preceding node. It is inevitable to know which of the paths leading to the previous node causes the costs which are stored in the currently considered label. Thus, besides the preceding node, the index of the preceding label is also stored in each label. For the case of CSO, i.e., for the case of cost functions c_T and c_E, labels are defined as a 6-tuple, i.e., an ordered set consisting of six entries. A label $L := (c_T, c_E, v^{pre}, n^{pre}, v^{cur}, n^{cur})$ belonging to a node v^{cur} contains information about the time and energy-consumption costs that arise from the starting node to node v^{cur} on the path that is encoded by L. Moreover, it stores information which allows identifying the preceding label uniquely, i.e., the node v^{pre} to which the preceding label belongs and the corresponding label-index n^{pre}. Finally, due to notational reasons, information for describing the label itself, i.e., the node v^{cur} and the label index n^{cur}, are stored.

Now, algorithm A is applied to the small graph shown in Figure 4.3 in order to explain how it works and simultaneously to illustrate the idea of extended labels. Analogously to Dijkstra's algorithm, there is a set of labels $\mathcal{L}_{perm}$ and a set of labels $\mathcal{L}_{temp}$ used as storage for permanent and temporal labels, respectively. Table 4.1 displays the proceeding of algorithm A. As a is the

Algorithm A		
Iteration	$\mathcal{L}_{temp}$	$\mathcal{L}_{perm}$
	$L_a^1 := (0, 0\%, \emptyset, 0, a, 1)$	
It. 1	$L_b^1 := (1, 20\%, a, 1, b, 1)$, $L_c^1 := (1, 40\%, a, 1, c, 1)$	L_a^1
It. 2	L_c^1, $L_c^2 := (2, 50\%, b, 1, c, 2)$	L_a^1, L_b^1
It. 3	L_c^2 , $L_d^1 := (5, 90\%, c, 1, d, 1)$	L_a^1, L_b^1, L_c^1
It. 4	$L_d^2 := (4, 70\%, c, 2, d, 3)$, L_d^1	L_a^1, L_b^1, L_c^1, L_c^2
It. 5	L_d^1	L_a^1, L_b^1, L_c^1, L_c^2, L_d^2

Table 4.1: Proceeding of algorithm A for the example from Fig. 4.3

starting node, the first label which is created during the initialization is $L_a^1 := (0, 0\%, \emptyset, 0, a, 1)$. The first two entries, which encode the cumulated costs, clearly have to be equal to zero. Since there is no preceding node, entries three and four are filled with dummy-values. The last two entries are a consequence of the fact that this first label belongs to node a and that it is the first label assigned to node a. Node a is not the destination and with $L_a^1 \in \mathcal{L}_{temp}$, the set of temporal labels isn't empty. Thus, algorithm A enters the while-loop. Label L_a^1 is taken from the set of

temporal labels, defined as the currently considered label L^{cur} in line 2, and afterwards added to the set of permanent labels. Note that always the lexicographically smallest label is taken from $\mathcal{L}_{temp}$:

For two n-dimensional vectors $\hat{y} := (\hat{y}_1, \hat{y}_2, ..., \hat{y}_n)$, $\bar{y} := (\bar{y}_1, \bar{y}_2, ..., \bar{y}_n) \in \mathbb{R}^n$, vector $\hat{y}$ is denoted as **lexicographically** smaller than $\bar{y}$ if one of the following two conditions hold: Either $\hat{y} = \bar{y}$ or $\hat{y}_j < \bar{y}_j$ with $j := \min\{i : \hat{y}_i \neq \bar{y}_i,\ i\ \in \{1, ..., n\}\}$. This means that the first entries of a vector are most important for comparison. The definition is taken from section 5.1 in (*41*). One also writes $\hat{y} \leq_{lex} \bar{y}$.

For algorithm A, a label $\hat{L} := (\hat{c}_T, \hat{c}_E, \hat{v}^{pre}, \hat{n}^{pre}, \hat{v}^{cur}, \hat{n}^{cur})$ is called lexicographically smaller than a label $\bar{L} := (\bar{c}_T, \bar{c}_E, \bar{v}^{pre}, \bar{n}^{pre}, \bar{v}^{cur}, \bar{n}^{cur})$ if the accumulated costs encoded by $\hat{L}$ are lexicographically smaller[32] than the accumulated costs encoded by $\bar{L}$, i.e., if

$$(\hat{c}_T, \hat{c}_E) \leq_{lex} (\bar{c}_T, \bar{c}_E). \tag{4.38}$$

In line 5 of algorithm A, all neighbours of node v^{cur} are considered and labels for these nodes are created in lines 6 to 12 by adding the costs for the corresponding edges to the accumulated costs and by using label L^{cur} as predecessor. At this point, algorithm A differs significantly from Martins' algorithm. In contrast to Martins' algorithm, dominated labels are also added to $\mathcal{L}_{temp}$. It is worth mentioning that $n^{max}(v)$ denotes the highest index that has been assigned to a label which belongs to node v. Whenever a new label that belongs to $n^{max}(v)$ is generated, this number is increased by one (see line 10). By doing this, it can be ensured that each generated label can be uniquely identified by the node to which it belongs and by the index which is assigned to it. A further difference to Martins' algorithm is that algorithm A includes the path feasibility condition in line 13.

Note that the development of sets $\mathcal{L}_{perm}$ and $\mathcal{L}_{temp}$, which result when applying algorithm A to the graph from Figure 4.3, is shown in Table 4.1. The i-th row shows the situation after the while-loop has been executed the i-th time. Here, two iterations are remarkable: During the second iteration, i.e., when the label L_b^1 is added to the set of permanent labels, a second label belonging to node c is added to $\mathcal{L}_{temp}$. By following the preceding labels it can be seen that L_c^1 encodes path $[a, c]$, whereas L_c^2 encodes path $[a, b, c]$. The second interesting iteration is the last one, when the first label belonging to the destination node d is made permanent and algorithm A returns the time optimal and feasible path $[a, b, c, d]$. Then, according to line 1 of algorithm A, no more iterations are started and the algorithm terminates. This is also a difference to Martins' algorithm, which computes the whole set of Pareto optimal solutions by maintaining the

[32] According to the defintion taken from (*41*), a vector x is denoted as lexicographically smaller than a vector y, even if $x = y$. This also explains writing $\leq_{lex}$ and not $<_{lex}$ in equation 4.38.

while-loop in any case until set $\mathcal{L}_{temp}$ is empty. However, it is used that Martin's algorithm is a label-setting algorithm and that, due to this, the route search can be stopped as soon as the destination is reached, since computing one solution is assumed to be sufficient here.

On the basis of the pseudo-code of algorithm A, the following theorem can be shown (a corresponding proof can be found in appendix A):

Theorem 1. *Let a finite and directed graph $\vec{G} = (V, \vec{E})$, a starting node s, a destination node d, cost functions c_T and c_E (as described in section 4.1.2), and a starting state of charge SOC_S be given. Furthermore, let there be no cycle on $\vec{G}$ that leads to time costs of zero and let at least one path from s to d on $\vec{G}$ exist which is feasible under the given conditions. Then, algorithm A terminates with finding a label that encodes a time optimal and feasible s-d-path.*

According to Theorem 1, algorithm A is able to ensure feasible and time optimal solutions in a very general setting. Neither the FIFO-property for c_T, nor the cost consistency for c_E are required during the proof. Also the conditions concerning the graph are very weak, since the existence of an optimal solution, as well as the absence of zero-time cycles are, from a practical perspective, negligible restrictions. However, this flexibility causes high computational effort: With Martins' algorithm, algorithm A is based on a rather slow approach. Moreover, it even leaves out the deletion of dominated subpaths, a fact that raises computation times even more. On the other hand, it can be expected that, besides the premature termination of algorithm A when reaching the destination node, especially the feasibility condition in line 13 prunes the search space significantly. This is because the lexicographic selection of candidate labels in lines 2 to 3 ensures that algorithm A primarily constructs time minimal charging strategies. Such strategies naturally tend to suggest few and short charging processes and thus often violate the feasibility condition. As a result, many labels can be discarded early during the route search process. Still, even though it will not be explicitly tested within this thesis, the analyses of the properties of the considered cost functions in section 4.2 prompt that computation time does not allow applying algorithm A on large graphs.

Algorithm B: Modification of Algorithm A for Accelerated Computation

```
...
13      If L^new is not dominated by another label in L_temp or L_perm that belongs
14      to v^cur and if SOC_S − c_E^new > 0, then:
15          add L^new to L_temp and delete all labels belonging to v^cur in L_temp that
16          are dominated by L^new.
17      End if.
...
```

Figure 4.11: Pseudo-code of algorithm B as an extension of algorithm A

One possibility to counter this problem is to include the deletion of labels which encode dominated subpaths. The corresponding algorithm is here denoted with algorithm B. It results by replacing lines 13 to 15 in algorithm A by the pseudo-code stated in Figure 4.11. In this context, it has to be considered that new labels are not added to the set of temporary labels $\mathcal{L}_{temp}$ if they are dominated. Moreover, existing labels, i.e., labels which were already added to $\mathcal{L}_{temp}$ during previous iterations of the while-loop, are also deleted if they are dominated by a recently constructed label. Despite this modification, algorithm B proceeds analogously to algorithm

Algorithm B		
Iteration	$\mathcal{L}_{temp}$	$\mathcal{L}_{perm}$
	$L_a^1 := (0, 0\%, \emptyset, 0, a, 1)$	
It. 1	$L_b^1 := (1, 20\%, a, 1, b, 1)$, $L_c^1 := (1, 40\%, a, 1, c, 1)$	L_a^1
It. 2	L_c^1	L_a^1, L_b^1
It. 3	$L_d^1 := (5, 90\%, c, 1, d, 1)$	L_a^1, L_b^1, L_c^1
It. 4	$\emptyset$	L_a^1, L_b^1, L_c^1, L_d^1

Table 4.2: Proceeding of algorithm B for the example from Fig. 4.3

A. To illustrate this, Table 4.2, analogously to Table 4.1 for algorithm A, provides an overview of the iterations of algorithm B if it is applied to the example depicted in Figure 4.3. When comparing both tables, the first difference can be observed during the second iteration, where algorithm B, in contrast to algorithm A, does not add the dominated label L_c^2 to $\mathcal{L}_{temp}$. This fact eventually explains that label L_d^2 is not constructed. Hence, the optimal solution to the stated problem, which is encoded by L_d^2, is not computed. Even though deleting dominated labels during the route search leads to the already discussed loss of optimality for solutions generated by algorithm B, this proceeding still seems to be reasonable. If some strategy 1 leads to a certain location in less time and with a higher state of charge than a strategy 2, it appears to be reasonable to assume that strategy 1 is at least not much worse than strategy 2. Correspondingly, it can be expected that algorithm B in most cases computes the same or a comparably good solution as algorithm A. This conjecture is confirmed in (*69*). In this work, the author describes a case study, where both algorithms were compared with regard to computational effort and achieved solution qualities. The findings indicate that algorithm B leads in almost all cases to the same solution as algorithm A. A further clear advantage of algorithm B can be observed in Table 4.2: The number of iterations and of constructed labels is already lower for this very small example than for algorithm A. In (*69*), this observation is confirmed, too. The effect becomes even more significant with increasing graph size. Nevertheless, algorithm B is also not expected to be applicable for graphs of sizes which occur in practical applications.

However, algorithm B at least offers a perspective. One could, for instance, think of combining algorithm B with established speed-up methods for shortest path algorithms. More details about this will be given later on in chapter 9.

4.4 Model Assessment with Regard to Research Objectives

As mentioned, the introduced MDP is used as reference model in order to assess the formulation of the problem of finding optimal charging strategies as an SPP. It particularly allows identifying restrictions of other models with regard to RO 1a. Now, when comparing the MDP formulation from chapter 3 to the formulation as a deterministic SPP from chapter 4, then three major differences can be named: The first difference is that the set of possible charging decisions is no longer continuous. The original decision spaces $\mathcal{U}_k$ with $k \in V_D^{cs}$ (i.e., the decision spaces which refer to charging decisions) are replaced by a finite set of decision possibilities $\mathcal{U}_k^{\Delta}$. The second one is that there exist charging policies that cannot be represented by solutions of the deterministic SPP. The last difference is that, for the MDP, a generic description of performance measure f is given. For the SPP, on the contrary, f is specified rather concretely as a function depending on deterministic edge cost functions c_T and c_E. Each of these differences influence up to which degree the requirements defined by ROs 1a to 1c can be fulfilled by the new problem formulation.

RO 1a: The MDP allowed modelling the problem of finding optimal charging strategies realistically and very generally. The above mentioned differences between the MDP and the deterministic SPP, however, have some influence on the SPP's ability to achieve the same. In this context, it can be expected that the influence of discretized decision stages is rather small. Reasons for this assumption have been provided in section 4.1.1. The author also assumes that the SPP's missing ability to represent all possible charging policies via paths is not very relevant, at least from a practical point of view. The main reason for this conjecture is that in practice, a navigation system can be expected to recompute charging strategies during trips. Therefore, the driver is not bound to the initially recommended sequence of route and charging instructions. If necessary, these recommendations can be adjusted to react to recent incidents. A regular updating of charging strategies gets very close to the idea of charging policies. There may still be some situations in which such an on-trip recomputation of charging strategies does not achieve the same results as a charging policy, but the author assumes this to be very unlikely in reality.

In contrast to discretized decision spaces and the restriction to compute charging strategies instead of charging policies, the suggested concretizations are assessed to be very critical with regard to RO 1a. The main issue is the assumption of deterministic travel times and energy consumption. Due to individual driving style and the influence of non-recurrent traffic incidents, such as accidents, it is not realistic to expect travel time and energy consumption predictions

to be absolutely correct. Particularly if the realized energy consumption only slightly exceeds the energy consumption which is presumed according to $\grave{c}_E$, i.e., according to the deterministic model, BEVs may run out of energy even though following charging strategies which are assumed to be feasible. The deterministic SPP does correspondingly not satisfy the requirements that need to be fulfilled for an implementation in practice.

RO 1b: The definition of f which is suggested in section 4.1.3 basically includes both efficiency and, up to some degree, reliability. Efficiency is achieved by penalizing charging strategies which cause high travel times, reliability by penalizing charging strategies that lead to an empty battery. On the other hand, the suggested framework has no possibility to handle uncertainties. It suffers in this context from the same problems as former models for CSO (compare the literature review in section 2.1.3). Thus, the achieved level of reliability is unable to mirror the original intention of RO 1b.

RO 1c: The discretization of the decision spaces makes it possible to transform the MDP to an SPP, which again makes it possible to handle the problem numerically. The reduction to a deterministic framework reduces the expected computational effort for solving the problem. The analyzes conducted in section 4.2, on the other hand, suggest that solving the introduced deterministic SPP is still expensive. Nevertheless, the developed algorithm B probably offers, in combination with additional speed-up techniques, a possibility to compute near optimal charging strategies even on graphs that are large enough to represent the road networks of whole regions or countries.

Conclusions: In conclusion, the introduced deterministic SPP is not able to achieve RO 1a. Correspondingly, an adjustment of this model has to be developed. This reformulation has to allow taking uncertainty into account. It is, furthermore, important to ensure that the adjusted problem formulation does not cause a significant increase of computation times.

4.5 Summary

The suggested interpretation of CSO as an MDP, which was described in chapter 3, is generic, but can hardly be addressed numerically. Hence, an alternative formulation as an SPP was introduced in chapter 4. SPPs consist of two main components: A graph and an objective function. The construction of graph $\vec{G}_D^{\Delta}$, which is based on the decision graph $\vec{G}_D$ from chapter 3, was carried out in section 4.1.1. In this context, a discretization of the originally continuous decision spaces $\mathcal{U}_k$ became necessary. Moreover, it turned out that $\vec{G}_D^{\Delta}$ allows associating paths with charging strategies, but not with arbitrary charging policies. To be able to rate, compare and hence optimize such strategies, a rating criterion was introduced. For this purpose,

two deterministic edge cost functions, assigning energy consumption costs and time costs, respectively, to edges, were described in section 4.1.2. Energy consumption costs were used to introduce the notion of feasible charging strategies. These are strategies which allow reaching the destination without running out of energy. Time costs were used to actually rate charging strategies. For the final formulation of the problem of finding optimal charging strategies as a deterministic SPP, both aspects (travel time and feasibility) were taken into account: Charging strategies leading to low travel times are preferred, but infeasible charging strategies are directly excluded from consideration. The resulting problem formulation can be interpreted as a (deterministic) constrained SPP.

The properties of the derived SPP were analyzed in section 4.2. This was necessary to understand how shortest path algorithms behave when being applied to the problem. Based on this analysis, it turned out that the described SPP is at least $\mathcal{NP}$–complete. Moreover, Bellman's optimality principle does not hold. As a consequence, the time necessary for computing optimal solutions is expected to rise very quickly with the size of graph $\vec{G}_D^{\Delta}$. Nevertheless, two algorithms for solving the problem were suggested and discussed in section 4.3. The first one guarantees optimality of generated paths. The other one ignores the absence of Bellman's optimality principle. This allows improving computation times at the cost of risking suboptimal solutions. Finally, in section 4.4, the developed SPP was analyzed with regard to ROs 1a to 1c. In contrast to the MDP from chapter 3, achieving RO 1a was identified to be critical. The main issue is the missing possibility to take the existence of uncertainties into account. Thus, it was concluded that the proposed formulation as a constrained SPP needs further adjustments.

Chapter 5

Charging Strategy Optimization as a Shortest Path Problem under Uncertainty

The formulation of CSO as a deterministic SPP significantly simplifies the former formulation as a sequential MDP. The discretization of the decision spaces, as well as the missing possibility to represent decision policies were mentioned. However, the suggested reduction from a stochastic to a deterministic system is most critical. If realized energy consumption only slightly exceeds the consumption which is presumed within the model, then following feasible charging strategies may still lead to an empty battery. As a consequence, an adjusted problem formulation is necessary, which achieves robustness against uncertainties, especially uncertainties of energy consumption predictions. Such a reformulation is provided in the following. In this context, over-cautious strategies also need to be avoided. Otherwise, too many and too long rechargings are suggested or it is stated in situations, in which the considered BEV could be used safely for the intended trip, that a reliable arrival cannot be guaranteed.

Chapter 5 is structured as follows: In section 5.1, edge costs are modeled as random variables and notations are adjusted correspondingly. Based on this, an exemplary formulation of the problem of finding optimal charging strategies as a stochastic SPP is stated in section 5.2. It is argued that this formulation allows handling uncertainty adequately, but at the same time causes a significant increase of computation times. Since solving the suggested deterministic problem is already expected to cause high computational effort, any further negative impact on computation times has to be avoided. Consequently, an alternative problem formulation is proposed in section 5.3. The original deterministic framework is maintained, but an extended interpretation of the feasibility probability is introduced, where charging strategies are

excluded from consideration as soon as states of charge fall below a certain threshold. Different approaches for defining this threshold dynamically along paths are suggested and their algorithmic implementation are discussed.

5.1 Non-deterministic Edge Costs

First, the problem of finding optimal charging strategies is reformulated in such a way that non-deterministic edge costs can be represented. For this purpose, let it be assumed that two probability density functions $g_T(e, t, \omega_T)$ and $\grave{g}_E(e, t, \omega_E)$ are given. Function $g_T(e, t, \omega_T)$ describes the distribution of the travel time which is necessary for passing an edge $e = (v_i, v_j)$, when starting at time t at node v_i. Analogously to chapter 4.1.2, ω_T is again interpreted as an object which describes the available information about factors which influence travel time, such as traffic conditions or driving behavior. Also information which allows describing correlations to other edges may now be included in ω_T. Function $\grave{g}_E(e, t, \omega_E)$ represents the distribution of the energy consumption which is necessary for passing edge e, when starting at time t at node v_i. Object ω_E describes factors that influence energy consumption, such as the current state of charge, vehicle specific parameters (*57*), traffic conditions (*86*) (*123*), driving behavior (*57*), weather conditions (*66*), and road steepness (*92*). Note that graph $\vec{G}_D^{\Delta}$ can remain the same as for the deterministic setting from chapter 4.

In the following, a function $\grave{C}_E$ representing energy consumption and a function C_T representing time consumption are defined. Their dependency on objects ω_T and ω_E is again not explicitly considered within the notation to keep the notation simpler. Functions $\grave{C}_E$ and C_T assign random variables to edges[33]:

$$C_T(e, t, SOC) \sim g_T(e, t, SOC) \tag{5.1}$$

$$\grave{C}_E(e, t) \sim \grave{g}_E(e, t) \tag{5.2}$$

It is worth mentioning that $C_T(e, t, SOC)$ and $\grave{C}_E(e, t)$ are random variables, whereas C_T and $\grave{C}_E$ are functions assigning random variables to edges in dependency of time or the state of charge. In a next step, analogously to chapter 4, energy consumption distributions are adjusted in such a way that unrealistic states of charge are avoided (compare equation 4.10):

$$C_E(e, t, SOC) := \begin{cases} SOC - 1 & \text{if } SOC - \grave{C}_E(e, t) > 1 \\ SOC & \text{if } SOC - \grave{C}_E(e, t) < 0 \\ \grave{C}_E(e, t) & \text{else} \end{cases} \tag{5.3}$$

[33] "$X \sim g$" means that random variable X is distributed according to the probability density function g or cumulative distribution function g, respectively.

Note that typically significant spatial correlations exist between the cost distributions of different edges (*136*). Hence, the assumption that accurate probability distributions of edge travel times and edge energy consumption are known for all relevant edges of a graph which represents a realistic road network is a very strong requirement (*112*).

5.2 Rating Paths under Random Edge Costs

Having defined edge costs as random variables, some resulting issues shall be described within the current section. To achieve this, the following formulation of a stochastic SPP in the context of charging strategies is considered:

$$\begin{aligned} \min \quad & \mathbb{E}[F_M(P, t_S, SOC_S)] \\ \text{subject to} \quad & P \text{ is a } v_0\text{-}v_{K+1}\text{-path on } \vec{G}_D^{\Delta} \end{aligned} \tag{5.4}$$

Variables t_S and SOC_S again denote the starting time and starting state of charge, respectively. Performance measure F_M is understood to penalize situations in which the BEV runs out of energy:

$$F_M(P, t_S, SOC_S) := \begin{cases} C_T(P, t_S, SOC_S) & \text{if } P \text{ does not lead to an empty battery} \\ M & \text{else} \end{cases} \tag{5.5}$$

The cumulated time costs of a path P are denoted by $C_T(P, t_S, SOC_S)$, which is again a random variable. Note that M is a large positive number. This ensures that the expected time costs of any path are well-defined, which may not be the case if M was replaced by ∞. Applying the expected value operator, i.e., to consider $\mathbb{E}[F_M]$ instead of F_M as the objective function, is necessary to ensure that the objective function returns values in $\mathbb{R}$.

It has already been stated in the state of the art in chapter 2 that computing shortest paths on the basis of randomly distributed edge costs leads to an increase of computation times in comparison to problem formulations where deterministic edge costs are presumed. Two main reasons for this are typically mentioned in literature: First, for many stochastic SPPs, again Bellman's optimality principle does not hold. This is the case, as soon as the objective function value which is assigned to a path cannot be expressed as the sum of the ratings of its edges. This can happen if, for instance, edge costs are correlated (*136*). The consequence of the absence of Bellman's optimality principle is that, as mentioned in section 4.2.3 when considering general time dependent edge cost functions, many labels need to be created and managed during the route search. However, for CSO, Bellman's optimality principle has already been lost in the deterministic case. Due to this, it could be expected that considering randomly distributed

edge costs do not lead to a significant increase of computation times in comparison to the deterministic case. To explain this conjecture more clearly: When applying algorithm A to the deterministic SPP 4.32, then in fact all available decision possibilities are considered during the route search as long as the feasibility condition holds. There is no intelligence included in algorithm A that would allow reducing the search space. Thus, since the considered graph $\vec{G}_D^{\Delta}$ and along with it the set of possible decisions remains the same for the suggested stochastic SPP, the search space is not enlarged. Actually, only the rating scheme is different. Consequently, algorithm A (and algorithm B, too) probably does not need much more time to find solutions for the stochastic SPP than for the deterministic SPP.

The second source of increased computational effort occurs whenever cost-dependent edge costs are considered. A typical example of cost-dependent costs are time costs that depend on arrival times. The critical aspect is that for general edge cost distributions, it is not possible to derive a closed form probability distribution of path costs (*136*). This means, for example, that it is in general not possible to analytically derive a distribution $g_T(P, t_S, \omega_T)$ with $P = [v_1, ..., v_Q]$, even if the edge cost distributions $g_T((v_i, v_{i+1}), t, \omega_T)$ are known for all possible arrival times t and all relevant edges (v_i, v_{i+1}). Instead, path cost probability distributions typically need to be estimated numerically by solving a sequence of recursively defined integrals. For the example of time-dependent travel time costs, recursively defined integrals are caused by the need to compute arrival time distributions based on travel time distributions of previously passed edges. The consequence is that simply rating single paths can lead to huge computational effort. An example illustrating this fact can be found in appendix B. This example actually shows that even in a very simple setting, in which the random edge costs C_T and $\grave{C}_E$ do neither depend on arrival times, nor on the state of charge, the effort for computing the costs of a path rises quickly with the number of edges of the path. Therefore, the already high computational effort for solving the deterministic SPP from chapter 4 would be increased even further if edge costs are considered as random variables. This considerations suggest that the problem of finding optimal charging strategies should not be modeled as a stochastic SPP. Instead, it is probably more meaningful to adjust the (up to this point) risky deterministic SPP in such a way that uncertainties can be handled.

5.3 The Concept of Energy Buffers

According to section 4.2, the interpretation of CSO as a deterministic SPP already leads to significant computational effort. Hence, despite the goal to achieve robustness against uncertainties (especially against the uncertainty of energy consumption predictions), computational effort should not be increased any more – or at least not significantly. At the same time, the current version of the feasibility condition is considered to be very risky. Issues may occur whenever states of charge only slightly higher than zero are expected, i.e., whenever for some path $P = [v_1, ..., v_Q]$ the accumulated energy consumption costs $c_E(P_{1:i}, t_S, SOC_S)$ from node v_1 to node v_i almost reach the starting state of charge SOC_S. In such situations, the

corresponding path is considered to be feasible, but if realized energy consumption exceeds the predicted energy consumption only marginally, then the BEV may run out of energy. Due to this, a modified version of feasibility is suggested to reduce this risk:

A strategy associated with a path $P = [v_1, ..., v_Q]$ is denoted as **energy secure** with respect to (w.r.t.) SOC_{min} if

$$SOC_S - c_E(P_{1:i}, t_S, SOC_S) > SOC_{min}(\omega) \quad \forall i \in \{2, 3, ..., Q\}. \tag{5.6}$$

In this context, SOC_{min} is a real-valued function. It is from here on denoted as **energy buffer function** and the values it returns as **minimal energy buffers**. Function SOC_{min} depends on a set of (not yet specified) variables and parameters ω. Condition 5.6 means that a strategy is denoted as energy secure as long as the predicted state of charge never falls below the lower bound defined by SOC_{min}. It is important to mention that whenever it is referred to the „predicted“ state of charge or the „predicted“ energy consumption, the values resulting from considering edge cost functions $\grave{c}_E$ and c_T are meant, i.e., the values resulting according to the framework from chapter 4. The bigger the value $SOC_{min}(\omega)$ is, the lower the risk of running out of energy becomes for charging strategies which are energy secure w.r.t. $SOC_{min}(\omega)$. Assuming that SOC_{min} returns independently of ω a static value of, for example, five percent ensures that the destination is reached as long as the realized accumulated energy consumption never exceeds the predicted accumulated energy consumption by more than five percent of the capacity of the battery. Note that the idea of energy- or fuel-buffers, respectively, has already been considered in (*82*) and (*141*). However, only static buffers have been suggested in these prior works. For the described research, the size of the energy buffer is intended to be only as big as necessary. This means, for instance, that the size of the energy buffer is rather big in situations in which energy consumption predictions are expected to be less reliable. On the other hand, in situations in which it is very unlikely that energy consumption is underestimated significantly, the buffer should be chosen smaller. The ability of an energy buffer function to adequately adjust the size of the minimal energy buffer is from here on denoted as **adaptivity**.

Replacing the feasibility condition with the energy security condition can be expected to cause not much additional computational effort when solving the corresponding SPP. In fact, additional computation times result primarily from computing SOC_{min}. If evaluating this function does not become too expensive, the corresponding effects should be negligible. A clear drawback of the suggested adjustment, particularly in comparison to the formulation as a stochastic SPP in section 5.2, is that uncertainties of travel time predictions and, along with this, their impact on energy consumption are not considered at all.

In the following, possible definitions of function SOC_{min} and parameter set ω are introduced

and discussed to illustrate this yet rather abstract concept. However, before this is done, one property is postulated, which any function SOC_{min} is assumed to fulfill: SOC_{min} is intended to avoid that incorrectly predicted energy consumption causes an empty battery. As soon as the BEV reaches a charging station, this cannot happen until the BEV again leaves the charging station. Thus, SOC_{min} is set equal to zero for edges which represent parts of a charging process.

5.3.1 Relative Energy Buffer

One of the most intuitive ideas for defining an energy buffer function is to use a certain percentage of the predicted energy consumption for buffering. This type of function is from here on denoted with $SOC^{r,z}_{min}(\omega)$ ("r" for "relative"). Parameter $z \geq 0$ defines the percentage according to which the size of the energy buffer is quantified. In Figure 5.1, the pseudo-code of a corresponding algorithm for computing $SOC^{r,z}_{min}$ along a path can be found. Based on this

Algorithm for Computing Relative Energy Buffers along a Path

Input: A directed graph $\vec{G}^{\Delta}_{D}$, a path $P = [v^P_1, v^P_2, ..., v^P_N]$ on $\vec{G}^{\Delta}_{D}$ with $N \in \mathbb{N}$, a node $v^P_{N^*}$ for which the minimal energy buffer has to be computed, a starting time t_S, costs functions c_T and $\grave{c}_E$ as described before, a starting state of charge SOC_S, a positive number z

Initialization: $SOC^{old}_{min} := 0$, $n := 2$

$t^{n-1} := t_S$
$SOC^{n-1} := SOC_S$
While $n \leq N^*$:
    If edge $e_n := (v^P_{n-1}, v^P_n)$ represents a road segment:
        $SOC^{r,z}_{min}(e_n, t^{n-1}, SOC^{old}_{min}; z) := SOC^{old}_{min} + z \cdot \mid \grave{c}_E(e_n, t^{n-1}) \mid$
    else (i.e., if e_n is part of the charging process):
        $SOC^{r,z}_{min}(e_n, t^{n-1}, SOC^{old}_{min}; z) := 0$
    End if.
    $SOC^{old}_{min} := SOC^{r,z}_{min}(e_n, t^{n-1}, SOC^{old}_{min}; z)$
    Compute $c_E(e_n, t^{n-1}, SOC^{n-1})$ according to equation 4.10
    $SOC^n := SOC^{n-1} - c_E(e_n, t^{n-1}, SOC^{n-1})$
    $t^n := t^{n-1} + c_T(e_n, t^{n-1}, SOC)$
    $n := n + 1$
End while.
$SOC^{r,z}_{min} := SOC^{old}_{min}$.
Return $SOC^{r,z}_{min}$.

Figure 5.1: Pseudo-code to compute energy buffer $SOC^{r,z}_{min}$ along a path.

pseudo-code, the set ω consists of the currently considered edge $e_n = (v^P_{n-1}, v^P_n)$, the time t^{n-1} and the state of charge SOC^{n-1} when reaching the start of this edge, and the energy

buffer SOC_{min}^{old} that is assumed to be necessary until node v_{n-1}^{P} (which is the start of edge e_n) is reached. It can be observed that $SOC_{min}^{r,z}$ grows along sequences of edges which represent road segments. For each road segment e_n which is passed, a certain percentage of the corresponding predicted energy consumption $\grave{c}_E(e_n, t^{n-1})$ is added to the energy buffer (see line 6 in 5.1). The minimal energy buffer is set back to zero whenever an edge representing a part of a charging process is passed. Note that taking the absolute value of the predicted energy costs (in line 6) ensures that negative edge costs do not reduce the size of the buffer. Instead it grows also if energy gains are predicted due to recuperation. This is done to compensate for unexpectedly low energy gains.

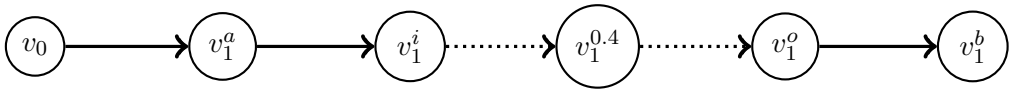

nodes	v_0	v_1^a	v_1^i	$v_1^{0.4}$	v_1^o	v_1^b
SOC [%]	70	40	10	40	40	10
edge leading to node		(v_0, v_1^a)	(v_1^a, v_1^i)	$(v_1^i, v_1^{0.4})$	$(v_1^{0.4}, v_1^o)$	(v_1^o, v_1^b)
$SOC_{min}^{r,z}$ [%] for $z = 1/6$		5	10	0	0	5

Figure 5.2: Development of the expected state of charge and the relative energy buffer for $z = 1/6$ along an exemplary path.

To explain how $SOC_{min}^{r,z}$ works, Figure 5.2 shows the development of $SOC_{min}^{r,z}$ along an example path $P := [v_0, v_1^a, v_1^i, v_1^{0.4}, v_1^o, v_1^b]$, i.e., for a charging strategy which suggests charging at charging station 1 up to a state of charge of 40 percent. For simplicity, it is assumed that energy consumption $\grave{c}_E(e, t)$ is equal to 30 percent for any edge which embodies a road segment, independently of the arrival state of charge or the arrival time. Furthermore, a z-value of $1/6$ is considered and a starting state of charge of 70 percent. The table shown at the bottom of Figure 5.2 provides information about the development of the predicted state of charge SOC (when arriving at the corresponding nodes) and about the minimal energy buffer $SOC_{min}^{r,z}$, which describes the state of charge which has to remain after passing the corresponding edge. The SOC-values after passing edges representing road segments result directly by subtracting 30 percent from the state of charge at the start of the edge. The SOC–values at nodes $v_1^{0.4}$ and v_1^o are computed according to section 4.1.2 and simply show a recharging up to 40 percent. The values of $SOC_{min}^{r,z}$ are computed according to the pseudo-code given in Figure 5.1. Based on the stated values of z and $\grave{c}_E(e, t)$, the minimal energy buffer increases with each passed road segment by five percent ($= z \cdot \mid \grave{c}_E(e, t) \mid$). However, it is instantly reduced to zero percent as soon as an edge that represents a part of a charging process is passed. As a consequence, it can be observed that the energy buffer increases until a charging process is conducted at a charging station. Afterwards, the buffer starts increasing again. The idea behind this is that

between two successive charging processes, uncertainty can be assumed to increase along with the covered distance[34]. However, as soon as a charging process is completed, the resulting state of charge is known. It is defined by the considered path, i.e., by the considered charging strategy itself, and it is independent of previous energy consumption – always assuming that the charging station can at least be reached. Consequently, the energy buffer can be reset to zero at charging stations. This also avoids that energy buffers become extremely big if paths are very long and several charging stops are necessary. If the energy buffer were not regularly reset to zero, relative energy buffers would increase further and further. Consequently, in many cases no energy secure charging strategy could be provided for long-distance trips due to the high requirements concerning the size of the energy buffer. This would not be reasonable.

Note that if the energy consumption for driving from the lastly visited charging station to the currently visited charging station has been underestimated, then the time consumption caused by the suggested charging process increases. If it has been overestimated, then charging times are lower than expected. Since energy consumption is assumed to be time-dependent, this may also have impact on the accuracy of energy consumption estimations for the following edges. However, as already mentioned, the effect of incorrectly predicted arrival times on the uncertainty of energy consumption predictions won't be taken into account by any of the suggested energy buffer functions.

Its growth along edges leads to the fact that $SOC_{min}^{r,z}$, in contrast to energy or time consumption, does not only depend on the currently considered edge e_n, the time t^{n-1}, and the state of charge SOC^{n-1} when reaching the start of this edge. Moreover, also the old energy buffer SOC_{min}^{old} needs to be included. This means that $SOC_{min}^{r,z}$ always has to be computed along whole paths and not for each edge separately. Hence, in order to adjust algorithms A and B in such a way that the concept of energy buffers is applied, it is not sufficient to replace the feasibility condition by the energy security condition. Moreover, the definition of labels has to be extended again. The pseudo-code in Figure 5.3 shows how this can be done. The suggested algorithm is denoted as algorithm A-2. It is a modified version of algorithm A. Instead of the feasibility condition, now the energy security condition can be found (see line 14). A further difference to the original version of algorithm A in Figure 4.10 is that each label contains seven instead of six values. The size of the „old“ energy buffer is additionally stored. Otherwise, the computation of $SOC_{min}^{r,z}$ in line 10 of algorithm A-2 could not be executed. The computational effort for applying algorithm A-2 instead of A remains almost unaltered. Additional effort is solely caused by evaluating the minimal energy buffer function. For the case of $SOC_{min}^{r,z}$, this is not expensive.

[34]Here, increasing uncertainty means that a deviation from the deterministic energy consumption costs of (for instance) five percent of the maximal battery capacity is more likely to happen on a 100 kilometer trip than on a 10 kilometer trip.

Algorithm A-2: Finding Optimal Charging Strategies

Input: A directed graph $\vec{G}_D^{\Delta} = (V_D^{\Delta}, \vec{E}_D^{\Delta})$, a starting node v_0, a destination node v_{K+1}, a starting time $t_S := 0$, cost functions c_T and $\grave{c}_E$ as described above, a starting state of charge SOC_S, a positive number z

Initialization: Create label $L = (0, 0\%, \emptyset, 0, v_0, 1)$ for node v_0. Define set of temporal labels $\mathcal{L}_{temp} := \{L\}$ and set of permanent labels $\mathcal{L}_{perm} := \emptyset$; define for each node the highest existing index: $n^{max}(v_0) := 1$, $n^{max}(v) := 0 \qquad \forall v \neq v_0$

1 While $\mathcal{L}_{temp} \neq \emptyset$ and no label belonging to v_{K+1} was added to $\mathcal{L}_{perm}$, do:
2 $L^{cur} = (c_T^{cur}, c_E^{cur}, SOC_{min}^{old}, v^{pre}, n^{pre}, v^{cur}, n^{cur})$:= the lexicographically
3 smallest label in $\mathcal{L}_{temp}$.
4 Remove L^{cur} from $\mathcal{L}_{temp}$ and add it to $\mathcal{L}_{perm}$.
5 For all $v^{new} \in V$ such that $e := (v^{cur}, v^{new}) \in \vec{E}$ do:
6 Compute $SOC^{cur} := SOC_S - c_E^{cur}$
7 Compute $c_T^{new} := c_T^{cur} + c_T(e, t_S + c_T^{cur}, SOC^{cur})$
8 Compute $c_E(e, t_S + c_T^{cur}, SOC^{cur})$ according to equation 4.10
9 Compute $c_E^{new} := c_E^{cur} + c_E(e, t_S + c_T^{cur}, SOC^{cur})$
10 Compute $SOC_{min}^{new} := SOC_{min}^{r,z}(e, t_S + c_T^{cur}, SOC_{min}^{old}; z)$
11 Compute $n^{max}(v^{new}) := n^{max}(v^{new}) + 1$
12 Compute $n^{new} := n^{max}(v^{new})$
13 Create $L^{new} := (c_T^{new}, c_E^{new}, SOC_{min}^{new}, v^{cur}, n^{cur}, v^{new}, n^{new})$
14 If $SOC_S - c_E^{new} > SOC_{min}^{new}$, then:
15 add L^{new} to $\mathcal{L}_{temp}$
16 End if.
17 End for.
18 End while.
19 If possible, return a label $\bar{L} \in \mathcal{L}_{perm}$ that belongs to node v_{K+1},
20 otherwise return "No feasible solution found".

Figure 5.3: Pseudo-code of algorithm A-2

Note that algorithm B can be modified analogously, leading to algorithm B-2. Moreover, function $SOC_{min}^{r,z}$ in line 10 can be replaced by other energy buffer functions. Further examples for such functions will be given in the following sections. For some of these functions, even more information will be necessary, making further extensions of the definition of labels necessary.

5.3.2 Quantile-based Approach

Let it be assumed that besides predicted edge costs $\grave{c}_E(e,t)$, also energy consumption distributions $\grave{g}_E(e,t)$ of variables $\grave{C}_E(e,t)$ are known[35]. Then, function $SOC_{min}^{q,\alpha}(\omega)$ („q“ for „quantile“) is defined for some $\alpha \in [0,1]$ as the sum of the differences between the α-quantiles of the random edge costs, and the predicted edge costs. Function $SOC_{min}^{q,\alpha}$ is from here on denoted as quantile-buffer function. The set of input quantities ω remains the same as for relative energy buffers (location, arrival time, state of charge, former energy buffer). The pseudo-code for computing $SOC_{min}^{q,\alpha}$ results if line 5 of the pseudo-code in Figure 5.1 is replaced by lines 5 to 7 from Figure 5.4 (and z is replaced by α for the remaining lines). Analogously to $SOC_{min}^{r,z}$, function $SOC_{min}^{q,\alpha}$ grows along edges representing road segments and is set equal to zero as soon as a charging station is reached. Note that in the right-hand side of the assignment in line 7, the energy buffer does not get reduced if q_α is smaller than the corresponding predicted edge costs. Besides replacing $SOC_{min}^{r,z}$ by $SOC_{min}^{q,\alpha}$ in algorithm A.2, no more adjustments are necessary for using algorithm A-2 to compute charging strategies which are energy secure w.r.t. to $SOC_{min}^{q,\alpha}$.

Algorithm for Computing Quantile-based Energy Buffers

```
4 | ...
5 |     Compute ċ_E^n := ċ_E(e_n, t^{n-1})
6 |     Compute q_α := α-quantile of random variable Ċ_E(e_n, t^{n-1})
7 |     SOC_min^{q,α}(e_n, t^{n-1}, SOC_min^old; α) := SOC_min^old + max{0, q_α − ċ_E^n}
8 | ...
```

Figure 5.4: Pseudo-code to compute minimal energy buffer for an edge.

Parameter α allows adjusting the sizes of the energy buffers resulting from functions $SOC_{min}^{q,\alpha}$. Obviously, higher values of α lead to bigger energy buffers and thus to more reliability. In this context, it has to be mentioned that $1-\alpha$ does not describe the probability of running out of energy for a charging strategy which is energy secure w.r.t. $SOC_{min}^{q,\alpha}$. This is a consequence of the occurring differences between realized energy consumption and the predicted energy consumption. Hence, the real state of charge may not develop as predicted. The consequence is that following a charging strategy and charging up to a certain recommended state of charge may take more or less time than originally expected. Along with that, the time at which further edges are reached change. Therefore, possibly not the correct probability density function $\grave{g}_E(e,t)$, which depends on this arrival time, is considered when computing $SOC_{min}^{q,\alpha}$. Along with this, even setting α equal to 1.0 does not ensure an absolutely save arrival.

[35] The predicted values $\grave{c}_E(e,t)$ are typically assumed to be equal to the expected value of $\grave{C}_E(e,t)$.

5.3.3 Trajectory Buffer

In literature, predicting the energy consumption a BEV needs to pass a specific road segment is typically done in two steps (*74*) (*86*) (*90*) (*123*): First, one or more potential driving trajectories[36] are predicted based on available information about, for instance, prevailing traffic conditions or historical traffic data. Second, a microscopic energy consumption model is applied to these driving trajectories to receive energy consumption values. Within a deterministic framework – and the SPP that results from including the energy security condition remains a deterministic SPP, even though uncertainties can be handled up to some degree – it is often assumed that one unique driving trajectory exists and that it can be predicted precisely. This is a strong presumption. Driving trajectories depend on some highly dynamic and hardly measurable factors, such as traffic conditions and the driver's driving style. Hence, instead of predicting solely one trajectory and hoping that it will mirror the future reality perfectly, it seems more expedient to generate a whole set of reasonable driving trajectories. Such a set of trajectories can then be applied to produce a set of corresponding energy consumption values. In the following, this set of energy consumption values is considered to estimate the maximal possible energy consumption. The difference between this estimated maximal possible energy consumption and the predicted energy consumption is then used as the energy buffer.

Before such an energy buffer function can be defined, some preparatory notation concerning trajectories is introduced. Let from here on be assumed that for any edge e and any time t, a set of $NT+1$ auxiliary trajectories can be computed. NT is a natural number and the corresponding driving trajectories are denoted by $T^{nt}(e,t)$ with $nt \in \{0,1,...,NT\}$. It is assumed that always the same nt auxiliary trajectories are assigned to a tuple (e,t). The travel time that results from a trajectory $T^{nt}(e,t)$ is denoted by $c_T(T^{nt}(e,t))$. Analogously, it is assumed that for any path $P = [v_1^P, ..., v_N^P]$ with $N \in \mathbb{N}$, a set of auxiliary trajectories $\{T^{nt}(P,t_S)\}_{nt=0,...,NT}$ can be computed. For the proceeding, it is not important how these trajectories are generated[37], but it is essential that for all $nt \in \{0,1,...,NT\}$, trajectory $T^{nt}(P,t_S)$ is equal to the concatenation of the trajectories $T^{nt}(e_n, t_S + c_T(T^{nt}(P_{1:n-1}, t_S)))$. These are the trajectories belonging to edges $e_n = (v_{n-1}^P, v_n^P)$ of path P. This postulation allows computing auxiliary trajectories $T^{nt}(P,t_S)$ step-wise along the edges of path P, which is of relevance when computing trajectories along paths during route search. Besides the possibility to compute sets of reasonable trajectories, it is assumed that a microscopic version of energy consumption model $\grave{c}_E$ is given. It assigns energy consumption values to edges in dependency of driving trajectories:

$$\grave{c}_E(e,t,T^{nt}(e,t),\omega_E) \quad \forall e \in \vec{E}_D^{\Delta},\ \forall t \geq t_S. \tag{5.7}$$

[36] A driving trajectory describes the location of a vehicle depending on time. Typically, a driving trajectory is given as a sequence of points $\{(t^k, x^k)\}_{k=1,2,...,K}$, where x^k refers to a location and t^k refers to a point in time.

[37] A possible procedure for the generation of such sets of driving trajectories will be discussed in chapter 6 in detail.

Here, ω_E again abstractly denotes a set of additional factors (for instance, outdoor temperature), which are considered for the computation of energy consumption[38]. As was done in previous chapters and sections, ω_E is left out in the following.

Algorithm for Computing Relative Energy Buffers along a Path

Input: A directed graph $\vec{G}_D^{\Delta}$, a path $P = [v_1^P, v_2^P, ..., v_N^P]$ on $\vec{G}_D^{\Delta}$ with $N \in \mathbb{N}$, a node $v_{N^*}^P$ for which the minimal energy buffer has to be computed, a starting time t_S, costs functions c_T, $\grave{c}_E$ and c_E as described before, a starting state of charge SOC_S, a number $NT \in \mathbb{N}_{\geq 2}$

Initialization: $n = 2$

$t_{pre}^{n-1} := t_S$, $t_{nt}^{n-1} := t_S \quad \forall nt \in \{0, 1, ..., NT\}$
$SOC_{pre}^{n-1} := SOC_S$, $SOC_{nt}^{n-1} := SOC_S \quad \forall nt \in \{0, 1, ..., NT\}$
While $n \leq N^*$:
  If edge $e_n := (v_{n-1}^P, v_n^P)$ represents a road segment:
    Compute $c_T^n := c_T(e_n, t_{pre}^{n-1})$
    Compute $\grave{c}_E^n := \grave{c}_E(e_n, t_{pre}^{n-1})$
    Compute c_E^n based on $\grave{c}_E^n$ and SOC_{pre}^{n-1}
    Compute $SOC_{pre}^n := SOC_{pre}^{n-1} - c_E^n$
    Compute $t_{pre}^n := t_{pre}^{n-1} + c_T^n$
    For $nt = 0$ to NT
      Generate driving trajectory $T^{nt}(e_n, t_{nt}^{n-1})$
      Compute travel time $c_T^{n,nt}$ from $T^{nt}(e_n, t_{nt}^{n-1})$
      Compute $\grave{c}_E^{n,nt} := \grave{c}_E(e_n, t_{nt}^{n-1}, T^{nt}(e_n, t_{nt}^{n-1}))$
      Compute $c_E^{n,nt}$ based on $\grave{c}_E^{n,nt}$ and SOC_{nt}^{n-1}
      Compute $SOC_{nt}^n := SOC_{nt}^{n-1} - c_E^{n,nt}$
      Compute $t_{nt}^n := t_{nt}^{n-1} + c_T^{n,nt}$
      $SOC_{min}^{nt} := max\{SOC_{nt}^n - SOC_{pre}^n, 0\}$
    End for.
    $SOC_{min}^{t,NT}(e_n) := max\{SOC_{min}^{nt} \mid nt \in \{0, ..., NT\}\}$
  else (i.e., if e_n is part of the charging process):
    $SOC_{min}^{t,NT}(e_n) := 0$
    $t_{nt}^n := t_{pre}^n := t_{pre}^{n-1} + c_T(e_n, t_{pre}^{n-1}, SOC_{pre}^{n-1}) \; \forall \; nt \in \{0, 1, ..., NT\}$
    $SOC_{nt}^n := SOC_{pre}^n := SOC_{pre}^{n-1} - c_E(e_n, SOC_{pre}^{n-1}) \; \forall \; nt \in \{0, 1, ..., NT\}$
  End if.
  $n := n + 1$
End while.
Return $SOC_{min}^{t,NT}(e_N)$.

Figure 5.5: Pseudo-code to compute energy buffer $SOC_{min}^{t,NT}$ along a path.

[38] Actually, trajectory $T^{nt}(e, t)$ can be understood as a part of object ω_E. Here, both inputs are listed separately to emphasize the relevance of $T^{nt}(e, t)$.

Given a microscopic energy consumption model $\grave{c}_E$ and the possibility to compute driving trajectories T^{nt}, the energy buffer function $SOC_{min}^{t,NT}$ can be introduced in the following. It is defined as the maximum over all differences between the states of charge which result when applying $\grave{c}_E$ to trajectories $T^{nt}(e,t)$, and the predicted state of charge. In Figure 5.5, the pseudo-code of an algorithm for computing $SOC_{min}^{t,NT}$ along a path $P = [v_1^P, ..., v_N^P]$ can be found. The algorithm can be separated into two parts: In the first part, it computes the predicted arrival times and the predicted states of charge analogously to algorithms A and B from chapter 4. For edges representing road segments, this happens in lines 5 to 9 of the code. Value t_{pre}^n („pre“ for „predicted“) describes the predicted arrival time at node v_n^P and SOC_{pre}^n describes correspondingly the predicted state of charge when reaching node v_n^P. Note that it is not uncommon that the predicted energy consumption $\grave{c}_E(e_n, t_{pre}^{n-1})$ is computed on the basis of a trajectory, too. This means that for an edge e_n and a starting time t_{pre}^{n-1}, a unique trajectory $T^{pre}(e_n, t_{pre}^{n-1})$ is generated for which the following equation holds:

$$\grave{c}_E(e_n, t_{pre}^{n-1}) = \grave{c}_E(e_n, t_{pre}^{n-1}, T^{pre}(e_n, t_{pre}^{n-1})). \tag{5.8}$$

It is from here on assumed that predicted arrival times and energy consumption values are based on trajectories.
For edges representing parts of charging processes, predicted arrival times and predicted states of charge are computed in lines 22 and 23 in the algorithm from Figure 5.5. There is no difference to former chapters.

In the second part, the algorithm does basically the same as in the first part, but now auxiliary trajectories T^{nt} are used as basis. Assuming that trajectory $T^{nt}(P_{1:n}, t_S)$ describes the movement of the BEV, variable t_{nt}^n denotes the time at which node v_n^P is reached and SOC_{nt}^n denotes the corresponding state of charge. For edges representing road segments, the computation of states of charge and arrival times is done in lines 11 to 16. Otherwise, in lines 22 and 23. In this context, it is remarkable that as soon as a charging station is reached, all trajectories are assumed to leave the charging station at the same time. Let this proceeding be explained considering Figure 5.6. This figure visualizes for an exemplary graph the proceeding of the algorithm described by the pseudo-code in Figure 5.6. A path $P = [v_1^P, ..., v_6^P]$ consisting of six nodes and five edges is illustrated at the left the figure. Edges e_4 and e_5 represent parts of a charging process, the remaining edges represent road segments. All trajectories which are necessary for the computation of $SOC_{min}^{t,NT}$ (with $NT = 1$) are displayed. Trajectories T^{pre} are represented by black arrows, auxiliary trajectories T^{nt} by gray arrows. Within the described example, the BEV starts driving along path P at time t_S. To compute the size of the energy buffer at node v_2^P, altogether three driving trajectories are generated: The predicted trajectory $T^{pre}(e_2, t_S)$ and $NT + 1$ auxiliary trajectories ($T^0(e_2, t_S)$ and $T^1(e_2, t_S)$). Based on these three trajectories, arrival times t_{nt}^2 and t_{pre}^2, and states of charge SOC_{nt}^2 and SOC_{pre}^2

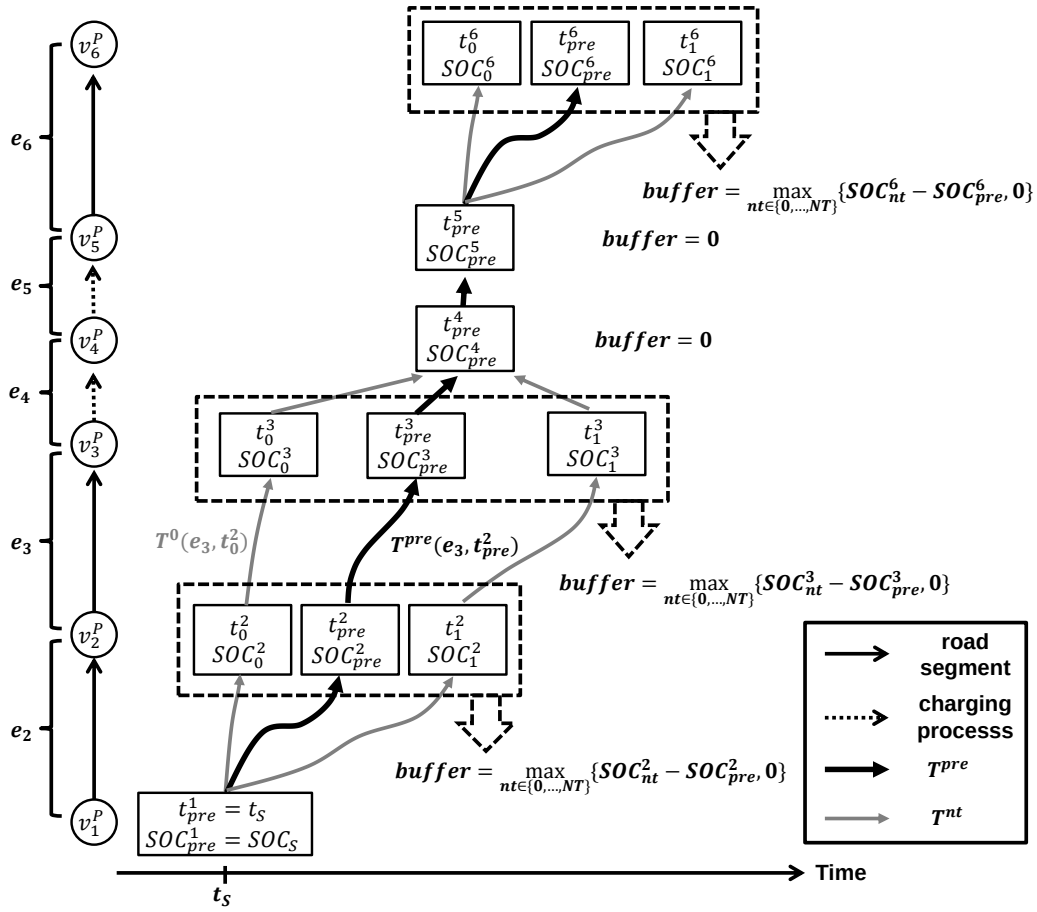

Figure 5.6: Trajectory generation scheme for energy buffer quantification.

are computed for $nt \in \{0, ..., NT\}$ (see lines 5 to 9 and 12 to 16 in Figure 5.6). The size of the energy buffer at node v_2^P results as the maximum difference between the states of charge resulting from the auxiliary trajectories and the state of charge resulting from the predicted driving trajectory[39] (see line 19). To compute the size of the energy buffer for node v_3^P, all three trajectories are extended up to node v_3^P, i.e., trajectories $T^{pre}(e_3, t_{pre}^2)$, $T^0(e_3, t_0^2)$ and $T^1(e_3, t_1^2)$ are generated and corresponding arrival times and states of charge are derived. The buffer itself is computed analogously as for node v_2^P. The most interesting aspect can then be observed for the next edge, which represents a part of a charging process. Instead of maintaining $NT + 2$ separate trajectories and, along with that, computing $NT+2$ different arrival times and $NT+2$ different states of charge for node v_4^P, all arrival times and all states of charge are set equal to the predicted arrival time and the predicted state of charge, respectively (lines 22 and 23). This is done for each edge belonging to a charging process. The consequence is that the resulting

[39]The energy buffer function is modified within the given pseudo-code in such a way that negative energy buffers are avoided.

buffer size (which is defined as the maximal difference between the states of charge resulting from auxiliary trajectories T^{nt}, and the predicted state of charge) is equal to zero in such a case[40]. As soon as a road segment needs to be passed again, separate trajectories are computed.

Note that the pseudo-code stated in Figure 5.5 can be included into algorithms A-2 and B-2 similarly to the codes for relative and quantile buffers. Though, it is necessary to further extend the definition of labels for this purpose. Here, all values t^n_{nt} and SOC^n_{nt} for $nt \in \{0, 1, ..., NT\}$ need to be stored, leading to $2 \cdot (NT + 1)$ additional entries for each label. In contrast to $SOC^{r,z}_{min}$, it is not necessary to store the size of the energy buffer of previous edges. Note also that the usefulness of $SOC^{t,NT}_{min}$ depends on the considered set of auxiliary trajectories T^{nt}. If this set is able to represent the set of all possible driving trajectories adequately, then it can be expected that using $SOC^{t,NT}_{min}$ for CSO works well. An adequate representation means two things in this context: First, it needs to be probable for any edge e and any arrival time t_S that the real future driving trajectory looks similar to at least one of the generated auxiliary trajectories $T^{nt}(e, t_S)$. Otherwise, the corresponding buffer may be too small. Second, any auxiliary trajectory $T^{nt}(e, t_S)$ has to be reasonable. Unrealistic trajectories may cause the buffer to become too big.

5.3.4 Comparison of Energy Buffer Types

Table 5.1: Comparison of energy buffer concepts.

	Relative Buffer	Quantile-based Buffer	Trajectory Buffer
Notation	$SOC^{r,z}_{min}$	$SOC^{q,\alpha}_{min}$	$SOC^{t,NT}_{min}$
Reliability Parameter	$z \geq 0$	$\alpha \in [0, 1]$	$NT \in \mathbb{N}$
Computational Effort	$++$	$++$	$-(-)$
Requirements	$++$	$--$	$\bigcirc$
Adaptivity	$\bigcirc$	$++$	$+(+)$

Three energy buffer functions have been suggested. In the following, they are assessed with regard to the additional computational effort they cause, to the requirements that need to be fulfilled to be able to apply these functions, and with regard to their adaptivity. Recall that adaptivity describes in this context the ability of an energy buffer function to adequately adjust the size of an energy buffer in dependency of the reliability of the predicted energy consumption. Table 5.1 provides a short overview of the advantages (indicated by plus signs) and

[40] Recall that keeping energy buffer sizes equal to zero when passing edges belonging to charging processes was postulated for all energy buffer functions.

drawbacks (indicated by minus signs) of the introduced approaches with regard to these three criteria. Circles indicate that no clear statement is possible. Additionally, the parameters (z, α and NT) which are part of the three introduced energy buffer functions are listed. Since these parameters have influence on the size of the resulting energy buffers and, along with this, on the reliability of the corresponding charging strategies, they are denoted from here on as reliability parameters.

Relative Buffer: The relative energy buffer function $SOC_{min}^{r,z}$ can be computed easily and, moreover, needs no additional information in comparison to the original formulation of the deterministic SPP from chapter 4, in which the feasibility condition was applied as a constraint instead of the energy security condition. At the same time, a certain level of adaptivity is achieved, since the size of this buffer increases along with the predicted energy consumption. The idea is that if a long distance has to be covered to reach the next charging station, then this tends to cause a rather high level of uncertainty and consequently a rather large amount of energy should be reserved. A critical situation for relative buffers occurs if a sequence of edges represents a long road corridor, but the sum of the corresponding predicted energy costs is close to zero. This can happen, for instance, if significant energy gains are expected due to recuperation. In such a case, the size of a relative energy buffer does not grow much, even though significant uncertainties probably still exist. The energy gain due to recuperation may be lower than expected or energy consumption may be higher than expected. To reduce the risk resulting from this issue, a static component could be added to $SOC_{min}^{r,z}$. However, no details are considered here[41].

Quantile Buffer: The quantile-based approach causes high requirements concerning the availability of information, since the distribution of energy consumption needs to be known for all possible combinations of arrival times and locations. Furthermore, correlations of these distributions are also relevant. On the other hand, computing quantiles (under the assumption of given probability distributions) should not increase computation times significantly. Moreover, a high level of adaptivity can be expected for function $SOC_{min}^{q,\alpha}$, as this buffer type is explicitly constructed on the basis of the probability distributions of energy consumption. This means that $SOC_{min}^{q,\alpha}$ leads particularly in situations in which real energy consumption is very likely to exceed predicted values to big buffers. This is also an advantage in comparison to relative energy buffers: The size of a relative energy buffer solely depends on the predicted energy consumption. It is not taken into account how reliable this prediction is. Therefore, the quantile-buffer function does not lead to the same issue for situations in which, due to recuperation, the predicted energy consumption is close to zero.

[41] One could think of a variety of different energy functions which combine static components, components growing linearly with the predicted energy consumption or components that grow nonlinearly (exponential functions, higher order polynomials) with the predicted energy consumption.

Trajectory Buffer: For the last method, which is based on computing a range of possible driving trajectories, computational effort definitely increases. How big this increase is depends on how expensive the generation of the sets of trajectories is. This again depends on the applied trajectory generation method and on the number of generated trajectories. Also the level of adaptivity and the requirements, which have to be fulfilled to allow deriving the trajectories, primarily depend on the trajectory generation method. It can be expected that some additional information is necessary, but that this information can be obtained easier than the information which is needed for the quantile-based approach. If the considered sets of trajectories are able to represent the sets of all possible trajectories adequately, then a rather high level of adaptivity can be expected, too.

In conclusion, all three energy buffer approaches appear to be reasonable. Relative buffers are simple and the mentioned issue concerning close-to-zero energy consumption predictions won't be too relevant in practice, since it can be expected that many kilometers lie between two consecutive charging stops. Thus, it is very unlikely that it is predicted that recuperation keeps energy consumption close to zero. The quantile buffer function probably has the potential to achieve the best results of the three suggested types of buffer functions, i.e., the highest efficiency along with the highest reliability. Its main drawback is the requirement that energy consumption probability distributions need to be known. If the available probability distributions are unable to mirror reality accurately, then the resulting charging strategies are also of low quality. Since, from a practical perspective, it seems hardly possible to identify for all edges and arbitrary arrival times the corresponding probability distributions of energy consumption, quantile-buffer functions will not be considered in the following chapters. The description of the last type of energy buffer function, the trajectory buffer function, is quite generic in its current form. It has not been specified yet, how the necessary trajectories are generated. The benefits and drawbacks of the trajectory buffer function can be expected to depend significantly on the applied trajectory construction algorithm. Until such an algorithm has not been stated, a reasonable evaluation of $SOC_{min}^{t,NT}$ is hardly possible.

5.4 Model Assessment with Regard to Research Objectives

Even though the replacement of the feasibility condition by the energy security condition is the only difference between the deterministic SPPs from chapters 4 and 5, the degree up to which the new problem formulation is able to fulfill ROs 1a to 1c changes significantly:

RO 1a: The problem formulation from chapters 4 and 5 are based on the same graph $\vec{G}_D^{\Delta}$. Hence, some model limitations, such as discretized decision stages and the fact that solutions of the optimization problem cannot represent arbitrary charging policies, are maintained. The huge difference is the ability of the new problem formulation to handle uncertainty. Hence, presuming that an appropriate energy buffer function is applied, resulting charging strategies

can be expected to ensure a reliable arrival also if they are applied in practice. Nevertheless, some restrictions still exist in this context. The most important one is that the concept of energy buffers does not allow taking uncertainties of travel time predictions explicitly into account. Along with this, also the influence of unexpected arrival times on energy consumption predictions cannot be considered explicitly[42].

RO 1b: The definition of f is the same as in chapter 4. Consequently, efficiency is achieved by penalizing charging strategies which cause high travel times, reliability by penalizing risky charging strategies. „Risky“ denotes in this context charging strategies which do not fulfill the energy security conditions. Excluding not only infeasible, but also risky strategies from consideration offers some additional modeling opportunities. The understanding of risky strategies is represented the applied energy buffer function. This function allows making trade-offs between reliability and efficiency. In theory, it can be designed in such a way that the driver's level of risk-aversion is mirrored. In conclusion, the new deterministic SPP from chapter 5 is able to take both reliability and efficiency into account and even provides lots of flexibility for defining a compromise between these two criteria.

RO 1c: If $SOC_{min}^{t,NT}$ is applied as the energy buffer function, then computation times could rise in comparison to the problem formulation from chapter 4. This increase depends on the applied method for generating driving trajectories and on the number of generated trajectories NT. If relative or quantile buffers are applied, then replacing the feasibility condition by the energy security condition should not cause a significant increase of the computational effort. Hence, the concept of energy buffers offers the possibility to keep computation times on the same level, which the optimization problem from chapter 4 achieved.

Conclusions: The modified version of the deterministic SPP, which is described in chapter 5, cannot represent occurring uncertainties perfectly. To obtain this, the influence of incorrectly predicted travel times on energy consumption had to be considered. However, ignoring this aspect allows preventing a further increase of computational effort (in comparison to the originally suggested SPP from chapter 4). Moreover, the introduction of energy buffers makes it possible to handle uncertainties of energy consumption predictions. It can be ensured that charging strategies become robust against underestimated energy consumption values and, at the same time, are still efficient. In sum, the suggested reformulation of the deterministic SPP fulfills the requirements defined by ROs 1a to 1c rather well. Therefore, from a theoretical perspective, there remains no critical issue preventing an implementation of the corresponding model in reality. Still, it is not yet absolutely certain whether computation times can be kept low enough and whether the suggested idea of finding a compromise between reliability and efficiency is really practicable.

[42] Recall in this context that energy consumption values are assumed to depend on arrival times.

5.5 Summary

In the introduction of chapter 5, it was stated that under realistic conditions, in which energy and time consumption typically cannot be precisely predicted, the feasibility condition is not enough to achieve charging strategies which can be expected to ensure a reliable arrival. Motivated by these considerations, a potential formulation of the problem of finding optimal charging strategies as stochastic SPP has been suggested and analyzed in section 5.2. It turned out that even under simplest assumptions, this reformulation causes a significant increase of the already high computation times for solving the corresponding optimization problem. To be able to avoid a further increment of computational effort, the deterministic SPP from chapter 4 is considered again. In order to be able to handle inaccuracies of energy consumption predictions, the feasibility condition is replaced with the so-called energy security condition. A charging strategy is denoted as energy secure if the states of charge which are expected never get too close to zero. This means that some part of the battery is used as an energy buffer to compensate for unexpectedly high energy consumption. Essential in this context is that the size of the energy buffer varies along the considered path. Three different concepts for defining the size of the energy buffer have been introduced and compared in section 5.3. Chapter 5 ends with an assessment of the reformulated deterministic SPP. The central result of this evaluation is that, on the basis of the new model, all three subobjectives of RO 1 can be achieved simultaneously – at least up to a degree that should make a practical implementation of CSO possible.

Chapter 6

Using Error-prone Traffic Information for Charging Strategy Optimization

Chapters 3 to 5 focused on RO 1, i.e., on developing an appropriate mathematical formulation for the problem of finding optimal charging strategies. The motivation for chapter 6 – and later on for chapter 7 – is to achieve RO 2, i.e., to test the developed formulation as a deterministic SPP and to assess its ability to handle uncertainties in such a way that charging strategies of „practicable“ quality can be ensured. The testing is done via a simulation study. This appears to be reasonable, since making robust statements about reliability probably makes lots of tests under various conditions necessary. In order to be able to conduct simulation runs, the still abstract problem formulation as a deterministic SPP has to be concretized. This means particularly that specific models that enable a numerical computation of (in the best case) realistic travel times and energy consumption values have to be provided. Moreover, a source of uncertainty has to be included into the simulation.

Chapter 6 is intended as a preparation for the description of the simulation study, which takes place afterwards in chapter 7. Three preparatory steps are conducted in chapter 6. To motivate these steps, at first the structure of a single simulation run of the executed simulation study is explained: A single simulation run represents the trip of a BEV along a very long road corridor under various conditions. Several charging stations can be found along this road corridor. Furthermore, it is assumed that the BEV is equipped with a navigation system which provides charging strategies as an on-trip information, i.e., these charging strategies are updated frequently during the trip. The computation of the charging strategies is based on a set of input data, such as data on the available charging infrastructure, the BEV's current state of charge, and data on outdoor temperature. Furthermore, also different types of simulated real-time traffic information (RTTI) are taken into account for the computation of the charging strategies. The RTTI is used to predict the BEV's future driving trajectories, which are again used to predict travel times and energy consumption values. Note that the simulated RTTI is not absolutely correct – in contrast to all other types of input data. Due to this, the simulated BEV

partly experiences traffic situations during a simulation run that differ from the situations which were presumed for the computation of the charging strategy it follows. The magnitude of these differences depends on the type of RTTI, i.e., these types show different levels of similarity to the real traffic situation. The described simulation approach allows analyzing the ability of the concept of energy buffers to handle uncertainties, at least for the case of uncertainty that is caused by error-prone RTTI.

The first of the aforementioned three preparatory steps takes place in section 6.1. There, the proposed formulation of the problem of finding optimal charging strategies as a deterministic SPP is concretized by introducing a model which allows computing energy consumption and travel times based on RTTI[43]. In section 6.2, a method to quantitatively measure the quality of RTTI is described. This allows analyzing the dependency of charging strategy quality on the quality of the simulated RTTI and, along with that, the dependency of charging strategy quality on the level of uncertainty. Additionally, the proposed measure is of relevance in section 6.3, where the yet abstract concept of trajectory buffers is specified by describing an approach for computing sets of auxiliary trajectories on the basis of available RTTI. Consequently, it is not only possible to test relative buffers within the simulation study, but also to test trajectory buffers.

6.1 Considering Imperfect Real-time Traffic Information

Up to this point, the proposed optimization problems are formulated in a quite generic way. To conduct simulation runs, however, concrete models are necessary, which make it possible to explicitly compute energy consumption values and travel times. Moreover, it is necessary to include some source of uncertainty into the simulation. For the remainder of the described research, the subsequently described setting is presumed in order to achieve both concrete models and the inclusion of uncertainty.

First and foremost, it is expected from here on that energy consumption is predicted on the basis of driving trajectories, which again are derived solely from RTTI. In order to estimate energy consumption on the basis of driving trajectories, it is assumed that a corresponding energy consumption model $\grave{c}_E$ (see equation 5.7 in section 5.3.3) is available. Note that travel times result directly from driving trajectories, since they describe location in dependency of time. Moreover, it is assumed that at time t_0, which is the time at which a charging strategy recommendation is requested, a function $V_{RTTI}^{t_B}$, which represents RTTI, is available for all relevant locations and times. The value $t_B \in \mathbb{R}_{\geq 0}$ denotes in this context the time at which the RTTI is broadcasted. Since function $V_{RTTI}^{t_B}$ needs to be available at time t_0, the corresponding

[43] Recall that RTTI refers to both traffic state estimations and traffic predictions (see the beginning of section 2.3), i.e., it describes current and predicts future traffic states.

RTTI cannot be broadcasted after time t_0, i.e., $t_B \leq t_0$[44]. Function $V_{RTTI}^{t_B}$ is given as a spatio-temporal speed function, i.e., it assigns a speed value to any pair (x, t), where x is a location along an edge of the considered graph $\vec{G}_D^{\Delta} = (V_D^{\Delta}, \vec{E}_D^{\Delta})$ and t a point in time with $t \geq t_B$.

In this work, driving trajectories are derived from spatio-temporal speed functions (this topic has been intensively discussed in (*149*)). For this purpose, let $e \in \vec{E}_D^{\Delta}$ be an edge that represents a road segment and let t_S be the time at which a vehicle starts passing this edge[45]. The (spatial) start of e is denoted with $\underline{e}$ and its end with $\overline{e}$. Furthermore, let V be a spatio-temporal function describing the development of driving speeds along e for any time $t \geq t_S$. If a vehicle starts passing edge e at time t_S while facing traffic conditions described by V, then a unique driving trajectory $T(e, t_S, V)$ can be derived by solving the ordinary differential equation

$$\frac{dx}{dt} = V(x(t), t) \tag{6.1}$$

with initial condition $x(t_S) = \underline{e}$. The computation is terminated as soon as $\overline{e}$ is reached. It is worth mentioning that x is interpreted in equation 6.1 as a function of time.

Available RTTI is not expected to mirror future traffic situations perfectly. To account for this, it is differentiated between the real (current and future) macroscopic driving speeds V_{Real} and the RTTI speeds $V_{RTTI}^{t_B}$. The real traffic situation V_{Real} itself is unknown at time t_0 and it is interpreted from here on as a random variable, i.e., $V_{Real}(x, t)$ denotes a real-valued random variable instead of an explicit speed value. The function returning realizations of V_{Real} for any point (x, t) is denoted by $\bar{V}_{Real}$. This means that $\bar{V}_{Real}(x, t) \in \mathbb{R}_{\geq 0}$ is equal to the speed with which cars are driven at a specific location x at a specific time t[46]. The higher the similarity between functions $V_{RTTI}^{t_B}$ and $\bar{V}_{Real}$ is, the higher the quality of the RTTI is rated. Note that with increasing similarity between $V_{RTTI}^{t_B}$ and $\bar{V}_{Real}$, also the similarity between the predicted driving trajectory $T(e, t_S, V_{RTTI}^{t_B})$ and the real driving trajectory $T(e, t_S, \bar{V}_{Real})$ and hence between predicted and real energy consumption tends to improve.

For the simulation and for the further considerations in chapter 6, predicted time costs c_T and predicted energy consumption costs $\grave{c}_E$ are computed on the basis of the available RTTI

[44] $t_B \leq t_0$ means that a charging strategy computation can be based on traffic prediction which have been made previously. Usually, it is reasonable to assume that $t_B = t_0$.

[45] Here, distinctions are made between three different times: The planned start of the trip t_S, the time at which a charging strategy is requested t_0, and the time at which the RTTI is broadcasted t_B.

[46] Speed value $\bar{V}_{Real}(x, t)$ is here interpreted in a macroscopic sense, i.e., it is intended to describe macroscopic average driving speeds.

function $V_{RTTI}^{t_B}$, i.e.:

$$\grave{c}_E(e,t) := \grave{c}_E(e,t,T(e,t_S,V_{RTTI}^{t_B})) \tag{6.2}$$

$$c_T(e,t) := c_T(T(e,t_S,V_{RTTI}^{t_B})) \tag{6.3}$$

Note that the resulting energy consumption and time costs can only be understood as a „best guess“ of the yet unknown real future energy consumption and the yet unknown time costs that result from trajectory $T(e,t_S,\bar{V}_{Real})$. The issue is that $\bar{V}_{Real}$ is not known at time t_0, at which the charging strategy is requested. In contrast, the typically imperfect function $V_{RTTI}^{t_B}$ is available at that time. For the simulation study, different types of (partly artificially generated) RTTI, which show different levels of similarity to $\bar{V}_{Real}$, are applied for CSO. The simulated vehicles are assumed to follow the recommended strategies while facing the real traffic situation and, along with that, energy consumption and time costs which differ from those which were presumed during the optimization. It is analyzed up to which degree different energy buffer functions are able to handle the resulting uncertainties.

Various reasons for incorrectly predicted energy consumption values and travel times exist. Though, RTTI[47] shows some properties which make it particularly interesting to consider RTTI as a source of uncertainty: First of all, traffic conditions have significant influence on both energy consumption (*86*) (*123*) and travel times (*148*) (*164*). This leads, in comparison to uncertainty that solely affects one of both costs functions, to additional dynamics during the simulation runs, since energy buffers are not able to handle travel time uncertainty (and its influence on energy consumption) directly. Another reason for considering error-prone RTTI as a source of uncertainty is that the driver does not have much influence on prevailing traffic conditions. Admittedly, she/he is in most cases able to adjust her/his route to avoid certain traffic conditions, but this is not always possible or reasonable. This powerlessness, which is probably one of the main reasons for range-anxiety, represents a contrast to other aspects that could also be considered to be sources of uncertainty for energy consumption or travel time predictions. The driver has, for example, significant influence on her/his driving style, which again has influence on travel times and energy consumption (*57*). In situations, in which it is unclear whether the next charging station or the destination, respectively, can be reached, she/he can adjust her/his driving behavior in order to extend the remaining driving range. However, it is (usually) not possible to adjust prevailing traffic conditions. The third reason for concentrating on imperfect RTTI as a source of uncertainty is that traffic, in contrast to most other factors on which the driver has no influence (such as weather conditions, the road network or road steepness), is highly dynamic and hardly predictable even for comparably short prediction periods. As a consequence, it is very likely that RTTI is prone to errors in reality. This has been

[47] The considerations of chapter 6 are not restricted to the case of „real-time“ traffic information. In most cases, they are also applicable for other kinds of traffic information. Still, it will usually be spoken of RTTI.

confirmed in prior studies (*19*) (*84*).
These reasons make the influence of RTTI quality on travel times, on energy consumption prediction, and, along with this, on charging strategy quality very interesting – from a scientific, as well as from a practical point of view. In order to simplify considerations, RTTI errors are assumed to be the only source of uncertainty in the following. This does not mean that other potential sources of uncertainty are not relevant. Instead, the suggested procedure can be understood as a first step, where the focus is set on the probably most crucial aspect. Future work can then build upon this fundament and extend the stated considerations by including other sources of uncertainty.

6.2 Measuring Errors of Real-time Traffic Information

Within the simulation study in chapter 7, different types of artificially generated RTTI are applied for the computation of charging strategies. These types of RTTI show different levels of similarity to the simulated reality and are used to analyze the dependency of charging strategy quality on the quality of the available traffic information. The idea is to find a relation between the level of uncertainty, which is represented by the quality of the error-prone RTTI, and the quality of the resulting charging strategies. The findings of the conducted analyses allow drawing conclusions on the developed framework's ability to achieve RO 2. In order to be able to analyze the relation between charging strategy quality and RTTI quality, a framework for measuring RTTI quality has to be introduced. The proposed approach, which is described in the following, shows similarities to prior works about RTTI quality: First, a traffic state reconstruction is carried out on the basis of inductive loop detector data. This traffic state reconstruction is then used as the reference, to which the RTTI being assessed is compared. Quality is in this context interpreted as the level of similarity between the RTTI and the traffic state reconstruction. But before a method for assessing the quality of RTTI can be described, a methodology for bringing RTTI into a reasonable and numerically treatable form is explained. Furthermore, a detailed discussion about reasons leading to imperfect RTTI is provided.

6.2.1 Numerical Representation of Real-time Traffic Information

RTTI is assumed to be information about macroscopic driving speeds. In practice, a provider of commercial RTTI updates this information regularly, i.e., the period between an provision of information and the following update is constant. For the remainder of this work, this time period is denoted with $\Delta t^{RTTI} \in \mathbb{R}_{>0}$. Nowadays, Δt^{RTTI} is often equal to one minute. Each speed value that is part of the broadcasted RTTI is sent along with an identification key. This key can be associated with road segments and thus allows assigning broadcasted speed values to locations. As mentioned in section 2.3, the keys and the set of possible road segments are defined by standardized digital maps, which are typically available for both the traffic content provider and the receiver of the RTTI. In order to represent RTTI in a numerically treatable form, let a single road corridor in one driving direction be considered. This road corridor is

represented by an interval $X = [\underline{X}, \overline{X}[\subset \mathbb{R}_{\geq 0}$. Here, $\underline{X} \in \mathbb{R}_{\geq 0}$ denotes the start of the road corridor and $\overline{X} \in \mathbb{R}_{\geq 0}$ denotes its end[48]. Road corridor X is partitioned into the aforementioned RTTI induced road segments $\{S_i^{RTTI}\}_{i=1,2,...,I}$, i.e.,:

$$\begin{gathered} X = \bigcup_{i=1,...,I} S_i^{RTTI}. \\ S_{i_1}^{RTTI} \cap S_{i_2}^{RTTI} = \emptyset \quad \forall i_1,\ i_2\ \in \{1, 2, ..., I\}. \end{gathered} \tag{6.4}$$

It is assumed that these road segments are arranged along road corridor X, i.e., the first road segment is S_1^{RTTI}, the second S_2^{RTTI} and so on. Furthermore, let this road corridor be considered during a time period $T = [\underline{T}, \overline{T}[\subset \mathbb{R}_{\geq 0}$. $\underline{T}$ and $\overline{T}$ define the start and the end of this time period. It is also assumed that this time period is partitioned into time intervals $\{T_j^{RTTI}\}_{j=1,2,...,J}$. At the beginning of each of these time intervals, the RTTI is updated. Therefore, the length of these time intervals is equal to Δt^{RTTI}. Based on these notations, a spatio-temporal speed function V_{RTTI} is introduced with

$$V_{RTTI} : X \times T \longrightarrow \mathbb{R}_{\geq 0}. \tag{6.5}$$

This function is not intended to represent traffic predictions, but solely to represent estimations of current traffic states. It returns for any location $x \in X$ and any time $t \in T$, the driving speed which has been estimated most recently by the considered traffic content provider. Recall that RTTI is updated at the beginning of each time interval T_j^{RTTI}. Given a time $t \in T$, the time $t_B(t) \in T$ („B“ for „broadcasted“) denotes the latest point in time at which RTTI has been provided:

$$t_B(t) := \max_{j=1,...,J} \{\underline{T}_j^{RTTI} : \underline{T}_j^{RTTI} \leq t\}. \tag{6.6}$$

Time $\underline{T}_j^{RTTI} \in T$ denotes the start of interval T_j^{RTTI}. Due to the way RTTI is provided, function V_{RTTI} returns the same speed value for all points (x, t) which are part of the same spatio-temporal cell $S_i^{RTTI} \times T_j^{RTTI} \subseteq X \times T$. This means that V_{RTTI} is piecewise constant on the spatio-temporal plane. The result is that V_{RTTI} shows a grid structure as visualized exemplarily in Figure 6.1 for the time period between 16:25 and 17:05 for the part of the road network in Figure 2.3 which is marked by the dashed rectangle. The situation at 16:45 is displayed. The considered road corridor (driving from south to north) is separated into seven road segments S_i^{RTTI} with $i \in \{1, 2, ..., 7\}$ and an update rate Δt^{RTTI} of five minutes is assumed. The grid resulting from road segments S_i^{RTTI} and time intervals T_j^{RTTI} is from here on denoted as RTTI induced grid.

[48] Any interval that is considered within this work does not contain its upper border. This ensures that any point within the original interval can be assigned uniquely to one of the smaller intervals if an interval is partitioned further.

If traffic state estimations are considered together with traffic predictions, then the corresponding spatio-temporal speed function is denoted with $V_{RTTI}^{t_B}$:

$$V_{RTTI}^{t_B} : X \times [t_B, \overline{T}[\longrightarrow \mathbb{R}_{\geq 0} \tag{6.7}$$

The value $V_{RTTI}^{t_B}(x,t)$ for some $t \geq t_B$ describes the speed value which the traffic content provider predicts at time t_B for time t. In contrast to V_{RTTI} (compare equation 6.6), there is no direct relation between the time t_B, at which the RTTI is broadcasted, and the time t, for which the speed value is predicted. Hence, it is written $V_{RTTI}^{t_B}(x,t)$ instead of $V_{RTTI}(x,t)$. The relation between V_{RTTI} and $V_{RTTI}^{t_B}$ can be described as follows:

$$V_{RTTI}(x,t) = V_{RTTI}^{t_B(t)}(x,t) \tag{6.8}$$

Note that there exists only one function V_{RTTI} for time period T and this function cannot be provided until the last time information is broadcasted during period T, i.e., until $\overline{T} - \Delta t^{RTTI}$. On the contrary, there exists a separate function $V_{RTTI}^{t_B}$ for each $t_B \in \{\underline{T}_j^{RTTI}\}_{j=1,\ldots,J}$. For

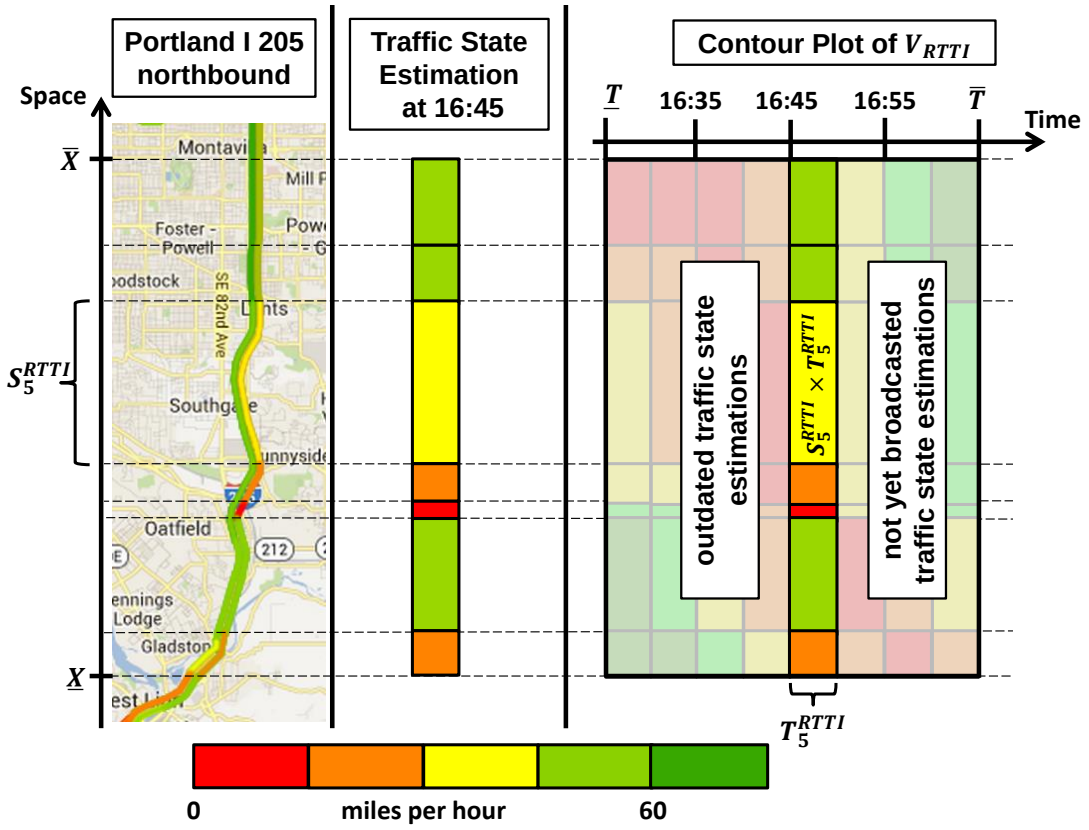

Figure 6.1: Grid structure resulting from an ex post arrangement of real-time traffic state estimations.

simplicity, it is assumed in this research that function $V_{RTTI}^{t_B}$ shows the same temporal discretization as function V_{RTTI}, i.e., speed predictions remain the same during intervals T_j^{RTTI}:

$$V_{RTTI}^{t_B(t)}(x,t) = V_{RTTI}^{t_B(t)}(x,t_B(t)) \quad \forall\,(x,t)\ \in X \times T \tag{6.9}$$

Correspondingly, $V_{RTTI}^{t_B}$ is also piecewise constant within cells $S_i^{RTTI} \times T_j^{RTTI}$.

6.2.2 Reasons for Imperfect Real-time Traffic Information

In practice, the lengths of single segments S_i^{RTTI} can be huge. For so-called traffic message channel (TMC) messages, segment lengths of more than ten kilometers occur. TMC messages are probably the most widely applied type of commercial RTTI. TMC is a standard (*1*) which defines how traffic messages can be delivered via radio (or to be more precise: via the radio data system). To broadcast a traffic message according to TMC, the location of a traffic related incident, as well as the type of this incident have to be encoded in a specific way. The encoding of the location is done according to the so-called TMC location code list, which is an example of a standardized digital map[49]. It allows differentiating between 64000 different locations per country. This number is typically too low to allow the representation of all parts of the road network of a country. Figure 6.2 shows exemplarily the part of the road network around Munich that can be represented via TMC (upper part) and the network coverage which is achieved by a digital map provided by TomTom (lower part). It can be observed that TMC is restricted to freeways, federal roads, and urban arterials. The TomTom map, which is intended for usage within navigation devices, offers much more details. Note that not only TMC messages refer to the TMC location code list, but also other types of traffic information. However, the relevance of TMC is diminishing. The TMC standard has been developed during the late eighties. Due to the limited technical possibilities in terms of data transmission at that time, TMC was designed in such a way that the amount of data that are necessary for encoding traffic related information is kept as low as possible. To achieve this, limitations, such as the already mentioned limited spatial coverage and resolution, were accepted. During the last years, more sophisticated location referencing methods were developed. These methods do not assign spatial information to spatial objects (road segments, spatial areas, etc.) which are parts of standardized digital maps. Instead, an abstract description of the spatial extent of a traffic related incident (or any other spatial information) based on GPS data and possibly also on further information is used to locate this incident on arbitrary digital maps. As a consequence, limited resolution or coverage are no longer a problem. An example of such an advanced geo-coding approach is OpenLR (*75*) (*145*).

[49] Recall from section 2.3 that the idea of such standardized maps is that both the provider of RTTI and the receiver have the same map. Any kind of information is sent from the provider to the receiver along with a identification key, which refers to a specific part of this map, such as a road segment or a spatial area. This makes it possible for the receiver to locate the information.

(a) TMC road network

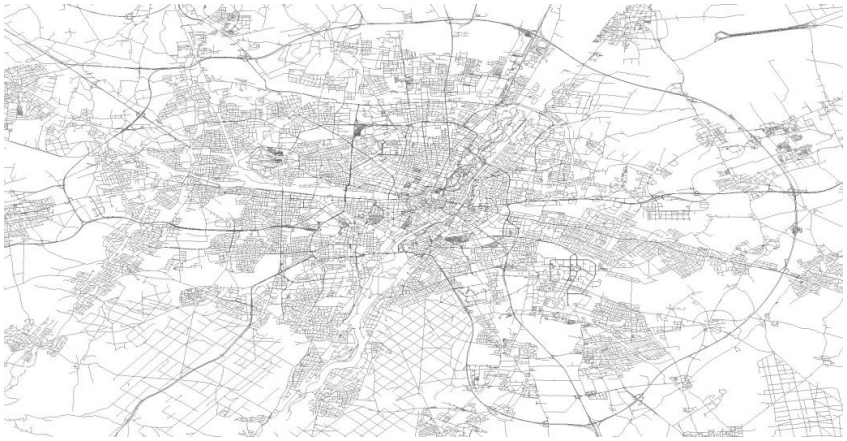

(b) Routing-ready road network

Figure 6.2: Comparing the TMC-coverage of Munich with the coverage provided by TomTom routing devices

Prior studies have indicated that commercial RTTI sometimes does not mirror the real traffic situation adequately (*19*) (*84*). In these studies, primarily traffic state estimations have been analyzed, i.e., potential prediction errors have not even been considered. However, even for the – in comparison to predictions – simple case of traffic state estimations, there exist many reasons which may lead to inaccuracies. The most important among them are

1. Provision limitations, for instance, a limited spatial resolution
2. Delays caused by detection, data preparation or transmission processes
3. Missing, insufficient, contradictory or misinterpreted data
4. System stability

The problems resulting from provision limitations, especially a restricted spatial resolution, have already been discussed. Another issue is that traffic content providers can solely broadcast information about a change of prevailing traffic conditions if they know about it. If the traffic content provider primarily uses probe data to estimate traffic states, then at least a few vehicles from which the RTTI provider receives information need to have experienced such a change before a corresponding information can be broadcasted. If the traffic content provider relies primarily on stationary detector data, then changes are not detected unless they reach locations which are covered by these detectors. Either way leads to detection delays. Unfortunately, detection delays are not the only consequence of the limited availability of traffic data. Some incidents may not even be detected at all or the available data may lead to misinterpretations. This can be the case if vehicles show a non-representative driving behavior, for instance, if data from vehicles searching for parking spots or data from trucks on freeways are received. Besides gathering data, traffic content providers have to aggregate, process, and interpret data. Afterwards, the resulting information is broadcasted and received by the customer of the RTTI service, who possibly again needs some time to process the received RTTI and include it in her/his own traffic related service. Most of these steps can reduce data accuracy (*19*) and each of these steps consumes time. Analyses of different types of RTTI proved that delay is still an issue in practice: In (*113*), empirical tests that were executed in 2011 in Germany showed a maximal duration of three minutes between the time at which a TMC-message has been broadcasted and the time of its visual provision by typical navigation devices. In the same year, the whole process of gathering traffic data, generating a TMC-message and visualizing the information on the display of a navigation device took, in Austria, on average 10 minutes (*118*). Another study, in which RTTI provided by INRIX (a professional traffic content provider) is analyzed, indicate that the average period between a change within the prevailing traffic conditions and the time at which the corresponding information is received by customers was equal to six minutes in 2014 (*84*).
A further issue is that RTTI has to be provided continuously, i.e., 24 hours a day, seven days a week. Even if no or only sparse traffic data are available on certain parts of the road network, traffic data providers are still supposed to broadcast RTTI. Historical traffic data are typically applied in such cases as a supplement, but they limit the maximal possible information quality. Furthermore, no system works perfectly. If the system is operating in real-time, such as RTTI services do, detecting and correcting errors can lead to interruptions and breakdowns.

6.2.3 Traffic State Reconstruction

To be able to measure differences between RTTI and reality, a reference to which the RTTI can be compared, is usually applied. This reference, which is typically denoted as the ground truth (GT), has to represent the „real“ traffic situation adequately and it must be in a form that can be handled numerically. There exist different ideas for the construction of the ground truth. Basic information concerning this topic was provided in section 2.3. For the remainder of this work,

a spatio-temporal speed function showing average driving speeds in dependency of time and location is used as reference. The corresponding speed functions are constructed according to the method described in (*146*). Speed data gathered by inductive loop detectors form the basis[50]. Due to the high costs for inductive loop detectors, often only small parts of the entire

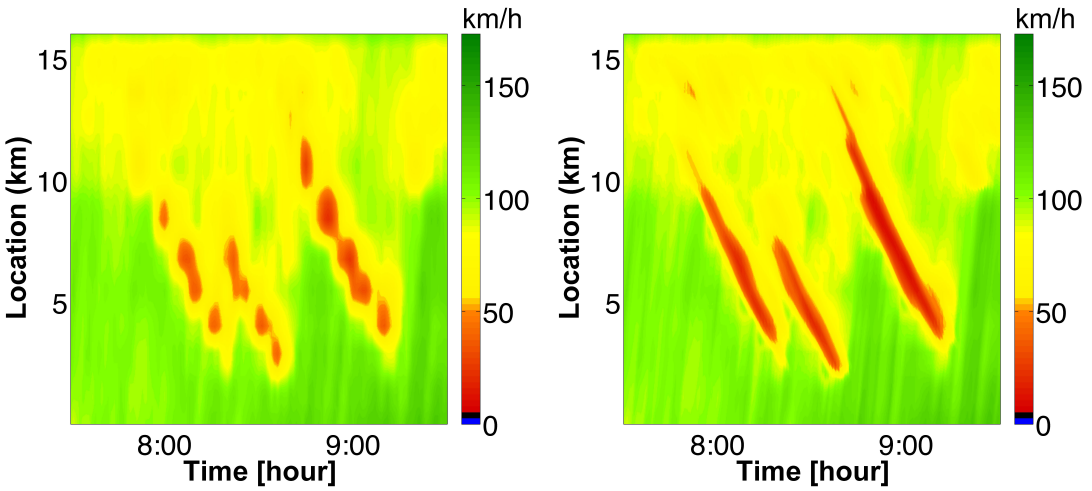

(a) Isotropic Interpolation (b) Anisotropic Interpolation

Figure 6.3: Difference between isotropic and anisotropic interpolation

road network are equipped with them. Moreover, distances between successive detectors of several kilometers occur frequently, at least in Germany. As a consequence, the detectors cannot observe the real traffic situation continuously. To fill (spatial, but also temporal) detection gaps and thus to portray the traffic situation for a road corridor during a certain time period comprehensively, a spatio-temporal interpolation is carried out. There are different ways for realizing this. The most intuitive approach is to do a simple isotropic interpolation, i.e., the influence of measured speed values on the speed estimation for a point on the spatio-temporal plane for which no measurement is available is inversely proportional to the distance (on the spatio-temporal plane) between the point of measurement and the point for which the speeds have to be estimated. The left part of Figure 6.3 visualizes such a traffic state reconstruction resulting from an isotropic interpolation[51]. It shows a 16 kilometers long road corridor on the German autobahn A99, between the interchange Munich north and the interchange Munich east, on November 3rd, 2003 between 7:30 and 9:30, southbound. Fourteen inductive loop detectors are located along the illustrated corridor. Red areas indicate spatio-temporal regions at which only low driving speeds were realized, green areas indicate free-flow. Note that three

[50]The inductive loop detector data which are considered in this work provide information about traffic related quantities at one-minute resolution. All detector data are gathered on freeways. The delivered data are only available per direction, i.e., the data are averaged over all lanes. The averaging is done according to the procedure described in (*154*).

[51]A detailed description of the isotropic interpolation approach that has been applied for the generation of this picture can be found in (*68*).

different jam waves can be identified. However, these waves seem to be interrupted, an observation that cannot be made in reality, where jam waves typically propagate steadily against the driving direction. Such unrealistic observations can be the result when applying isotropic interpolation schemes.
In order to avoid such behavior, in (*146*), an adaptive interpolation scheme is proposed. The corresponding approach is usually denoted as **adaptive smoothing method** (ASM). The ASM takes the typical propagation speeds of information in freeway traffic into account. These speeds are assumed to be very similar all over the world: In congestion, information is transmitted with roughly 18 kilometers per hour in upstream direction. In free-flowing traffic conditions, it moves with about 80 kilometers per hour downstream. The result of applying the ASM to inductive loop detector data is a spatio-temporal speed function, which is from here on denoted by V_{GT}[52]. If detector data for a road corridor X during a time period T are available, then V_{GT} returns for any location $x \in X$ and any time $t \in T$ the corresponding „real“ macroscopic driving speed $V_{GT}(x,t)$. The right part of Figure 6.3 visualizes V_{GT} for the same situation as considered in the left part. Each of the aforementioned jam waves is now represented by a connected red area. The slope of the jam waves mirrors the presumed upstream propagation speed of 18 kilometers per hour.

Note that the contour plot on the right side of Figure 6.3 was not generated by applying the original version of the ASM from (*146*). Instead, a speed-up version of the ASM, as stated in (*132*), was executed. This modified method makes use of fast Fourier transforms. Accelerations in computation time up to a factor of 100 are achieved. At the same time, quality reductions remain negligible. The parameters that were used for generating V_{GT} in Figure 6.3 are oriented towards those of (*132*). The corresponding list of values can be found in appendix C. There, besides presumed propagation speeds, further parameters are listed. Among these parameters, the most important for the following sections are $\Delta x^{GT} = 40$ meters and $\Delta t^{GT} = 20$ seconds. They describe the spatial and the temporal resolution of V_{GT}. The implementation of the ASM which is applied throughout this work returns a set of triples. Each triple consists of a specific location x_i, a specific point in time t_i, and the corresponding speed values $V_{GT}(x_i, t_i)$. The in fact continuous function V_{GT} is described by these triples. The set of points (x_i, t_i) form a grid on the spatio-temporal plane. The spatial and the temporal distance between successive points are denoted by Δx^{GT} and Δt^{GT}. From here on, V_{GT} is interpreted as a piecewise constant speed function, which returns for any (x,t) the speed value $V_{GT}(x_i, t_i)$ which is assigned to the point (x_i, t_i) that lies closest to (x,t):

$$\begin{aligned} V_{GT}(x,t) &= V_{GT}(x_i,t_i) \\ &\forall (x,t) \in [x_i - 0.5 \cdot \Delta x^{GT}, x_i + 0.5 \cdot \Delta x^{GT}[\times [t_i - 0.5 \cdot \Delta t^{GT}, t_i + 0.5 \cdot \Delta t^{GT}[\end{aligned} \tag{6.10}$$

[52] The relation between V_{GT} and V_{Real} will be explained later on.

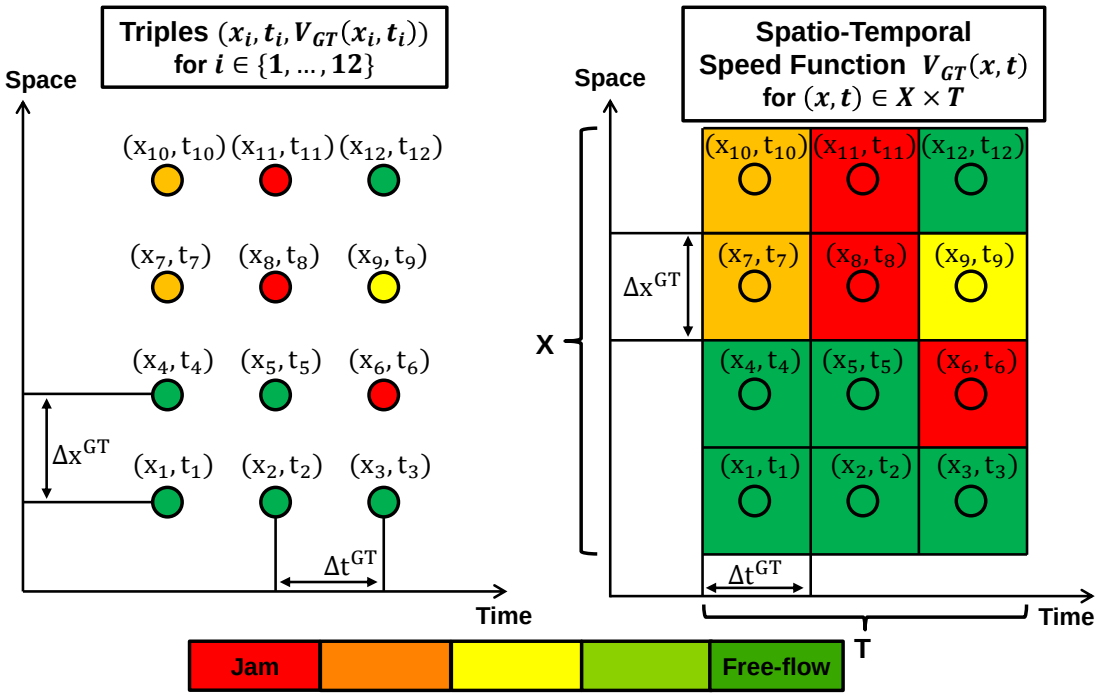

Figure 6.4: Construction of ASM-grid.

Similarlarly to the case of RTTI, the road segments and time intervals that are defined by this grid are denoted by S_k^{GT} and T_l^{GT}, respectively. The interpretation as a piecewise constant function will later on allow deriving a rather simple quantification of differences between V_{GT} and broadcasted driving speeds, which are, as already described, also interpreted as piecewise constant speed functions. In Figure 6.4, the idea of interpreting the available set of triples $(x_i, t_i, V_{GT}(x_i, t_i))$ (left side) as a spatio-temporal speed function (right side) is illustrated.

It is worth mentioning that a traffic state reconstruction is already done by the traffic content providers to generate the broadcasted RTTI. This raises the question why function V_{GT}, which is intended to be used to assess the quality of RTTI, should mirror reality more accurately than the RTTI itself. Actually, there are several reasons for this: V_{GT} is typically constructed ex post, i.e., „at the end of the day“. Hence, there is no time pressure. The problem of latencies caused, for instance, by data transmission vanishes. Another aspect is that if during a specific time period not enough or (for some reason) only data that seem to be unreliable are available for the construction of V_{GT}, then the possibility exists to ignore this time period during the assessment process. An RTTI provider does not have this option as RTTI in most cases has to be provided continuously (24 hours a day, 7 days a week). Moreover, if the traffic situation for a specific time t is estimated and if this estimation is done ex post, then not only data gathered before or at time t are available. Also „future“ data, i.e., data that were collected after t, can

be taken into account. There exists methods for traffic state reconstruction, for instance the ASM, which make use of future data to achieve a more accurate traffic state reconstruction. An online-traffic state estimation, which has to be carried out by traffic content providers, can obviously not include such future data. Finally, traffic state reconstructions are in general not bound to standards that limit the amount of detail that can be represented, which may be the case for RTTI. Bringing all this together, it can be concluded that a posterior traffic state reconstruction is much simpler and in general has the potential to be more accurate than an online traffic state estimation. Note that even if the same data basis is used for both, it is very likely that differences occur.

One final remark shall be given at this point: Besides V_{GT}, which is a piecewise constant speed function that is reconstructed ex post on the basis of inductive loop detector data, function V_{Real} has been introduced, too. V_{Real} returns, depending on location and time, random variables $V_{Real}(x,t)$. These random variables are solely relevant from a modeling point of view. In fact, under the assumption that $\bar{V}_{Real}$ describes the real average driving speeds, function V_{GT} can be interpreted as an approximation of $\bar{V}_{Real}$. Whenever an ex post analysis of RTTI quality is carried out during the remainder of the described research, V_{GT} is applied as reference.

6.2.4 Error Measurement

In the following, the differences between broadcasted RTTI and the constructed ground truth are quantified for some road corridor $X \subset \mathbb{R}_{\geq 0}$ during a time period $T \subset \mathbb{R}_{\geq 0}$. Both functions V_{GT} and $V_{RTTI}^{t_B}$ are constant in each cell of a grid on the spatio-temporal plane. For V_{GT}, the corresponding grid is described by a set of spatial segments $\{S_k^{GT}\}_{k=1,...,K}$ and a set of time intervals $\{T_l^{GT}\}_{l=1,...,L}$, with K and $L \in \mathbb{N}$. Analogously, a set of spatial segments $\{S_i^{RTTI}\}_{i=1,...,I}$ and a set of time intervals $\{T_j^{RTTI}\}_{j=1,...,J}$, with I and $J \in \mathbb{N}$, describe the grid for $V_{RTTI}^{t_B}$ (or V_{RTTI}, respectively). Both sets of segments are supposed to be partitionings of X and both sets of time intervals to be partitionings of T, i.e., each point in $X \times T$ can be assigned to exactly one cell in both grids.

The measurement of the differences is done in three steps: First, based on the two already existing grids, a third grid, which is described by sets $\{S_m^U\}_{m=1,...,M}$ („U“ for „union“) and $\{T_n^U\}_{n=1,...,N}$ with M and $N \in \mathbb{N}$, is generated. It is essential that each cell $S_m^U \times T_n^U$ is completely covered by a single cell $S_k^{GT} \times T_l^{GT}$ and by a single cell $S_i^{RTTI} \times T_j^{RTTI}$. This means that for all $m \in \{1, ..., M\}$ and for all $n \in \{1, ..., N\}$, there exists exactly one index k^* $\in \{1, ..., K\}$, one index $l^* \in \{1, ..., L\}$, one index $i^* \in \{1, ..., I\}$ and one index $j^* \in \{1, ..., J\}$, such that the subsequent conditions holds

$$S_m^U \times T_n^U \subseteq S_{k^*}^{GT} \times T_{l^*}^{GT} \tag{6.11}$$

$$S_m^U \times T_n^U \subseteq S_{i^*}^{RTTI} \times T_{j^*}^{RTTI} \tag{6.12}$$

This ensures that V_{GT} and $V^{t_B}_{RTTI}$ (and V_{RTTI}) are constant within each cell of the new, dense grid. During the second step, the values both functions return are compared for each cell of the new grid separately. For this purpose, let $V_{GT}(S^U_m, T^U_n)$ denote the speed value that is returned by V_{GT} for any point (x, t) which is located in cell $S^U_m \times T^U_n$. Value $V^{t_B}_{RTTI}(S^U_m, T^U_n)$ is defined analogously. Furthermore, let a function d (for instance, this can be a metric) be considered that measures the difference between two values. The rating for a cell $S^U_m \times T^U_n$ is thus denoted by

$$d(V_{GT}(S^U_m, T^U_n), V^{t_B}_{RTTI}(S^U_m, T^U_n)). \tag{6.13}$$

During the third step, the computed difference ratings for all cells are aggregated to one single number by weighting them according to the spatio-temporal extent of the corresponding cell:

$$\begin{aligned} w_{m,n} &:= \int_{S^U_m}\int_{T^U_n} 1\ dt\ dx = (\overline{S}^U_m - \underline{S}^U_m) \cdot (\overline{T}^U_n - \underline{T}^U_n) \\ W &:= \int_X \int_T 1\ dt\ dx = \sum_{m=1}^{M}\sum_{n=1}^{N} w_{m,n}. \\ D(V_{GT}, V^{t_B}_{RTTI}, X \times T, d) &:= \frac{1}{W} \cdot \sum_{m=1}^{M}\sum_{n=1}^{N} w_{m,n} \cdot d(V_{GT}(S^U_m, T^U_n), V^{t_B}_{RTTI}(S^U_m, T^U_n)) \end{aligned} \tag{6.14}$$

The spatio-temporal extent of each cell is denoted with $w_{m,n}$ and the size of the area $X \times T$ with W. Dividing by W in equation 6.14 is necessary for normalization, i.e., to ensure that the computed difference value D does not depend on the size of $X \times T$.

Figure 6.5 is intended to illustrate the suggested approach for quantifying differences between ground truth and RTTI. Three contour plots are shown, all of them for a 34 kilometers long road corridor on the German autobahn A99 (southbound, starting about nine kilometers west of the interchange Munich north and ending roughly eight kilometers south of the interchange Munich east) for the time period between 16:30 and 20:00 on April 19th, 2012. The first one describes the ground truth, which is generated by applying the ASM on inductive loop detector data collected by 25 detectors along the road. Three jam waves between 17:45 and 18:45 can be observed. The second contour plot is based on commercial RTTI (only traffic state estimations, i.e., V_{RTTI}) received from a traffic content provider for the corresponding time and location. Traffic state estimations were updated at one-minute resolution and the TMC location code list is used for location referencing. This leads in total to 12 TMC road segments for the considered road corridor. Note that the dashed horizontal black lines in Figure 6.5 mark the spatial extent of the longest of these segments[53], which has a length of almost 5.6 kilometers. Based on the broadcasted RTTI, it is not possible to identify three separate jam waves. Solely a reduction of speed is indicated at the corresponding area on the spatio-temporal plane. The last contour

[53] Just as a remark: The corresponding TMC location code is „D01+12980“.

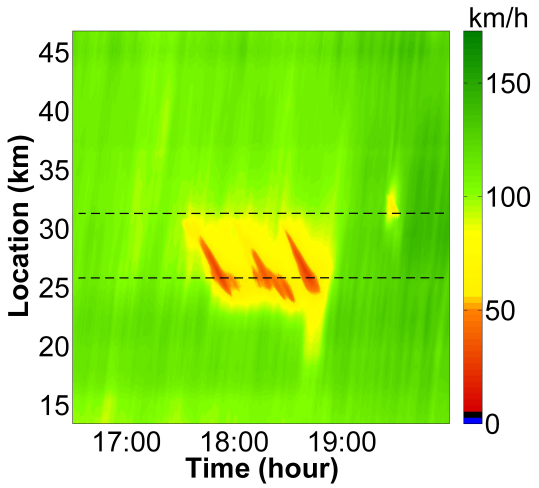

(a) Ground truth V_{GT}

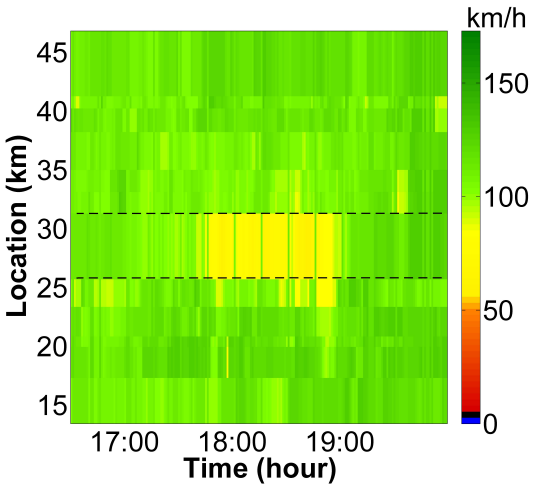

(b) Recorded RTTI V_{RTTI}

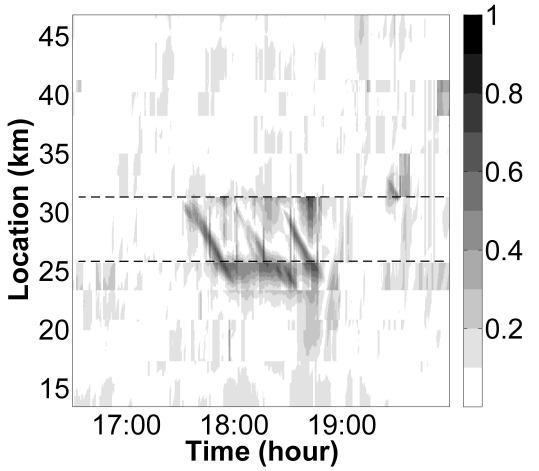

(c) Error plot: Visualization of absolute percentage differences between V_{GT} and V_{RTTI}

Figure 6.5: Visualization of ground truth, recorded RTTI, and the resulting relative errors for a corridor on a German freeway.

plot visualizes the resulting error ratings for each cell of the grid (spatial resolution Δx^{GT} of the ground truth grid is equal to 40 meters, temporal resolution Δt^{GT} is equal to 20 seconds). The absolute percentage error (APE) was applied for their computation, i.e., a measure d_{APE} is used with:

$$d_{APE}(a, b) := \frac{|\, b - a \,|}{b}. \tag{6.15}$$

The maximum of all occurring values $d_{APE}(V_{GT}(S_m^U, T_n^U), V_{RTTI}(S_m^U, T_n^U))$ is equal to 0.746. The resulting overall rating $D(V_{GT}, V_{RTTI}, X \times T, d_{APE})$, where X describes the road corridor and T the time period between 16:30 and 20:00 on April 19th, 2012, is equal to 0.083.

This means that the average[54] relative deviation between V_{GT} and V_{RTTI} is at about eight percent. It can be seen that errors occurred especially around congested areas. Unfortunately, adequate RTTI is most valuable in congested situations. One potential reason for these errors is the limited spatial resolution of the considered RTTI. For any TMC segment, the traffic content provider can only broadcast one speed value to describe the traffic situation along the whole segment. Particularly for the case of the TMC segment which is bordered by the dashed lines in Figure 6.5, the traffic content provider would have been unable to broadcast detailed information concerning the jam waves, even if the traffic content provider had been aware of them. These considerations motivate the generation of an alternative traffic state reconstruction, which takes a limited spatial, but also a limited temporal resolution of RTTI into account. This is considered in the following section.

6.2.5 Considering Restrictions of Resolution

For measuring the quality of RTTI, the applied reference is typically intended to approximate the real traffic situation as closely as possible. This proceeding seems to be reasonable since car drivers, who eventually use RTTI-based traffic services, compare the RTTI they receive to the real traffic situation – or at least to their perception of the real traffic situation. The left part of Figure 6.6 illustrates this idea. On the other hand, it has already been discussed that RTTI,

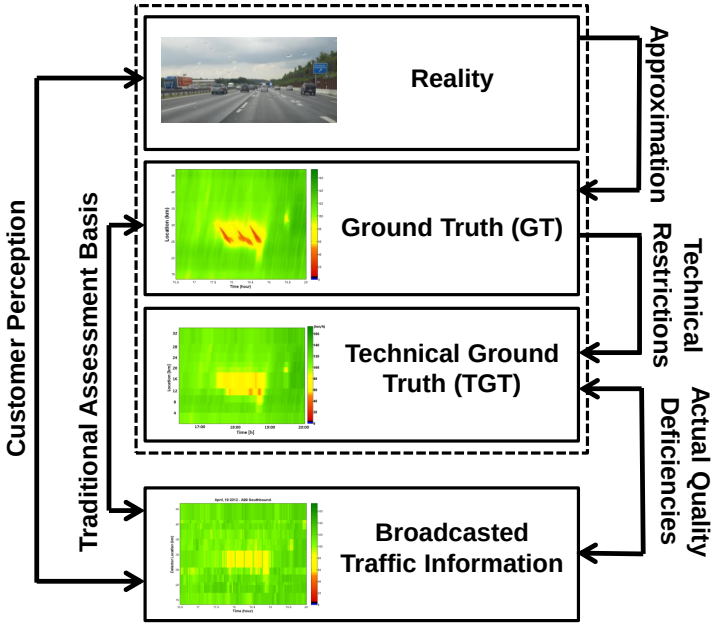

Figure 6.6: Scheme describing the idea of considering technical restrictions during the quality assessment process.

such as TMC-messages, often suffer from certain, primarily technical restrictions that limit the

[54] Due to the definition of D, „average“ is interpreted here in a spatio-temporal sense.

maximal possible quality that can be obtained. This aspect is especially important if companies, like car manufacturers, purchase commercial traffic data: The traffic content providers take lots of money for the supplied information. Accordingly, their industrial customers want certain quality standards to be fulfilled. If a costumer postulates that the spatial referencing of the broadcasted (commercial) RTTI needs to be based on the TMC location code list, then it seems unfair to make the provider responsible for inaccuracies caused by the technical limitations of TMC. However, this is exactly what traditional quality measurement methods do, since the best possible traffic state reconstructions are applied as reference, to which the RTTI is compared. Here, an alternative reconstruction scheme, denoted as **technical ground truth** (TGT), is suggested.

The central issue is that, even if a traffic content provider generated, based on the data that are available, the same ground truth which is later on used during the assessment, she/he still would not be able to broadcast it with all its details if the RTTI is bound to, for instance, the TMC location code list. In order to be able to mirror the perspective of the traffic content provider, the function V_{GT} is discretized according to the spatio-temporal grid defined by the RTTI that has to be assessed, i.e., according to road segments S_i^{RTTI} and time intervals T_j^{RTTI}. For this purpose, a harmonic mean speed is computed for each cell $S_i^{RTTI} \times T_j^{RTTI}$:

$$\begin{aligned} A_{i,j} &:= \int_{T_j^{RTTI}} \int_{S_i^{RTTI}} 1 dx\, dt \\ v_{harm}(S_i^{RTTI}, T_j^{RTTI}) &:= A_{i,j} \cdot \left(\int_{T_j^{RTTI}} \int_{S_i^{RTTI}} \frac{1}{V_{GT}(x,t)} dx\, dt \right)^{-1} \end{aligned} \tag{6.16}$$

In traffic, the harmonic mean is typically used to aggregate speed values. The arithmetic mean would lead to systematic bias when computing trajectory-based travel times on the basis of the corresponding spatio-temporal speed function. The harmonic mean avoids this effect (see Figure 4.10 in (*147*)). The discretized ground truth speed function is then defined by:

$$V_{TGT} : X \times T \to \mathbb{R}_{\geq 0} \tag{6.17}$$

$$V_{TGT}(x,t) := v_{harm}(S_i^{RTTI}, T_j^{RTTI}) \quad \forall (x,t) \in S_i^{RTTI} \times T_j^{RTTI}. \tag{6.18}$$

Obviously, V_{TGT} is constant within each cell $S_i^{RTTI} \times T_j^{RTTI}$. Recalling that V_{GT} is assumed to represent the real traffic situation, then V_{TGT} can be understood as the best possible approximation of the real traffic situation that can be achieved if one is bound to the grid that is induced by the spatial and temporal resolution of the considered RTTI. Note that function V_{TGT} is introduced here, since it will be used later on in section 6.3.2 for the derivation of auxiliary trajectories.

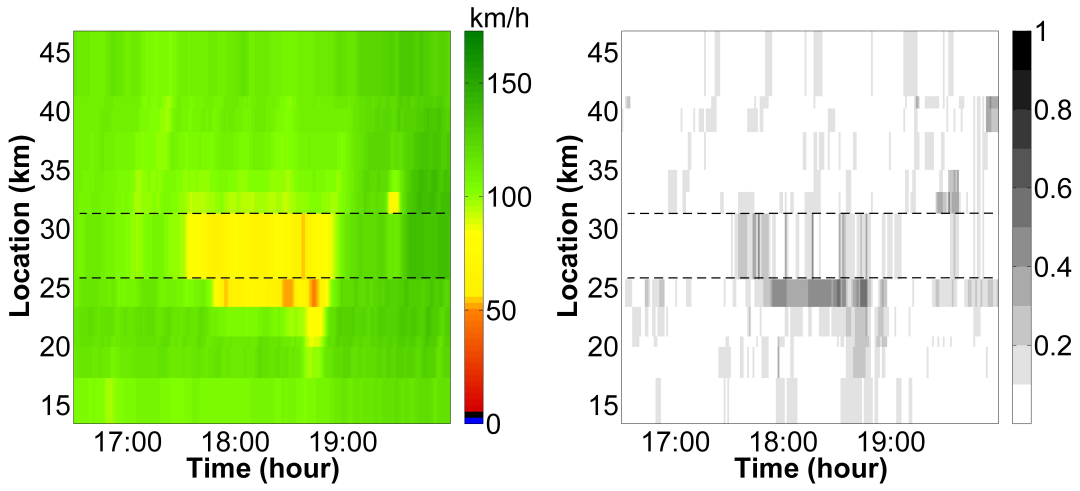

(a) V_{TGT}

(b) Error plot: Visualization of absolute percentage differences

Figure 6.7: Spatio-temporal visualization of differences between RTTI and the technical ground truth. Measure d_{APE} is applied here.

Figure 6.7 continues the example from Figure 6.5. The contour plot on the left shows V_{TGT}, the right contour plot the resulting differences to V_{RTTI}. It can be observed that the differences between V_{TGT} and V_{RTTI} are less significant than the differences between V_{GT} and V_{RTTI}. The main reason for this is that the three jam waves also vanish for V_{TGT}. Furthermore, the right part of Figure 6.7 indicates that real quality problems occur especially between kilometers 23 and 26. The considered RTTI overestimates average driving speeds there. In contrast, the situation for TMC segment D01+12980 (between the two dashed horizontal lines) is represented rather well, at least under the restriction that only one speed value can be broadcasted for the whole segment. Consequently, the quality deficiencies that can be observed in the error plot of Figure 6.5 for TMC segment D01+12980 (between the dashed lines) seem to be primarily caused by the limited spatial resolution of the considered RTTI[55].

6.3 Trajectory Buffer for Error-prone Traffic Information

One of the three tasks that has to be carried out in chapter 6 is the provision of a concrete formulation of the trajectory buffer function $SOC_{min}^{t,NT}$ in order to test it within the simulation study in chapter 7. The motivation for this is that, otherwise, after excluding quantile-based energy buffers from further consideration, solely relative buffers could be tested. Relative buffers show some advantageous properties, but the level of adaptivity which can be achieved by relative buffers is limited (see Table 5.1, where the three proposed energy buffer functions were

[55] Actually, these deviations between V_{GT} and V_{RTTI} could also be caused by the limited temporal resolution of V_{RTTI}. Here, this is not the case due to the RTTI's high update rate of one minute.

compared). This is because function $SOC^{r,z}_{min}$ only depends on the predicted energy consumption costs. As long as these costs remain the same, also the size of the relative energy buffer does not change – independently of how reliable the available RTTI or other relevant quantities are expected to be. Trajectory buffers, on the contrary, may be able to ensure a high level of adaptivity, but their ability to achieve this depends heavily on the applied method for generating sets of auxiliary trajectories. Up to this point, it has not been explained how sets of reasonable driving trajectories can be generated. Actually, this had been hardly possible due to the rather abstract problem formulation stated in chapter 5, where energy and time edge costs were simply assumed to be given. In the following, under the presumption that RTTI can be used to derive driving trajectories, a corresponding approach is described. Two goals are relevant in this context: First, the computational effort for generating sets of auxiliary driving trajectories has to be kept low in order to avoid any negative impact with regard to RO 1c. Second, a certain level of adaptivity shall be obtained, i.e., the resulting energy buffer function should take varying reliability of RTTI into account.

The proceeding in section 6.3 is the following: In section 6.3.1, the description of a method for generating sets of auxiliary trajectories is stated. The fundament of this method is a prediction of lower and upper bounds for (macroscopic) average driving speeds. This means that instead of one spatio-temporal speed function $V^{t_B}_{RTTI}$, which returns a single speed value in dependency of location and time, two spatio-temporal speed functions are applied, which return lower and upper speed bounds. These bounds have to be defined in such a way that it is very likelty that the real future driving speeds lie between these bounds. An approach to derive such speed bounds based on commercial RTTI is described in section 6.3.2. Finally, in section 6.3.3, some issues resulting from deriving driving trajectories (which actually are a microscopic type of data) from RTTI (which is typically interpreted as a macroscopic kind of data) are discussed.

6.3.1 Trajectory Buffer on the Basis of Speed Bounds

Figure 6.8 schematically illustrates the approach that is described subsequently. First, given a time t_B at which RTTI is broadcasted[56], it is intended to compute two spatio-temporal speed functions $V^{t_B}_{low}$ and $V^{t_B}_{up}$, which represent lower and upper bounds for random variable V_{Real}:

$$V^{t_B}_{low}(x,t) \leq \bar{V}_{Real}(x,t) \leq V^{t_B}_{up}(x,t) \quad \forall x \ \in e, \ t \geq t_B. \tag{6.19}$$

In literature, it is not uncommon for traffic prediction methods to return ranges instead of specific values (*80*) (*81*). As V_{Real} describes driving speeds, such bounds naturally exist. For instance, a speed of zero can be applied as a lower bound and the considered vehicle's maximal driving speed as an upper bound. However, to keep these ranges tight and thus interesting for

[56]To reduce notational complexity, it is from here on assumed that the time t_0, at which a charging strategy is requested, is equal to the time t_B, at which the RTTI is broadcasted. All approaches would work similarly if it was differentiated between these times.

applications, outliers are typically excluded from consideration by postulating bounds that hold solely with a certain probability $\alpha \in [0, 1]$:

$$\mathbb{P}(V_{low}^{t_B,\alpha}(x,t) < V_{Real}(x,t)) = \alpha \tag{6.20}$$

$$\mathbb{P}(V_{up}^{t_B,\alpha}(x,t) > V_{Real}(x,t)) = \alpha \tag{6.21}$$

In section 6.3.2, an approach for deriving such probabilistic speed bounds will be explained. For the moment, spatio-temporal speed functions $V_{low}^{t_B,\alpha}$ and $V_{up}^{t_B,\alpha}$, which fulfill the conditions defined in equations 6.20 and 6.21, can simply be assumed to be given. Note that the proposed definition of speed bounds provides a possibility to interpret reliability in the context of RTTI: It can be said that reliable RTTI allows deriving speed bound functions $V_{low}^{t_B,\alpha}$ and $V_{up}^{t_B,\alpha}$ which show small differences to each other even for high values of α. This means that that function $V_{RTTI}^{t_B}$ is „reliable“ if the probability that big errors occur is low.

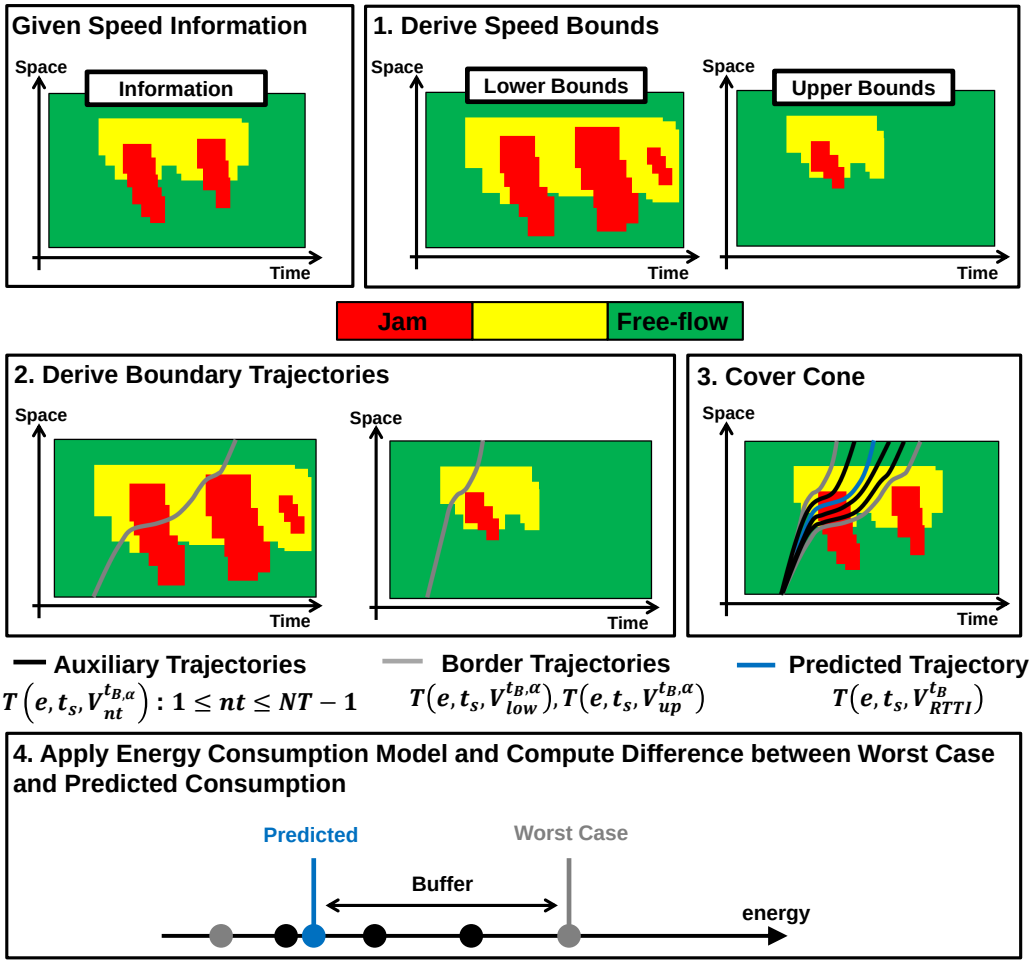

Figure 6.8: Generation of a trajectory set on the basis of speed bound functions.

In a second step, for some time $t_S \geq t_B$[57] and a specific road segment e, where $\underline{e}$ denotes its start and $\overline{e}$ denotes its end, speed functions $V_{low}^{t_B,\alpha}$ and $V_{up}^{t_B,\alpha}$ are applied to construct „boundary“ trajectories $T(e, t_S, V_{low}^{t_B,\alpha})$ and $T(e, t_S, V_{up}^{t_B,\alpha})$. To receive these trajectories, differential equation 6.1 has to be solved after replacing its right-hand side either by function $V_{low}^{t_B,\alpha}$ or by function $V_{up}^{t_B,\alpha}$. These two trajectories form a shape on the spatio-temporal plane that looks similar to a cone, where the vertex of the cone is given by $(\underline{e}, t_S)$. This is illustrated by the two gray trajectories which are placed in the contour plot under point three in Figure 6.8. If α is set equal to 1.0, then any possible driving trajectory $T(e, t_S, \bar{V}_{Real})$, independently of the realization $\bar{V}_{Real}$, is located between these boundary trajectories due to inequalities 6.20 and 6.21. If α is set close to 1.0, then at least most possible driving trajectories can be assumed to be located within the cone.

During the third step, a set of reasonable trajectories is generated which covers this cone comprehensively. This set is afterwards used to compute the size of the buffer according to the methodology described in section 5.3.3 (see also the fourth step in Figure 6.8). The idea is that at least one of the generated trajectories looks similar to the real, not yet known driving trajectory $T(e, t_S, \bar{V}_{Real})$. To generate auxiliary trajectories which cover the cone comprehensively, the following procedure is executed: Construct for each index $nt \in \{0, 1, ..., NT\}$ with $NT \in \mathbb{N}_{>0}$ a spatio-temporal speed function $V_{nt}^{t_B,\alpha}$ as described below (this could be done analogously if $V_{low}^{t_B}$ and $V_{up}^{t_B}$, and not $V_{low}^{t_B,\alpha}$ and $V_{up}^{t_B,\alpha}$ were considered):

$$V_{nt}^{t_B,\alpha}(x,t) := \frac{NT - nt}{NT} \cdot V_{low}^{t_B,\alpha}(x,t) + \frac{nt}{NT} \cdot V_{up}^{t_B,\alpha}(x,t). \tag{6.22}$$

It holds that $V_0^{t_B,\alpha} = V_{low}^{t_B,\alpha}$. With increasing nt, these functions turn from $V_{low}^{t_B,\alpha}$ to $V_{up}^{t_B,\alpha}$ with $V_{NT}^{t_B,\alpha} = V_{up}^{t_B,\alpha}$. For each of these functions, one auxiliary trajectory $T^{nt}(e, t_S) := T(e, t_S, V_{nt}^{t_B,\alpha})$ is computed. These trajectories cover the aforementioned cone equally (in a spatio-temporal sense).
If the reliability of $V_{RTTI}^{t_B}$ is low, then the range between $V_{low}^{t_B,\alpha}$ and $V_{up}^{t_B,\alpha}$ is comparably big even for small values of α. Along with this, the cone which is defined by the two boundary trajectories becomes wide. This leads to a set of trajectories $\{T^{nt}(e, t_S)\}_{nt=0,...,NT}$ which show more diversity, i.e., the differences between the auxiliary trajectories rise. It will turn out that under realistic conditions, particularly those driving trajectories that show very low or very high speeds cause high energy consumption. As a consequence, in most cases one of both border trajectories leads to the highest energy consumption values. A further consequence is that the size of the trajectory energy buffer tends to rise with the width of the cone, since wide cones lead to very low and very high speeds at its borders. If $V_{RTTI}^{t_B,\alpha}$ is expected to be reliable, it is

[57] Recall that t_S denotes the planned start of the trip and that this is not necessarily the time at which the charging strategy computation takes place.

the other way around and the energy buffer's size gets small. Consequently, the suggested trajectory generation method should be able, up to some degree, to achieve that $SOC_{min}^{t,NT}$ returns high values in situations in which RTTI tends to be less reliable, and low values in situations in which RTTI is reliable. Note that the size of the trajectory energy buffer also tends to become bigger if higher values of α are used, since the cone again becomes wider. Increasing the number of trajectories NT may also have some influence, but the proposed method for trajectory generation makes it, as already mentioned, unlikely that the highest energy consumption values result from non-border trajectories. Due to this, increasing the number of trajectories has only little influence on the resulting energy buffer.

It is worth mentioning that the suggested approach for generating a set of trajectories is computationally not too expensive. This allows including it into algorithms for computing optimal charging strategies. On the other hand, there is no guarantee that the real driving trajectory $T(e, t_S, \bar{V}_{Real})$ (or $T(e, t_S, V_{GT})$, respectively) looks similar to one of the constructed trajectories. Furthermore, it is up to this point not clear how speed bounds $V_{low}^{t_B}$ and $V_{up}^{t_B}$ (or $V_{low}^{t_B,\alpha}$ and $V_{up}^{t_B,\alpha}$, respectively) can be derived. However, a corresponding approach will be described during the next sections.

6.3.2 Prediction of Speed Bounds for Real-time Traffic Information

In this section, an approach to derive lower and upper speed bounds $V_{low}^{t_B,\alpha}$ and $V_{up}^{t_B,\alpha}$ is explained. For this purpose, it is assumed that commercial RTTI is received and represented by a spatio-temporal speed function $V_{RTTI}^{t_B}$. The section can be separated into three parts. During the first part, a random variable Y is introduced, which describes, depending on location and time, deviations between the RTTI and a reconstructed ground truth. It is conjectured that a relation exists between the distribution of Y and several, not yet identified explanatory variables[58] $E_1, E_2, ..., E_Q$ with $Q \in \mathbb{N}$. In the second part of this section, a set of potential explanatory variables is proposed. Finally, in the third part, a training set $\{y^m, e_1^m, e_2^m, ..., e_Q^m\}_{m=1,2,...,M}$, consisting of $M \in \mathbb{N}$ realizations y^m of random variable Y and the corresponding observations e_q^m of the explanatory variables, is used to derive probabilistic bounds for Y in dependency of the observations belonging to the explanatory variables. The idea is that at time t_B, at which the charging strategy is requested and, due to this, at which the speed bounds have to be constructed, the realizations of the set of explanatory variables are already available. The realizations of Y, on the contrary, are unknown. The derived bounds for Y are afterwards applied to generate functions $V_{low}^{t_B,\alpha}$ and $V_{up}^{t_B,\alpha}$. It is worth mentioning that the proposed approach can basically be used to generate speed bounds for any kind of spatio-temporal speed function and not only for the case of a function representing commercial RTTI. Though, some of the suggested explanatory variables explicitly refer to the case of commercial RTTI.

[58] Explanatory variables are often also denoted as predictors or independent variables.

Definition of the Dependent Variable The dependent variable Y is defined depending on location and time as the relative difference between ground truth driving speeds and the RTTI:

$$Y(S_i^{RTTI} \times T_j^{RTTI}) := D(V_{TGT}, V_{RTTI}^{t_B}, S_i^{RTTI} \times T_j^{RTTI}, d_{PE}). \tag{6.23}$$

Function D is here defined as stated in equation 6.14 and the difference measure d_{PE} denotes the relative difference between the first and the second input („PE“ for „percentage error“):

$$d_{PE}(v_1, v_2) := \frac{v_1 - v_2}{v_2}. \tag{6.24}$$

Note that the technical ground truth V_{TGT} is used as the reference[59] to which $V_{RTTI}^{t_B}$ is compared in equation 6.23. This is because $V_{RTTI}^{t_B}$ is constant in each cell $S_i^{RTTI} \times T_j^{RTTI}$. Most of the explanatory variables which will be considered later on are based on $V_{RTTI}^{t_B}$ and hence they are also constant in each cell $S_i^{RTTI} \times T_j^{RTTI}$. Due to this, the suggested approach hardly allows making distinctions between locations and points in time that are part of the same cell. This suggests discretizing V_{GT} to V_{TGT}. Furthermore, the discretization simplifies further notation, as solely one grid needs to be considered, and reduces computation times since the resolution of the RTTI-based grid is lower than the resolution of the ground truth grid.

For generating the set $\{y^m\}_{m=1,2,...,M}$, it solely remains to specify road segments $S_{i_m}^{RTTI}$, time intervals $T_{j_m}^{RTTI}$, and times t_B^m at which the RTTI is requested[60]. The realizations y^m of the dependent variable Y are then defined as stated below:

$$y^m := y(t_B^m, S_{i_m}^{RTTI}, T_{j_m}^{RTTI}) := D(V_{TGT}, V_{RTTI}^{t_B^m}, S_{i_m}^{RTTI} \times T_{j_m}^{RTTI}, d_{PE}) \tag{6.25}$$

Due to the definition of D and the fact that V_{TGT} and $V_{RTTI}^{t_B^m}$ are constant within each cell $S_{i_m}^{RTTI} \times T_{j_m}^{RTTI}$, this can also be written as:

$$y^m = y(t_B^m, S_{i_m}^{RTTI}, T_{j_m}^{RTTI}) = \frac{V_{TGT}(S_{i_m}^{RTTI}, T_{j_m}^{RTTI}) - V_{RTTI}^{t_B^m}(S_{i_m}^{RTTI}, T_{j_m}^{RTTI})}{V_{RTTI}^{t_B^m}(S_{i_m}^{RTTI}, T_{j_m}^{RTTI})}. \tag{6.26}$$

In equation 6.26, $V_{RTTI}^{t_B^m}(S_{i_m}^{RTTI}, T_{j_m}^{RTTI})$ denotes the speed value that $V_{RTTI}^{t_B^m}$ obtains in cell $S_{i_m}^{RTTI} \times T_{j_m}^{RTTI}$. Analogously, $V_{TGT}(S_{i_m}^{RTTI}, T_{j_m}^{RTTI})$ denotes the corresponding speed value for function V_{TGT}. The realizations of the dependent variable Y describe the deviations between RTTI and ground truth for the corresponding location and time. Usually, it is written y^m instead of $y(t_B^m, S_{i_m}^{RTTI}, T_{j_m}^{RTTI})$ to shorten notation.

[59] Usually, the denominator refers to the quantity which is used as the reference if percentage errors are computed. Here, it is the other way around. This will be of relevance later on.

[60] Here, it is written $S_{i_m}^{RTTI}$ and $T_{j_m}^{RTTI}$ instead of S_i^{RTTI} and T_j^{RTTI} to emphasize that possibly not all road segments and time intervals are included into the generation of the training set. This means that $i_m \in \{1, ..., I\}$ and $j_m \in \{1, ..., J\}$ for all $m \in \{1, ..., M\}$.

Identify Potential Explanatory Variables Now, a set of explanatory variables $E_1, ..., E_Q$ has to be identified which allows drawing conclusions on the distribution of the dependent variable Y. The goal is to make predictions about the reliability of the considered commercial RTTI. In this context, a critical aspect of working with commercial RTTI is that the receiver typically does not know how much and which types of raw traffic data (data from detectors, probe data, etc.) were used for the generation of the RTTI, nor does she/he know how the data were processed. Moreover, for the case of traffic predictions, the applied prediction procedure is usually unknown, too. Therefore, the set of potential explanatory variables is limited. In the following, an exemplary selection of five potential explanatory variables is discussed: Prediction horizon, historical relative speed averages, estimations of current relative driving speeds, the time of day, and so-called confidence values that are broadcasted along with the RTTI. For this purpose, it is assumed that, besides function $V_{RTTI}^{t_B}$, spatio-temporal speed functions V_{Hist} and V_{ff} are available. Function V_{Hist} describes historical driving speed averages depending on location and time. For simplicity, it is assumed that V_{Hist} is also piecewise constant within the cells $S_i^{RTTI} \times T_j^{RTTI}$ of the spatio-temporal grid which is induced by the RTTI. It contains no information about recent incidents and is solely based on historical traffic data. Function V_{ff} is independent of time. It assigns, probably also based on historical traffic data, estimated free-flow driving speeds to road segments S_i^{RTTI}. Function V_{ff} is used to compute relative driving speeds. Relative speeds means here that speeds are given in percent of free-flow speed. Furthermore, the availability of a function Cf^{t_B} („Cf“ for „confidence“) is expected. Nowadays, private traffic content providers typically deliver such confidence values to give their customers an idea of how much recently collected probe data were available for generating the broadcasted RTTI. Intuitively, it could be expected that with an increasing amount of available and recently collected traffic data, also the reliability of the RTTI increases.

The first and maybe most intuitive potential explanatory variable for the quality of RTTI is the prediction horizon, i.e., the time span between the time at which the information is received and the time for which speeds are predicted. Mathematically, the realizations of the corresponding predictor E_1 can be defined as follows:

$$e_1^m := e_1(t_B^m, S_{i_m}^{RTTI}, T_{j_m}^{RTTI}) := \underline{T}_{j_m}^{RTTI} - t_B^m \quad \forall m \in \{1, 2, ..., M\}. \tag{6.27}$$

In equation 6.27, the starting time of interval $T_{j_m}^{RTTI}$ is denoted by $\underline{T}_{j_m}^{RTTI}$. The idea for analyzing prediction horizons as potential predictors for RTTI quality is that the further one intends to look into the future, the less reliable traffic predictions probably become (*112*).

Congestion and along with it changing traffic conditions usually do not appear unless a certain level of road utilization is reached. If there are almost no cars on the road, then it is very unlikely that a change from free-flow to congestion (or the other way around) occurs. Due to this,

in situations in which road utilization can be expected to be extremely low, RTTI should be quite reliable, simply because there is nothing to report or broadcast, respectively. In order to determine road utilization, traffic volume needs to be known. Private traffic content providers, since they rely primarily on probe data and usually collect traffic data from only a few percent of all driving vehicles, probably cannot estimate traffic volume reliably. Stationary detectors, which are usually capable of measuring flows, cover the road network only sparsely. Consequently, it may be hard to achieve a comprehensive coverage of the entire road network with real-time flow data. As an alternative, the utilization can be estimated indirectly based on relative driving speeds. This is what is done in the following. For this purpose, it is used that low relative speeds indicate high utilization according to the fundamental diagram. Considering the available data, two types of speed information can be applied in order to achieve this, namely historical speeds and RTTI. Based on them, the realizations of two potential predictors are defined as subsequently described:

$$e_2^m := e_2(t_B^m, S_{i_m}^{RTTI}, T_{j_m}^{RTTI}) := \frac{V_{Hist}(S_{i_m}^{RTTI}, T_{j_m}^{RTTI})}{V_{ff}(S_{i_m}^{RTTI})} \quad \forall m \in \{1, 2, ..., M\} \tag{6.28}$$

$$e_3^m := e_3(t_B^m, S_{i_m}^{RTTI}, T_{j_m}^{RTTI}) := \frac{V_{RTTI}^{t_B^m}(S_{i_m}^{RTTI}, t_B^m)}{V_{ff}(S_{i_m}^{RTTI})} \quad \forall m \in \{1, 2, ..., M\} \tag{6.29}$$

Here, E_2 denotes historical relative speed averages and E_3 denotes the estimation of current relative driving speeds. $V_{Hist}(S_{i_m}^{RTTI}, T_{j_m}^{RTTI})$ denotes the speed values which V_{Hist} returns for any point $(x,t) \in S_{i_m}^{RTTI} \times T_{j_m}^{RTTI}$, $V_{ff}(S_{i_m}^{RTTI})$ denotes the speed value which V_{ff} returns for any location $x \in S_{i_m}^{RTTI}$, and $V_{RTTI}^{t_B^m}(S_{i_m}^{RTTI}, t_B^m)$ denotes the speed value which $V_{RTTI}^{t_B^m}$ returns for any point (x, t_B^m) with $x \in S_{i_m}^{RTTI}$.

The historical speed data provide historical speed averages depending on location and time. If on a certain road segment during a certain time interval congestion occurs frequently, then these average driving speeds also lie significantly below the corresponding free-flow speed. Conversely, if historical speed profiles show no reduction of average driving speeds, then this is interpreted as an indicator that congestion occurs only rarely. Under such typically stable conditions, there is (in most cases) not much which can be predicted incorrectly. As a consequence, it is concluded that RTTI quality is probably comparably high.

The same way as predictor E_2 is intended to characterize typical traffic conditions, predictor E_3 is intended to characterize current traffic conditions. If low relative speeds are broadcasted at time t_B, then it is likely that the corresponding road segment is congested at time t_B, which again possibly makes predicting the future evolution of traffic for this location harder than for the low-utilization case. Whether this suspicion is true or not depends on the prediction algorithms that are applied by the traffic content provider.

Note that besides characterizing regular or current traffic conditions, considering E_2 and E_3 in parallel may also be interesting: Huge differences between the currently estimated relative

driving speeds and the historical relative speed averages may indicate a very uncommon traffic situation. Hence, traffic prediction may not be able to describe future traffic situations as accurately as in other situations which show a more regular behavior.

The fourth of the suggested potential predictors is the time of day for which the traffic situation is predicted:

$$e_4^m := e_4(t_B^m, S_{i_m}^{RTTI}, T_{j_m}^{RTTI}) := \underline{T}_{j_m}^{RTTI} \quad \forall m \in \{1, 2, ..., M\}. \tag{6.30}$$

The idea for explanatory variable E_4 is, similar to E_2 and E_3, that it is easy to predict traffic if nothing is happening. During nights, traffic volume typically is very low. Along with that, congestion occurs very rarely. Therefore, it can be expected that there is free-flow during nights if the traffic content provider states free-flow. Admittedly, historical relative speed averages should be able to represent the in most cases stable traffic situations during nights, too. However, it could be imagined that congestion is in general less probable during nights than during off-peak periods (which also exist during the day), where historical data may show very high relative speed averages, too[61]. This could be an advantage of E_4 in comparison to E_2. Another important aspect is that roads exist, on which congestion occurs regularly during nights. This can be the case, for instance, if shift operations are typical for the local industry. As a consequence, predictor E_4 may not work well for all road segments.

Function $Cf^{t_B^m}$ forms the basis for the last of the suggested predictors:

$$e_5^m := e_5(t_B^m, S_{i_m}^{RTTI}, T_{j_m}^{RTTI}) := Cf^{t_B^m}(S_{i_m}^{RTTI}) \tag{6.31}$$

Whenever RTTI is broadcasted for a road segment, customers of traffic content providers usually receive a confidence value for this road segment, too. Confidence values are intended to represent, as already mentioned, the amount of recently collected data which are used to generate the broadcasted RTTI. Intuitively, it could be expected that high confidence values go hand in hand with better RTTI.

Derivation of Probabilistic Bounds Up to this point, it has been described how the training set $\{y^m, e_1^m, ..., e_Q^m\}_{m=1,2,...,M}$ is generated. Based on the training set, a regression equation is formed. The relation between the dependent variable Y and the explanatory variables $E_1, ..., E_Q$ is expressed by a function $R : \mathbb{R}^Q \to \mathbb{R}$ and a noise term $\epsilon : \mathbb{R}^Q \to \mathbb{R}$, which

[61] For clarification: Measuring average driving speeds during nights is sensitive to outliers due to the low traffic flow. Data delivered by trucks, for instance, may decrease historical relative speed averages significantly - even if always free-flow conditions prevail. This has influence on the explanatory power of E_2.

accounts for random scatter and the influence of unobserved explanatory variables:

$$Y = R(e_1, ..., e_Q) + \epsilon(e_1, ..., e_Q). \tag{6.32}$$

If RTTI perfectly mirrored real driving speeds, then it would hold that

$$R(e_1, ..., e_Q) \equiv \epsilon(e_1, ..., e_Q) \equiv 0. \tag{6.33}$$

An important difference to linear regression models, which is probably one of the most common approaches to derive relations between a dependent variable and a set of explanatory variables, is that no homoscedasticity is expected (see page 90 in (8)), i.e., the variance of the residuals ϵ is not expected to be constant. This is expressed by writing $\epsilon(e_1, ..., e_Q)$ instead of ϵ in equation 6.32. Actually, since it is intended to derive probabilistic bounds for Y depending on the realizations of $E_1, ..., E_5$, heteroscedasticity is implicitly conjectured. If Y was homoscedastic, the bounds could be chosen independently of these realizations of $E_1, ..., E_Q$, which would mean that the reliability of the considered RTTI depended not on $E_1, ..., E_Q$.

Another difference to typical regression approaches is that the goal is to estimate probabilistic bounds for Y. Correspondingly, it is not the goal to find a good regression function R, but to identify a quantile function R_α, which fulfills for $\alpha \in]0, 1]$ the following property:

$$R_\alpha(e_1, ..., e_Q) := inf\,\{y^* \in \mathbb{R} \mid \mathbb{P}(Y \geq y^*) \leq 1 - \alpha\} \tag{6.34}$$

Function R_α returns for a given vector of observations $(e_1, ..., e_Q)$ the α-quantile of random variable Y. Based on the definition of R_α, speed bounds $V_{t_B}^{low,\alpha}$ and $V_{t_B}^{up,\alpha}$, which fulfill the probabilistic boundary properties stated in inequalities 6.20 and 6.21, can be constructed as described below (see the definition of y^m in equation 6.26):

$$V_{t_B}^{low,\alpha}(x,t) := (1 + R_{1-\alpha}(e_1, ..., e_Q)) \cdot V_{RTTI}^{t_B^m}(x,t) \tag{6.35}$$

$$V_{t_B}^{up,\alpha}(x,t) := (1 + R_{\alpha}(e_1, ..., e_Q)) \cdot V_{RTTI}^{t_B^m}(x,t) \tag{6.36}$$

It is worth mentioning that the probability that V_{TGT} is located between $V_{t_B}^{low,\alpha}$ and $V_{t_B}^{up,\alpha}$ is only equal to $1 - 2 \cdot \alpha$, since both boundaries are violated with a probability of α.

To construct a quantile function R^α on the basis of a training set $\{y^m, e_1^m, ..., e_Q^m\}_{m=1,2,...,M}$, the realizations $\{e_1^m, ..., e_Q^m\}_{m=1,2,...,M}$ are separated into categories. Then, for each of these categories, the α-quantile over all corresponding realizations y^m is computed.
In a first step, the lowest and the biggest of all occurring realizations for each explanatory

variable E_q are calculated:

$$E_q^{min} := min\left\{e_q^m \mid m \in \{1,2,...,M\}\right\} \quad \forall q \in \{1,...,Q\} \tag{6.37}$$

$$E_q^{max} := max\left\{e_q^m + \delta \mid m \in \{1,2,...,M\}\right\} \quad \forall q \in \{1,...,Q\}. \tag{6.38}$$

A small positive value $\delta \in \mathbb{R}_{>0}$ is used to ensure that all realizations of explanatory variable E_q lie within the interval $[E_q^{min}, E_q^{max}[$. In a second step, each interval $[E_q^{min}, E_q^{max}[$ is sep-

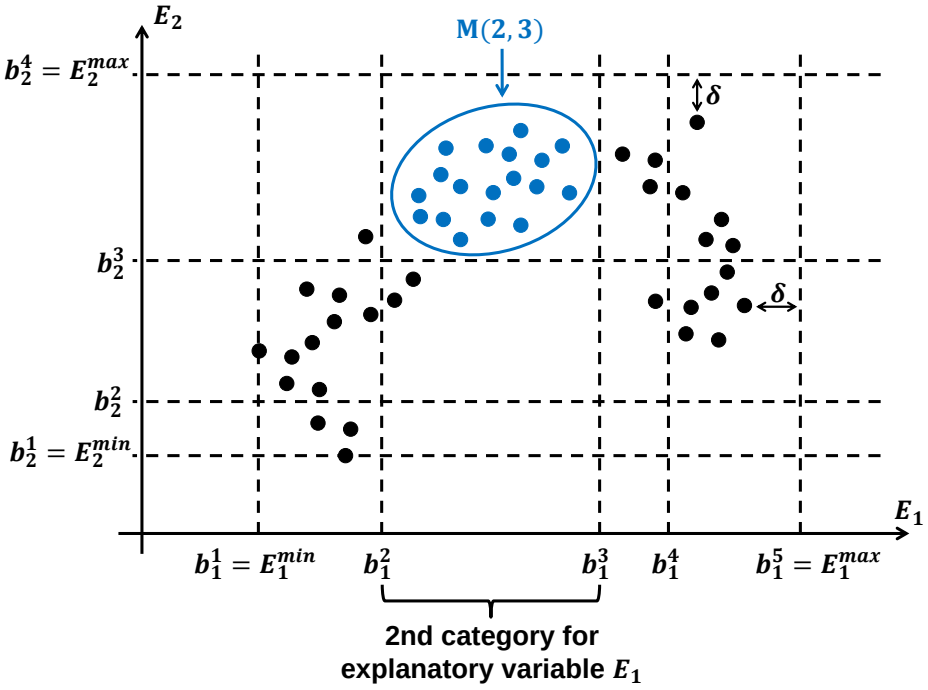

Figure 6.9: Illustration of notation which is relevant for the categorization of the training dataset according to realizations of the explanatory variables.

arated into a set of $B_q \in \mathbb{N}$ categories $[b_q^i, b_q^{i+1}[$ with $i \in \{1,2,...,B_q\}$. The borders b_q^i of these categories have to be chosen in such a way that they fulfill the subsequently described conditions:

$$E_q^{min} = b_q^1 < b_q^2 < ... < b_q^{B_q} < b_q^{B_q+1} = E_q^{max}. \tag{6.39}$$

These categories can be used to partition the set of indices $\{1,2,...,M\}$ into sets $M(i_1,...,i_Q)$ (with $i_1 \in \{1,...,B_1\}$, $i_2 \in \{1,...,B_2\}$, and so on) with:

$$M(i_1,...,i_Q) := \{m^* \in \{1,2,...,M\} \mid e_q^{m^*} \in [b_q^{i_q}, b_q^{i_q+1}[\quad \forall q \in \{1,...,Q\}\} \tag{6.40}$$

The result are $B_1 \cdot B_2 \cdot ... \cdot B_Q$ different index sets $M(i_1,...,i_Q) \subseteq \{1,2,...,M\}$. Most of the introduced variables are exemparily illustrated for the case of two explanatory variables in Figure 6.9. The black points represent an artificially generated set $\{e_1^m, e_2^m\}_m$. In a third step,

for each of these index sets, the α-quantile over all corresponding realizations y^m is computed:

$$r_\alpha(i_1, ..., i_Q) := \alpha\text{-quantile of } \{y^m \mid m \in M(i_1, ..., i_Q)\} \tag{6.41}$$

Finally, these quantiles r_α are applied in order to define the value which function R_α assigns to a vector $(e_1, e_2, ..., e_Q)$:

$$R_\alpha(e_1, e_2, ..., e_Q) := r_\alpha(i_1, ..., i_Q), \text{ where indices } i_1, ..., i_Q \text{ are defined as follows:} \tag{6.42}$$

$$i_q := \{i \in 1, 2, ..., B_q \mid e_q \in [b_q^i, b_q^{i+1}[\ \} \quad \forall q \in \{1, 2, ..., Q\} \tag{6.43}$$

For the case of one explanatory variable, an idea of the shape of such quantile functions is pro-

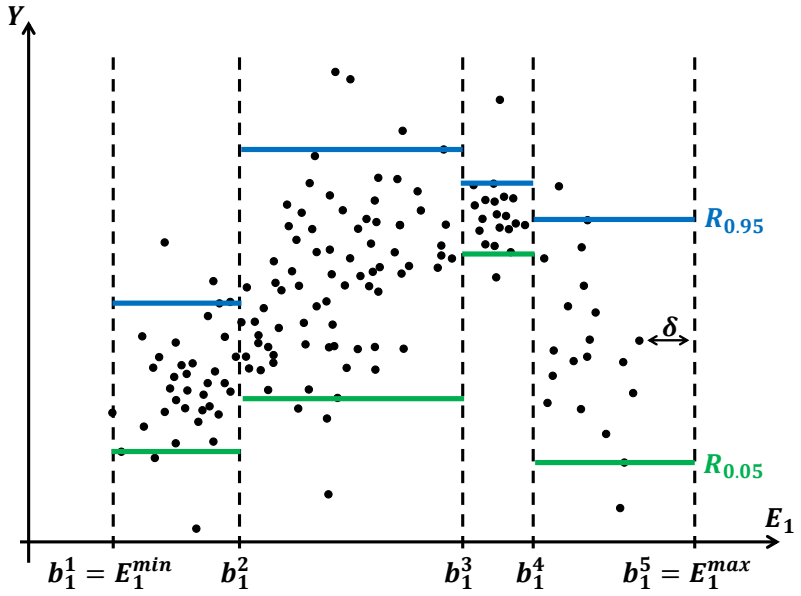

Figure 6.10: Illustration of the shape of quantile functions for .

vided by Figure 6.10. There, the black points represent an artificially generated set $\{y^m, e_1^m\}_m$, i.e., only one explanatory variable is considered. Note that functions R_α are constant within each of the defined categories. Furthermore, it can be seen that whenever the scatter of the points within one cell is small, the difference between the two displayed quantile functions is small, too.

In the following, in order to reduce the computational effort for constructing functions R_α, typically not all explanatory variables $E_1, ..., E_Q$ are taken into account simultaneously. To account for this, it is, for instance, written $R_\alpha(e_1, e_3)$ instead of $R_\alpha(e_1, ..., e_Q)$ if solely the first (prediction horizon) and the third (current relative speed estimations) explanatory variables are considered.

The suggested construction of R_α is intended to fulfill the idea of equation 6.34, i.e., that R_α

is intended to return for any realization $(e_1, ..., e_Q)$ the α-quantile of random variable Y. Certainly, this is a purely statistical and not an analytical approach. If the amount of available data is high and if a relation as described by equation 6.32 exists, then it can be expected that $V_{low}^{t_B,\alpha}$ and $V_{up}^{t_B,\alpha}$ fulfill the probabilistic boundary properties of inequalities 6.20 and 6.21 rather well. Note that also other, more sophisticated approaches for generating functions R_α could be applied, such as machine learning techniques. Typical regression approaches, on the other hand, are less suited. It will turn out that the relation between Y and the proposed explanatory variables $E_1, ..., E_5$ is neither linear, nor monotone. This, alongside the aforementioned heteroscedasticity of Y, makes them hardly applicable.

6.3.3 Individuality and Macroscopic Traffic Information

Function $V_{RTTI}^{t_B}$ provides information on a macroscopic scale. As a consequence, trajectory $T(e, t_S, V_{RTTI}^{t_B})$ has to be understood as a „macroscopic driving trajectory“. According to the author's experience, such trajectories do typically not have the same properties as microscopically recorded[62] trajectories. Due to data aggregation during the generation of $V_{RTTI}^{t_B}$ or due to a limited spatial resolution of $V_{RTTI}^{t_B}$, macroscopic trajectories tend to show less oscillation of speeds than microscopic trajectories do. Figure 6.11 illustrates this statement exemplarily for a recorded test drive on the German freeway A9, between the interchange Munich north and the exit ramp Pfaffenhofen. The recording started at 17:37 on November 6th, 2014. Location can be found on the x-axis and speed on the y-axis. The blue line describes microscopically recorded driving speeds[63]. The gray line describes speeds which result when deriving a corresponding macroscopic driving trajectory from RTTI[64] which has been broadcasted by a private traffic content provider for the corresponding time period and road corridor. The starting time and starting location of the microscopically recorded test drive is also used for the generation of the macroscopic trajectory on the basis of differential equation 6.1. The broadcasted RTTI is updated at one-minute resolution. The vertical red lines indicate the spatial resolution according to which the traffic content provider broadcasts speed information. Here, the TMC location code list defines the spatial resolution. The most important observation is that the blue line, even though the course of both lines is quite similar along the considered road corridor, shows much more fluctuations than the gray line. These fluctuations cannot solely be explained by noise caused by the recording process. Instead, it can be concluded that the microscopically recorded data provide more details. The critical aspect is that microscopic energy consumption models are intended to estimate energy consumption for single drives and usually need precise information about instantaneous accelerations (*86*) (*148*). The microscopically recorded speed profile indicates that accelerations which are derived from macroscopic trajectories cannot be

[62] „Microscopically recorded“ means in this context that a mobile device, which is put into the vehicle, is used for recording the vehicle's driving trajectories (for instance via GPS).

[63] For the described example, speeds were measured via the GPS signal of a cell phone

[64] The displayed macroscopic driving trajectory results from traffic state estimations of a traffic content provider, which the author recorded, i.e., V_{RTTI} is considered here.

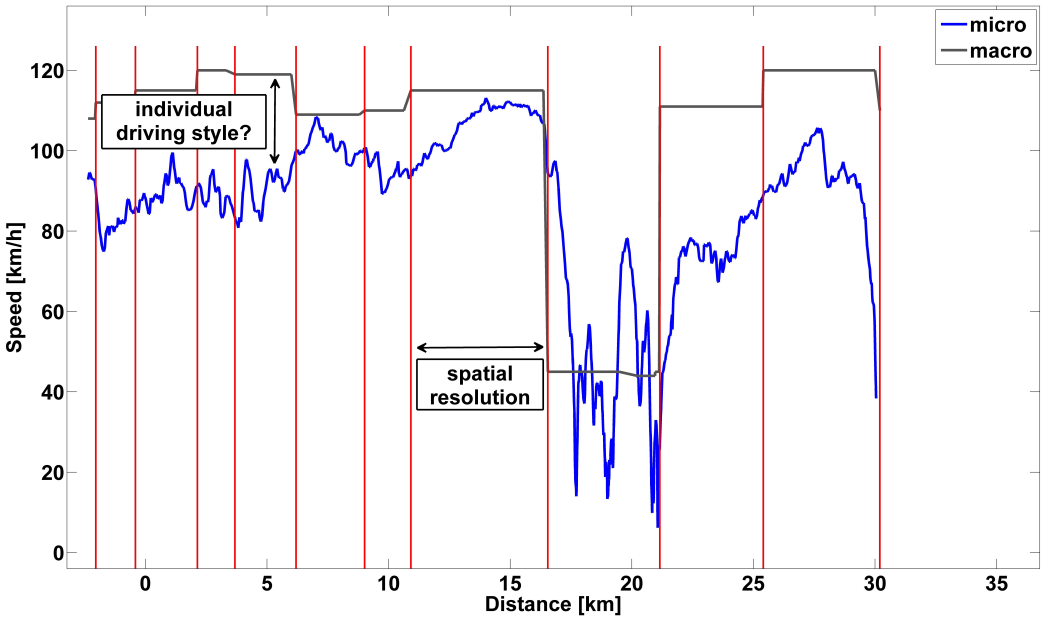

Figure 6.11: Tracked vehicle trajectory compared to RTTI-based macroscopic driving trajectory.

expected to be realistic. Thus, applying traditional microscopic energy consumption models to such macroscopically generated trajectories probably leads to unrealistic energy consumption values. These considerations suggest that $\grave{c}_E$ should not be based on a traditional microscopic energy consumption model. More about this topic will be provided later on in section 7.1.5.

Figure 6.11 shows another potential problem, which can be caused when considering solely macroscopic traffic information in the context of CSO: During the first seven kilometers, an average difference of about 25 kilometers per hour can be observed when comparing the gray line to the blue one. Intuitively, it could be assumed that the broadcasted driving speeds did not mirror the real traffic situation correctly, but this was not the case. The driver simply drove slower than most of the other drivers. The possibilities of macroscopic traffic information to represent such a level of individuality are limited. Typically, macroscopic traffic information is intended to represent an „average driver“. In the context of CSO, this leads especially in free-flow conditions to some issues. If traffic volume is low, it is up to the driver to decide how fast she/he drives. CSO is primarily intended for long distance trips. For such trips, typically freeways are used. Particularly on German freeways, where no general speed limit exists, driving speeds vary drastically under free-flow conditions. The energy consumption of BEVs, on the other hand, rises quickly if high driving speeds are increased further (this will be confirmed later on in section 7.1.5). The reason for this is that at high speeds, most energy consumption

results from overcoming air resistance, which grows quadratically with speed. Consequently, the energy consumption which is necessary to pass a certain road corridor significantly depends on the driver's preferred driving speed. If her/his preferences are unknown, then it is hardly possible to provide an adequate charging strategy. Due to this, it is from here on presumed that the driver's preferred driving speed $v_p \in \mathbb{R}_{>0}$ is known whenever a charging strategy is requested. Besides, it is assumed that the vehicle never reaches speeds above v_p – even if the macroscopic traffic state allowed this. Moreover, it is assumed that the driver is able to drive with her/his preferred driving speed whenever free-flow traffic conditions prevail. For any location x and any time t, the corresponding macroscopic traffic situations are interpreted as free-flow traffic condition if the real macroscopic driving speeds $\bar{V}_{Real}(x,t)$ are at least as high as the corresponding free-flow speeds $V_{ff}(x)$, i.e., if the following condition holds:

$$\bar{V}_{Real}(x,t) \geq V_{ff}(x). \tag{6.44}$$

Note that similar assumptions concerning the definition of free-flow traffic conditions and the behavior of drivers in free-flow traffic conditions are suggested by Kerner (compare page 13 in (*79*)). Given the real macroscopic driving speeds $\bar{V}_{Real}$, the presumed free-flow speeds V_{ff}, and a preferred driving speed v_p, these considerations lead to a trajectory $T(e, t_S, \bar{V}_{Real}, v_p)$ as stated below:

$$\bar{V}^{v_p}_{Real}(x,t) := \begin{cases} v_p & \text{if } \bar{V}_{Real}(x,t) \geq \min\{v_p, V_{ff}(x)\} \\ \bar{V}_{Real}(x,t) & \text{else} \end{cases} \tag{6.45}$$

$$T(e, t_S, \bar{V}_{Real}, v_p) := T(e, t_S, \bar{V}^{v_p}_{Real}) \tag{6.46}$$

Other spatio-temporal speed functions, such as $V^{t_B}_{RTTI}$, can be modified analogously. It is worth mentioning that the proposed method for considering individuality of drivers within CSO is rather intuitive, but also a clear simplification of reality. Drivers cannot be expected to strictly drive with the same speed in free-flow traffic conditions. Moreover, the driver's preferred driving speed probably varies during a trip. Also the assumption of time independent free-flow speeds seems to be unrealistic, since reduced speed limits during nights with the purpose of limiting noise emissions represent a counterexample. Note that uncertainty due to individual driving style is still not considered – even though the proposed approach for modeling driving behavior under free-flow traffic conditions is able to represent individuality up to some degree. Hence, imperfect traffic information or RTTI, respectively, remains the only source of uncertainty.

6.4 Summary

Chapter 6 can be divided into three parts according to the three tasks mentioned at the start of it: In the first part, in section 6.1, the formulation of the problem of finding optimal charging

strategies as a deterministic SPP was concretized. It was assumed that RTTI is available for the computation of charging strategies and that RTTI is applied to derive driving trajectories, which are again used to compute travel times and energy consumption values necessary for passing road segments. The most important aspects that were mentioned in this context are that RTTI was assumed to be error-prone, i.e., RTTI does not mirror the real traffic situation perfectly, and that RTTI represents the only source of uncertainty. This means that all other data which are relevant for CSO are expected to represent the real situation correctly. The proposed concretizations are essential for the simulation study in chapter 7 for two reasons: First, they allow bringing uncertainty into the simulation. Second, they form the basis for a realistic modeling of edge costs. In the second part, in section 6.2, a framework for assessing the quality of RTTI was developed. It was shown how RTTI can be brought into a numerically treatable form and reasons for the imperfection of RTTI in practice were discussed. Next, an approach to generate adequate representations of real traffic situations was described. These representations were intended to be applied as the references to which the available RTTI is compared. It was proposed to interpret the quality of the considered RTTI as the level of similarity between the RTTI and the corresponding traffic state reconstruction. The described framework for measuring the quality of RTTI is important to analyze the impact of imperfect input data on charging strategy quality. This is done in chapter 7. Finally, in section 6.3, the yet abstract concept of trajectory buffers was concretized by describing a method for generating sets of reasonable driving trajectories. A requirement for this method is the availability of two spatio-temporal speed functions. The first of these speed functions represents lower bounds for average driving speeds, the second one represents upper bounds. These boundary speeds are applied to estimate boundary trajectories, which are able to describe a region on the spatio-temporal plane, in which any reasonable driving trajectory is assumed to reside. It was suggested to generate a set of reasonable driving trajectories by covering this region equally with trajectories. Besides the method for generating sets of reasonable driving trajectories, also an approach to derive lower and upper speed bounds on the basis of (commercial) RTTI was proposed. Section 6.3 ended with a discussion about the consequences of deriving driving trajectories from macroscopic traffic state estimations. The main issues addressed in this discussion were the probably unnatural smoothness of such driving trajectories and the challenge to adequately model the behavior of drivers under free-flow traffic conditions.

Chapter 7

Simulation

In chapter 7, a simulation study is described and the results of the simulation runs are analyzed. The aspects which were described in chapter 6 form the fundament for this study, in which trips of BEVs under various conditions are simulated. The charging strategies that are provided to the BEVs are based on different types of artificially generated error-prone RTTI. The central motivation for the simulation study is, as already mentioned, to test the concept of energy buffers under the existence of uncertainties and to evaluate whether the resulting charging strategies show a quality that can be said to be practicable.
Chapter 7 is structured as follows: First, in section 7.1, the simulation environment itself is described. This description contains information about the simulated test site, the scheme for constructing different types of artificial RTTI is explained, the considered energy consumption model is introduced, and also information about the optimization framework, i.e., about the parameters concerning the problem formulation and the applied optimization algorithm, is provided. The main part of chapter 7, i.e., the analysis of the simulation results, is stated in sections 7.2 and 7.3. In section 7.2, the influence of the quality of different types of RTTI on the quality of the resulting charging strategies is analyzed in detail. The focus is set on relative energy buffers. The motivation for this analysis is to achieve a comprehensive understanding of the effects of applying error-prone RTTI for charging strategy computation. Furthermore, the analysis allows gaining an impression of the charging strategy qualities that can already be achieved by using a comparably simple type of energy buffer function. In section 7.3, two versions of trajectory buffers are considered in addition to relative buffers. The first of these trajectory buffer functions is based on the ideas of chapter 6, the second one represents a simpler alternative. The comparison of the results that can be achieved by either of the three energy buffer functions provides an idea of the charging strategy quality that can be achieved on the basis of the proposed optimization framework. This is finally used in section 7.4 to assess whether or not the developed framework is able to handle uncertainties in such a way that practicable charging strategy qualities can be ensured.

7.1 Simulation Environment

The simulation environment is implemented in Matlab. It allows simulating BEVs along a 362 kilometers long road corridor while facing traffic situations described by an artificial ground truth V_{GT}. These BEVs are guided during their trips by charging strategies. „During“ the trip means that the recommended strategies are regularly updated, i.e., the charging strategies are provided as an on-trip information. Moreover, the computation of the charging strategies is based on different types of artificially generated RTTI. Each of them shows, up to some degree, similarities to the ground truth, but typically does not mirror V_{GT} perfectly. Due to this, the simulated BEVs face traffic situations which differ from the traffic predictions on which the charging strategies are based. Different types of energy buffer functions can be applied to compensate for the resulting uncertainties.
The simulation study itself is structured as follows: It is differentiated between two types of parameters: **Setting parameters** and **scenario parameters**. Setting parameters describe the quantities which are actually of importance. For the described research, these parameters are

1. the method according to which the simulated RTTI is generated,
2. the function that is applied for quantifying the size of the energy buffer,
3. and the corresponding reliability parameter[65].

The scenario parameters, on the other hand, are intended to vary the conditions under which the setting parameters are tested. The motivation for this is to derive robust and generally valid conclusions. This means that one specific setting, i.e., one specific combination of values for the setting parameters, is tested for many different combinations of scenario parameters. For the described research, the setting parameters are

1. the starting time of the virtual trip,
2. the BEV's state of charge at the beginning of the trip,
3. parameters describing the charging infrastructure that is available along the route,
4. parameters describing the properties of the considered virtual BEV,
5. and the presumed outdoor temperature.

Detailed explanations concerning either type of parameter will be given later on.

Section 7.1 is structured as follows: First, in section 7.1.1, the general structure of the simulation study is described in detail. In section 7.1.2, an overview of the available traffic data is provided. These data form the basis for the construction of the simulated reality V_{GT}, which

[65] See Table 5.1 for an overview of the reliability parameters belonging to the different energy buffer functions.

is described in section 7.1.3, and for the generation of different types of artificial RTTI. These types of RTTI are introduced, alongside all other setting parameters, in section 7.1.4. The set of scenario parameters is described in section 7.1.5. In section 7.1.6, some remarks concerning further parameters that are relevant for the simulation study are given. Section 7.1 ends, in section 7.1.7, with a discussion about the different types of failures that can occur when providing charging strategies as an on-trip information.

7.1.1 Test Site and Structure of the Simulation

A schematic picture of the test site is displayed in the left side of Figure 7.1. Several charging stations can be found along a road corridor that starts at a charging station (denoted with charging station 1) and ends at a destination. No alternative routes are possible and the only available road corridor is from here on denoted as the „main road“. The location of charging stations and their number varies among the scenarios, but there is always a charging station at the start. The black arrows in Figure 7.1 mark decision stages and „target“ stages along the main road. The notion of target stages is relevant for describing the simulation environment in the following. More details will be given later on. Decision stages are locations at which the BEV's driver has to make decisions[66]. Correspondingly, new charging strategies are computed whenever the simulated BEV passes one of the decision stages. The decision stages can be found at the start, at the destination, and shortly before off-ramps allow leaving the main road in order to get to a charging station.

The flowchart on the right side of Figure 7.1 illustrates the structure of the simulation. A setting is defined by specifying the aforementioned setting parameters (type of energy buffer function, reliability parameter, type of RTTI). For each tested setting, it is iterated over a set of 1440 different scenarios. The proceeding in each simulation run is as follows: First, a scenario is selected. Then, an initial charging strategy computation is carried out, which takes scenario and setting parameters into account. The ground truth V_{GT} is typically assumed to be unknown. If this computation does not lead to a charging strategy, i.e., if no reliable charging strategy for the whole road corridor can be computed based on the given setting and scenario parameters, then the next scenario is considered. Otherwise, it is assumed that the BEV follows the recommended charging strategy. If charging is suggested at charging station 1, then the BEV's state of charge is increased correspondingly. Moreover, the time at which the BEV leaves charging station 1 is also adjusted. Next, a virtual driving trajectory leading to the first target stage is computed on the basis of V_{GT}. An energy consumption model, which is specified by the scenario parameters, is applied to this trajectory. Travel time and energy consumption are computed. If the simulated energy consumption which is based on V_{GT} exceeds at any time the energy which is available, then the BEV runs out of energy within the simulation. This is the worst-case scenario. Otherwise, the BEV successfully reaches the first target stage and

[66] According to chapter 3, decision stages are points in time and not locations. This was stated due to notational reasons. Here, instead the more intuitive idea of interpreting decision stages as locations is considered.

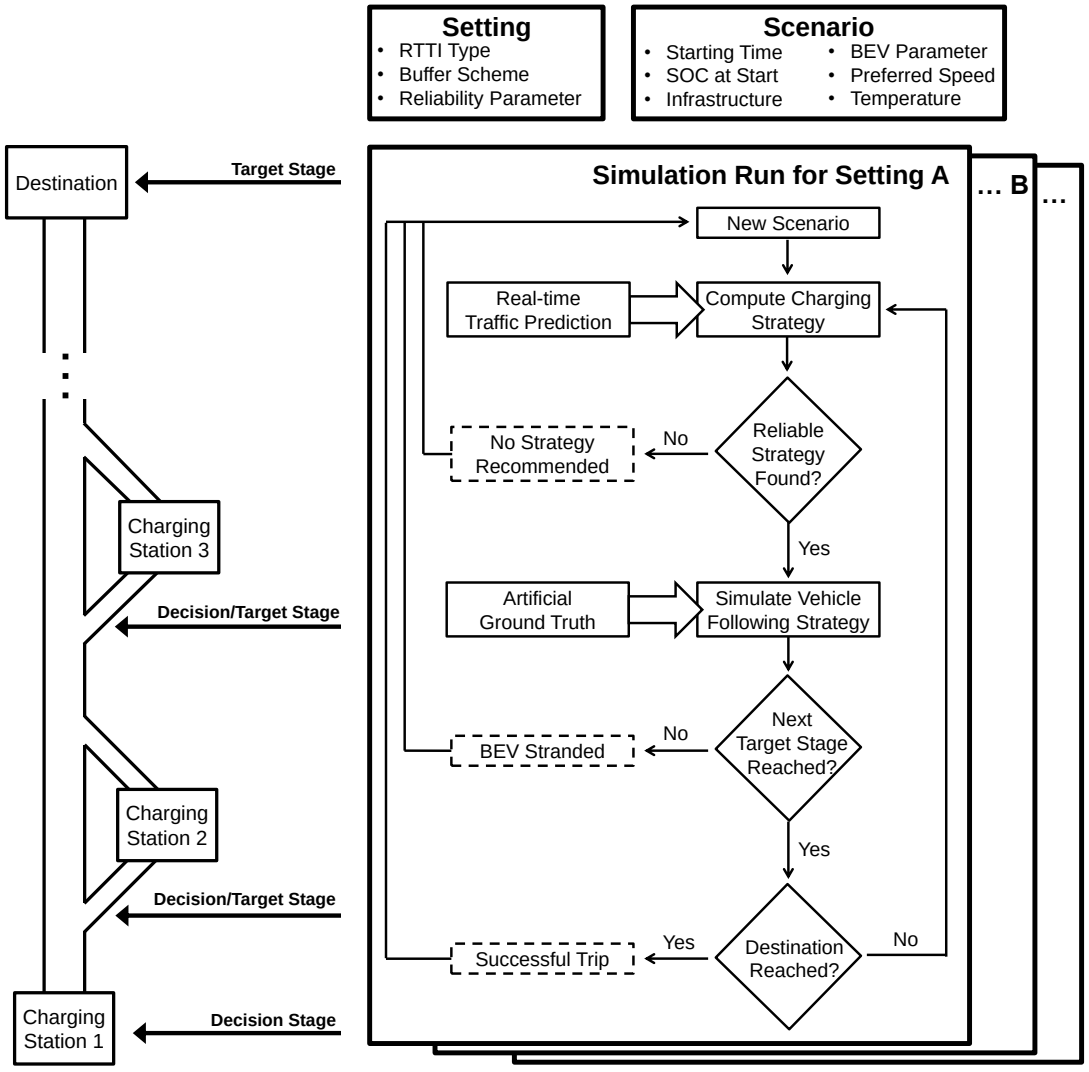

Figure 7.1: Structure of simulation.

a new charging strategy based on the BEV's current position, its current state of charge, the current time, and updated RTTI is computed. From here on, the proceeding remains the same. If a reliable strategy is found, the BEV's further trip is simulated on the basis of V_{GT} until it either reaches the destination, runs out of energy along the route or a reliable charging strategy can no longer be provided. Afterwards, the next scenario is considered until all 1440 scenarios have been simulated.

Note that the number of scenarios which are tested for each setting is rather high. This is important for two reasons: First, it ensures (up to some degree) robustness of the findings, i.e., the corresponding results are probably valid for a broad variety of situations a BEV might face. Second, it is extremely important for tools that provide charging strategies to achieve a high

level of reliability. Ensuring an arrival probability of 95 percent, which is a number that is often used in the context of robust travel time predictions, is not enough in this context. It would mean that the BEV does not reach its destination in one of 20 cases. To be able to analyze and compare the aforementioned settings at reliability levels close to 100 percent, a high number of tested scenarios is inevitable.
Testing many scenarios, on the other hand, makes it necessary to keep computation times reasonably low. For this purpose, algorithm B is used within the simulation. A detailed comparison between algorithms A and B with regard to computational effort and solution quality can be found in (*69*). The results show that algorithm B in almost all cases finds an optimal solution and, at the same time, can be computed much faster than algorithm A. Furthermore, allowing no route choices leads to a small graph $\vec{G}_D^{\Delta}$ and consequently further reduces the computational effort.

7.1.2 Available Traffic Data

Traffic related data from four different corridors on German freeways are relevant for the simulation runs: The first of these corridors is a stretch on the autobahn A9 at its southern end, near Munich, southbound (i.e., leading to Munich). To be more precise, a 26 kilometers long corridor between exit ramp Allershausen and interchange Munich north. The second road corridor is a part of the A9 between the interchange Munich north and exit ramp Geisenhausen, northbound (i.e., leading to Nürnberg). The third on is a part of the autobahn A99 leading to Salzburg, between exit ramp Ludwigsburg and exit ramp Hohenbrunn. Finally, the last of the relevant road corridors is a stretch of the A99 leading to Stuttgart, between exit ramp Ottobrunn and the freeway junction Munich – Feldmoching. Further information about these sites is given in Table 7.1, such as their lengths or the number of lanes. Note that the number of lanes varies for all of these freeways and thus the maximal and minimal number of lanes are stated in Table 7.1.

Table 7.1: Information on test sites.

corridor	**length of corridor [km]**	**number of lanes**	**number detectors**	**number of TMC segments**	**number of datasets**
A9 Nürnberg	39	3–4	27	12	31 (27 + 4)
A9 Munich	26	3–4	22	10	24 (18 + 6)
A99 Salzburg	33	2–5	26	13	26 (22 + 4)
A99 Stuttgart	35	2–5	29	14	27 (19 + 8)

Three types of traffic related data are available for each of these freeway corridors for a two and a half months period between April 11th and June 30th, 2015: Inductive loop detector data supplied by the South Bavarian Autobahn Authority, recorded commercial RTTI, and

historical average driving speeds. The recorded RTTI was broadcasted by a well-known private traffic content provider. The historical average driving speeds were generated by the same provider and are primarily used for long-term traffic predictions. The detector data form the basis for computing traffic state reconstructions. A more detailed description of the data can be found below. Before that, however, it is important to mention that some of the data that were gathered during the aforementioned period will not be considered. On some days, significant loop detector failures occurred. On others, either the RTTI recording procedure partly failed or RTTI was not provided continuously due to, for example, maintenance works on the data provider's servers. Only those days for which RTTI and detector data are comprehensively available (i.e., throughout the whole day) are taken into account within the following analyzes. The total number of analyzed days for each road corridor can be found in the last column of Table 7.1 outside the brackets. The meaning of the numbers in brackets will be explained later on.

Inductive Loop Detector Data The inductive loop detector data are given at one-minute resolution. They contain several types of traffic information, but for the following investigations, only recorded driving speeds are used. The available data are aggregated over all lanes and thus show no lane specific information. The number of detectors for each considered freeway corridor can be found in Table 7.1. The distances between two consecutive detectors range between a few hundred meters and more than three kilometers. Traffic state reconstructions are carried out based on these data as it has been described in section 6.2.

Historical Average Driving Speeds The available historical speed data were delivered by a professional traffic content provider. Unfortunately, no details concerning their generation process are available. These data represent historical average driving speeds in dependency of time (time of day and day of week) and location. A spatio-temporal speed function V_{Hist} is derived from these data. Function V_{Hist} shows a temporal resolution of one minute and uses the TMC location code list for spatial referencing.

Recorded Real-time Traffic Information The considered RTTI was broadcasted with an update rate of one minute (i.e., $\Delta t^{RTTI} = 1$ minute) by the same traffic content provider from whom also the historical speed averages were received. The RTTI refers spatially to the TMC location code list[67]. Hence, the spatial resolution is not very high. The numbers of TMC segments that (partly or completely) cover the four considered road corridors can be found in Table 7.1. Some of these segments span lengths of almost six kilometers. For each TMC segment

[67] It is worth mentioning that the originally provided historical speed data did not refer to the TMC location code list. These original data were aggregated according to the methodology that was described in section 6.2.5 to transform function V_{GT} to function V_{TGT}. This was done to avoid that, besides the spatio-temporal grids that are induced by V_{GT} and by the recorded commercial RTTI, a third grid has to be considered during the simulation runs.

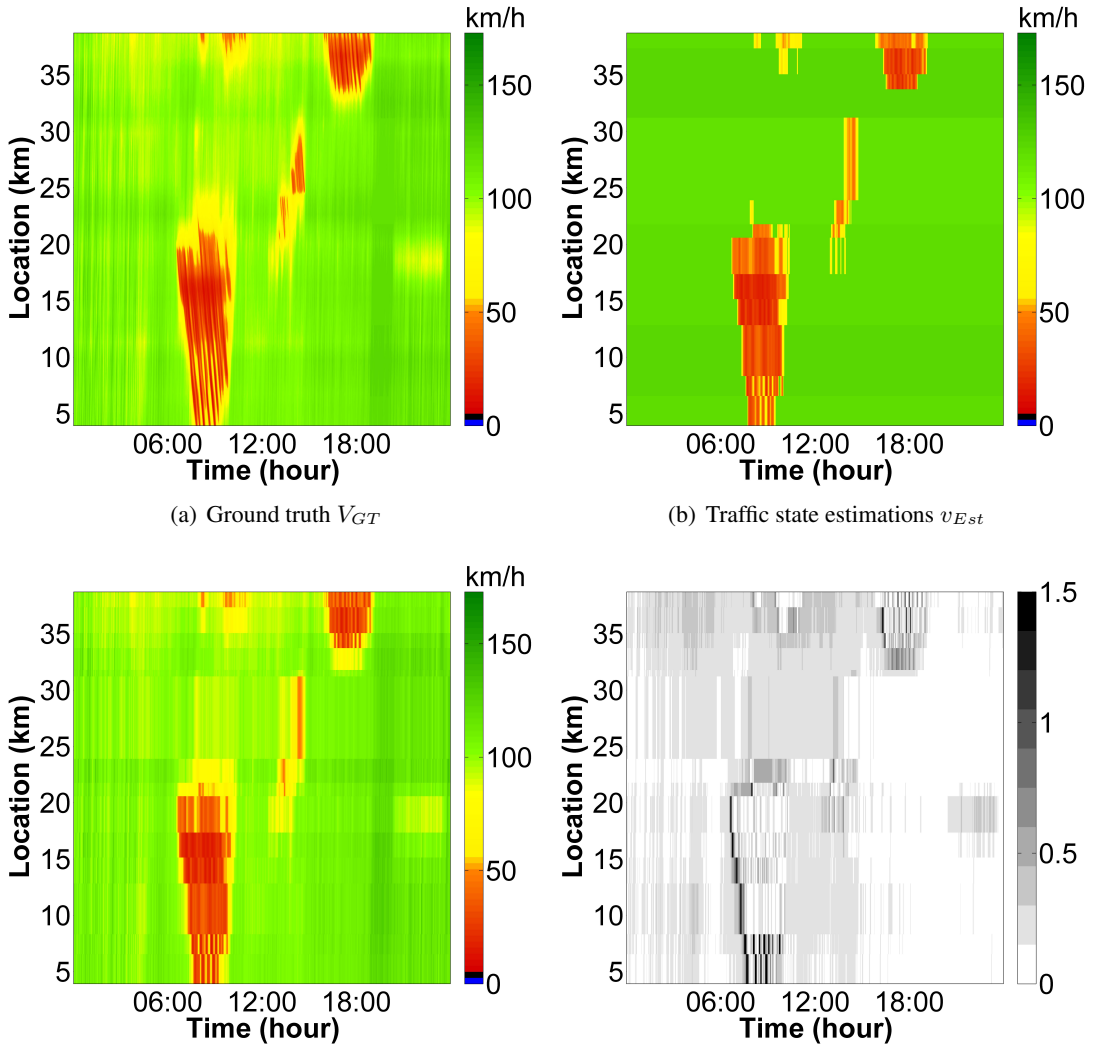

(a) Ground truth V_{GT}

(b) Traffic state estimations v_{Est}

(c) Technical ground truth V_{TGT}

(d) Error plot: Visualization of absolute percentage errors

Figure 7.2: Visualization of technical ground truth, recorded RTTI and the resulting relative errors on the freeway corridor A99, leading to Stuttgart, for April, 28th 2015.

and each minute, four different speed values were broadcasted: The first one is the estimated current driving speed $v_{Est}(S_i^{RTTI}, t_B)$. Variable t_B denotes the time at which the information is broadcasted. For simplicity, it is still assumed that t_B is equal to the time t_0, at which the optimization is computed. The other three speed values, here denoted with $v_{sho}(S_i^{RTTI}, t_B)$, $v_{mid}(S_i^{RTTI}, t_B)$ and $v_{lon}(S_i^{RTTI}, t_B)$, are intended to predict the future evolution of driving speeds for different prediction horizons. More information concerning the procedure for traffic state prediction on the basis of the recorded RTTI will be given later on.

The recorded RTTI shows some special properties: The traffic content provider defines for each TMC segment S_i^{RTTI}, a free-flow driving speed $V_{ff}(S_i^{RTTI})$. This free-flow speed is constant

over time. The broadcasted speed values are never higher than V_{ff}, independently of the raw traffic data the content provider receives. Furthermore, a speed reduction is solely broadcasted if at most 80 percent of the corresponding free-flow speeds are obtained. Thus, minor speed reductions are not represented by the RTTI. These properties can be seen in Figure 7.2. There, for April 10th, 2015, four contour plots for the aforementioned freeway corridor on the freeway A99, leading to Stuttgart, are displayed: Figure 7.2(a) shows V_{GT} based on inductive loop detector data, Figure 7.2(b) refers to v_{Est} (which is in fact function V_{RTTI}, i.e., the function that shows solely traffic state estimations), Figure 7.2(c) to V_{TGT}, and the last contour plot illustrates absolute percentage errors that result when comparing v_{Est} to V_{TGT}. Figures 7.2(b) to 7.2(d) show the expected low spatial resolution. Furthermore, when looking at v_{Est} in Figure 7.2(b), broadcasted speeds remain the same over large parts of the day. This is a consequence of ignoring minor speed reductions.

Besides speed values, the already mentioned confidence values $Cf^{t_B}(S_i^{RTTI})$ are also available. They are intended to rate the trustworthiness of the provided RTTI. The idea is that the more data are collected, the more reliable the corresponding traffic state estimation is. The confidence values range between 50 and 99, where 50 indicates a low confidence rating.

7.1.3 Construction of an Artificial Ground Truth

CSO is primarily intended for BEVs on long-distance trips. Hence, it seems expedient to consider a long road corridor within the simulation. „Long“ means here that a BEV needs to charge at least once to be able to pass the whole corridor. In order to simulate virtual BEVs and the influence traffic has on their trips, a ground truth V_{GT} representing the real traffic situation has to be provided for the considered road corridor. One of the best possibilities to ensure that V_{GT} shows realistic properties is to apply a traffic state reconstruction method to stationary detector data which are gathered on a real road corridor. Considering the traffic data which are available for the simulation (compare section 7.1.2), the corresponding road corridors are by far not long enough to reasonably test CSO. As a consequence, an artificial spatio-temporal speed function V_{GT} is constructed on the basis of the available inductive loop detector data. These data are separated into two parts. One dataset is intended later on for generating speed bounds as described in section 6.3.2, and the other one for testing, i.e., for the construction of V_{GT}. The test set consists of four days of data for the previously described road corridor on the autobahn A9 leading to Nürnberg, six days of data for the A9 leading to Munich, four days of data for the A99 leading to Salzburg, and eight days of data for the A99 leading to Stuttgart (see also the second of the two numbers in brackets in the last column of Table 7.1). These days are selected randomly from the set of all days for which traffic data are comprehensively available. Traffic state reconstructions are carried out by applying the ASM on each of these 22 datasets separately. As a result, one receives 22 spatio-temporal speed functions, each of them describing the traffic situation for one day and one of the four road corridors for which traffic

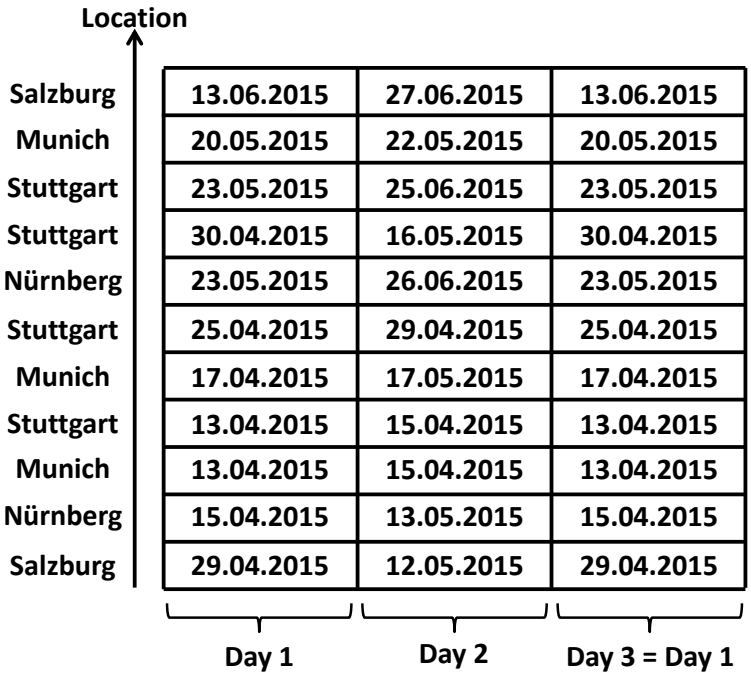

(a) Arrangement of datasets leading to V_{GT}.

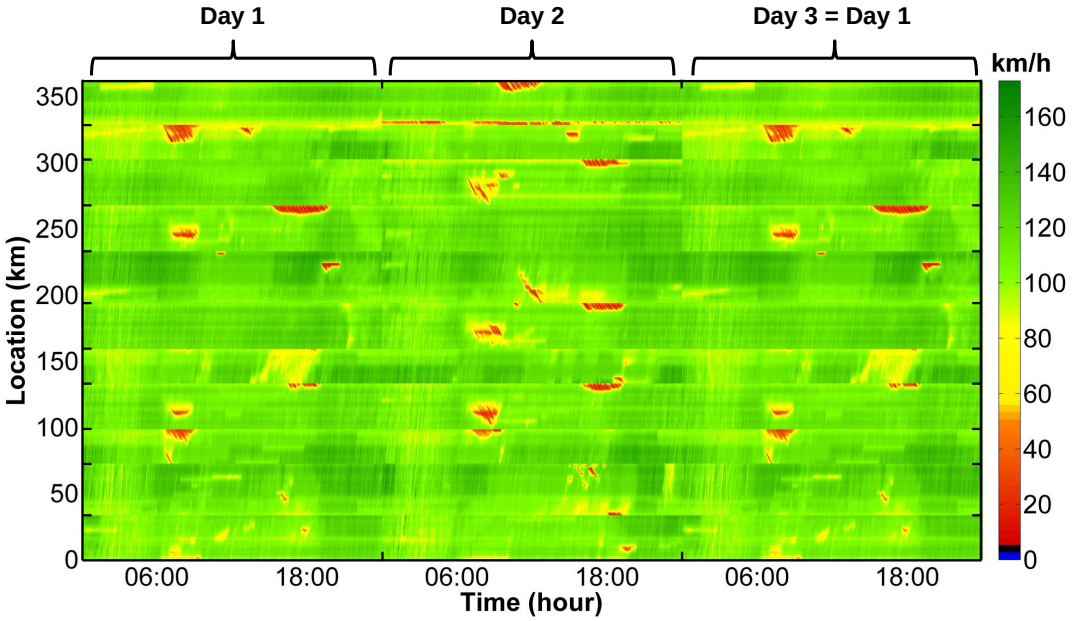

(b) Function V_{GT} which is used in simulation.

Figure 7.3: Construction of the ground truth which is used for the simulation runs.

data are available. These 22 speed functions are arranged as shown in Figure 7.3(a). There, the positions of these 22 datasets on the spatio-temporal plane can be seen. This arrangement

leads to an artificial ground truth V_{GT} for a three day period for a 362 kilometers long road corridor (see Figure 7.3(b)). The ground truth construction is carried out with Δt^{GT} equal to one minute and hence, as the RTTI is assumed to be updated every minute, it holds that $\Delta t^{RTTI} = \Delta t^{GT} = 1$ minute. Note that the first day is copied and used additionally as the third day. Generating a third is necessary, since the starting times of the simulated BEVs are distributed between the start of the first and the end of the second day[68]. Without the extension from two to three days, simulated BEVs that start their trip at the end of the second day would leave the spatio-temporal area for which macroscopic speed averages are available. The 362 kilometers long road corridor is denoted with X, the two days time period with $T_{2d} \subseteq \mathbb{R}_{\geq 0}$, and the three day time period with $T \subseteq \mathbb{R}_{\geq 0}$. Note that the available RTTI and historical average driving speeds are also arranged as shown in Figure 7.3(a).

The suggested arrangement of traffic state reconstructions has one significant drawback: Even though each of the applied spatio-temporal speed functions represents realistic traffic situations, the resulting arrangement of all speed functions cannot achieve that. Discontinuities occur at the spatial borders between these functions[69]. Such phenomena cannot be observed in reality. Consequently, computed driving trajectories show unrealistic speed drops and increases, since any simulated trajectory is in fact only a concatenation of realistic trajectories. This would be critical if the applied primary energy consumption models depended on accelerations which are derived from these trajectories. However, the consumption models, which will be proposed later on, solely depends on driving speeds. This allows interpreting the energy consumption which results from passing a section of the simulated road corridor that contains such a discontinuity as the sum of the energy consumption which results for passing the first part of this section, i.e., until the first discontinuity is reached, and the energy consumption that results for passing the remaining part of the section.

7.1.4 Setting Parameters

Recall that three types of setting parameters exist: The available RTTI, the applied energy buffer function, and the corresponding reliability parameter.

Types of imperfect traffic information For the computation of charging strategies, function V_{GT}, which is assumed to represent the real traffic situation within the simulation, is not known. Solely RTTI, which is assumed to approximate V_{GT} up to some degree, is available. Travel time and energy consumption predictions are based on driving trajectories that are derived from the

[68] Unfortunately, it was not possible to include further data into the testing dataset, since tests showed that the method for computing speed bounds, which was proposed in section 6.3.2, needs a lot of data in order to achieve reasonably good results.

[69] There are also discontinuities at the temporal borders. However, these discontinuities are very weak, since free-flow traffic conditions typically can be found on both sides of these borders, where speed values describing traffic situations at 00:00 am and at 12:00 pm meet.

available RTTI. The level of uncertainty that is caused by considering error-prone RTTI when computing optimal charging strategies depends on the similarity between V_{GT} and RTTI, i.e., it depends on the quality of the RTTI. In order to obtain a comprehensive understanding of the relation between RTTI quality and charging strategy quality, six different types of RTTI are considered during the simulation runs:

1. The real traffic situation (assumption of perfect information)
2. Free-flow driving speeds (assumption of no information)
3. Historical average driving speeds
4. Instantaneous travel times
5. Information based on recorded commercial RTTI which was broadcasted by a professional traffic content provider
6. An artificially generated spatio-temporal speed function which shows phantom jams

The first type of RTTI results when computing charging strategies on the basis of function V_{GT}. This means that perfect knowledge about current traffic states and the future development of traffic is presumed. Since incorrect RTTI represents the only source of uncertainty within the simulation, no energy buffer is necessary in this situation. The resulting charging strategies ensure minimal travel times – except for cases where algorithm B returns a suboptimal solution. Thus, the setting, where V_{GT} is available for CSO and where the size of energy buffers is constantly set equal to zero, is from here on considered as reference setting. All other types of RTTI are compared to this setting. In order to be able to differentiate formally between the function describing the ground truth and the function representing perfect RTTI, a function $V_{Perf}^{t_B}$ is introduced to denote the latter:

$$V_{Perf}^{t_B}(x,t) := V_{GT}(x,t) \tag{7.1}$$

Note that t_B is the time at which the charging strategy is computed and it is the time at which the RTTI, which is used for the charging strategy computation, is requested.

The second type of RTTI results by presuming free-flow speeds for all locations and times. This can be understood as a situation in which no information about the real traffic situation is available. Thus, it forms the counterpart to settings in which $V_{Perf}^{t_B}$ is available. The spatio-temporal speed function which represents this type of RTTI is defined as subsequently described:

$$V_{ff}^{t_B}(x,t) := V_{ff}(S_i^{RTTI}) \quad \forall x \in S_i^{RTTI} \tag{7.2}$$

Recall that, based on the considerations of section 6.3.3, a driver is assumed to be able to drive constantly with her/his preferred driving speed v_p in free-flow. Hence, it can also be written:

$$V_{ff}^{t_B}(x,t) := v_p \tag{7.3}$$

The third idea is to generate RTTI solely on the basis of historical speed averages:

$$V_{Hist}^{t_B}(x,t) := V_{Hist}(S_i^{RTTI},t) \quad \forall x \in S_i^{RTTI} \tag{7.4}$$

Note that V_{Hist} and $V_{ff}^{t_B}$ do not contain any recent traffic information, i.e., in fact, they are no „real-time“ traffic information. Though, both functions will allow analyzing the benefits of RTTI in comparison to such types of information.

Instantaneous traffic predictions represent the fourth method for generating RTTI which is considered in the following. The fundamental idea is to assume that the current traffic situation is known and that it won't change in the future:

$$V_{Inst}^{t_B}(x,t) := V_{GT}(x,t_B) \quad \text{for } t \geq t_B. \tag{7.5}$$

This approach is often applied in literature in order to artificially generate RTTI which behaves realistically (*43*) (*58*) (*97*). Note that also many navigation applications base their route computations on instantaneous travel times.

In (*53*), it is stated that former studies, which intended to analyze the influence that imperfect RTTI has on traffic related services, typically had to simulate the RTTI, i.e., to generate it artificially. This is in most cases, as already mentioned, done by using instantaneous travel times (*43*) (*58*) (*97*) or by adding random noise to the (reconstructed or simulated) real traffic situation (*94*) (*162*). Furthermore, it is emphasized in (*53*) that artificially generated RTTI lacks up to some degree realism. Some of the properties of real RTTI, such as a limited spatial resolution, are often not represented. Another important aspect that has to be considered in this context is that traffic content providers start going beyond simply using instantaneous travel times for traffic prediction purposes[70]. Correspondingly, a significant benefit compared to former studies is that in the following not only the impact of artificially constructed RTTI is analyzed, but also real commercial RTTI is considered. As mentioned before, the recorded RTTI contains four types of speed values v_{Est}, v_{sho}, v_{mid} and v_{lon}. These four values are used

[70]The recorded RTTI which is described within in this chapter is an example of RTTI including predictions.

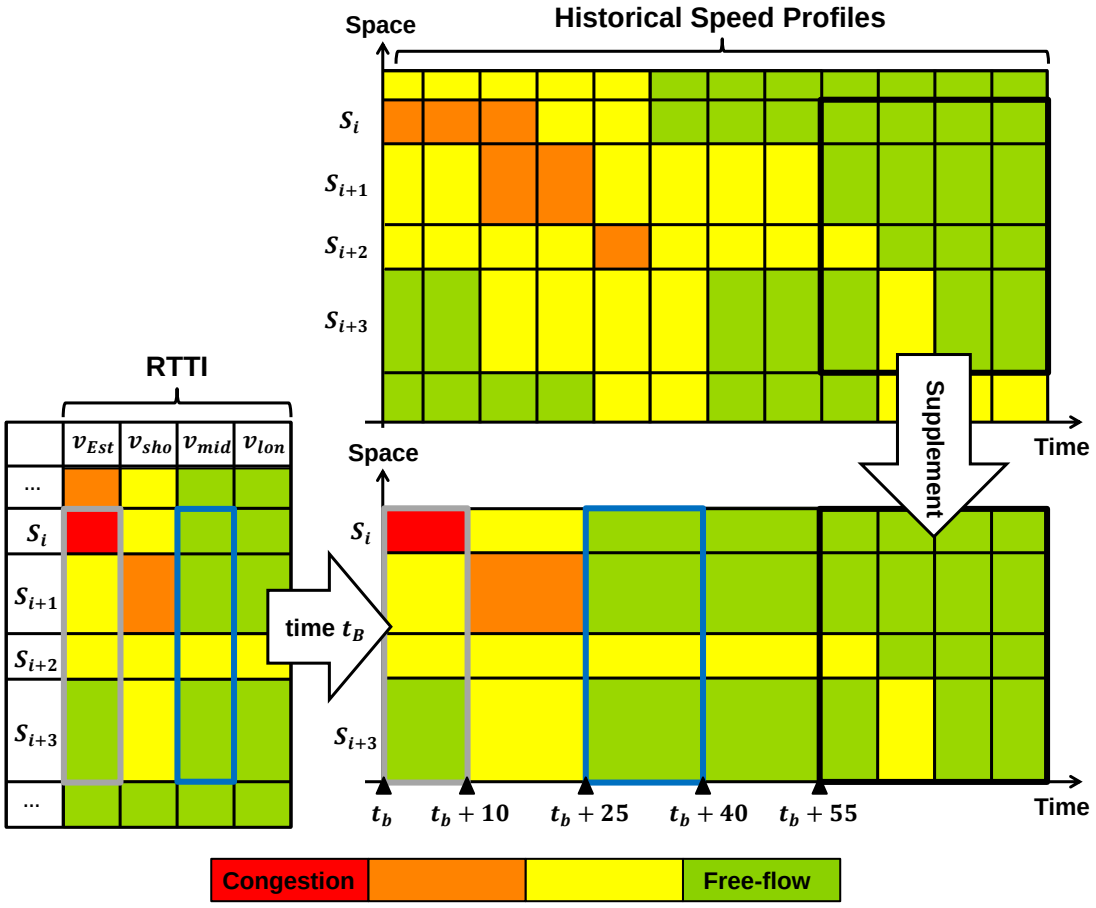

Figure 7.4: Generating a real-time traffic state prediction based on RTTI and historical speed profiles.

for traffic prediction purposes as stated below:

$$V_{Com}^{t_B}(x,t) = \begin{cases} v_{Est}(S_i^{RTTI}, t_B) & \text{if } x \in S_i^{RTTI} \text{ and } t_B \leq t \leq t_B + 10\text{min} \\ v_{sho}(S_i^{RTTI}, t_B) & \text{if } x \in S_i^{RTTI} \text{ and } t_B + 10\text{min} < t \leq t_B + 25\text{min} \\ v_{mid}(S_i^{RTTI}, t_B) & \text{if } x \in S_i^{RTTI} \text{ and } t_B + 25\text{min} \leq t < t_B + 40\text{min} \\ v_{lon}(S_i^{RTTI}, t_B) & \text{if } x \in S_i^{RTTI} \text{ and } t_B + 40\text{min} \leq t < t_B + 55\text{min} \\ V_{Hist}(S_i^{RTTI}, t) & \text{else} \end{cases} \tag{7.6}$$

Value v_{Est} is used for short-term prediction for the first ten minutes, v_{sho} for the period between minute ten and minute 25, v_{mid} for the period between minute 25 and 40, and v_{lon} for the period between minute 40 and 55. From minute 55 onward, historical traffic data are used to predict driving speeds. Figure 7.4 illustrates the construction of $V_{Com}^{t_B}$ („Com“ stands for „commercial“). On the left side, the broadcasted RTTI can be found. As already mentioned,

four speed values are broadcasted for each road segment and each minute. These speed values are applied to predict driving speeds for the next 55 minutes. The result is that $V_{Com}^{t_B}$ forms again a grid on the spatio-temporal plane, but this grid shows a very low temporal resolution. This changes as soon as prediction horizons of more than 55 minutes are considered. There, historical average driving speeds are applied as a supplement to the real-time information.

The sixth and last considered type of traffic information is generated as follows:

$$V_{Pha}^{t_B}(x,t) := \begin{cases} \min\{V_{GT}(x,t), V_{GT}(x,t+1 \text{ day})\} & \text{if } t \text{ is part of first or second day} \\ \min\{V_{GT}(x,t), V_{GT}(x,t-1 \text{ day})\} & \text{if } t \text{ is part of third day} \end{cases} \tag{7.7}$$

Recall that, in the simulation, V_{GT} represents a three day period, where the speeds belonging to first day are copied and also used for the third day. Function $V_{Pha}^{t_B}$ returns for any point (x,t) either the real driving speed $V_{GT}(x,t)$, or, if it is lower, the driving speed that is returned by V_{GT} on one of the neighbouring days for the corresponding location and time of day. Due to this, function $V_{Pha}^{t_B}$ is either equal to the simulated reality or underestimates driving speeds. The motivation for the construction of $V_{Pha}^{t_B}$ is that traffic congestion is reported in situations in which no congestion can be found in reality and that this traffic congestion shows a reasonable spatio-temporal extent[71]. Function $V_{Pha}^{t_B}$ represents in some sense also a counterpart to V_{ff}, which reports no congestion, even if congestion can be found in reality for the corresponding time and location.

Three remarks concerning the way the different types of RTTI are included into the simulation have to be made: First, during the simulation, predicted driving trajectories are based on RTTI, „real“ driving trajectories are based on the ground truth V_{GT}. In either case, the applied speed function is adjusted with regard to the driver's presumed preferred driving speed v_p. This means that all generated trajectories show a speed of v_p whenever the considered spatio-temporal speed function exceeds the free-flow speed defined by V_{ff} or the preferred driving speed v_p. The formal description of this adjustment was provided in equation 6.45. Second, all considered speed functions refer to grids. The set of cells for which functions $V_{Hist}^{t_B}$, $V_{ff}^{t_B}$ and $V_{Com}^{t_B}$ are piecewise constant is denoted by $\{S_i^{RTTI} \times T_j^{RTTI}\}_{i,j}$, the set of cells for which functions V_{GT}, $V_{Perf}^{t_B}$, $V_{Inst}^{t_B}$ and $V_{Pha}^{t_B}$ are piecewise constant is denoted by $\{S_i^{GT} \times T_j^{GT}\}_{i,j}$. Due to this, the RTTI induced grid and the ground truth grid are the same if functions $V_{Perf}^{t_B}$, $V_{Inst}^{t_B}$ and $V_{Pha}^{t_B}$ are used as RTTI. Third, if it is written $V_{RTTI}^{t_B}$, then not a specific type of RTTI function is considered. Instead, $V_{RTTI}^{t_B}$ can be interpreted as a placeholder, i.e., $V_{RTTI}^{t_B}$ may

[71] „Pha“ stands for „phantom“. The idea behind this notation is that $V_{Pha}^{t_B}$ shows „phantom traffic jams“, i.e., traffic jams that cannot be found in reality.

represent any of the described RTTI functions:

$$V_{RTTI}^{t_B} \in \left\{ V_{Perf}^{t_B}, V_{Inst}^{t_B}, V_{Pha}^{t_B}, V_{Hist}^{t_B}, V_{ff}^{t_B}, V_{Com}^{t_B} \right\} \tag{7.8}$$

Energy buffer function and reliability parameter Three different approaches for quantifying the size of the energy buffer are considered. Relative energy buffer function $SOC_{min}^{r,z}$ are used during the analysis of the dependency of the quality of recommended charging strategies on the quality of the available RTTI. Afterwards, in section 7.3, relative buffers are compared to two different types of trajectory buffers. The sets of auxiliary trajectories are derived as described in section 6.3.1 for both trajectory buffer functions. They solely differ with regard to the method according to which lower and upper speed bounds are generated. More details about this will be given later on in section 7.3.

7.1.5 Scenario Parameters

Each scenario is described as a 6-tuple consisting of the starting time of the trip t_S, the state of charge at the start SOC_S, the infrastructure setting, vehicle related parameters such as the consumption model describing the BEV's energy consumption, the driver's preferred driving speed v_p, and the outdoor temperature Tp. The sequence of scenarios which are tested in each simulation run remains the same – independently of the setting parameters. Starting times are chosen in steps of two minutes, starting at 00:00 in the morning of the first day and ending at 23:58 at the end of the second day for which V_{GT} is constructed. This leads in total to 1440 scenarios. For each starting time, SOC_S and Tp are chosen randomly between zero and 100 percent, and -10°C and $+35$°C, respectively. A uniform distribution is applied in both cases for the generation of the random numbers. Moreover, four different infrastructure scenarios are considered. The first infrastructure scenario is assigned to the first scenario (assuming that the scenarios are ordered according to their starting times), the second infrastructure scenario to the second scenario and so forth. When reaching the fifth scenario, the first infrastructure scenario is used again. Afterwards, one proceeds analogously (i.e., second infrastructure scenario is assigned to the sixth scenario, ...) until all scenarios have received an infrastructure scenario. The same procedure is applied to assign one of three possible vehicle models and one of five possible preferred driving speeds to each scenario (see Table 7.2 for illustration).

Infrastructure Scenarios The infrastructure scenarios differ particularly in terms of the number of charging stations: The first scenario provides seven, the second one nine, the third one eleven, and the last one thirteen charging stations. Considering the current situation along most German freeways (compare for instance the freeway A9 between Munich and Leipzig, which will be considered in chapter 8 for real world test drives), an average distance between two successive fast-charging stations of 40 kilometers and more can be found. Thus, the first and second infrastructure scenarios can be understood as examples representing the current

Table 7.2: Description of scenarios

Scenario Number	t_S	SOC_S	Tp	**Infrastructure**	v_p	**BEV Model**
1	00:00 day 1	87.1 %	4.2°C	scenario 1 (7 stations)	90 km/h	standard
2	00:02 day 1	17.3 %	22.6°C	scenario 2 (9 stations)	100 km/h	city
3	00:04 day 1	17.2 %	8.7°C	scenario 3 (11 stations)	110 km/h	high-range
4	00:06 day 1	37.2 %	-4.5°C	scenario 4 (13 stations)	120 km/h	standard
...						
1440	23:58 day 2	91.1 %	22.0°C	scneario 4 (13 stations)	130 km/h	high-range

situation. The third and the fourth scenarios can be understood as a vision of a future situation, for which a higher density of charging infrastructure is probable. In each of the four scenarios, one charging station can be found at the starting location. The other charging stations are distributed randomly along the main road. To be more precise, one random vector is generated for each of the four infrastructure scenarios. A uniform distribution between zero and 362 kilometers is applied. The entries of the vector are used to mark the locations of the exit ramps which lead to the charging stations. To ensure that a reliable charging strategy exists, at least for most of the considered scenarios, new random vectors are generated until the maximal distance between two successive charging stations and the distance between the last charging station and the destination are, at most, equal to 80 kilometers. Moreover, new random vectors are also generated until the smallest of the occurring distances between two successive charging stations and between the last charging station and the destination is bigger than three kilometers[72]. The second condition is intended to achieve a realistic distribution of exit ramps, as a situation where several exit ramps are located at almost the same position cannot be observed very often in reality (at least not in Germany).

Preferred Driving Speeds Five different possible preferred driving speeds v_p are assumed: 90, 100, 110, 120 and 130 kilometers per hour. These speeds seem to be chosen rather low considering that there is no general speed limit on German freeways. On the other hand, initial simulation runs showed that (for the presumed BEV models) the lowest total travel times can be achieved for speeds slightly above 100 kilometers per hour. The main reason for this is that energy consumption becomes extremely high for high driving speeds. Moreover, high preferred driving speeds lead frequently to situations in which no reliable charging strategy exists, even

[72]The method of generating random vectors until they fulfill a set of additional constraints is often denoted as „rejection sampling“.

if perfect knowledge of the future development of traffic is presumed. In order to avoid such special situations and, along with this, to guarantee that for each scenario a charging strategy exists which allows reaching the destination, the maximal possible preferred driving speed is kept low.

Vehicle Parameters There are three different features of BEVs which are varied among the scenarios: The energy consumption model, the capacity of the battery, and the charging durations. It is started with describing the different energy consumption models.

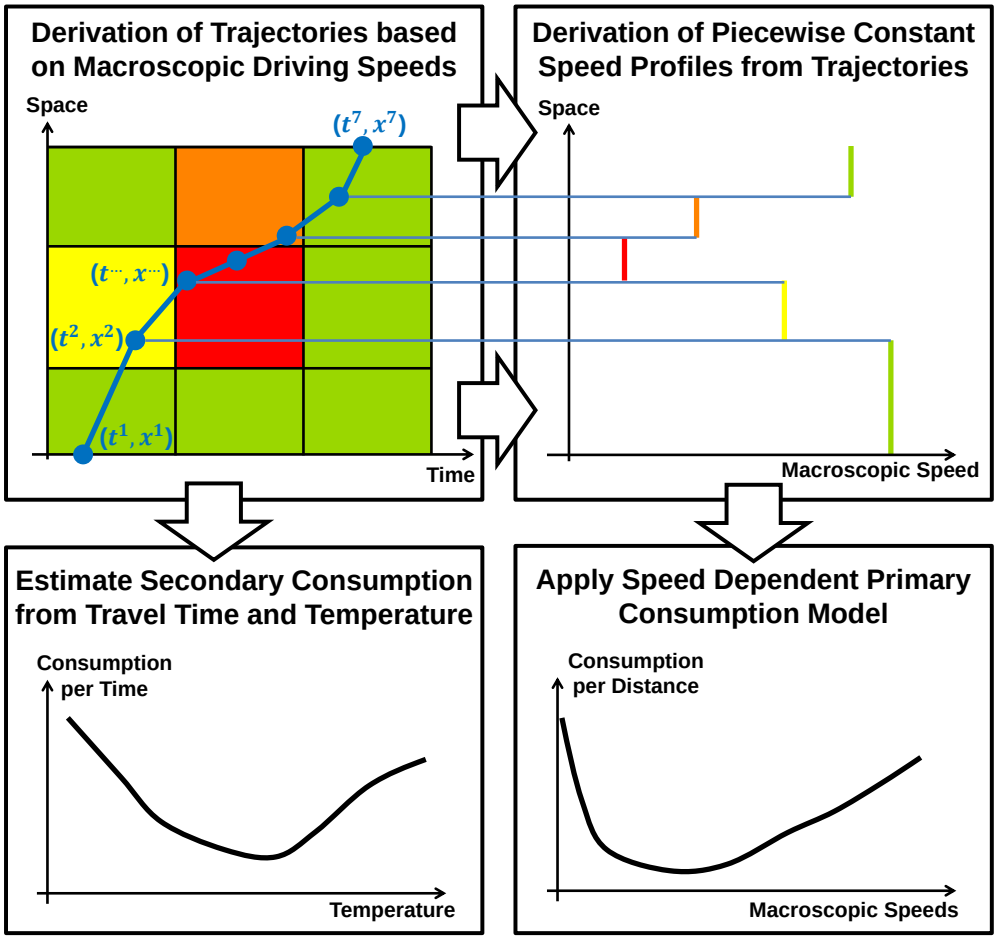

Figure 7.5: Computing energy consumption based on macroscopic driving trajectories.

Energy consumption of BEVs consists of two components, namely the primary energy consumption $\grave{c}_{Prim}$ and the secondary energy consumption $\grave{c}_{Sec}$. The primary energy consumption results from driving itself, i.e., from acceleration, deceleration, overcoming air resistance, recuperating energy and so on. The secondary energy consumption refers to energy consumption

which does not result directly from driving, such as energy consumption caused by the automotive electronics or air-conditioning. Figure 7.5 illustrates the methodology according to which primary and secondary energy consumption are derived from virtual (macroscopic) driving trajectories within the simulation study. Based on given traffic information $V_{RTTI}^{t_B}$, a virtual driving trajectory $T(e,t,V_{RTTI}^{t_B})$ is derived for some road segment e and some time t. This driving trajectory is defined as a sequence of points $\{(t^k,x^k)\}_{k=1,2,...,K}$ on the spatio-temporal plane:

$$T(e,t,V_{RTTI}^{t_B}) = \left[(t^1 = t_S, x^1 = \underline{e}), (t^2,x^2), ..., (t^K, x^K = \overline{e})\right]. \tag{7.9}$$

Variable $\underline{e}$ marks the start of edge e. A small excerpt of an exemplary contour plot showing a piecewise constant speed function and a resulting driving trajectory can be found in the upper left part of Figure 7.5. From such a trajectory, a piecewise constant speed profile SP is derived, which describes driving speeds along the road corridor. This speed profile can be understood as a function of space:

$$SP\left(x, T(e,t,V_{RTTI}^{t_B})\right) := V_{RTTI}^{t_B}(x^k,t^k) \quad \forall x \in [x^k, x^{k+1}[\tag{7.10}$$

A corresponding illustration can be found in the right upper part of Figure 7.5. Speed profiles are used to estimate primary consumption and travel times $t^K - t^1$ to estimate secondary consumption.

To get from speed profiles to energy consumption, a function EC_{Prim} („EC“ for „energy consumption“) will be derived later on. This function returns, given a macroscopic driving speed v, an average energy consumption per distance traveled. This value can be measured, for example, in joules per meter. The primary energy consumption resulting from a whole speed profile is then computed by multiplying traveled distances with the corresponding speed dependent energy consumption per distance:

$$\begin{aligned}\grave{c}_{Prim}(e,t,T(e,t,V_{RTTI}^{t_B})) &:= \grave{c}_{Prim}(e,t,V_{RTTI}^{t_B}) = \\ &= \sum_{k=1}^{K-1}(x^{k+1}-x^k)\cdot EC_{Prim}\left(SP\left(x^k, T(e,t,V_{RTTI}^{t_B})\right)\right).\end{aligned} \tag{7.11}$$

Note that $\grave{c}_{Prim}(e,t,T(e,t,V_{RTTI}^{t_B}))$ is replaced by $\grave{c}_{Prim}(e,t,V_{RTTI}^{t_B})$ in equation 7.11, since the driving trajectory is a direct result of e, t and $V_{RTTI}^{t_B}$. To compute secondary energy consumption, a function EC_{Sec} is applied which returns, depending on outdoor temperature Tp, an average energy consumption per time. This value can be measured, for example, in joules per second. The secondary energy consumption resulting from a trajectory $T(e,t,V_{RTTI}^{t_B})$ is then derived as subsequently described:

$$\grave{c}_{Sec}(e,t,T(e,t,V_{RTTI}^{t_B}),Tp) := \grave{c}_{Sec}(e,t,V_{RTTI}^{t_B},Tp) := (t^K - t^1)\cdot EC_{Sec}(Tp). \tag{7.12}$$

The focus is set on the dependency of secondary consumption on Tp, since energy necessary for air conditioning contributes most to secondary consumption for BEVs (*66*). The amount of energy which is typically necessary for air conditioning again depends significantly on the outdoor temperature. Finally, energy consumption costs are defined as the sum of primary and secondary consumption:

$$\grave{c}_E(e, t, V_{RTTI}^{t_B}, Tp) := \grave{c}_{Prim}(e, t, V_{RTTI}^{t_B}) + \grave{c}_{Sec}(e, t, V_{RTTI}^{t_B}, Tp). \tag{7.13}$$

To achieve reasonable results in the context of CSO, it is important to derive realistic energy consumption models EC_{Prim} and EC_{Sec}. For this purpose, a primary energy consumption model is derived which is based on a dataset containing information about almost eleven thousand trips of altogether 23 BEVs[73]. The 23 vehicles, each of them was a BMW i3 (without range extender), were either privately owned or part of company fleets. The vehicles were equipped with sensors for measuring quantities, such as driving speeds and (instantaneous) primary energy consumption. The data were recorded with a frequency of ten hertz. Information on location or road steepness was not gathered.

Since the derivation of vehicle trajectories during the simulation is based on macroscopic traffic state estimations and predictions, respectively, it cannot be expected that corresponding accelerations are realistic. This has already been discussed in section 6.3.3. This fact, together with the missing possibility to locate the equipped vehicles' driving paths[74] prevents constructing a precise physical energy consumption model as it is done, for instance, in (*148*). Still, the available energy consumption data are applied to derive a realistic relation EC_{Prim} between macroscopic driving speeds and energy consumption. A detailed description of the derivation of this model can be found in the appendix, in chapter D.2.

Due to a nondisclosure agreement with BMW, the author is not allowed to provide specific information on the derived relation between energy consumption per distance and driving speed. However, an idea of the shape of EC_{Prim} is sketched in the lower right part of Figure 7.5. It can be stated that EC_{Prim} is a convex function which shows lowest consumption values for speeds between 40 and 50 kilometers per hour. Significant increases of consumption can be observed for low and high speeds. Function EC_{Prim} is steeper for low speeds than for high speeds (i.e., the derivative of EC_{Prim} is very negative for low speeds and, in comparison, less positive for high speeds).

[73]The recording of the data took place in the project „PREMIUM“ and was funded by the (German) Federal Ministry for the Environment, Nature Conservation, Building and Nuclear Safety.

[74]The absence of information on location makes it hardly possible to gain information about road steepness or road classes. Moreover, it is also hardly possible to reliably decide whether the recorded data refer to urban or non-urban traffic.

The function which is applied within the simulation to describe secondary energy consumption EC_{Sec} depending on temperature Tp is provided by BMW[75]. Again, no details can be shown, but the shape of this function shows no surprises (see lower left part in Figure 7.5): Low temperatures lead to the highest possible energy consumption, but secondary consumption is also significantly increased at high temperatures. Note that primary consumption is typically the dominating factor, i.e., driving contributes more to the total energy consumption than the secondary consumers do ($EC_{Prim} > EC_{Sec}$).

Concerning the charging behavior, a time period of 60 minutes is used as the maximal charging duration d_{max}. The function S, which describes the charging behavior of a BEV (compare equation 4.23), is defined as follows:

$$S(d) := \begin{cases} \frac{d}{30 \text{ minutes}} \cdot 80\% & \text{if } d \leq 30 \text{ minutes} \\ 80\% + \frac{d-30 \text{ minutes}}{30} \cdot 20\% & \text{if } 30 \text{ minutes } < d \leq d_{max} \\ 100\% & \text{else} \end{cases} \tag{7.14}$$

Function S returns for a given duration $d \in \mathbb{R}_{\geq 0}$ the state of charge which is reached when recharging a completely empty battery during this duration. This means that a recharging process from zero to 80 percent takes 30 minutes, recharging the remaining 20 percent consumes the same amount of time. Function S is based on the charging behavior of a BMW i3 (*17*). Also the battery capacity of a BMW i3 of 67,680,000 joules is used within the simulation (*18*).

The described energy consumption model $\grave{c}_E$ (see equation 7.13) is from here on denoted as the „standard“ model. As already mentioned, two further consumption models are introduced: The „city“ model and the „high-range“ model. The idea of the city model is to suit the needs of urban traffic. Therefore, its primary energy consumption is, in comparison to the standard model, reduced for low speeds and increased for high speeds. This could be the case for vehicles which are equipped with a very efficient system for recuperation and which show a comparably high air resistance. Furthermore, the battery capacity of the city model and, along with this, the durations for charging are reduced by ten percent. This leads to a capacity of 60,912,000 joules and to a maximal charging duration of 54 minutes, whereby recharging from zero to 80 percent is done in 27 minutes. Secondary consumption is assumed to be slightly smaller than for the standard model. The high-range model is understood as a premium version of a BEV. Its battery capacity is increased by 40 percent. Charging durations are correspondingly increased by 40 percent. Also primary and secondary energy consumption are higher than for the standard model. Especially for low driving speeds, a significant increase of primary consumption is presumed.

[75]The provision of this function took place in the project „DC-Ladestation am Olympiapark“, which was funded by the (German) Federal Ministry of Transport and Digital Infrastructure.

7.1.6 Further Parameters

Time and energy costs for driving along the main road are based on driving trajectories, which are derived from spatio-temporal speed functions. For leaving the main road and getting to a charging station, a reduction of the state of charge of two percent is assumed, independently of the leaving time or the applied energy consumption model. The time costs for leaving the main road and approaching one of the charging stations are set equal to three minutes. Acceleration or deceleration processes are not considered. Since it is assumed that the BEV starts at charging station 1, no additional time or energy costs result for approaching this station. The costs for returning from station 1 to the main road, however, are defined analogously to other stations. Note that any energy which is necessary for leaving or returning to the main road is not taken into account by any of the applied energy buffer functions. This means that trajectories for the trajectory buffer are solely computed for the main road and relative energy buffers do not take the aforementioned costs of two percent into account. This simplification allows avoiding the need to find a reasonable approach to generate border trajectories for the way from and to the charging stations. Relative buffers ignore the energy costs to conserve consistency of all applied energy buffer functions. Concerning waiting times, it is assumed that no waiting times occur at charging stations, i.e., waiting time c_T^W is set equal to zero. Time costs c_T^A are set equal to three minutes (see section 4.1.2 for the interpretation of c_T^A). The charging step length Δ is set equal to five percent.

7.1.7 Types of Failures

As mentioned before, different settings are tested by simulating virtual BEVs facing various scenarios. The quality of charging strategies is measured with regard to realized travel times, i.e., the average time needed by a BEV within the simulation to reach the destination, and failure probabilities. Different settings can be compared with each other on the basis of computed average travel times and failure probabilities. Concerning the latter, a BEV following a navigation system which provides charging strategies as an on-trip information (i.e. regular updates during the trip based on recent information), as it is assumed for the described simulation, can basically experience four different situations:

1. The BEV reaches the destination.
2. The navigation system is at the beginning of the trip not able to provide a charging strategy which fulfills the energy security condition.
3. A decision stage is reached during the trip and the navigation system is not able to provide for the remaining part of the route a charging strategy which fulfills the energy security condition.
4. The BEV runs out of energy during the trip while following the instructions of the navigation system.

Scenarios that lead to the first situation are counted as a success, scenarios leading to the last situation are counted as failures. For the second situation, it is not that simple. As already mentioned, the setting where perfect traffic information $V_{Perf}^{t_B}$ is available and the energy buffer is set constantly equal to zero, is considered as the reference setting to which all other settings are compared. However, even though perfect information is presumed for the reference setting, it is still possible that scenarios exist for which no charging strategy recommendation can be made. This means that there exists no strategy which would allow reaching the destination. This could be the case, for instance, if a very long distance between two successive charging stations occurs. It would not be counted as a failure if a setting leads for such a scenario to the second situation. In fact, the best a navigation system can do in this case is to tell the driver that she/he cannot reach the destination reliably. On the other hand, if under perfect information a charging strategy can be provided, but the currently considered setting does not lead to a recommendation, then it is indeed counted as a failure. Since this failure occurs before the driver starts her/his trip, it is from here on denoted as **pre-trip failure**. Note that for all of the 1440 considered scenarios, the destination can be reached if perfect traffic information is available. The third situation is counted as a failure, too. Compared to the second situation, the third situation is less desirable as the driver has already started the trip at the time when the navigation system informs her/him that an arrival at the destination cannot be ensured anymore. Nevertheless, some options remain under such circumstances. For instance, the navigation system could suggest to the driver to reduce her/his driving speed below her/his preferred driving speed to reduce future energy consumption. Another possibility is to adjust the reliability parameter in such a way that more risky strategies are still considered to be reliable enough. Both approaches could also be combined. Unfortunately, both approaches either change scenario or setting parameters and are thus not considered within the simulation. All failures which occur during the trip are denoted as **on-trip failures**.

7.2 The Impact of Real-time Traffic Information Quality

The structure of the simulation study has been explained in detail in section 7.1. Based on these explanations, analyses concerning the dependency of charging strategy quality on the quality of the applied RTTI are conducted in the following. Recall that the central motivation for the simulation study is to achieve RO 2, i.e., to test the suggested problem formulation (i.e., the formulation of the problem of finding optimal charging strategies as a deterministic SPP in combination with the idea of using energy buffers to compensate for uncertainty) under the existence of uncertainties and to assess its ability to handle these uncertainties in such a way that charging strategies of practicable quality can be obtained. This means that particularly a high level of reliability of the resulting charging strategies has to be ensured.

In section 7.2, the quality of charging strategies resulting from applying relative energy buffers to compensate for the uncertainty caused by various types of RTTI is analyzed. This makes

it possible to understand the dependecy of charging strategy quality on the magnitude of the existing uncertainties. Furthermore, it is possible to gain an idea of the charging strategy qualities that can already be achieved by relying on a comparably simple method for energy buffer quantification. This knowledge will be particularly relevant when discussing up to which degree RO 2 can be fulfilled on the basis of the developed framework.

Section 7.2 is structured as follows: At the beginning, in section 7.2.1, the qualities which different types of RTTI achieve are analyzed in detailed. In section 7.2.2, a list of the simulated settings is provided and the resulting charging strategy qualities are illustrated. Based on this, several conclusions concerning the relation between charging strategy quality and RTTI quality are drawn. Finally, in section 7.2.3, additional simulation runs are considered in order to explicitly test the impact of two of the scenario parameters on the relation between RTTI quality and charging strategy quality.

7.2.1 Analysis of Real-time Traffic Information Quality

RTTI quality is again understood as the level of similarity between the RTTI and the ground truth, which is constructed according to section 7.1.3. The quality of the following functions is analyzed: $V_{Perf}^{t_B}$ (knowledge of ground truth), $V_{ff}^{t_B}$ (free-flow assumption), $V_{Hist}^{t_B}$ (historical average driving speeds), $V_{Inst}^{t_B}$ (instantaneous travel times), $V_{Com}^{t_B}$ (recorded commercial RTTI), and $V_{Pha}^{t_B}$ (phantom traffic jams). The level of similarity is, in principle, measured according to the ideas of section 6.2. However, to achieve a detailed understanding of the quality of the considered types of RTTI, the measurement is done in dependency of the prediction horizon. The prediction horizon $t_h \in \mathbb{R}_{\geq 0}$ is defined as the temporal difference between the time t_B, at which the prediction is made, and the time t, for which the prediction is made:

$$t_h := t - t_B. \tag{7.15}$$

In order to measure RTTI quality in dependency of the prediction horizon, the real driving speeds $V_{GT}(x,t)$ are compared to the driving speeds $V_{RTTI}^{t_B}(x,t)$ with $t = t_B + t_h$. For this purpose, let the following function be introduced:

$$\begin{aligned} T_{2d}^{t_h} &:= [\underline{T}_{2d} + t_h, \overline{T}_{2d} + t_h[\\ V_{RTTI,t_h} &: T_{2d}^{t_h} \longrightarrow \mathbb{R}_{\geq 0} \\ V_{RTTI,t_h}(x, t + t_h) &:= V_{RTTI}^{t}(x, t + t_h) \quad \forall (x,t) \in X \times T_{2d} \end{aligned} \tag{7.16}$$

This function returns for a time $t + t_h$ the speed value which has been predicted t_h minutes earlier. Due to its construction, function V_{RTTI,t_h} is defined for the two day period $T_{2d}^{t_h}$, which is the same as the two day period T_{2d}, but shifted by t_h. The construction idea for this function is

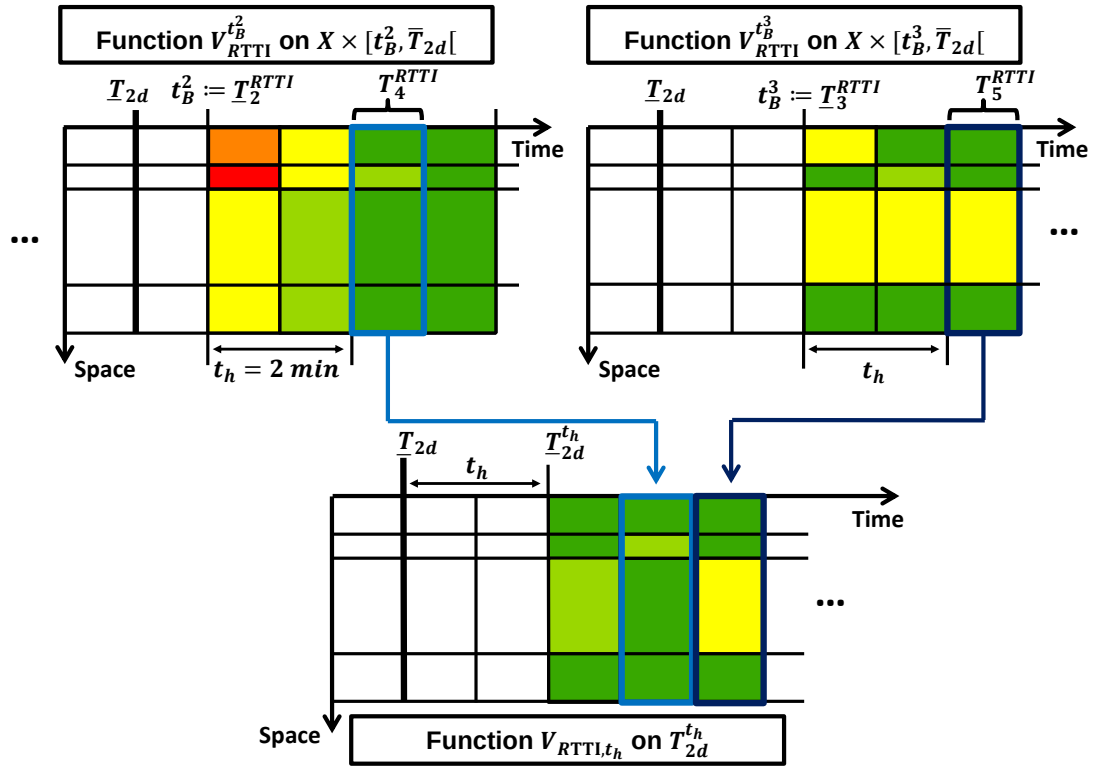

Figure 7.6: Ex post construction of function V_{RTTI,t_h} for $t_h = 2$ minutes.

illustrated in Figure 7.6 for an exemplary prediction horizon of $t_h = 2$ minutes. For the following analyses, the average difference $D(t_h) \in \mathbb{R}_{\geq 0}$ between ground truth driving speeds and predicted driving speeds is computed for each prediction horizon $t_h \in \{0 \text{ min}, 1 \text{ min}, ..., 180 \text{ min}\}$ according to the following rule:

$$D(t_h) := D(V_{GT}, V_{RTTI,t_h}, X \times T_{2d}^{t_h}, d) \tag{7.17}$$

The absolute percentage error d_{APE} is applied as the distance measure and errors are solely measured for the two day period $T_{2d}^{t_h}$, since otherwise some errors would be counted twice[76]. A plot showing the average prediction errors $D(t_h)$ in dependency of prediction horizon t_h can be found in Figure 7.7. The gray line refers to $V_{ff}^{t_B}$, the yellow line to $V_{Hist}^{t_B}$, the green line to $V_{Inst}^{t_B}$, the red line to $V_{Com}^{t_B}$ and the blue line to $V_{Pha}^{t_B}$. The orange line will be of relevance later on and refers to V_{TGT}, i.e., to the technical ground truth resulting from adjusting function V_{GT} to the RTTI induced grid. Note that there is no line displayed which refers to $V_{Perf}^{t_B}$. Trivially, such a line would run horizontally through zero, since under the assumption of perfect information, independently of the prediction horizon, no deviations occur.

[76]Recall that the third day of the considered three day period T, for which V_{GT} provides information, is just a copy of the first day.

It can be observed that $V_{ff}^{t_B}$ leads, with an average absolute percentage error of about 0.15, to the worst results. This is not surprising, since always assuming free-flow traffic conditions is a significant simplification, especially as the underlying traffic data refer to two of the most congested freeways in Germany. However, it is remarkable that the similarity between $V_{ff}^{t_B}$ and V_{GT} does not depend on the prediction horizon. This is a result of the definition of $V_{ff}^{t_B}$ in equation 7.2: Values $V_{ff}^{t_B}(x,t)$ do not dependent on the broadcasting time t_B and are also independent of time t. Due to this, these values are independent of the prediction horizon $t - t_B$. Functions $V_{Hist}^{t_B}$, $V_{Pha}^{t_B}$, and V_{TGT} also show no dependency on the prediction horizon. They are, in contrast to $V_{ff}^{t_B}$, time-dependent, but they do not depend on the broadcasting time t_B. This means, for instance, that function $V_{Hist}^{t_B}$ for some time t always returns the same speed value – independently of the time of prediction t_B:

$$V_{Hist}^{t_B^1}(x,t) = V_{Hist}^{t_B^2}(x,t) \quad \forall (x,t) \text{ and } \forall t_B^1 \neq t_B^2 \tag{7.18}$$

The similarity between V_{GT} and instantaneous traffic predictions $V_{Inst}^{t_B}$, on the other hand, depends significantly on the prediction horizon. This can be observed clearly in Figure 7.7. At

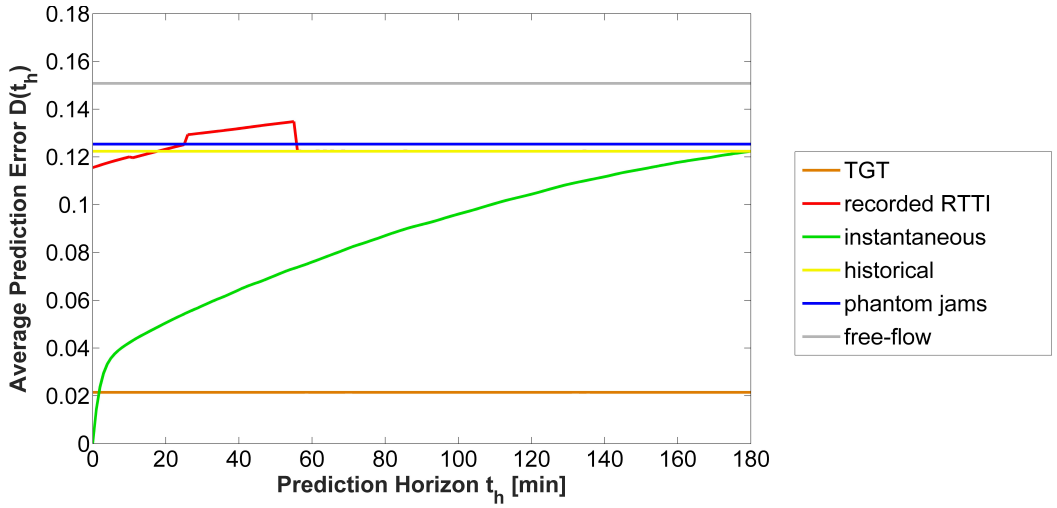

Figure 7.7: Quality of traffic prediction approaches in dependency of prediction horizon.

the beginning, i.e., for a prediction horizon of zero minutes, instantaneous traffic predictions which are based on ground truth data show no deviations from the ground truth. With increasing prediction horizon, the deviations between $V_{Inst}^{t_B}$ and V_{GT} rise. Particularly during the first few minutes, this happens quickly. Despite this growth of dissimilarity, a prediction horizon of almost three hours is necessary until $V_{Inst}^{t_B}$ leads to worse results than $V_{Hist}^{t_B}$. This is surprising, since historical speed averages are often applied for prediction horizons of less than three hours. A discussion concerning this observation will be provided later on.

The most irregular behavior can be observed for the red curve, which belongs to $V_{Com}^{t_B}$. As described in section 7.1.4, $V_{Com}^{t_B}$ is constructed from four different values which are broadcasted

in real-time, and from historical traffic data. Each of these types of speed values is applied for a certain range of prediction horizons. These ranges are from zero to ten minutes, from ten to 25 minutes, from 25 to 40 minutes, from 40 minutes to 55, and historical traffic data are applied for any further prediction horizon. Hence, the red curve vanishes behind the yellow line in Figure 7.7 for all prediction horizons above 55 minutes. The construction scheme of function $V_{Com}^{t_B}$ leads to discontinuities of the red curve in Figure 7.7 whenever the border between two such ranges is reached[77]. Remarkable is the fact that $V_{Com}^{t_B}$ leads to rather bad results. Concerning traffic state estimations, i.e., for a prediction horizon equal to zero minutes, this does not mirror the author's experiences. Throughout any preparatory analysis, the recorded commercial RTTI seemed to represent the real traffic situation rather accurately (compare also Figures 7.2(a) and 7.2(b)). A closer look at the underlying reasons appears to be necessary at this point.

Considering the properties of the recorded commercial RTTI, two reasons which probably lead to differences between V_{GT} and $V_{Com}^{t_B}$ can be found: The commercial RTTI's limited spatial resolution and the fact that only speed reductions of more than 20 percent with regard to the presumed free-flow speeds are broadcasted[78].
The orange curve in Figure 7.7 shows the quality which results when comparing V_{GT} to the technical ground truth V_{TGT} by using the measure described in equation 7.17. From all spatio-temporal speed functions that are restricted to the RTTI induced grid, function $V_{RTTI}^{t_B}$ can be understood as the speed function which achieves the highest possible similarity to V_{GT}. Since the orange curve in Figure 7.7 indicates very small error values, it can be concluded that large parts of the differences between V_{GT} and $V_{Com}^{t_B}$ are not a result of the limited spatial resolution of $V_{Com}^{t_B}$.

As a result, it may be conjectured that $V_{Com}^{t_B}$ basically describes significant speed drops quite well, but significantly differs from V_{GT} at higher speed levels. In order to confirm this conjecture, a preferred driving speed v_p of 90 kilometers per hour is presumed in the following. The ground truth is adjusted according to equation 6.45, which means that for any (x, t) with a ground truth speed higher than V_{ff} or v_p, a speed of 90 kilometers per hour is considered:

$$V_{GT}^{v_p}(x,t) := \begin{cases} v_p & \text{if } V_{GT}(x,t) \geq min\{v_p, V_{ff}(x)\} \\ V_{GT}(x,t) & \text{else} \end{cases} \tag{7.19}$$

[77] The discontinuity at a prediction horizon of 40 minutes is not as big as for minutes 10, 25 or 55, since the recorded values $v_{mid}^{t_B}$ and $v_{lon}^{t_B}$ were often identical.

[78] Note that it holds: $V_{Com}^{t_B}(x,t) \notin [0.8 \cdot V_{ff}^{t_B}(x,t), 1.0 \cdot V_{ff}^{t_B}(x,t)[$. This is a consquence of the missing ability to represent minor speed reductions.

All types of RTTI are adjusted analogously:

$$V_{RTTI}^{t_B,v_p}(x,t) := \begin{cases} v_p & \text{if } V_{RTTI}^{t_B}(x,t) \geq min\{v_p, V_{ff}(x)\} \\ V_{RTTI}^{t_B}(x,t) & \text{else} \end{cases} \tag{7.20}$$

Based on these adjustments of the relevant spatio-temporal speed functions, again error values depending on prediction horizon are computed. The resulting plot can be found in Figure 7.8. For a person intending to drive with a speed of 90 kilometers per hour whenever possible, the displayed curves describe the „relevant“ quality of the different types of RTTI. The idea is that for such drivers, it does not really matter whether the applied RTTI is unable to mirror V_{GT} at speed levels which lie above 90 kilometers per hour. It can be observed that, in comparison to Figure 7.7, all curves show smaller difference values. This is simply a consequence of the fact that for all spatio-temporal regions for which ground truth speeds and RTTI speeds lie above v_p, difference values of zero are computed. Furthermore, it can be seen that $V_{Hist}^{t_B}$ reaches

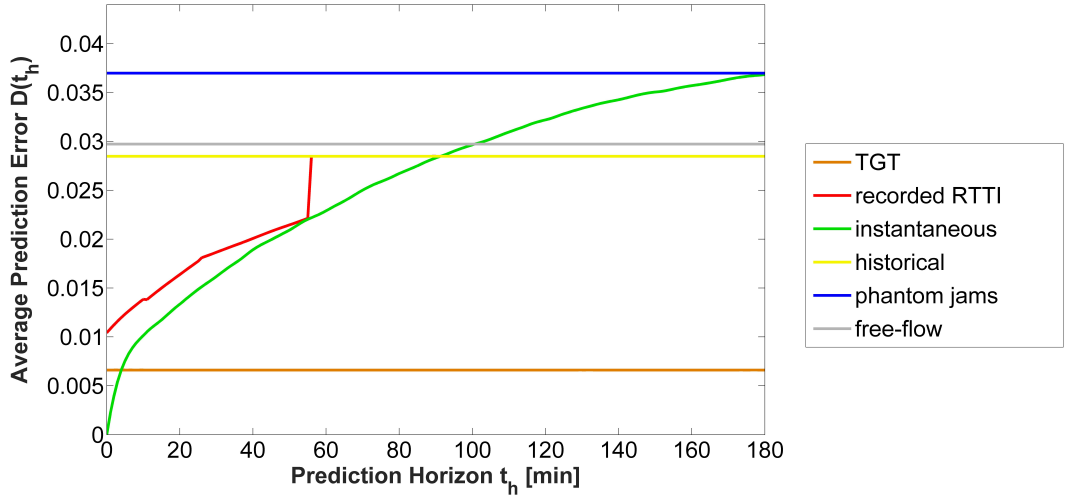

Figure 7.8: Relevant RTTI quality in dependency of prediction horizon with an presumed preferred driving speed of 90 kilometers per hour.

the same level of similarity as function $V_{Inst}^{t_B}$ already for prediction horizons of about 80 minutes. This indicates that $V_{Hist}^{t_B}$ differs from V_{GT} for higher speed levels more than $V_{Inst}^{t_B}$ does. Moreover, it can be observed that $V_{Com}^{t_B}$ is now able to provide significant benefits regarding short-term predictions in comparison to $V_{Hist}^{t_B}$. This was not the case in Figure 7.7. Hence, it is very likely that the aforementioned 80 percent rule has a significant negative impact on the similarity between V_{GT} and $V_{Com}^{t_B}$. Note that, even though $V_{Com}^{t_B}$ also improved in comparison to $V_{Inst}^{t_B}$, the traffic state predictions which are based on the recorded commercial RTTI are hardly able to reach the same quality level as instantaneous travel time predictions do. The latter represents a quite simple approach for predicting traffic. This indicates that the ability of

the recorded commercial RTTI to predict traffic is limited. However, the orange curve in Figure 7.8 shows that this is again partly caused by the limited spatial resolution of function $V_{Com}^{t_B}$.

Within the simulation study, the prediction of driving trajectories and the simulation of real driving trajectories depend on the presumed preferred driving speed v_p. The presumed preferred driving speed varies, since it is a scenario parameter. This has to be taken into account when analyzing the influence of RTTI quality on charging strategy quality. Therefore, it is important to consider Figure 7.7, as well as Figure 7.8.

7.2.2 Relation between Real-Time Traffic Information Quality and Charging Strategy Quality

In order to analyze the relation between RTTI quality and charging strategy quality, all introduced RTTI functions are tested within the simulation study. For each of these functions, the relative energy buffer function $SOC_{min}^{r,z}$ with $z \in \{0.0, 0.025, 0.05, 0.1, 0.2\}$ is applied to compensate for uncertainties. The resulting charging strategy qualities are one of the most central outcomes of the simulation study. Thus, it will be explained it detail, how the relation between reliability parameter, traffic prediction method, and the quality of the resulting charging strategies is illustrated. This explanation is based on Figure 7.9. Two graphs are displayed and several comments marked with numbers ranging from „1“ to „5“ are shown. Let the upper graph be considered at first. It shows the results for RTTI function $V_{Perf}^{t_B}$. Average total travel times can be found on the x-axis and the number of failures on the y-axis. Each triangle[79] in Figure 7.9 marks the average travel time and the number of failures for one specific setting, i.e., each triangle results from 1440 simulated trips. The numbers written near the triangles denote the value (in percent) of the reliability parameter z belonging to the corresponding setting and the color for the curve indicates the traffic prediction methods. **Comment 1** in Figure 7.9 exemplarily describes the interpretation of the triangle that can be found next to „30“: This triangle results when using perfect RTTI $V_{Perf}^{t_B}$ and while applying a relative energy buffer with a reliability parameter of 30 percent. During the 1440 simulation runs, 47 failures occurred and the remaining 1393 scenarios led to an average total travel time of about 394 minutes. Note that scenarios leading to failures are not included into the computation of average travel times.

Let in the following, the tested reliability parameters be considered in detail, starting with $z = 0$ (see also **comment 2** in Figure 7.9): If z is equal to zero, this actually means that no energy buffer has been applied. Hence, any charging strategy is interpreted as reliable if it fulfills the feasibility condition. If an error-prone type of RTTI was considered, then this would be critical, since no buffer to compensate for unexpectedly high energy consumption was available. However, function $V_{Perf}^{t_B}$ is used here and, along with this, no uncertainty exists at all in

[79] Triangles indicate that relative buffers are used for generating the corresponding point, other symbols will later on indicate alternative buffer functions.

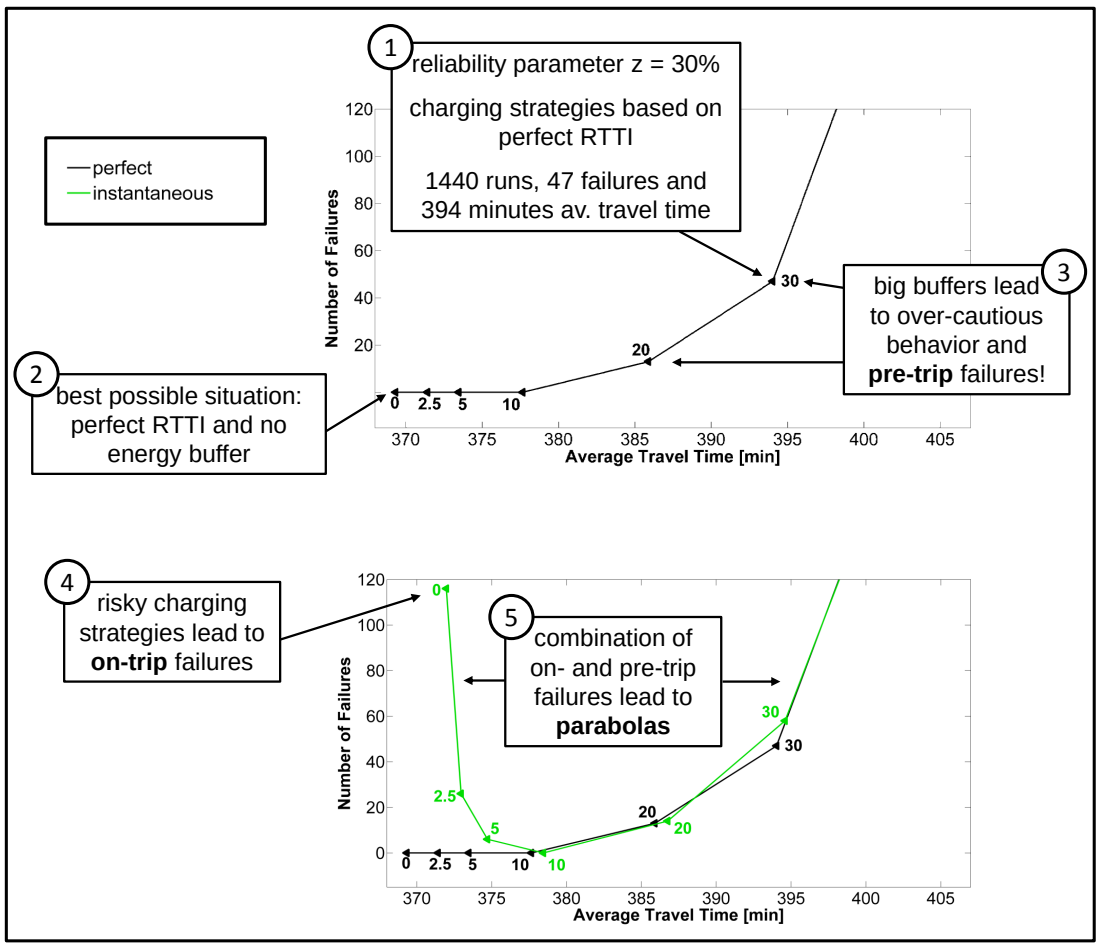

Figure 7.9: Explanation of graphs describing relation between reliability parameter, traffic prediction method, and the quality of the resulting charging strategies.

the analyzed setting. In a situation in which no uncertainty exists, energy buffers would cause that charging strategies are considered to be unreliable that actually are sufficient to get to the destination. Particularly very efficient charging strategies, which suggest comparably few and short rechargings and where the state of charge may often get close to zero, would be excluded, though it is not necessary to be able to react to unexpectedly high energy consumption. Note that this setting, where no uncertainties exist and no buffer is applied, necessarily leads to the best charging qualities. The reason for this is that with increasing z, the number of charging strategies that are able to fulfill the corresponding energy security condition becomes lower and lower. Hence, the set of possible solutions is reduced, which again reduces optimization potential and, along with this, average total travel times are increased. At some point, the number of energy secure charging strategies is reduced down to zero for some of the simulated scenarios. This is when pre-trip failures start occurring, i.e., no charging strategy can be recommended at the beginning of the trip (see also **comment 3** in Figure 7.9). This can be interpreted as

over-cautious behavior. Note that pre-trip failures not only occur for function $V_{Perf}^{t_B}$, but, as can be seen in the lower graph in Figure 7.9, also for error-prone types of RTTI: The green curve belonging to function $V_{Inst}^{t_B}$ shows higher failures rates for high reliability parameters. Important is that, as soon as an error-prone type of RTTI is considered, failures also occur if the reliability parameter is chosen too low. **Comment 4** in Figure 7.9 emphasizes this fact. It can be seen that that the simulated BEV experiences almost 120 failures if no energy buffer is applied and charging strategies are computed during the simulation runs on the basis of $V_{Inst}^{t_B}$. These failures are on-trip failures and primarily indicate that the simulated BEV ran out of energy. The combination of on-trip failures for small buffers and pre-trip failures for big buffers lead to the fact that all curves belonging to error-prone types of RTTI (i.e., all curves except for the black one[80]) show a shape similar to a parabola (see **comment 5**). Considering that low average travel times and low failure numbers are desirable, it can be concluded that all settings belonging to the right branch of one of these parabola are dominated by the vertex of the parabola. Consequently, choosing big buffers, where „big“ means that the corresponding setting can be found on the right branch of a parabola, has to be avoided. Clearly, this conclusion is only true as long as on- and pre-trip failures are treated equally. Alternatively, failures could be weighted according to their severeness, i.e., pre-trip failures could be weighted less than on-trip failures. Chapter D.1 in the appendix illustrates the effects of such inhomogeneous weightings exemplarily for the curve belonging to function $V_{Hist}^{t_B}$.

In the following, the relation between RTTI quality and the quality of the corresponding charging strategies will be analyzed in more detail. For this purpose, let Figure 7.10(a) be considered. It shows for all six types of RTTI functions the relation between reliability parameter z and the resulting charging strategy qualities. Figures 7.10(b) and 7.10(c) are generated similarly, but the number of on-trip and pre-trip failures, respectively, is visualized and not the total number of failures. Based on these figures, the different types of RTTI are sorted according to the quality of the resulting charging strategies. A possible approach to conduct this sorting is to set the focus on on-trip failures and state that an RTTI function A performs better than an RTTI function B if the curve belonging to A is located left and below the curve belonging to function B in Figure 7.10(b)[81]. Based on this rule, it can be concluded that the availability of perfect RTTI (black curve) leads to the best results, followed by functions $V_{Inst}^{t_B}$ (green curve), $V_{Com}^{t_B}$ (red curve), $V_{ff}^{t_B}$ (gray curve), $V_{Pha}^{t_B}$ (blue curve), and finally $V_{Hist}(t_B)$ (yellow curve).
Similar to the way the different types of RTTI are sorted according to the quality of the resulting charging strategies, it is also attempted to sort them according to their level of similarity to the

[80] The availability of perfect RTTI makes on-trip failures impossible, since the real energy consumption is always equal to the the predicted energy consumption.

[81] Such a sorting could hardly be conducted if both on- and pre-trip failures would be taken into account. The reason for this is that the corresponding curves (see Figure 7.10(b)) show a parabolic shape. Thus, most possible pairs of curves show intersections and hence, no clear order can be derived. The focus is here set on on-trip failures and not on pre-trip failures, since on-trip failures are assumed to be more critical for drivers.

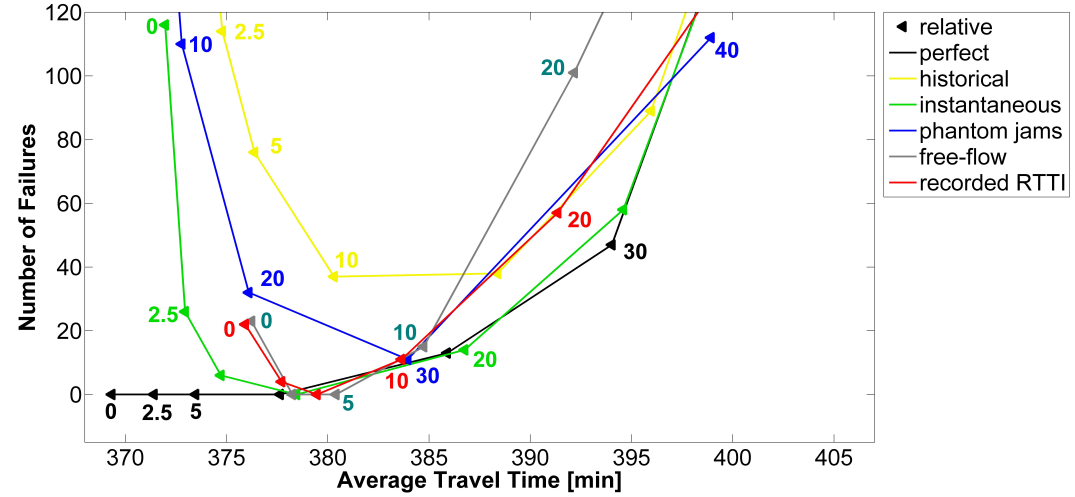

(a) All failures included.

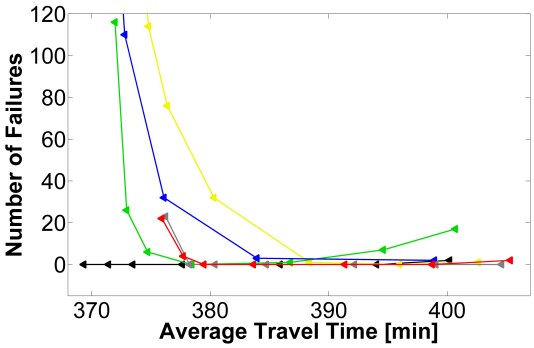

(b) Solely on-trip failures included.

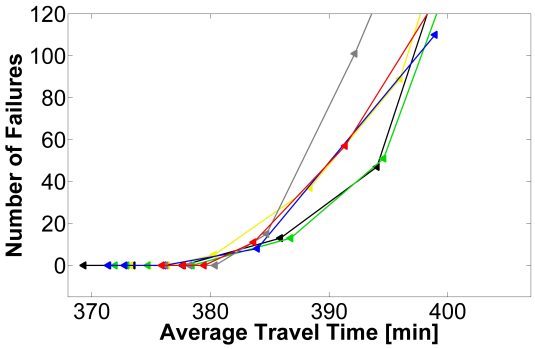

(c) Solely pre-trip failures included.

Figure 7.10: Dependency of average travel times and the number of failures on the applied traffic prediction method and reliability parameter z.

ground truth. This is not trivial. Depending on whether Figure 7.7 or Figure 7.8 is considered, a different order is the result. The dependency of the similarity between RTTI and ground truth on the prediction horizon additionally complicates making clear statements. Nevertheless, two statements, which will be of relevance for the following considerations, can be made: First, $V_{Perf}^{t_B}$ trivially leads to the highest similarity. Second, historical speed averages achieve better results than simply presuming free-flow driving conditions.

The relations between RTTI quality and the quality of the corresponding charging strategies turns out to be complex, but still some generally valid conclusions can be drawn:

- High RTTI quality ensures high charging strategy qualities
- When comparing two types of RTTI, then higher RTTI qualities not necessarily lead to improved charging strategies

- If differences between RTTI and ground truth lead to a systematic over- or underestimation of energy consumption values, then the corresponding charging strategy qualities are comparable to those which result if bigger or smaller, respectively, energy buffers are applied
- Travel times are not affected much when applying different types of RTTI

Details concerning these conclusions are provided in the following.

High RTTI Qualities As mentioned, $V_{Perf}^{t_B}$ leads to the best charging strategies of all tested types of RTTI. This is not surprising. Current and future traffic situations are known perfectly. Thus, travel time and energy consumption prediction errors are not possible. Along with this, no on-trip failures can occur[82] and no unnecessary charging stops are conducted. Note that it is very likely that for all types of RTTI which show only minor differences to V_{GT} the achievable charging strategy qualities do not drop significantly in comparison to those which are achieved when using $V_{Perf}^{t_B}$. See appendix D.3 for an example that supports this conjecture. Consequently, it is concluded that good RTTI (and not only perfect RTTI) leads to good charging strategies.

No Simple Dependency Another observation that can be made when comparing the results achieved by functions $V_{Hist}^{t_B}$ and $V_{ff}^{t_B}$ is that a higher RTTI quality not necessarily leads to better charging strategies: In Figure 7.7 as well as in Figure 7.8, RTTI based on historical speed averages achieves a higher level of similarity to the ground truth than RTTI which constantly states free-flow. At the same time, the former leads to significantly worse charging strategy qualities, at least as long as the focus is set on on-trip failures (compare Figure 7.10(b)). Based on these considerations, it can be concluded that a higher RTTI quality not necessarily leads to better charging strategies.
This surprising observation can be explained as follows: The quality of charging strategies depends on the quality of energy consumption predictions. RTTI solely describe driving speeds. The relation between driving speeds and energy consumption is neither linear nor monotone. Function EC_{Prim}, which describes the dependency of primary[83] energy consumption on macroscopic driving speeds, shows a parabolic shape (see Figure 7.5). Due to this, it is possible that significantly different macroscopic driving speeds lead to almost the same energy consumption. The consequence is that incorrect RTTI does not necessarily cause inaccurate energy consumption predictions.

[82] Pre-trip failures, on the other hand, may still occur. Though, this happens only if energy buffers, which are in fact not necessary if perfect knowledge is available, become extremely big, such that the sum of the energy consumption that is predicted to be necessary to reach the next charging station and the energy that is part of the buffer surpasses the maximal energy that can be stored by the battery.

[83] Secondary energy consumption has some influence on the total energy consumption of BEVs, too. However, primary energy consumption is, in most situations, much bigger and thus the dominating factor.

It is worth mentioning that the stated similarities between the different types of RTTI and the ground truth depend on the measure that is used for quantifying differences to the ground truth. If, instead of d_{APE}, another distance measure had been applied to generate Figures 7.7 and 7.8, then the magnitude of the differences between $V_{Hist}^{t_B}$ to $V_{ff}^{t_B}$ could have been different. However, for this specific pair of spatio-temporal speed functions, it seems very likely that traffic state estimations and traffic predictions which are based on historical speed averages achieve higher similarities to the ground truth than RTTI which simply states free-flow speeds. This should be the case for most possible distance measures.

Systematic Over- and Underestimation of Energy Consumption All curves in Figure 7.10, except for the black curve, are parabolas. It is remarkable that the sizes of the left branches of these parabolas differ drastically. For functions $V_{Com}^{t_B}$ and $V_{ff}^{t_B}$, the left branch is tiny. Even if no energy buffer is used, only about 20 failures occur as long as one of these two speed functions is applied. For function $V_{Pha}^{t_B}$, in contrast, the left branch is huge (see Figure D.2 for an illustration of the whole left branch of the curve belonging to $V_{Pha}^{t_B}$). Relative buffers of 20 percent are necessary to keep the number of failures at least below 40.
The reason for these enormous differences is that functions $V_{Com}^{t_B}$ and $V_{ff}^{t_B}$ lead to a systematic overestimation of energy consumption values, whereas function $V_{Pha}^{t_B}$ frequently causes underestimations of energy consumption values (reasons for these observations will be provided later on). A systematic overestimation of energy consumption results, similarly to the situation when applying big energy buffers, in a low number of on-trip failures. Hence, the left branch of the corresponding parabola looks like it is cut off near the vertex. A systematic underestimation of energy consumption values leads analogously to the opposite effects: Big buffers are necessary to keep failure rate reasonably low, whereas low buffer sizes lead to extremely high failure rates. Therefore, the left branch of the parabola belonging to such a speed functions becomes big.

The systematic overestimation of energy consumption values that results when applying the recorded commercial RTTI $V_{Com}^{t_B}$ can be explained as follows: Function $V_{Com}^{t_B}$ shows some very specific properties. Particularly the restriction that no minor speed reductions are broadcasted becomes interesting in the context of energy consumption predictions. This restriction often causes an overestimation of driving speeds when prevailing traffic conditions show comparably high driving speeds (i.e., speed near free-flow). Recall that the ground truth function V_{GT}, which is considered during the simulation study, returns high driving speeds for large parts of the spatio-temporal plane $X \times T$ (compare Figure 7.3(b)). The result is that such overestimations of driving speeds occur quite frequently during the charging strategy computations. If the speed level is high, then also primary energy consumption increases along with driving speeds due to the parabolic shape of function EC_{Prim} (primary energy consumption). Thus, the overestimation of high driving speeds induces an overestimation of future energy

consumption. Note that further analyses revealed that function $V_{Com}^{t_B}$ tends to underestimate speeds in situations where low driving speeds are expected, i.e., the predicted development of traffic congestion is often worse than it is in reality (no details are shown here). Primary energy consumption increases if a BEV, which drives with a low speed, further reduces its driving speed. The result is that the underestimation of low driving speeds induces again an overestimation of energy consumption.
The systematic overestimation of energy consumption values that result when applying function $V_{ff}^{t_B}$ can be explained similarly: Always presuming free-flow leads to an overestimation of driving speeds and, along with this, to an overestimation of energy consumption at high speed levels. For low speeds, energy consumption is often also overestimated when applying $V_{ff}^{t_B}$. The reason for this is that driving speeds need to be extremely low (less than ten kilometers per hour) to lead to energy consumption values that are as high as or higher than those which result at high[84] driving speeds. The frequently underestimated driving speeds that occur for function $V_{Pha}^{t_B}$ are a direct result of its construction[85]. Underestimations of energy consumption values at high speed levels are the consequence. A already mentioned, large parts of the traffic state reconstruction V_{GT} show high speed levels. Thus, energy consumption is frequently underestimated when applying function $V_{Pha}^{t_B}$.

Travel Time Robustness When comparing the parabolas belonging to the different types of RTTI functions in Figure 7.10, then it can be stated that the influence of different RTTI qualities on average travel times is minor. If, for example, the leftmost triangles (settings where no energy buffer is considered) of the parabolas in Figure 7.10 are compared to each other, then differences of average travel times of less than ten minutes can be observed. The same holds if the average travel times belonging to the vertices of the parabolas are compared. These are negligible deviations considering that the average total travel time lies above six hours.
Note that average travel times also increase only moderately with increasing buffer sizes (i.e., with an increasing value of z). The x-axis distances between triangles representing a buffer size of zero and the triangles which mark the vertex of the corresponding parabola lie for all of the considered types of RTTI below 15 minutes. For a driver, it is probably not too important whether travel times of 370 or 385 minutes are experienced. The moderate increase of travel times suggests using big energy buffers rather than small energy buffer.

Note that the identified relations between charging strategy quality and the differences between the applied types of RTTI to the ground truth function V_{GT} will be of relevance in section 7.4, where it is discussed up to which degree the idea of energy buffers allows achieving RO 2.

[84] If it is spoken of „high“ driving speeds, then it can be thought of speeds of more than 100 kilometers per hour.
[85] Actually, generating a function that causes underestimations of driving speeds is the motivation for the construction of function $V_{Pha}^{t_B}$. Due to this, $V_{Pha}^{t_B}$ can be understood as a counterpart to function $V_{ff}^{t_B}$, which ensures that driving speeds are systematically overestimated.

7.2.3 The Influence of Charging Infrastructure and Vehicle Range

In the previous section, it has been shown that the dependencies of charging strategy quality on the quality of the available RTTI is complex. The fact that the energy consumption models, which are applied within the simulation, do not grow or fall monotonically with driving speeds has been identified as one of the main reasons for this observation. If these consumption models had been different, then also the results of the executed simulation runs would have been different. However, it can be expected that BEVs in general need a comparably high amount of energy when driving with very low or very high speeds. For other aspects of the simulation model, on the contrary, alternative parameter, which differ significantly from the applied ones, are reasonable, too. Some of these aspects have influence on the dependency of charging strategy quality on RTTI quality. This implies that even if a specific type of RTTI is considered, it may not be possible to make a general statement about whether the quality of this type of RTTI leads to good charging strategies. In order to clarify this statement, the results of exemplary simulation runs are investigated in the following. Within these simulation runs, charging station density and battery capacity are varied. It is shown how these modifications affect the dependency of charging strategy quality on RTTI quality.

For the announced computations, most parts of the simulation environment remain the same. Though, the considered infrastructure scenarios are changed. Again, four different infrastructure scenarios are applied. The difference between them is the number of charging stations that are placed between the start and the destination. Eight charging stations are available in the reference scenario (plus one charging station at the start). The other scenarios show six (i.e., 75 percent of the charging stations of the reference scenario), twelve (150 percent) and sixteen (200 percent) charging stations. In contrast to all former simulation runs, charging stations are equally spaced along the main route for any of these new infrastructure scenarios. This ensures a certain level of regularity and makes the interpretation of the resulting charging strategy qualities clearer.

Besides adjusted infrastructure conditions, also battery capacities are varied. The original parameterization is here applied as the reference scenario. This means that three different vehicle types are considered with capacities of 67,680,000 (standard model), 60,912,000 (city model) and 94,752,000 (high-range model) joules. Besides the reference scenario, three further capacity scenarios are tested, where the battery capacity of each of the three BEV models is changed to 75, 150 and 200 percent of its original value. Furthermore, it is assumed that the amount of absolute energy[86] which can be charged per second remains the same, independently of the capacity scenario. Thus, charging durations decrease/increase proportionally with the battery capacity.

It is important to mention that for each simulation run, i.e., for each analyzed setting, the

[86] The absolute amount of energy is measured in joule and not in percent of the battery capacity.

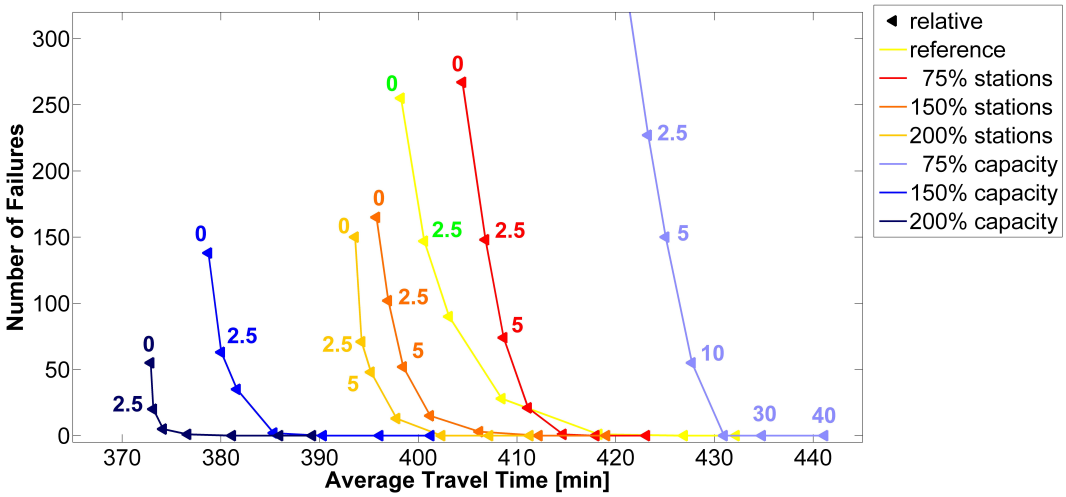

Figure 7.11: The impact of infrastructure and energy capacity on charging strategy quality when applying historical speed averages.

considered infrastructure and battery capacity scenarios remain the same for all 1440 simulated vehicles. Thus, it seems more reasonable to speak of infrastructure and battery capacity „settings“ in this section and not of „scenarios“. Solely the starting times, vehicle models, temperatures, and the preferred driving speed change during a setting. Also the battery's state of charge at the beginning of the trip does no longer vary. It is always set equal to zero percent. This guarantees that the absolute amount of energy that is available at the start does not depend on the considered capacity setting. Otherwise, a simulated vehicle starting with a state of charge of 50 percent would cover more distance before it needs to be recharged for the first time in a high capacity setting than in a low capacity setting. Therefore, due to the additional starting energy, the total amount of energy that needs to be recharged during the whole trip would probably be slightly smaller, which again would reduce travel times. Consequently, a direct comparison between low and high capacity settings would be biased if starting states of charge unequal to zero are considered.

Figure 7.11 shows exemplarily for function $V_{Hist}^{t_B}$ how the described infrastructure and capacity settings influence achievable charging strategy qualities. The yellow curve corresponds to the reference setting, i.e., to the situation with 100 percent infrastructure and 100 percent capacity. The blue curves refer to different infrastructure settings, the red and orange curves to different capacity settings. Relative energy buffers with $z \in \{0, 0.025, 0.05, 0.1, 0.2, 0.3, 0.4\}$ are considered. It can be seen that charging strategy quality, i.e., travel times and failure rates, improves with increasing charging station numbers and battery capacities. For the blue curves, reduced travel times are primarily a result of an enlarged set of possible charging strategies. This bares additional optimization potential. Moreover, it is clear that more charging stations

also provide more possibilities to adjust charging strategies during a trip. Consequently, it can be reacted more often and more promptly to prediction errors, which again reduces the probability of on-trip failures. For the read and orange curves, having the ability to store more energy reduces the number of necessary charging processes. Thus, less travel time is the consequence, since the main route is left less frequently. The improvements in terms of failure rates, on the other hand, are primarily the consequence of the way the energy buffer is defined here: Along with battery capacity, also the absolute amount of energy that is consumed between two consecutive charging processes increases on average. Thus, the absolute amount of energy which is used as an energy buffer increases, too. The reason for this is that relative energy buffers reserve a certain percentage of the energy which is expected to be consumed until the next charging stop is conducted. If it is expected that a lot of energy is consumed until the next charging stop, then also a lot of energy is used for buffering. Due to this, underestimations of future energy consumption can be compensated more easily if more energy can be stored. An interesting observation is that the impact of changing battery capacities is significantly higher than the impact of changing the number of charging stations, at least if the quality of the 75 percent infrastructure setting is compared to the 75 percent capacity setting (or if the 150 and 200 percent settings are compared).
It is also worth mentioning that no pre-trip failures can be observed in Figure 7.11. This is a result of spacing the charging infrastructure equally along the main route. Hence, the maximal distance which occurs between two consecutive charging stations is much smaller than it is for the original infrastructure scenarios. There, the locations of charging stations are randomly distributed along the main route. This leads to a maximal distance between consecutive charging stations of 70 kilometers for the infrastructure scenario with seven charging stations (61/49/61 kilometers for the nine-/eleven-/thirteen-station infrastructure scenario). Even for the infrastructure setting with only six equally spaced charging stations, the maximal distance (which actually is also equal to the minimal distance) is only 51.7 kilometers. This number results when dividing the total route length of 362 kilometers by seven. Covering a distance of about 50 kilometers with a fully recharged battery is, in contrast to covering 70 kilometers, no problem for any of the considered BEVs or any of the applied reliability parameters. Consequently, pre-trip failures are, for the described settings, no longer an issue.

So far, it can be concluded that the reliability of charging strategies does not solely depend on the quality of the applied type of RTTI, even though the latter represents the only source of uncertainty. The conducted changes to the available infrastructure already lead to the disappearance of pre-trip failures. Moreover, the number of on-trip failures and the average travel times also change drastically if battery capacities or the density of the available charging infrastructure are varied. It can be observed in Figure 7.11 that, for example, a relative energy buffer of only five percent is already enough to keep the number of occurring failures only

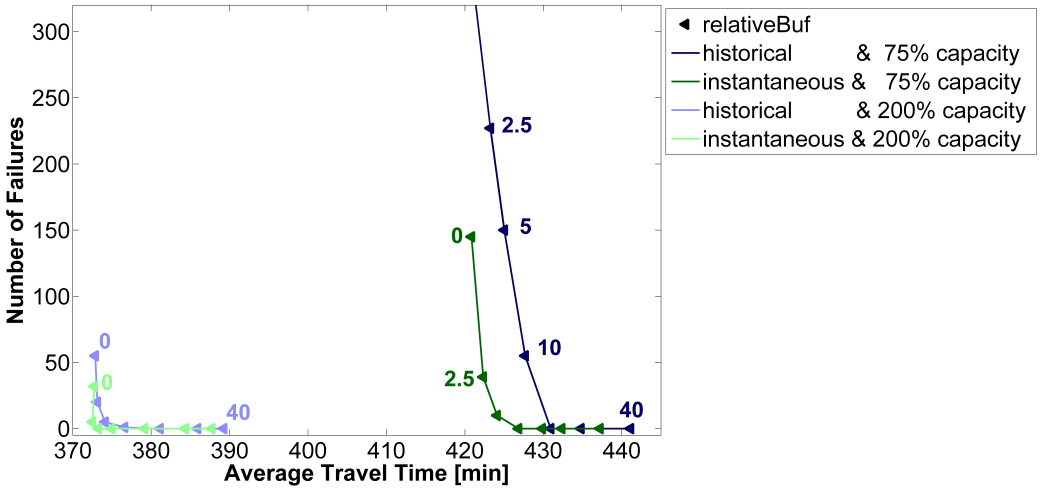

Figure 7.12: Differences between historical and instantaneous travel time prediction for the case of two different capacity settings.

slightly above zero if battery capacity is increased to 200 percent (recall that equally distributed charging stations are presumed). Due to this, function $V_{Hist}^{t_B}$, i.e., a type of RTTI that causes comparably bad charging strategy qualities (recall Figure 7.10(a)), leads to reasonably good results according to Figure 7.11. Also the usefulness of applying better or worse types of RTTI depends on the „overall-setting“. This is illustrated in Figure 7.12. There, for the case of the 75 and 200 percent capacity setting, the quality of charging strategies that results when applying $V_{Hist}^{t_B}$ is compared to the quality that is achieved when applying $V_{Inst}^{t_B}$. In contrast to $V_{Hist}^{t_B}$, function $V_{Inst}^{t_B}$ achieves a rather high level of similarity to the ground truth. For the 75 percent setting, similar to the findings of Figure 7.10(a), significant differences can be observed, particularly for small energy buffers (i.e., low values of z). For the 200 percent capacity setting, the resulting differences between using $V_{Hist}^{t_B}$ and $V_{Inst}^{t_B}$ vanish almost completely.

7.3 Comparison of Energy Buffer Approaches

Section 7.2.2 showed that, if parameter z is chosen appropriately, relative energy buffers lead, for most of the introduced types of RTTI, to failure rates equal or close to zero. This means that, despite applying a comparably simple energy buffer method, reasonable charging strategy qualities are achieved. Still, this is not possible for all of the tested RTTI functions. Particularly $V_{Hist}^{t_B}$ causes high failure rates for all tested values of z. In this context it has to be considered that relative energy buffers represent only one possible way to quantify the size of energy buffers. In order to get a better idea of the best possible charging strategy qualities that can be achieved on the basis of the concept of energy buffers, further approaches have to be tested. For this purpose, three different energy buffer functions are compared within this section. It is investigated which of them leads to the best charging strategies. The first of the tested energy

buffer functions is again $SOC_{min}^{r,z}$ (relative energy buffer). Moreover, two different trajectory buffer functions are considered. Both use speed bounds to generate a set of auxiliary driving trajectories, but the way these speed bounds are derived is different. For the first type of speed bounds, speed function $V_{RTTI}^{t_B}$ is simply multiplied by a fixed positive number. If this number is bigger than one, then the resulting spatio-temporal speed function is used as an upper bound, otherwise as a lower bound. The corresponding speed bounds are denoted by $V_{low}^{t_B,f}$ and $V_{up}^{t_B,f}$ for some $f \in [0,1]$. Their construction is done as subsequently shown:

$$V_{low}^{t_B,f}(x,t) := (1-f) \cdot V_{RTTI}^{t_B} \tag{7.21}$$

$$V_{up}^{t_B,f}(x,t) := (1+f) \cdot V_{RTTI}^{t_B} \tag{7.22}$$

The second type of speed bounds is computed according to the ideas of section 6.3.2. The corresponding speed bounds are denoted by $V_{low}^{t_B,\alpha}$ and $V_{up}^{t_B,\alpha}$ for some $\alpha \in [0,1]$. Their generation and some intermediate results are described in section 7.3.1. To be able to differentiate between the energy buffer function resulting from either type of speed bounds, the energy buffer function that results from speed bounds $V_{low}^{t_B,f}$ and $V_{up}^{t_B,f}$ is from here on be denoted with $SOC_{min}^{con,f}$ („con“ for „constant“). The other trajectory buffer function is denoted with $SOC_{min}^{ad,\alpha}$ („ad“ for „adaptive“). These two types of speed bounds are also denoted as „adaptive“ and „constant“ speed bounds, respectively. The number of generated auxiliary trajectories can no longer be found within the formulas, since it is set equal to two for the remainder of this work, i.e., $NT = 1$.

7.3.1 Generation of Adaptive Speed Bounds

The generation of speed bounds $V_{low}^{t_B,\alpha}$ and $V_{up}^{t_B,\alpha}$ is discussed in this section. For the construction of $V_{low}^{t_B,\alpha}$ and $V_{up}^{t_B,\alpha}$, it is necessary to define a set of explanatory variables $E_1, ..., E_Q$ and a training set $\{y^m, e_1^m, ..., e_5^m\}_{m=1,2,...,M}$. As explanatory variables, those which have already been introduced in section 6.3.2 are considered: Variable E_1 denoting the prediction horizon, E_2 denoting relative historical speed averages, E_3 denoting the estimation of current relative driving speeds, E_4 describing the time of day, and E_5 representing the broadcasted confidence values. In order to generate the training set, the days for which traffic related data are available are separated into two sets. This was already mentioned in section 7.1.2. There, inductive loop detector data from the first set of days were used to generate the ground truth V_{GT}. Data from these days are now also applied to derive a test set $\{y^n, e_1^n, ..., e_5^n\}_{n=1,2,...,N}$. The data that has been recorded during one of the other days form the basis for the training set $\{y^m, e_1^m, ..., e_5^m\}_{m=1,2,...,M}$.

Training Data: First, a set of triples $\{(t_B^m, S_{i_m}^{RTTI}, T_{j_m}^{RTTI})\}_{m=1,2,...,M}$ is generated with $M \in \mathbb{R}_{>0}$. The set of road segments $\{S_{i_m}^{RTTI}\}_m$ consists of the TMC road segments, according to which the recorded commercial RTTI was broadcasted. The set of considered broadcasting

times $\{t_B^m\}_m$ consists of all times at which the commercial RTTI were broadcasted during one of the days that are assigned to the training set. Since the commercial RTTI is updated every minute, this leads to 1440 different broadcasting times t_B^m for each day which belongs to the training set. Note that the number of minutes within one day is equal to $24 \cdot 60 = 1440$. Finally,

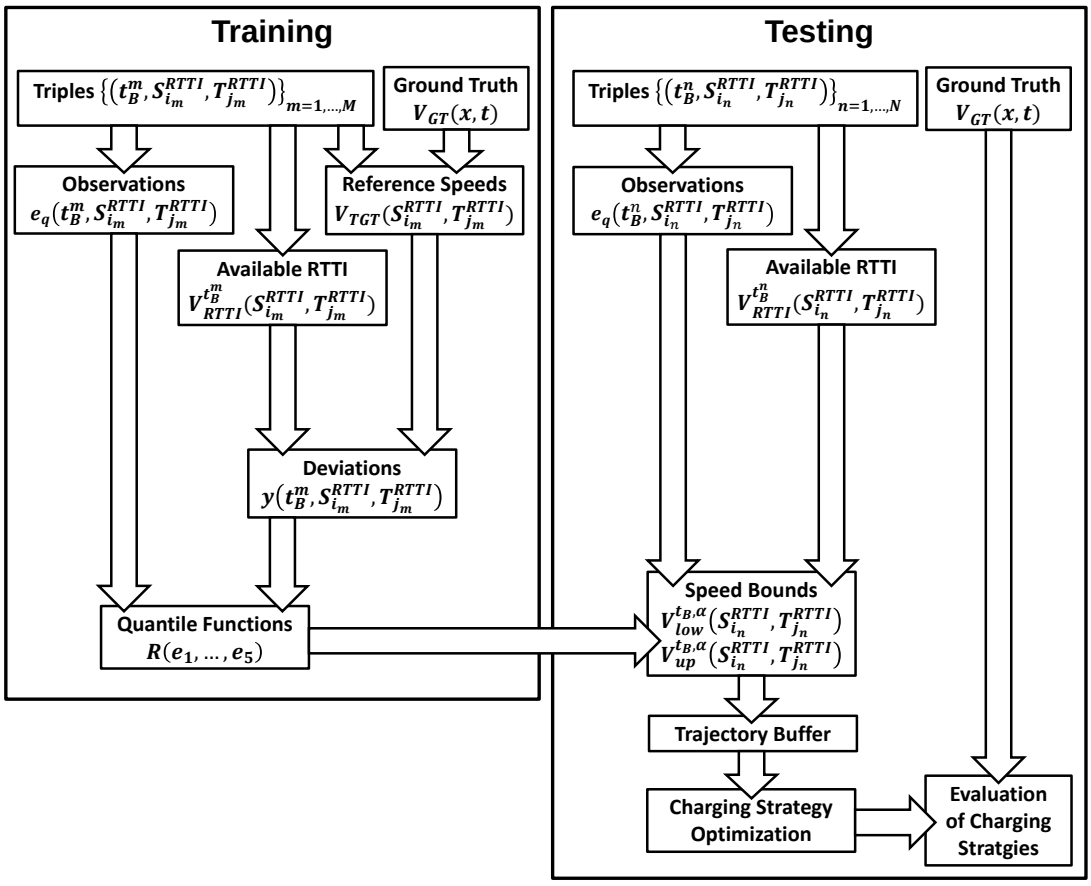

Figure 7.13: Generation and usage of adaptive speed bounds.

the set of prediction intervals $\{T_{j_m}^{RTTI}\}_m$ consists of the RTTI induced set of time intervals. In order to avoid that the size of the training set becomes too big, only prediction horizons of at most 91 minutes are considered here, i.e., $\overline{T}_{j_m}^{RTTI} - t_B^m \leq 91$ minutes for all $m \in \{1, ..., M\}$. For the road corridor A9 leading to Nürnberg, the described proceeding leads to more than 42 million triples $(t_B^m, S_{i_m}^{RTTI}, T_{j_m}^{RTTI})$ (see Table 7.1 for an overview of the relevant data):

$$12 \text{ segments} \cdot 27 \text{ days} \cdot 1440 \text{ broadcasting times} \cdot 91 \text{ prediction intervals} \approx 42.5 \text{ mio.} \quad (7.23)$$

For all four freeway corridors, about 138 million triples $(t_B^m, S_{i_m}^{RTTI}, T_{j_m}^{RTTI})$ are generated, i.e., $M \approx 138$ million.

The set $\{(t_B^m, S_{i_m}^{RTTI}, T_{j_m}^{RTTI})\}_{m=1,2,...,M}$ is applied to compute realizations y^m (deviations between RTTI speeds and ground truth speeds) according to equation 6.25 and to compute

observations $e_1^m, ..., e_5^m$ according to equations 6.27 to 6.31. This leads to the training set $\{y^m, e_1^m, ..., e_5^m\}_{m=1,2,...,M}$. The data belonging to days which are not part of the training set are analogously used to generate a test set $\{y^n, e_1^n, ..., e_5^n\}_{n=1,2,...,N}$. The training and the test set form the basis for all further steps until functions $V_{low}^{t_B,\alpha}$ and $V_{up}^{t_B,\alpha}$ are constructed. Figure 7.13 provides an overview of these steps, which are described in the following.

The values y^m show the relative deviation between broadcasted driving speeds and ground truth driving speeds. Consequently, these values depend on the applied RTTI function. The distribution of set $\{y^m\}_m$ resulting for function $V_{Com}^{t_B}$ can be found in Figure 7.14. It is slightly asymmetric with increased probabilities for negative values, leading to an arithmetic average over all y^m of -0.0263, i.e., values $V_{TGT}(S_{i_m}^{RTTI} \times T_{j_m}^{RTTI})$ are on average slightly higher than $V_{Com}^{t_B^m}(S_{i_m}^{RTTI} \times T_{j_m}^{RTTI})$. This is surprising, since the recorded commercial RTTI reports

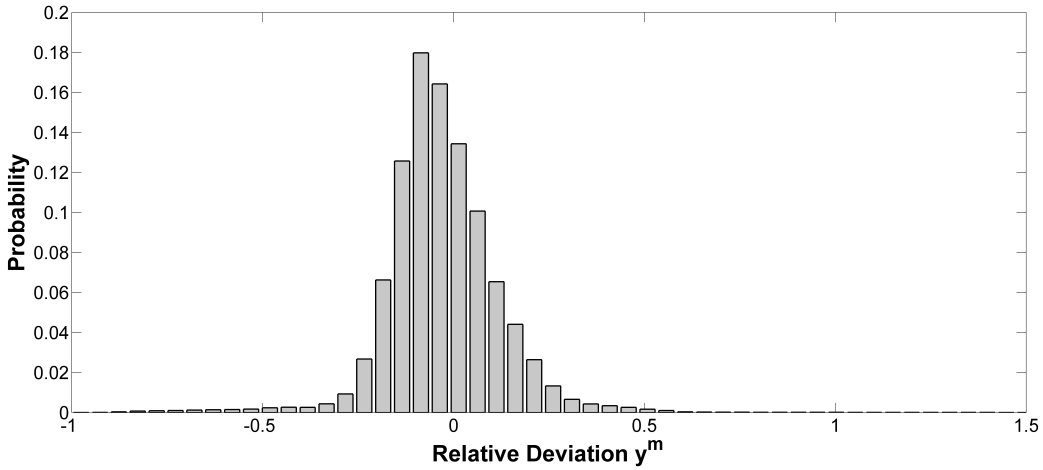

Figure 7.14: Analysis of the distribution of error values y^m.

free-flow unless significant speed drops are detected. Consequently, speeds should be overestimated. On the other hand, the recorded RTTI never reports speeds which are higher than the free-flow speeds V_{ff}. Especially during nights, the available inductive loop detector data frequently show speeds which lie significantly above the corresponding free-flow speeds. The consequence is that speeds are often significantly underestimated during nights. This explains the observed distribution. Note that for the simulation runs, extremely high values of V_{GT} have no influence, since all speed functions are adjusted according to the preferred driving speed v_p. Consequently, the adjusted ground truth function $V_{GT}^{v_p}$ returns v_p in such situations.
It is worth mentioning that not all of the occurring values of y^m are illusrtated in 7.14. Actually, the realizations of the dependent variable range from minus one to more than plus thirteen. This behavior indicates that it is probably not reasonable to apply speed bounds that hold with a probability of 100 percent, since the range between lower bounds $V_{low}^{t_B,\alpha}$ and upper bounds

$V_{up}^{t_B,\alpha}$ would become extremely big and, along with that, useless. Instead, such outliers need to be excluded from consideration.

Derivation of Quantile Functions: For the five proposed explanatory variables, Table 7.3 contains information about the minimum E_q^{min} of all occurring realizations e_q^m and the maximum E_q^{max}. Furthermore, the numbers of categories B_q, which are applied to construct functions R_α, are shown. The partitioning of the intervals $[E_q^{min}, E_q^{max}[$ is simply done by constructing B_q equidistant categories. The only exception is E_1, where the boundaries between the categories are defined as follows:

Table 7.3: Parameters applied for the generation of functions R_α.

	E_1	E_2	E_3	E_4	E_5
Meaning	prediction horizon	historical rel. speeds	currently estimated rel. speeds	time of day	confidence value
E_q^{min}	0 min	0.525	0.0	0 min	50
E_q^{max}	90 min	1.0	1.0	1440 min	99
B_q	13	20	20	20	20

$$b_1^i := \begin{cases} (i-1)\cdot 5 \text{ min} & \text{for } i \in \{1,2,...,12\} \\ 70 \text{ min} & \text{for } i = 13 \\ 90 \text{ min} & \text{for } i = 14 \end{cases} \tag{7.24}$$

Based on the parameters described in Table 7.3 and based on the training dataset, quantile functions $R_\alpha(e_{q_1})$, $R_\alpha(e_{q_1}, e_{q_2})$ and $R_\alpha(e_{q_1}, e_{q_2}, e_{q_3})$ are generated for any combination of explanatory variables, i.e., for any combination of indices q_1, q_2 and q_3 that fulfills the following properties:

$$\begin{aligned} &q_1,\ q_2,\ q_3 \in \{1,2,3,4,5\} \\ &q_1 \neq q_2,\ q_1 \neq q_3,\ q_2 \neq q_3 \end{aligned} \tag{7.25}$$

This means that at most three explanatory variables are considered in parallel. The reason for this restriction is that including four or all five explanatory variables would have led to unacceptably high computation times when generating functions R_α.

Note that not all five of the introduced explanatory variables are available or relevant for all types of RTTI. Confidence values, for example, do only exist for function $V_{Com}^{t_B}$. Moreover, taking the prediction horizon into account makes no sense if the available RTTI does not depend on the prediction horizon. This is the case for $V_{Perf}^{t_B}$, $V_{Hist}^{t_B}$, $V_{ff}^{t_B}$, and $V_{Pha}^{t_B}$. In the following, the analyzed combinations of indices q_1, q_2 and q_3 are reduced according to these considerations. For each relevant combination of explanatory variables, functions R_α are generated for

each α in $\{0.01, 0.02, 0.05, 0.1, 0.2, 0.5, 0.8, 0.9, 0.95, 0.98, 0.99\}$. If α is bigger than 0.5, then function R_α is used for the derivation of upper bounds. If α is smaller than 0.5, then R_α is used to construct lower speed bounds. The motivation for computing $R_{0.5}$ will be explained later on.

Figure 7.15 shows exemplarily functions $R_{0.02}(e_2)$, $R_{0.5}(e_2)$ and $R_{0.98}(e_2)$ for the case of applying recorded commercial RTTI (i.e., function $V_{Com}^{t_B}$ is used to estimate and predict traffic states). Recall that considering a function $R_\alpha(e_2)$, which takes exactly one explanatory variable as input, implies that solely the dependency between Y and E_2 is investigated, i.e., solely the dependency of relative deviations between RTTI-speeds and V_{TGT}-speeds on historical relative speed averages is taken into account. As already mentioned, functions R_α are constant

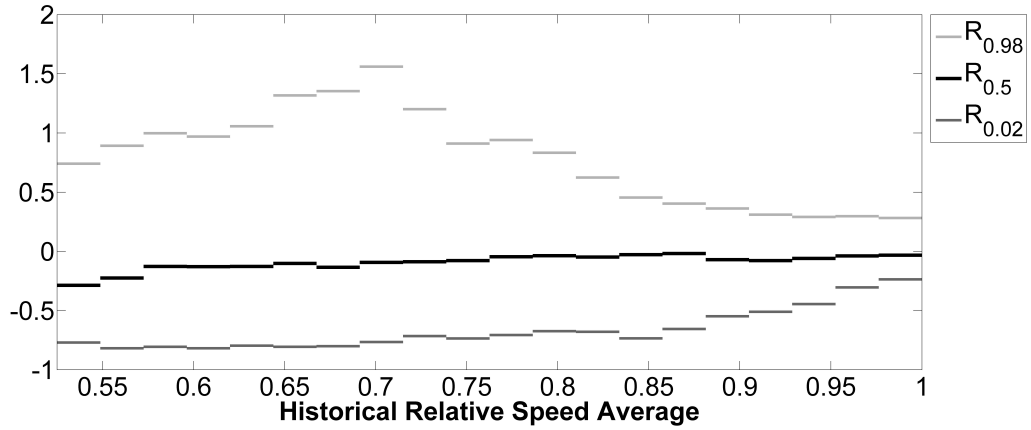

Figure 7.15: Plot of quantile function $R_\alpha(e_2)$ for different values of α for traffic prediction scheme $V_{Com}^{t_B}$.

within each category. Moreover, it can be seen in Figure 7.15 that for very high relative speeds (the rightmost categories), the range between functions $R_{0.02}$ and $R_{0.98}$ is rather small. This indicates that the reliability of $V_{Com}^{t_B}$ is high in situations where high historical relative speed averages occur. Let this statement be explained for the last category, i.e., for situations in which the average historical relative speed lies between 0.97525 and 1.0 (i.e., between b_2^{20} and b_2^{21}). For this category, function $R_{0.98}$ obtains a value of 0.28. According to the definition of R_α, this means that for 98 percent of all observed situations which show a historical relative average speed e_2^m that lies between 97.525 and 100 percent, the value returned by function $V_{Com}^{t_B}$ does not exceed the value returned by function V_{TGT} for more than 28 percent. Hence, small values of R_α for an α-value above 0.5 show that upper speed bounds can be kept tight. Analogously, it can be concluded that high values of function R_α for values of α below 0.5 lead to tight lower speed bounds. Due to this, small differences between $R_{0.02}$ and $R_{0.98}$ indicate a high reliability of function $V_{Com}^{t_B}$. However, the most important observation is that functions $R_{0.02}$ and $R_{0.98}$

are not constant. Instead, they significantly depend on the observations of E_2. This confirms that the reliability of $V_{Com}^{t_B}$, at least for the considered data, indeed depends on historical relative speed averages. Similar statements can be made for the case of applying $V_{Com}^{t_B}$ for all five suggested explanatory variables. See appendix D.4 for the corresponding plots of $R_\alpha(e_1)$, $R_\alpha(e_3)$, $R_\alpha(e_4)$ and $R_\alpha(e_5)$. Also other types of RTTI show comparable dependencies on the proposed explanatory variables.

Similarly to the case of considering one explanatory variable, also two explanatory variables

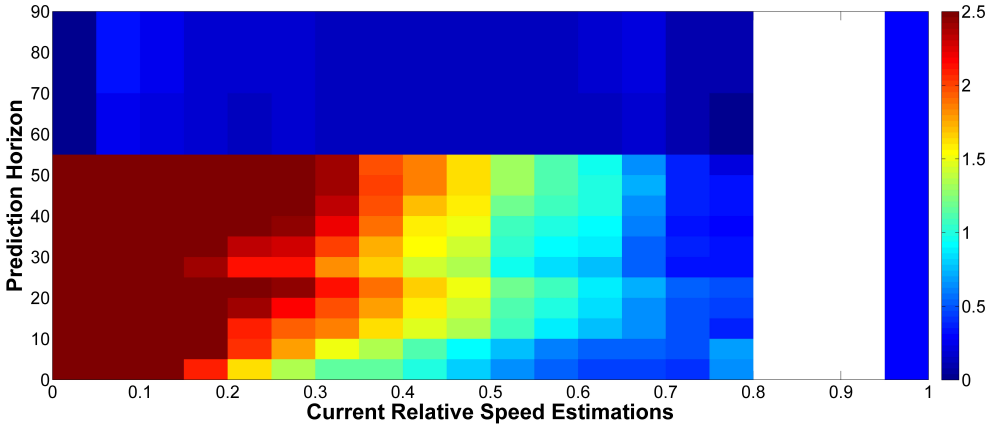

Figure 7.16: Plot of step function $R_{0.98}(e_1, e_3)$.

can be taken into account simultaneously. Figure 7.16 shows exemplarily function $R_{0.98}(e_1, e_3)$ for the case of using recorded commercial RTTI (i.e., function $V_{Com}^{t_B}$). The coloring indicates for each existing two-dimensional category the corresponding value of $R_{0.98}(e_1, e_3)$, i.e., the 0.98-quantile that results from the training dataset. Red indicates high values and thus bad upper bounds. Blue indicates low values and, correspondingly, tight upper bounds. Let, for instance, the deep blue area at the top left of Figure 7.16 be considered. It refers to situations in which the currently broadcasted relative speeds are below five percent of the free-flow speed and the prediction horizon lies above 55 minutes[87]. The blue color shows that it happens very rarely in such a situation that reported driving speeds lie significantly above the corresponding V_{TGT}-speeds. Correspondingly, very low/tight upper bounds can be chosen. An explanation for this observation is that if speeds are very low at the moment, then it often takes more than 55 minutes for traffic to recover. This means that real speeds remain below historical speed averages. In contrast to predictions which are based on historical data, it can be seen in Figure 7.16 that high upper bounds are necessary if the prediction horizon is below 55 minutes and the currently estimated relative speeds are low.

[87] Recall that function $V_{Com}^{t_B}$ is up to a prediction horizon of 55 minutes based on RTTI, afterwards it is based on historical speed averages.

Note that there is a white region for currently broadcasted relative speeds above 80, but below 100 percent. White is here used to indicate that, for the corresponding situations, no or only very few data points (less than 100) can be found in the training dataset. In such situations, it is hardly possible to make robust statements about probabilities or quantiles. The white area in Figure 7.16 is reasoned by the fact that the recorded commercial RTTI reports free-flow speeds unless the estimated (or predicted, respectively) relative drivings speeds fall below 80 percent of the presumed free-flow driving speeds V_{ff}.

The most important observation in Figure 7.16 is that the values which are returned by function $R_{0.98}(e_1, e_3)$ seem to change almost continuously in dependency of the current relative driving speeds and the prediction horizon. Significant discontinuities can only be found in those regions of the figure where the speed values that are used for the construction of function $V_{Com}^{t_B}$ change from v_{Est} to v_{sho} (at a prediction horizon of ten minutes), from v_{sho} to v_{mid} (at a prediction horizon of 25 minutes), and from v_{lon} to V_{Hist} (at a prediction horizon of 55 minutes). The smooth change of function $R_{0.98}(e_1, e_3)$ along the x- and the y-axis indicates that similar situations lead to a similar reliability of $V_{Com}^{t_B}$. Therefore, it can be expected that the values which function $R_{0.98}(e_1, e_3)$ returns do not depend too much on the applied categorization parameters. A comparably „continuous“ behavior can be observed for most other combinations of explanatory variables, too. This is also the case if not $V_{Com}^{t_B}$, but other types of RTTI are analyzed.

Evaluation of Speed Bounds: A lot of effort is necessary for the construction of adaptive speed bounds $V_{low}^{t_B,\alpha}$ and $V_{up}^{t_B,\alpha}$, especially in comparison to simple static bounds $V_{low}^{t_B,f}$ and $V_{up}^{t_B,f}$. Due to this, their generation is only reasonable if significant quality improvements are achieved. Here, the quality of speed bounds is measured according to the ideas that are described in (*80*): Speed bounds are good if they hold with a high probability and, at the same time, are tight, i.e., the distance between both bounds has to be small.

In the following, the quality of speed bounds $V_{low}^{t_B,\alpha}$ and $V_{up}^{t_B,\alpha}$ is compared to the quality of speed bounds $V_{low}^{t_B,f}$ and $V_{up}^{t_B,f}$. For this purpose, let two functions $V_{low}^{t_B,\alpha}$ and $V_{up}^{t_B,\alpha}$ be considered which are computed on the basis of the already described quantile functions R_α, which again are derived from the training set $\{y^m, e_1^m, ..., e_5^m\}_{m=1,...,M}$. These bounds are then applied to the test set $\{y^n, e_1^n, ..., e_5^n\}$. Figure 7.17 shows resulting average relative ranges and success rates exemplarily for the case that functions $R_\alpha(e_3)$, $R_\alpha(e_3, e_4)$ and $R_\alpha(e_3, e_4, e_5)$ are used to generate speed bounds $V_{low}^{t_B,\alpha}$ and $V_{up}^{t_B,\alpha}$ for function $V_{Com}^{t_B}$ [88]. In this context, the average relative range is defined as the average over all differences between $V_{up}^{t_B,\alpha}$ and $V_{low}^{t_B,\alpha}$

[88]The abbreviation „cur“ in Figure 7.17 represents „estimation of current relative speeds“, „time“ represents „time of day“, and „conf“ represents „confidence value“.

divided through the reported speed:

$$\frac{1}{N} \cdot \sum_{n=1}^{N} \frac{V_{up}^{t_B^n,\alpha}(S_{i_n}^{RTTI} \times T_{j_n}^{RTTI}) - V_{low}^{t_B^n,\alpha}(S_{i_n}^{RTTI} \times T_{j_n}^{RTTI})}{V_{Com}^{t_B^n}(S_{i_n}^{RTTI} \times T_{j_n}^{RTTI})} \tag{7.26}$$

The success rate is computed as the probability with which the speed bounds hold[89]:

$$\frac{1}{N} \cdot \left| \left\{ n \in \{1, ..., N\} : \begin{matrix} V_{low}^{t_B^n,\alpha}(S_{i_n}^{RTTI} \times T_{j_n}^{RTTI}) & \leq V_{TGT}(S_{i_n}^{RTTI} \times T_{j_n}^{RTTI}), \\ V_{TGT}(S_{i_n}^{RTTI} \times T_{j_n}^{RTTI}) & \leq V_{up}^{t_B^n,\alpha}(S_{i_n}^{RTTI} \times T_{j_n}^{RTTI}) \end{matrix} \right\} \right| \tag{7.27}$$

In Figure 7.17, the qualities for a selection of adaptive speed bounds and also the qualities of static speed bounds $V_{low}^{t_B,f}$ and $V_{up}^{t_B,f}$ for different values of f can be seen. Each curve belongs to exactly one pair of speed bounds. The different dots along a curve result from different parameters α and f, respectively. The colored numbers describe the values of these parameters for the corresponding dots. It can be seen, for instance, that speed bounds $V_{low}^{t_B,\alpha}$ and $V_{up}^{t_B,\alpha}$, which are based on functions $R_{1-0.9}(e_3, e_4, e_5)$ and $R_{0.9}(e_3, e_4, e_5)$ (the blue curve), lead for $\alpha = 0.9$ to a relative range of 0.3 and a success rate of about 83 percent.

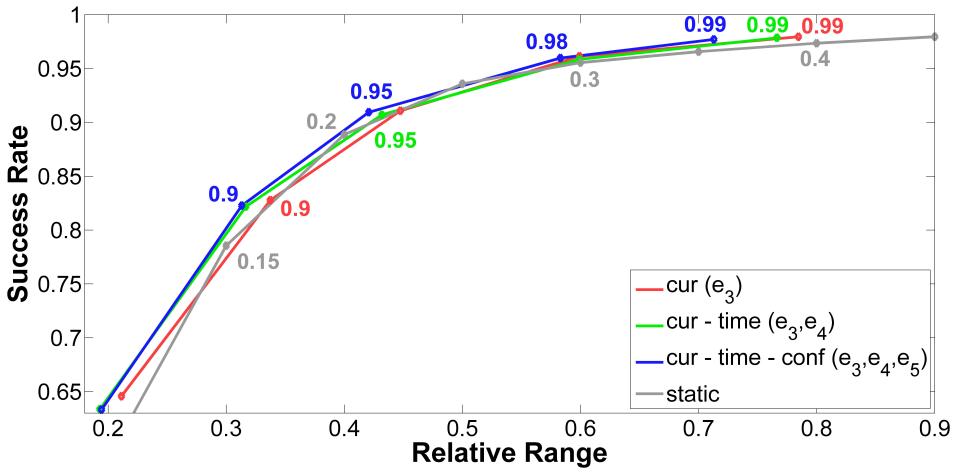

Figure 7.17: Success rates and ranges that are achieved for different speed bounds for the RTTI function $V_{Com}^{t_B}$

When comparing the qualities of the illustrated speed bounds, then it can be observed that the adaptive bounds in most cases lead to better results than the static bounds (grey curve). Furthermore, it can be stated that the quality of adaptive speed bounds improves if the number of explanatory variables, which are taken into account, increases. This is not only for the displayed combinations of explanatory variables the case (see also Figure D.4 in appendix

[89] | {set A} | describes the cardinality of set A, i.e., the number of elements of which set A consists.

D.5). Admittedly, the differences between the illustrated curves are rather small. Significant deviations can only be found for high success rates. For instance, achieving a success rate of at least 98 percent causes static speed bounds to show a relative range of about 0.9 (consider the grey dot at the edge of the right upper corner of Figure 7.17). The blue curve shows that adaptive speed bounds can do the same already for a relative range of about 0.7 (the rightmost blue dot).
In conclusion, it can be stated that adaptive speed bounds lead in comparison to constant speed bounds to improvements (at least for function $V_{Com}^{t_B}$), but these improvements are not very significant. Since no clear statements can be derived from these first observations, it appears to be reasonable to test within the simulation study trajectory buffer functions which are based on both types of speed bounds (constant and adaptive).

Extension: Compensate for Systematic Prediction Errors An interesting observation in Figure 7.15 is that function $R_{0.5}$, which describes the median of set $\{y^m\}_{m=1,...,M}$ in dependency of E_2, drops significantly for low historical relative speed averages. This indicates that in such situations, function $V_{Com}^{t_B}$ tends to lie above V_{TGT}. Such systematic RTTI errors can be seen for other explanatory variables and combinations of explanatory variables and for other types of RTTI, too (see, for example, Figure D.3(d) in the appendix D.4). To compensate for these errors, the RTTI itself is no longer applied to predict driving trajectories. Instead, the speed values which are returned by the applied RTTI function $V_{RTTI}^{t_B}$ are adjusted as described below:

$$V_{RTTI}^{t_B,med}(x,t) := (1 + R_{0.5}\left(e_1(x,t,t_B),...,e_Q(x,t,t_B)\right)) \cdot V_{RTTI}^{t_B}(x,t). \tag{7.28}$$

In equation 7.28, $e_q(x,t,t_B)$ describes the observation of E_q for location x and times t and t_B. For function $V_{Com}^{t_B}$, for instance, this means that $e_5(x,t,t_B)$ is equal to the confidence value that has been broadcasted at time t_B for the TMC segment which covers location x, and $e_3(x,t,t_B)$ is equal to the relative driving speed that is estimated at time t_B for the TMC segment which covers location x. Function $V_{RTTI}^{t_B,med}$ („med“ for „median“) shifts the reported RTTI in such a way that, if realizations y^m had been computed on the basis of $V_{RTTI}^{t_B,med}$ and not on the basis of $V_{RTTI}^{t_B}$, the corresponding function $R_{0.5}$ would have been constantly equal to zero, independently of the observations of $E_1,...,E_Q$. Figure 7.18 shows how the similarity between ground truth and reported speeds is increased if $V_{Com}^{t_B,med}$ is applied instead of $V_{Com}^{t_B}$. Again, training set $\{y^m, e_1^m,...,e_Q^m\}_{m=1,...,M}$ is used to derive a set of quantile functions $R_{0.5}$. Each of these quantile functions takes a different selection of explanatory variables into account. These quantile functions are afterwards used to compute $V_{Com}^{t_B,med}$ according to equation 7.28. The circles in Figure 7.18 mark for any possible combination of at most three explanatory variables, the average absolute percentage error that results when comparing $V_{Com}^{t_B,med}$ to V_{TGT}

based on the testing data, i.e., the following values are illustrated by the circles:

$$\frac{1}{W} \cdot \sum_{n=1}^{N} w_{i_n,j_n} \cdot d_{APE}\left(V_{TGT}(S_{i_n}^{RTTI}, T_{j_n}^{RTTI}), V_{RTTI}^{t_B^n,med}(S_{i_n}^{RTTI}, T_{j_n}^{RTTI})\right), \tag{7.29}$$

with

$$\begin{aligned} w_{i_n,j_n} &:= \int_{S_{i_n}^{RTTI}} \int_{T_{j_n}^{RTTI}} 1 \; dt \; dx \\ W &:= \sum_{n=1}^{N} w_{i_n,j_n} \\ d_{APE}(a,b) &:= \frac{\mid b-a \mid}{b}. \end{aligned} \tag{7.30}$$

Similar to the definition of difference value $D(V_{GT}, V_{RTTI}^{t_B}, X \times T, d)$ in equation 6.14, variable w_{i_n,j_n} describes the spatio-temporal extent of cell $S_{i_n}^{RTTI} \times T_{j_n}^{RTTI}$ and W the sum of the spatial extents of all cells belonging to the test set. The combination of explanatory variables which is taken into account for the computation of $V_{RTTI}^{t_B,med}$ can be found along the x-axis in Figure 7.18. The notation is the same as in the legend of Figure 7.17 (i.e., „conf“ stands for „confidence value“, and so on). Moreover, abbreviation „hor“ stands for „prediction horizon“ and „hist“ for „historical relative speed averages“. The black cross shows the average error which results when comparing $V_{Com}^{t_B}$ to V_{TGT} and not $V_{Com}^{t_B,med}$ to V_{TGT}. It can be observed that the proposed modification significantly reduces deviations between RTTI speeds and ground truth speeds. The improvements tend to grow with the number of explanatory variables which are taken into account by functions R_α. The highest improvement results if the prediction horizon, the time of day and the broadcasted confidence value are considered to generate function $V_{Com}^{t_B,med}$. The original average percentage deviation is reduced from 0.128 to 0.1. This is a relative reduction of the prediction error of about 20 percent.

Besides circles, plus-signs can also be found in Figure 7.18. They result if the expected value of the training set $\{y^m\}_{m=1,\ldots,M}$ is applied in equation 7.28 to construct function $V_{RTTI}^{t_B,med}$ instead of the median. Even though this procedure still leads to improvements in comparison to using the original function $V_{RTTI}^{t_B}$, it can be noticed that these improvements are less significant for all considered cases. Thus, systematic error correction is done according to equation 7.28.

Function $V_{RTTI}^{t_B,med}$ is used to generate macroscopic driving trajectories, which are again used to predict energy consumption and travel times. Whether function $V_{RTTI}^{t_B,med}$ or function $V_{RTTI}^{t_B}$ is applied has no influence on the computation of speed bounds, nor does it have influence on the resulting set of auxiliary trajectories. Note that for the described research, function $V_{RTTI}^{t_B,med}$ is considered if and only if $SOC_{min}^{ad,\alpha}$ is used to quantify energy buffers. This means that energy consumption values and travel times still are based on function $V_{RTTI}^{t_B}$ (and not on function $V_{RTTI}^{t_B,med}$) if relative buffers or constant trajectory buffers are used. The reason for this

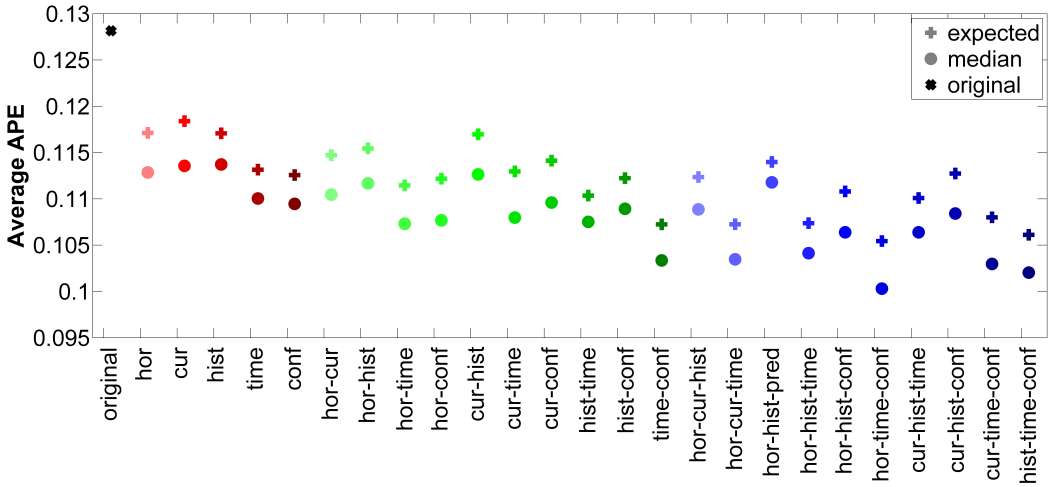

Figure 7.18: Average absolute percentage errors resulting from RTTI function $V_{Com}^{t_B}$ and adjusted speed function $V_{Com}^{t_B,med}$.

is that it would be a lot of additional effort to compute $V_{RTTI}^{t_B,med}$ for these cases, since it would be necessary to generate a training set $\{y^m, e_1^m, ..., e_Q^m\}_{m=1,...,M}$ and quantile functions $R_{0.5}$. When applying buffer function $SOC_{min}^{ad,\alpha}$, on the other hand, quantile functions R_α need to be generated anyway. Computing these functions for one additional value of α, namely $\alpha = 0.5$, is not much additional effort, since the training dataset is already prepared. Note also that a further advantage of replacing $V_{RTTI}^{t_B}$ by $V_{RTTI}^{t_B,med}$ is that it can be guaranteed that $V_{RTTI}^{t_B,med}$ lies between the adaptive speed bounds (as long as $\alpha \in [0.5, 1.0]$), i.e.:

$$V_{low}^{t_B,\alpha}(x,t) \leq V_{RTTI}^{t_B,med}(x,t) \leq V_{up}^{t_B,\alpha}(x,t) \quad \forall\, x,t,t_B. \tag{7.31}$$

This statement not necessarily holds when applying function $V_{RTTI}^{t_B}$ for traffic state estimation and traffic prediction.

7.3.2 Evaluating Different Types of Energy Buffers

In the following, the charging strategy qualities resulting from applying trajectory buffers that are based on constant and adaptive speed bounds are compared to charging strategy qualities that are achieved when applying simple relative energy buffers. Different values for the corresponding reliability parameters are used. An overview of these values can be found in Table 7.4. The number of auxiliary trajectories which are considered for the computation of trajectory buffers is set equal to two, i.e., $NT = 1$. This is done since preparatory analyses showed that increasing NT any further has almost no influence on the size of the resulting energy buffers and, along with this, it has almost no influence on the resulting charging strategy qualities. This observation can be explained by the fact that energy consumption is particularly high for very

Table 7.4: Overview of the tested energy buffer functions and the tested parameter values.

buffer method	buffer function	set of values
relative buffers	$SOC_{min}^{r,z}$	$z \in \{0\%, 2.5\%, 5\%, 10\%, 20\%, 30\%, 40\%\}$
trajectory buffer (constant bounds)	$SOC_{min}^{con,f}$	$f \in \{0.05, 0.1, 0.2, 0.3, 0.7\}$ $NT = 1$ (two auxiliary trajectories)
trajectory buffer (adaptive bounds)	$SOC_{min}^{ad,\alpha}$	$\alpha \in \{0.8, 0.9, 0.95, 0.98, 0.99\}$ $NT = 1$ (two auxiliary trajectories)

low and for high speeds. Thus, typically one of the two border trajectories, as already mentioned in section 6.3.1, leads to the highest energy consumption of all auxiliary trajectories T^{nt} (with $nt \in \{0, ..., NT\}$). For the comparison of the three described energy buffer functions, the following types of RTTI are considered: $V_{Perf}^{t_B}$, $V_{Hist}^{t_B}$, $V_{Inst}^{t_B}$, and $V_{Com}^{t_B}$.

Figure 7.19 shows the charging strategy qualities resulting from different combinations of RTTI functions and energy buffer functions. There is one graphic for each of the four considered types of RTTI. Again, triangles mark curves that result when applying relative energy buffers (each triangle belongs to one value of z), stars represent settings where trajectory buffers that are based on constant speed bounds are applied (each star belongs to one value of f), and circles belong to settings where trajectory buffers that are based on adaptive speed bounds are used (each circle belongs to one value of α). Note that the colored numbers which are displayed in Figure 7.19 show, for a selection of the tested settings, which value of the corresponding reliability parameter leads to this specific triangle/star/circle. In order to simplify differentiation, the values belonging to parameter z are stated in percent, the values belonging to parameters f and α are stated as numbers between 0.01 and 1.0. For the case of RTTI based on historical speed averages, the adaptive speed bounds that are applied for generating Figure 7.19(b) result from taking explanatory variables E_2 (historical relative speed averages) and E_4 (time of day) into account. For instantaneous traffic predictions, adaptive speed bounds are based on E_1 (prediction horizon), E_2 and E_3 (current relative speed estimations). For the case of $V_{Com}^{t_B}$, adaptive speed bounds are computed by considering E_3, E_4 and E_5 (confidence values). If function $V_{Perf}^{t_B}$ is applied, then it is not important which combination of explanatory variables is taken into account. Function $V_{Perf}^{t_B}$ is equal to the ground truth. Consequently, no RTTI errors occur at all. Along with this, function R_α is constantly equal to zero – independently of the realizations of any explanatory variable. Due to this, the lower and upper bounds $V_{low}^{t_B,\alpha}$ and $V_{up}^{t_B,\alpha}$ are equal to V_{GT} and, therefore, all auxiliary trajectories are equal to the ground truth trajectory. This again ensures that $SOC_{min}^{ad,\alpha}$ is equal to zero – independently of the explanatory variables that are taken into account for the generation of the adaptive speed bounds on which $SOC_{min}^{ad,\alpha}$ is based. Note that also for other types of RTTI functions, the influence of taking

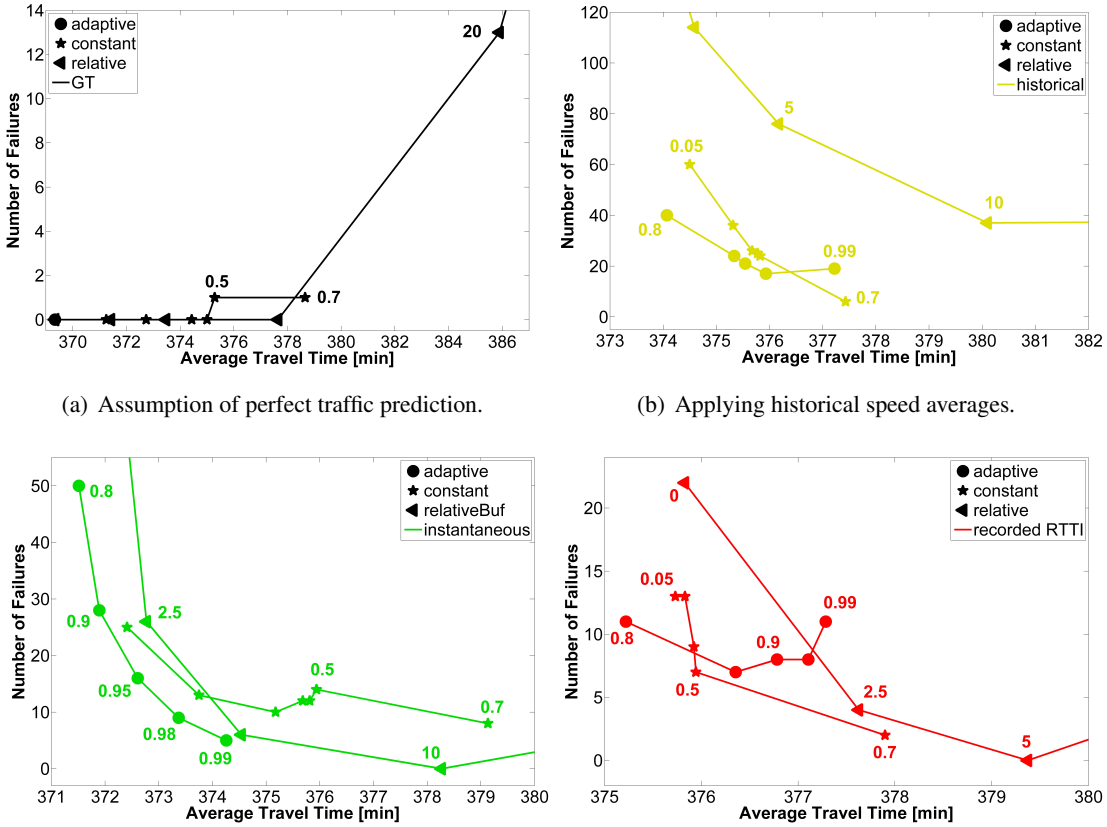

(a) Assumption of perfect traffic prediction.

(b) Applying historical speed averages.

(c) Applying instantaneous travel time predictions.

(d) Using recorded RTTI.

Figure 7.19: Comparison of different energy buffer methods for four traffic prediction schemes.

different combinations of explanatory variables into account is limited. See appendix D.6 for some examples supporting this statement.

In Figure 7.19(a), no curve belonging to $SOC_{min}^{ad,\alpha}$ can be seen. Since $SOC_{min}^{ad,\alpha}$ leads for the described setting to energy buffers of size zero, average travel times and failure numbers are the same as for the reference setting, where a buffer size of zero and the availability of perfect RTTI are presumed. The consequence is that all circles in Figure 7.19(a) are located at the same position as the reference setting (the leftmost point in Figure 7.19(a); its position is at $(369, 0)$). Relative energy buffers and trajectory buffers which are based on constant speed bounds, by contrast, do not include information about the quality of the applied RTTI. Thus, with increasing reliability parameters z and f, the size of the energy buffers and, due to this, average travel times and pre-trip failures rise in Figure 7.19(a).

When considering RTTI based on historical speed averages, then it can be seen in Figure 7.19(b) that the differences that result from using adaptive or constant speed bounds for the generation of trajectory buffers are rather small, but both trajectory buffer functions achieve

significantly better results than relative energy buffers. The minimal occurring number of failures, for instance, can be reduced from 37 (relative buffers) down to 6 (constant speed bounds) and 17 (adaptive speed bounds), respectively.
Though, such clear improvements cannot be seen for all of the analyzed types of RTTI functions. In Figures 7.19(c) and 7.19(d), trajectory buffers are unable to outperform relative buffers[90]. In Figure 7.19(c), for example, the curve belonging to the energy buffer functions $SOC_{min}^{ad,\alpha}$ is located left and below the curve belonging to function $SOC_{min}^{r,z}$. Thus, it could be argued that $SOC_{min}^{ad,\alpha}$ leads to better results than $SOC_{min}^{r,z}$. On the other hand, relative energy buffers allow achieving a failure rate of zero for z equal to ten percent. Unfortunately, it cannot be stated on the basis of the illustrated results, whether the number of failures can be reduced down to zero on the basis of the trajectory buffer approaches. A similar observation can be made in Figure 7.19(d) for trajectory buffers that are based on constant speed bounds and a z-value of five percent.

The results that are illustrated in Figure 7.19 show that none of the three tested energy buffer functions is in general better than the other two. Particularly the two trajectory buffer approaches seem to behave in most cases quite similarly[91]. However, it can also be observed that different types of energy buffer functions lead to different charging strategy qualities and it can be stated that these differences depend on the considered type of RTTI. Additionally to an analysis of the charging strategy qualities which can be achieved when applying the three proposed energy buffer functions, the conducted simulation runs allow drawing further conclusions: First of all, applying trajectory buffers increases the computation time for solving the corresponding optimization problem in comparison to applying relative energy buffers by about 60 percent during the conducted simulation runs. The main reason for this increase is the additional effort necessary for generating auxiliary trajectories. Note that an increase of 60 percent cannot be expected to hold in general. Depending on the implementation, the number of auxiliary trajectories and the analyzed setting, this value may vary.
Besides worse computation times, the conducted analyses revealed that trajectory buffers suffer from another drawback in comparison to relative energy buffers: During the simulation, trajectory buffer functions frequently lead to extremely small energy buffers, independently of the applied reliability parameter (the reason for this will be explained later on). The low failure rates achieved by trajectory buffers (see Figure 7.19) show that these small energy buffers are not critical during the simulation. However, presuming that the proposed framework is intended to be applied in practice, it can hardly be expected that the driver of a BEV constantly drives exactly according to an a priori stated preferred driving speed whenever this is possible.

[90] It has to be considered that the scale of the axes is different for each of the four graphics in Figure 7.19.

[91] To be able to apply energy buffer functions $SOC_{min}^{ad,\alpha}$, a lot of preparatory steps are necessary. Since functions $SOC_{min}^{con,f}$ achieve for most of the tested RTTI functions results that are comparable to those which are achieved when applying $SOC_{min}^{ad,\alpha}$, it can be concluded that it is more reasonable to rely on functions $SOC_{min}^{con,f}$ to compensate for uncertainties than applying functions $SOC_{min}^{ad,\alpha}$.

Even under the assumption that no RTTI errors occur, a driver sometimes may increase her/his driving speed, for example, to overtake another vehicle. Therefore, the real energy consumption may surpass the predicted energy consumption. This is very dangerous if no energy buffer or a very small energy buffer is reserved. Consequently, from a practical point of view, relative energy buffers may ensure more reliable charging strategies than trajectory buffers do.
The low energy buffer sizes that result when applying one of the two suggested trajectory buffer functions can be explained as follows: The presumed ground truth function V_{GT} returns for large parts of the considered spatio-temporal plane $X \times T$ rather high drivings speeds, which often lie close to or even above the presumed free-flow speeds V_{ff} (see Figure 7.3(b), which shows the ground truth function V_{GT} that is used within the simulation). The same holds for upper speed bounds $V_{up}^{t_B,f}$ and $V_{up}^{t_B,\alpha}$, irrespective of the actual values of f and α. Recall in this context that if a speed function returns for some point $(x,t) \in X \times T$ a speed value that is higher than the minimum of the preferred driving speed v_p and the presumed free-flow speed V_{ff}, then this function is assumed to return instead the value v_p (see equation 7.20). The corresponding functions are here denoted with $V_{GT}^{v_p}$, $V_{up}^{t_B,f,v_p}$ and $V_{up}^{t_B,\alpha,v_p}$. As a consequence, after the ground truth and the upper speed bounds are adjusted according to this rule, they often return the same speed value, i.e.:

$$V_{GT}^{v_p}(x,t) = V_{up}^{t_B,f,v_p}(x,t) = V_{up}^{t_B,\alpha,v_p}(x,t) = v_p. \tag{7.32}$$

If this happens for many points (x,t), then the ground truth driving trajectory and the upper border trajectory become very similar and, along with that, also the corresponding energy consumption values. The result is that if in such situations the upper border trajectory causes the highest energy consumption of all auxiliary trajectories, and this is typically the case for high driving speeds[92], then the size of the trajectory buffer is close to or, in many cases, even equal to zero. Increasing reliability parameters f or α solely increases the values which functions $V_{up}^{t_B,f}$ or $V_{up}^{t_B,\alpha}$, respectively, return. The issue remains the same, since these speed values are again reduced to v_p.

7.4 Evaluation of Simulation Results with Regard to Research Objectives

The findings from section 7.2 (analysis of the dependency of charging strategy quality on RTTI quality) and section 7.3 (comparison of the different types of energy buffer functions) form the basis for the following considerations. The question that has to be answered on the basis of these simulation results is up to which degree RO 1c (practicable computation times) and

[92] It has already been mentioned that, due to the properties of the applied primary energy consumption models, trajectories which are based on upper speed bounds usually cause in near free-flow situations the highest energy consumption values.

particularly RO 2 are achieved.

RO 1c: Even though the focus of the analyses which were conducted in chapter 7 was set up to this point on RO 2, the computation times which were experienced during the simulation runs allow drawing conclusions on RO 1c, too. When applying a computer which is equipped with 16 GB RAM and an Intel Xeon processor X3450 (dual core, 2.67 GHz, 8M Cache), then the average computation time for providing an initial charging strategy (i.e., a charging strategy leading from the start to the destination) was equal to 1.11 seconds if relative energy buffers were applied. The average computation time increased to 1.78 seconds if trajectory buffers (two auxiliary trajectories) were applied.
The computer on which the tests were conducted probably provides more computational power than typically navigation devices or navigation systems do. Nevertheless, the stated numbers indicate that reasonable computation times are possible if only a single route, and not a whole road network, is considered.

RO 2: In order to achieve RO 2, the developed framework has to be tested under the existence of uncertainties and it has to be evaluated whether it allows handling these uncertainties in such a way that charging strategies of practicable quality can be ensured. The testing itself was done by conducting the described simulation runs. This can be interpreted as a first proof of concept and hence, RO 2 is already partly fulfilled[93]. It remains to be analyzed whether the computed charging strategy qualities can be said to be practicable. For this purpose, it is firstly necessary to explain how the term „practicable“ is interpreted in this context.

Charging strategy quality is measured with regard to failure rates (reliability) and travel times (efficiency). Clearly, if charging strategies are intended to be applied in practice, then on-trip failures should not occur. Since the conducted simulation runs represent solely an exemplary selection of scenarios, it appears to be reasonable to postulate that charging strategy qualities are only interpreted as „practicable“ if no or almost no on-trip failures occur. This suggests applying big energy buffers. At the same time, the number of pre-trip failures should be kept low. Otherwise, if many situations exist in which no charging strategy can be recommended, i.e., if charging strategies can only be recommended for comparably simple scenarios in which also drivers probably have no problem to find a reasonable charging strategy, then the usefulness of the whole approach becomes questionable. Due to this, energy buffers are not allowed to become too big. Note that travel times can be assumed to be not relevant in this context. Considering the results displayed in Figure 7.10 (illustration of charging strategy qualities for

[93] Proofing the concept will be primarily considered in chapter 8, where experiences gained during real world test drives are described

different types of RTTI), it can be concluded that increasing buffer sizes lead to an unacceptable number of pre-trip failures far before it causes a critical rise of travel times.

According to the described considerations, charging strategies can be denoted as practicable if no on-trip failures occur and only a few pre-trip failures. However, providing specific values for the maximum number of on- and pre-trip failures that can be accepted is not trivial. Fortunately, this question does not need to be answered for most of the tested types of RTTI. According to Figure 7.10, relative energy buffers are able to completely avoid failures for functions $V_{Perf}^{t_B}$, $V_{Inst}^{t_B}$, $V_{Com}^{t_B}$ and $V_{ff}^{t_B}$. As a consequence, it can be stated that for most of the tested types of RTTI, relative energy buffers are – according to the conducted simulation study – able to lead to practicable charging strategy qualities. For function $V_{Pha}^{t_B}$, it is at least possible to achieve a number of on-trip failures of three, and a number of pre-trip failures of eight (by setting reliability parameter z equal to 30 percent). These values appear to be still reasonable and testing further values for z may even allow reducing the number of on-trip failures down to zero without increasing the number of pre-trip failures too much. Furthermore, it has to be taken into account that, due to its artificial construction, function $V_{Pha}^{t_B}$ probably shows properties that cannot be found when applying RTTI provided by professional traffic content providers. Unfortunately, the charging strategy qualities that are achieved for function $V_{Hist}^{t_B}$ are significantly worse. Either 37 on-trip (for $z = 10$ percent) or 38 pre-trip failures (for $z = 20$ percent) have to be accepted for the tested values of z. At this point, it can be questioned whether or not a 2.6 percent ($= 38/1440$) probability for pre-trip failures prohibits a practicable implementation. On the other hand, there may exist other reasonable types of RTTI[94] that cause even worse results. Consequently, it can be concluded that relative energy buffers ensure practicable charging strategy qualities for many different types of error-prone RTTI, but probably not for all.

Note that the findings of section 7.2 show that the quality of the applied RTTI not necessarily allows deciding whether or not relative energy buffers are able to ensure high charging strategy qualities. Due to this, it needs to be tested (for instance, via simulation) which charging strategy qualities can be achieved on the basis of relative energy buffers. If these tests indicate that relative energy buffers are unable to lead for a given RTTI function to sufficiently good results, then two alternatives can be considered. First, another type of energy buffer could be applied. The tests which were described in section 7.3 show that the proposed trajectory buffer approaches are partly able to achieve significant improvements in comparison to the application of relative energy buffers. Though, this does not hold for all of the tested types of RTTI. The second alternative is to ignore the available RTTI and, instead, use function $V_{ff}^{t_B}$. The idea

[94] In contrast to function $V_{Pha}^{t_B}$, applying historical average drivings speed is indeed a common approach to predict driving speeds. Due to this, from a practical point of view, the developed framework has to be able to handle the corresponding uncertainties.

behind this is that function $V_{ff}^{t_B}$ can be obtained quite easily, since it is just necessary to obtain a reasonable free-flow speed value for each relevant road segment. At the same time, the results from section 7.2 indicate that presuming always free-flow allows achieving sufficiently good charging strategy qualities[95]. This is a very strong statement. It means that it may be beneficial to ignore existing information – even though this information describes, in most cases, the real situation rather accurately.

Conclusions: In conclusion, the results of the simulation study indicate that applying relative energy buffers or one of the two alternatives allows achieving practicable charging strategy qualities for most possible RTTI functions[96]. However, it can solely be stated that the developed framework allows deriving practicable charging strategies for the tested scenarios (and probably for most possible RTTI functions). Thus, under different conditions, the suggested framework may no longer be able to achieve the same. The results of section 7.2.3, where different infrastructure and capacity settings were analyzed, support this conjecture. There, failure numbers of zero could be achieved even if function $V_{Hist}^{t_B}$ was used for traffic prediction. It was argued that this is a result of the fact that the maximal distances, which occurred between two successive charging stations, were rather small. Therefore, thinking the other way around, increasing the distances between successive charging stations at some point makes it impossible to compute charging strategies of practicable quality. This conclusion is trivial, but it implies that the ability to compute sufficiently good charging strategies does not only depend on the method that is applied to handle uncertainties. It is also a question of the considered scenarios or settings, respectively. Due to this, the question stated in RO 2 cannot be answered in general, i.e., it cannot be decided in general whether the developed framework allows handling uncertainties in such a way that charging strategies of practicable quality can be ensured. Instead, the question should be reformulated to „Under which conditions is a developed framework able to lead to practicable charging strategy qualities?“ Nevertheless, the conducted simulation study shows that for a set of rather realistic scenarios, the formulation of the problem of finding optimal charging strategies as a deterministic SPP, along with the concept of energy buffers, is able to handle uncertainties in a way, which let a future implementation in practice appear to be reasonable.

[95] The whole simulation study refers to freeways. Presuming free-flow speeds may not work well if other road categories are taken into account. On the other hand, it can be expected that the fast-charging infrastructure, which is in fact necessary to conduct charging processes during trips, can primarily be found along freeways. Hence, this approach probably works for most of the situations which are relevant in practice.

[96] It is very likely that a set of scenarios and settings, respectively, can be constructed for which none of the suggested approaches works well, but this represents probably not the regular case.

7.5 Summary

In chapter 7, a simulation study was described that allows analyzing the relations between different types of error-prone RTTI functions, three types of energy buffer functions which are applied to compensate for uncertainties, and the resulting charging strategy qualities. The chapter started in section 7.1 with a detailed description of the simulation environment itself. In section 7.2, the influence that different types of RTTI have on charging strategy quality was investigated. It turned out that the quality of charging strategies significantly depends on the applied RTTI. Further investigations showed that this dependency cannot be described easily. Better RTTI not necessarily leads to better charging strategies. On the other hand, it can be expected that good RTTI ensures a high quality of the corresponding charging strategies. Furthermore, even though RTTI errors were the only source of uncertainty within the simulation runs, it was observed that the quality of charging strategies also depends on other aspects of the simulation environment, such as the available charging infrastructure or the driving ranges of the simulated BEVs.

In contrast to section 7.2, where always relative energy buffers were applied to compensate for uncertainty, the impact of three different types of energy buffer functions on charging strategy quality was analyzed in section 7.3. The computational results indicate that the two proposed trajectory buffer functions, even though significantly more complex than relative energy buffers, are unable to generally achieve better charging strategy qualities than relative energy buffers. Moreover, both trajectory buffer functions caused increased computation times and it could be observed that, due to the way preferred driving speeds are taken into account within the simulation, trajectory buffers often led to extremely low energy buffer sizes. It was argued that the last point may be critical from a practical point of view.

Chapter 7 ends with an evaluation of the simulation results with regard to the stated research objectives, particularly with regard to RO 2. It was concluded that the simulation results indicate that the developed framework (i.e., the formulation of the problem of finding optimal charging strategies as a deterministic SPP plus the idea to handle uncertainties via energy buffers) is indeed able to ensure charging strategies of practicable quality. However, it was also pointed out that it is not clear whether this statement can be made in general or only for the set of scenarios tested within the simulation study.

Chapter 8

Test Drives

In chapter 3, a very flexible, but numerically hardly treatable formulation of the problem of finding optimal charging strategies as an MDP was proposed. This formulation was adjusted in chapters 4 and 5 to a deterministic SPP, which allows applying rather efficient numerical optimization algorithms in order to compute solutions. Then, in chapters 6 and 7, the deterministic SPP was concretized and a simulation study was executed. Considering the sequence of topics covered in chapters 3 to 7, it can be observed that the focus of the described research shifted more and more from purely theoretical considerations to practice relevant aspects. Hence, it appears to be reasonable to continue this development by testing the proposed framework in reality. For this purpose, field tests, where a PHEV with an official electric driving range of 170 kilometers (*18*) was used to cover (purely electrical) a distance of more than 400 kilometers, were conducted. During these field tests, the test drivers were supported through a prototypic software tool which allows receiving charging strategies during the test drives. These charging strategies were based on the developed models and algorithms. This switch of perspective – from theoretical and computational analyses to practical experiences – leads back to the original motivation of this thesis, which is to provide a first basis for a later inclusion of CSO functionalities into real world navigation systems.

The execution of the field tests is described in chapter 8. It is structured as follows: First, in section 8.1, information about the test site, the test vehicle and the applied prototypic implementation of a tool for CSO are provided. Next, in section 8.2, data gathered during the field tests are evaluated and further observations, which were made during the test drives, are stated. Finally, in section 8.3, the consequences which the experiences that were gained during the field tests have on assessing the developed framework's ability to achieve the ROs are discussed.

8.1 Setting

During the field tests, a PHEV was used to get from a specific starting location to a specific destination. Start and destination location remained the same for all executed test drives. The distance between them was significantly higher than the applied PHEV's maximal electrical driving range. In order to support the test drivers, charging strategies were provided to them. These charging strategies were computed on the basis of the framework which was developed in previous sections. The drivers followed these charging strategies. Details are described subsequently:

The Vehicle The PHEV which was used for the test drives was a BMW i3 which was equipped with a possibility for fast-charging and a so-called range extender. The latter means that, besides an electric battery and an electric motor, a fuel tank and a petrol engine were additionally available. This allows recharging the battery by electricity that is generated by the petrol engine[97] whenever the state of charge falls below 6.5 percent. This happens during the trips, i.e., while the vehicle is driving. The nine liter tank extends the official driving range from 170 (purely electrical, battery capacity of 18,8 kWh presumed) to a „customer oriented" (*18*) driving range of about 250 kilometers (*130*)[98].

Test Site The test drives were conducted on a 412 kilometer long road corridor (primarily freeways) starting in Munich and ending near Leipzig (Germany). This implies that charging strategies were again not computed on the basis of a whole road network, but solely for a predetermined road corridor. Altogether nine fast-charging stations, which are located along this route, were taken into account during the test drives: One is located in Munich at the southern end of the route, one at its northern end, near Leipzig, and seven additional charging stations are located in between. The distances between successive exit ramps, which lead to fast-charging stations, vary between 12 and 91 kilometers. The whole situation is illustrated in Figure 8.1. Note that the set of considered charging stations depends on the driving direction. The reason for this is that when driving from north to south, the charging station near Ingolstadt which is used when driving from south to north cannot be accessed. Due to this, another charging station, which is located significantly further away from the test route, has to be added to the set of charging possibilities. Note that there existed alternative fast-charging stations in Munich, in Ingolstadt, and near Lauf. Hence, different or further charging stations could have been taken into account. However, there existed no alternative fast-charging stations for the remaining parts of the test route.

[97] A BMW i3 that is equipped with a range extender is actually a serial PHEV (recall the differentiation between different types of HEVs from section 2.1.1).

[98] „Customer oriented" means that the corresponding value is intended to describe the ranges that can be obtained in reality more accurately than the official driving range typically does.

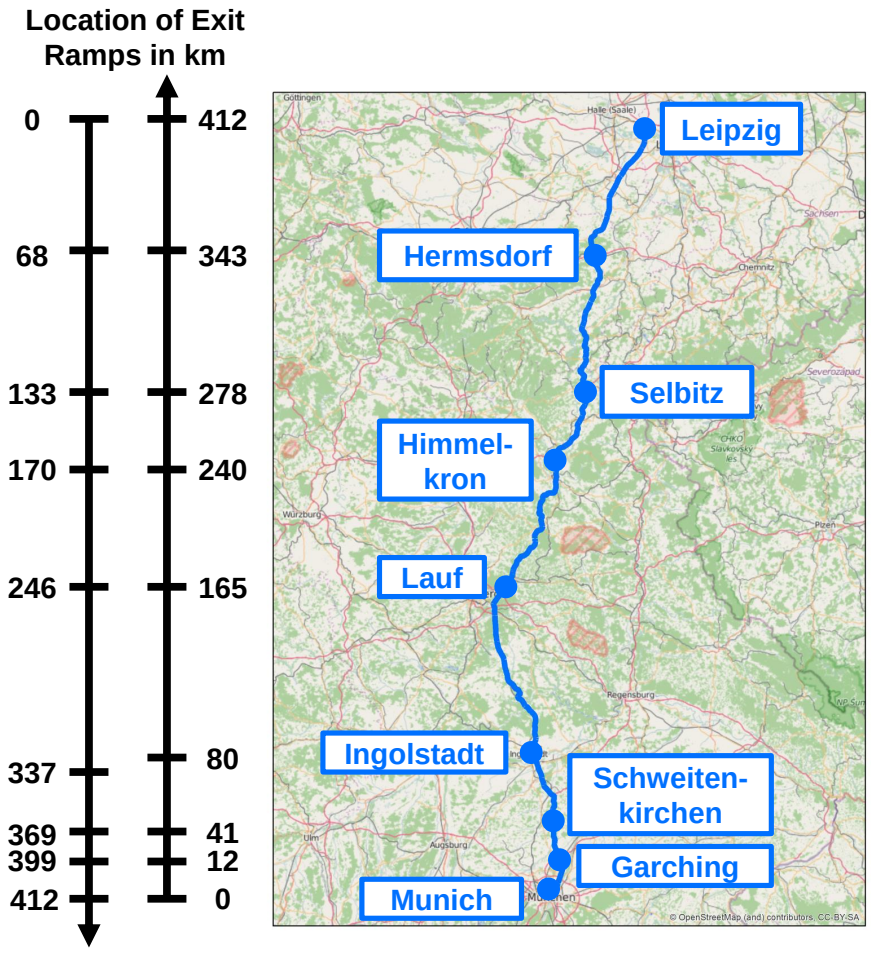

Figure 8.1: Test site and positions of fast-charging stations along the test route.

Available Traffic Information Historical speed averages were available for the whole road corridor. Moreover, commercial RTTI was additionally available for the most southern 42 kilometers of the road corridor, but only when driving from south to north, i.e., only for one direction. Both types of traffic information were generated analogously to the way functions $V_{Hist}^{t_B}$ and $V_{Com}^{t_B}$ were generated for the simulation study. This means that the same traffic content provider supplied the traffic data and the processing of the data was done the same way as described in sections 7.1.2 and 7.1.4. Note that also graph G_D^{Δ} was constructed on the basis of a digital map which was received from the same traffic content provider.

Energy Consumption Model For the computation of charging strategies for the test drives, energy consumption was predicted similarly as it was done for the simulation study in chapter 7. The same secondary consumption function E_{Sec}, which returns energy consumption per time in dependency of outdoor temperature, was applied. Estimations of current outdoor temperature and predictions of future outdoor temperature were received automatically from a

web-service providing weather data (*135*).
The primary energy consumption function EC_{Prim}, on the other hand, was slightly modified in comparison to the primary energy consumption function from chapter 7. A BMW i3 which was equipped with a range extender was used for the test drives. For the simulation study, by contrast, data gathered by people driving a BMW i3 without range extender formed the basis for EC_{Prim}. To take this into account, a new primary energy consumption function EC_{Prim} was constructed on the basis of energy consumption data that were gathered by people driving a BMW i3 with range extender. The data were gathered by 17 different vehicles during about 10,000 trips. The data were processed the same way as described in section 7.1.5, i.e., analogously to the data for the BMW i3 without range extender[99]. The resulting speed-dependent energy consumption values were slightly higher than those belonging to the BMW i3 without range extender. This increase can be explained by the fact that the range extender raises the vehicle's mass by about 120 kilograms.
Besides considering a different type of vehicle, another difference to the primary energy consumption model from chapter 7 was that also elevation data were taken into account. These data were also received from a web-service (*70*). A graph showing the elevation above sea level

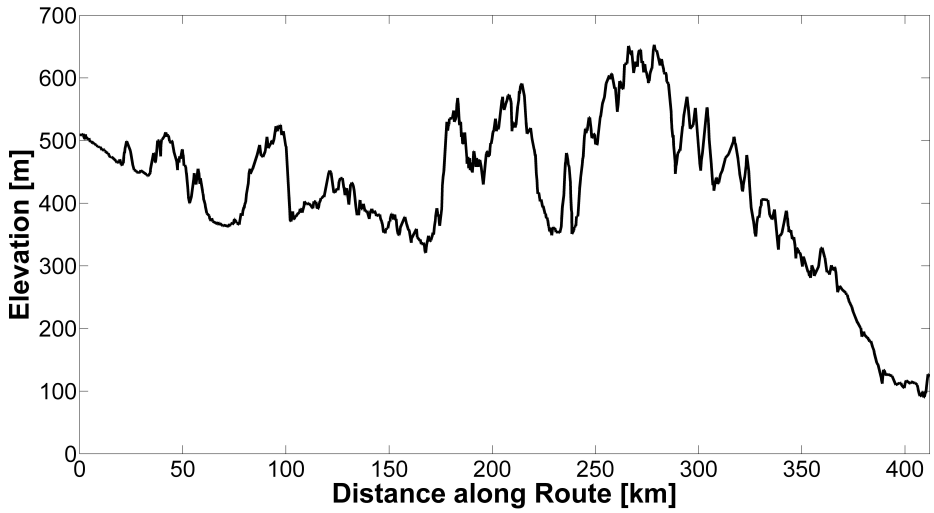

Figure 8.2: Elevation above sea level along test route from Munich to Leipzig.

along the test route can be found in Figure 8.2. In order to take elevation into account when predicting energy consumption, a second type of primary energy consumption function E_{Prim}^{elev} („elev" for „elevation"), similar to the one which is described in (*74*), was applied. Function

[99]The recording of the data took again place in the project „PREMIUM", which is funded by the (German) Federal Ministry for the Environment, Nature Conservation, Building and Nuclear Safety.

E^{elev}_{Prim} is defined for any edge $e \in \vec{E}^{\Delta}_{D}$ as follows:

$$E_{Pot}(e, m_{Veh}) := m_{Veh} \cdot g \cdot (elev(\overline{e}) - elev(\underline{e})) \text{ (change in potential energy)} \tag{8.1}$$

$$E^{elev}_{Prim}(e) := \begin{cases} \frac{E_{Pot}(e, m_{Veh})}{\eta_{mot}} & \text{if } elev(\overline{e}) \geq elev(\underline{e}) \\ \eta_{rec} \cdot E_{Pot}(e, m_{Veh}) & \text{else} \end{cases} \tag{8.2}$$

Function $elev$ assigns the elevation above sea level in meters to starts and ends of edges, m_{Veh} denotes the mass of a BMW i3 with range extender[100], g denotes the acceleration due to gravity, E_{Pot} the vehicle's change of the potential energy, $\eta_{mot} \in [0, 1]$ the electric drive overall efficiency, and $\eta_{rec} \in [0, 1]$ the recuperation efficiency. Function E^{elev}_{Prim} returns the battery energy that is necessary to lift the vehicle by $elev(\overline{e}) - elev(\underline{e})$ meters if the elevation above sea level is at the end of edge e higher than it is at its start. Otherwise, it returns the amount of energy that is recuperated. Note that the values which were assigned to parameters η_{mot} and η_{rec} were provided by BMW and again cannot be stated due to a nondisclosure agreement. Note that presuming that these parameters do not depend on driving speeds or accelerations represents a significant simplification.

Optimization Algorithm Basically, energy buffer function $SOC^{ad,0.99}_{min}$ was applied for the computation of charging strategies during the test drives. However, function $SOC^{ad,0.99}_{min}$ was modified by increasing the size of the energy buffer by 6.5 percent of the battery capacity. This was done to avoid that the range extender activates and, along with this, to ensure that the trips are conducted purely electrically. As a consequence, a test drive was counted as an on-trip failure whenever the state of charge reached 6.5 percent. The range extender was only intended as a fallback, but not for usage during the conducted drives.
The preferred driving speed was set equal to 110 kilometers per hour. For higher preferred driving speeds, preliminary tests showed that it often happened that no adequate charging strategy could be provided (i.e., pre-trip failures occurred or not reliable charging strategy existed at all). For significantly lower preferred driving speeds, predicted total travel times rose[101]. Furthermore, it was assumed that no waiting times occur at charging stations, parameter c^{A}_{T} was set equal to three minutes, and Δ equal to five percent. Charging durations were assumed to be the same as for the BMW i3 without range extender.

Provision of Charging Strategies Charging strategies were provided during the test drives as an on-trip information. To achieve this, a prototypic version of algorithm B-2 was implemented in matlab. This implementation allowed computing charging strategies for both directions

[100] For the prediction of energy consumption values, a mass of 1,550 kilograms was presumed. This number results when adding the estimated weight of two test drivers of 160 kilograms to the vehicle's mass of 1390 kilograms.

[101] Interestingly, if a charging strategy was returned for a preferred driving speed of, for example, 120 kilometers per hour, then the predicted total travel times typically were higher than for 110 kilometer per hour.

of the described test route under the assumption that a BMW i3 which is equipped with a range extender is used for driving. A simple user interface was added and the corresponding software was installed on a computer at the University of the Federal Armed Forces Munich. Furthermore, a software that enabled controlling this computed remotely via a smart phone was installed, too. Whenever the BMW i3 was recharged during one of the test drives, a smart phone was used to get access to the computer at the university. The preferred driving speed, the current state of charge, the driving direction (either to Munich or to Leipzig), and the current position were entered via the user interface. Based on these inputs, a charging strategy for the remaining part of the route was returned.

8.2 Observations made during the Test Drives

Test drives were conducted on three days (28th of April, 6th of May, and the 12th of May, 2016). The drivers started in the morning from Munich to Leipzig and returned in the evening. This leads in total to six test drives. The first two of them, i.e., the first drive from Munich to Leipzig and the first drive from Leipzig to Munich, are not considered in the following. They were intended as preparatory drives to explore differences between model assumptions and reality. The preparatory drives showed that, as already mentioned, the originally selected charging stations near Ingolstadt could not be accessed when driving from Leipzig to Munich. Additionally, a short part of the autobahn A9 was blocked due to road works. This caused detours of several kilometers when trying to get from Hermsdorf to Leipzig and the other way around (compare Figure 8.1). The findings of the first two explorative test drives were included into the software tool.

During the actual test drives (on the 6th of May, and the 12th of May, 2016), a protocol was written. It contained information about the vehicle's state of charge at the start, at the visited charging stations, and at the destination. Furthermore, it contained the corresponding arrival times, the durations of the conducted charging processes, and the states of charge after charging. Besides information about the course of the real test drives, recommended charging strategies were also recorded, i.e., the protocol contained information about predicted arrival times, predicted states of charge, and about the charging strategy itself. A new charging strategy was requested whenever the vehicle was charged.

Analyzing Observed Travel Times Figure 8.3 illustrates for the test drive from Leipzig to Munich, which was executed on 6th of May, the times at which charging stations were reached and the experienced charging durations. Similar figures for the three other test drives can be found in chapter E of the appendix. The x-axis shows time, the y-axis shows the position of the charging stations along the route. The bold black line illustrates the position of the BMW i3 in dependency of time. This curve allows reconstructing at which time the charging stations were reached, whether a charging process was conducted and, if this was the case, how long the corresponding charging process lasted. It can be seen, for example, that the trip on the 6th

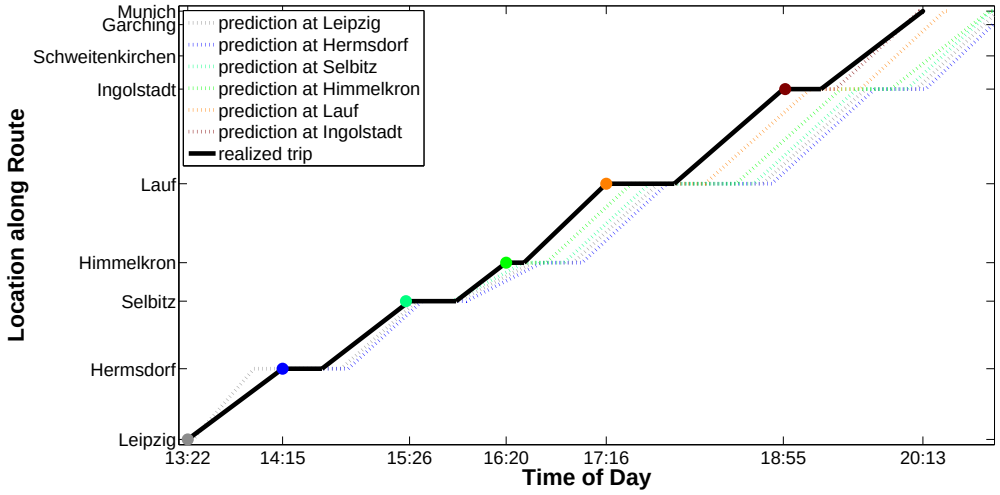

Figure 8.3: Development of arrival times for the test drive from Leipzig to Munich (southbound) on 6th of May, 2016.

of May from Leipzig to Munich was started at 13:22, the first charging station (in Hermsdorf) was reached at 14:15, and the destination in Munich was reached at 20:13. Note that whenever a line runs horizontally, then it shows that the vehicle remained at the corresponding position. This indicates a charging process.
The dotted lines represent provided charging strategies, i.e., these lines represent the movement of the BMW i3 that would have resulted if any prediction concerning travel times or energy consumption had been absolutely correct (always presuming that the driver followed the recommended charging strategy). Since a new charging strategy was computed whenever the vehicle was charged, a new dotted line starts at each location at which the vehicle was charged. The colored circles mark at which time and location the corresponding charging strategy was computed.

Comparing the dotted lines with the bold black line, it can be concluded that the real trip significantly differed from the predictions which formed the basis for the charging strategy recommendations. For the case of the trip which is illustrated in Figure 8.3, there exist two main reasons for this: Let the first road segment be considered, i.e., the road corridor from Leipzig to Hermsdorf. The single dotted line on the left of the bold black line indicates that the travel time that was predicted to be necessary to get from the starting location in Leipzig to the first charging station in Hermsdorf was significantly lower than the realized travel time. Since this prediction was made at 13:22, i.e., at the time the vehicle was located at the first charging station near Leipzig, the corresponding dotted line is denoted with „prediction at Leipzig“ within the legend of Figure 8.3. The huge difference between predicted and realized travel times was the result of a traffic jam caused by road works near Hermsdorf. Since travel time

predictions concerning this road segment were solely based on historical speed averages, the traffic jam was not detected and the resulting travel time prediction was too optimistic.

Another reason for the differences between predictions and the real trip, which holds for all conducted test drives, can be found in Figure 8.4. Each of the illustrated points (x_i, y_i) belongs

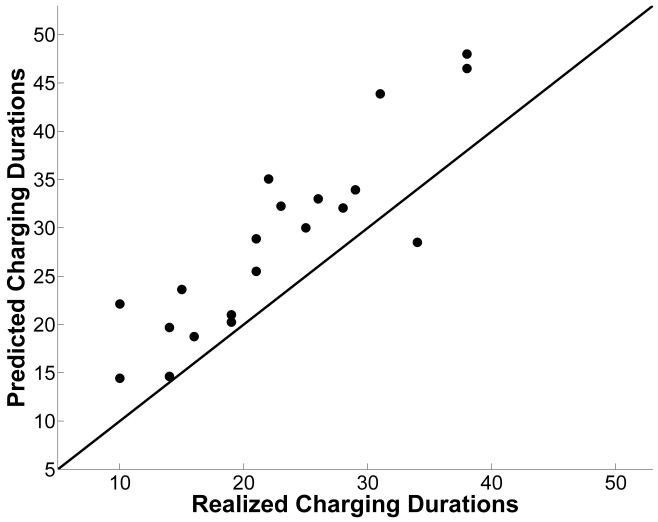

Figure 8.4: Comparison of realized and predicted charging durations.

to one charging process which was conducted during one of the four evaluated test drives. The x-coordinates x_i of the displayed points refer to the recorded durations of the corresponding charging process, i.e., these coordinates represent the real charging durations. To explain the meaning of the y-coordinates y_i, let for each displayed x_i the state of charge at the beginning of the corresponding charging process be denoted by SOC_i^S, and the state of charge at the end of the corresponding charging process by SOC_i^E. Furthermore, let the function which is used to model the charging behavior of a BMW i3 with range extender be denoted by S. The y-coordinates result if function S is used to estimate the charging duration which is necessary to recharge the battery from SOC_i^S to SOC_i^E (recall equation 4.26):

$$y_i = S^{-1}(SOC_i^E) - S^{-1}(SOC_i^S) \tag{8.3}$$

The black line in Figure 8.4 represents the set of points that could result if the observed (real) charging durations had mirrored the applied model S perfectly, i.e., if $x_i = y_i$. It can be observed that almost all points (x_i, y_i) lie above this line. This means that the real charging durations were typically shorter than the durations which would have been necessary according to

the model S. Hence, the applied model leads to a systematic overestimation of charging durations[102]. When returning to Figure 8.3, this observation explains why the predicted total travel times (dotted lines) are higher than the real total travel time (bold black line). An adjustment of function S seems to be necessary to avoid such systematic errors in the future.

Analyzing Observed States of Charge Analogously to the way Figure 8.3 shows the relation between vehicle position and time for the test drive from Leipzig to Munich on the 6th of May, Figure 8.5 illustrates the development of the state of charge along the test route. The bold black line again refers to the real situation and the dashed lines to the development of the states of charge which would have resulted if energy consumption and travel time predictions had been absolutely correct. Differences between the predictions and reality can be seen, but these

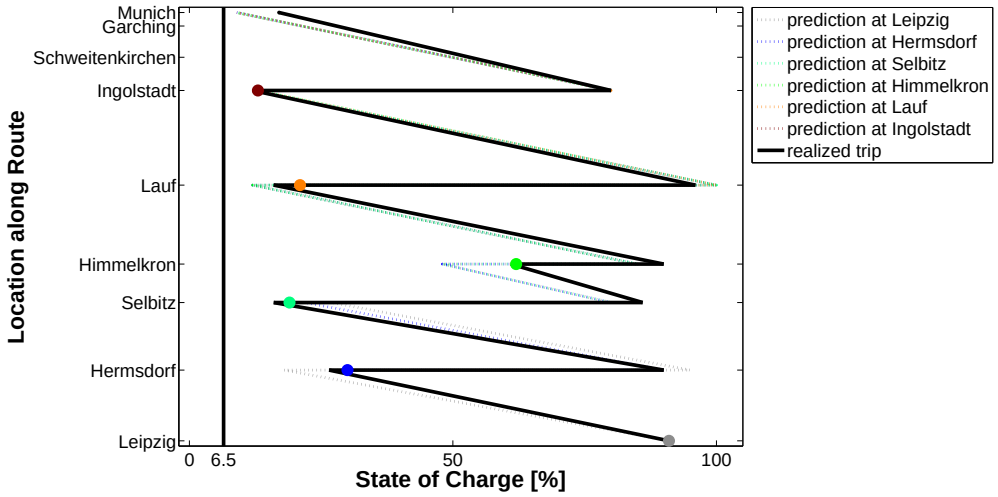

Figure 8.5: Development of states of charge for the test drive from Leipzig to Munich (southbound) on the 6th of May, 2016

differences are less significant than those which can be observed in Figure 8.3. An explanation for both the existence of differences and their minor magnitude can be found in Figure 8.6. The x-coordinates of the displayed points represent the energy (in percent of the battery capacity) which was necessary to get from one charging process to the next[103] during one of the four analyzed test drives, i.e., the x-coordinates represent the real energy consumption which occurred between two successive charging processes. The y-coordinates of the points which are displayed in Figure 8.6 refer to the amount of energy which was predicted to be necessary to get to the next charging process. In this context, the latest prediction is considered, i.e., the

[102] The outlier in Figure 8.4 (the only point below the black line) and the significant scatter the other points show indicate that charging durations probably cannot be predicted precisely. Instead, charging durations may be interpreted as random variables.

[103] Here, it is written „charging processes“ instead of „charging stations“, since the PHEV was not charged at each charging station during the test drives.

energy consumption prediction which was made at the end of the first of the two considered successive charging processes. The bold black line again represents all locations indicating an absolutely correct prediction.
First of all, it can be observed that the applied energy consumption prediction model did not work perfectly. An absolute percentage deviation of 12.7 percent can be computed. This deviation is significant, but it is much smaller than the absolute percentage deviation of 32.3 percent that results when comparing predicted and realized charging process durations (recall Figure 8.4). Due to this, the differences between the bold black curve and the dotted curves are less

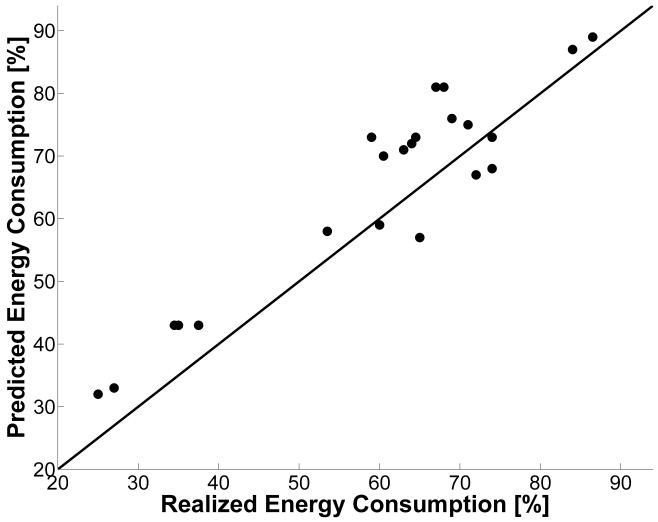

Figure 8.6: Comparison of realized and predicted energy consumption values between two charging stops.

significant in Figure 8.5 than they are in Figure 8.3. On the other hand, the applied model again systematically overestimates the observed values. The reason for the overestimation is probably that the test drivers drove rather steadily with a speed of 110 kilometers per hour. It is very likely that such a driving behavior differs from the „average“ driving behavior. Less accelerations and decelerations, and thus less energy consumption are the consequence. The applied energy consumption model EC_{Prim}, however, is the result of averaging recorded energy consumption values of trips which probably showed a less constant speed profile.

Further Observations Besides comparing observed and predicted travel times and states of charge, two remarkable observations were made during the test drives: First, it never happened that a test driver had to wait due to an occupied charging station. Considering that in total, i.e., when including the test drives of all three days (28th of April, 6th of May, and the 12th of May, 2016), more than 30 charging processes were conducted, this observation at least indicates that

large parts of the existing fast-charging infrastructure along German freeways were not utilized much at that time.
Second, it happened twice during the test drives that a recommended charging process could not be executed due to (temporarily) broken fast-charging stations. On the 6th of May, this was the case for the charging station in Lauf when driving from Munich to Leipzig (see Figure E.2), and on the 12th of May, the charging station in Ingolstadt did not work on the way back from Leipzig (see Figure E.3). To still be able to finish the corresponding test drives, the range extender was activated to get to the next charging station. As soon as the next station was reached, the range extender was again deactivated. Note that road segments which were passed by using the range extender, i.e., which were not passed purely electrically, are marked by a dashed black line instead of a solid black line. Moreover, there was a technical problem with the charging station in Schweitenkirchen when driving on the 12th of May back to Munich. It was not possible to release the cable at the time the recommended amount of energy was charged. The technical support of the charging station had to be called and it was necessary to restart the charging station. As a consequence, the BMW i3 was charged longer than originally intended (this can be seen in Figure E.1). These incidents indicate that the available charging infrastructure was prone to failures at the time the test drives were conducted. Since three different charging stations, which were operated by two different companies, were affected by these problems, it is very likely that similar issues still occur.

8.3 Evaluation of Test Drives

The observations which were described in section 8.2 lead to the following conclusions: The applied model for predicting charging durations has to be significantly adjusted. Moreover, weighting times at charging stations currently seem to occur only rarely (at least at fast-charging stations along German freeways) and thus it may not be too important at the moment to take them into account. Furthermore, the applied model for predicting energy consumption probably can be improved. Note that no information exists that would allow analyzing which part of the prediction errors was caused by incorrectly predicted primary consumption, by incorrectly predicted secondary consumption, or by the way the impact of elevation data on energy consumption was taken into account. Still, even though no detailed analysis is possible, it appears to be most probable that the frequent overestimation of energy consumption is a result of the already mentioned extraordinarily steady driving behavior of the test drivers. If this conjecture is true, then the frequent overestimation of energy consumption indicates that individual driving behavior can have a significant influence on energy consumption. Hence, individual driving style can be expected to lead to a significant amount of uncertainty and thus may be considered explicitly by future energy buffer functions – similar to the way traffic prediction uncertainties are considered by the adaptive trajectory buffer function. Finally, the gained experiences also allow drawing conclusions on RO 2:

RO 2: The test drives indicate that charging station failures occur quite often in practice. If a BEV without range extender had been used, then particularly the failure that was experienced on the 6th of May would have been a problem, since no other fast-charging station (neither the next along the test route, which was more than 70 kilometers away, nor any other fast-charging station in this area) could have been reached with the remaining energy. Thus, it would have been necessary to get to a nearby „slow"-charging station[104]. This would have increased total travel time drastically.

Considering that the recommended charging strategies would have led for two of the four evaluated test drives to an empty battery, it appears to be reasonable to conclude that the proposed framework for CSO is unable to provide charging strategies of practicable quality. However, three aspects have to be considered in this context: First, the failures occurred due to broken charging infrastructure. If the charging stations had worked correctly, the gathered data indicates that the trips would have been finished successfully. Second, for the considered test route and the used test vehicle, it was not possible to make the energy buffers big enough to be able to compensate for the breakdown of the charging station in Lauf. If this charging station does not work, an electrical vehicle has to pass a 160 kilometers long road corridor (between Ingolstadt and Himmelkron) without charging to reach the destination. With a speed of 110 kilometers per hour, the BMW i3 possibly can achieve 120 or 130 kilometers under realistic conditions – without taking any uncertainties due to, for instance, imperfect traffic predictions into account. This means that, irrespective of the method for computing charging strategies, no charging strategy recommendation could have been made as long as the driver is not willing to ignore the risk that this charging station may not be working. Note that the charging station in Lauf represents the most evident example, as the distances to its neighbour stations are rather high (about 75 and 85 kilometers). Failures of other charging stations along the test route would lead to similar, but less crucial issues.

Third, up to this point the author did not take the possibility of failing charging stations into account. Thus, the developed framework is not intended to handle such incidents. Since it is not unlikely that new technologies do not work very reliably at the beginning, it is probably reasonable to assume that, after a short period in which experiences are gathered by those who operate charging stations, charging station failures will occur only rarely. Alternatively, the problem formulation could be modified in such a way that the possible existence of charging station failures is explicitly taken into account. A potential idea for such a modification is sketched in chapter 9. Note that the fact that the developed framework is unable to represent and handle the possibility of charging station failures could also be considered in the context of RO 1a.

[104] It can be seen in Figure E.2(b) that the charging station in Lauf did work for several minutes before failing and, consequently, some energy was recharged. The failure occurred at a state of charge of about 50 percent. This state of charge would not have been sufficient to reach the next fast-charging station along the route, but it would have been enough to get to one of a few nearby conventional charging stations.

Conclusions: The number of conducted test drives is very low. Consequently, it is not possible to make credible statements on the ability of the developed framework to handle uncertainties in such a way that charging strategies of practicable quality can be ensured. On the other hand, running out of energy in 50 percent of the conducted test drives appears to be a clear indicator that the proposed optimization problem, even though it achieves reasonably good results in theory, still faces some issues in reality it cannot handle. The author supposes that the reliability of charging stations will rise quickly. If this assumption is true, the results of the test drives can be interpreted differently, since the recommended charging strategies have worked well whenever the charging infrastructure was working. Nevertheless, further field tests are inevitable to be able to guarantee that recommended charging strategies ensure a reliable arrival.

8.4 Summary

In chapter 8, field tests conducted on the freeway A9 between Munich and Leipzig were described. A BMW i3, with an experienced electrical driving range of about 120 kilometers, was used to cover this more than 400 kilometer long road corridor. In order to support the test drivers, regularly updated charging strategies were provided to them during the trips. In section 8.1, the test route, the test vehicle, and the assumptions on which the charging strategy computation was based, were explained in detail. In section 8.2, the test drives themselves were described by illustrating arrival times, charging durations, and the development of the state of charge for the four considered test drives. Furthermore, deviations between the observed travel times and energy consumption values, and the corresponding predictions, on which the charging strategy computations were based, were analyzed. However, the most important aspect discussed in section 8.2 was that it happened two times during the test drives that a charging process could not be conducted due to a charging station failure. This topic also dominated the discussion in section 8.3, in which the gathered data were analyzed with the purpose to draw conclusions on the ROs. Based on this discussion, it was stated that the mathematical framework, which was developed in chapters 3 to 5, is hardly able to handle charging station failures.

Chapter 9

Summary, Conclusions and Outlook

9.1 Summary

In this work, a framework was developed, which allows computing (near-)optimal charging strategies by solving a deterministic SPP. The focus was set on two aspects: First, different possibilities to model the problem of finding optimal charging strategies were discussed and compared. Second, the quality of charging strategies which are computed under uncertainty was intensively analyzed. The findings indicate that it is likely that the suggested approach is, in contrast to prior approaches, able to provide charging strategies of practicable quality even under the existence of uncertainties.

At the beginning of this work, in chapter 1, it is stated that advanced navigation applications for BEVs have the potential to reduce or even eliminate range anxiety. This conjecture motivates the development of a framework which makes the computation of charging strategies possible. The goal is to form the basis for a later implementation of CSO functionalities into real world navigation systems. Charging strategies are intended to guide drivers of BEVs in such a way that, on the one hand, unnecessary charging stops are avoided and, on the other hand, it is ensured that the BEV does not run out of energy during the trip. A literature review, which was conducted in chapter 2, revealed that the main drawback of existing approaches for the computation of charging strategies is that they provide no or only limited possibilities to handle uncertainties. Hence, since (particularly under realistic conditions) it cannot be expected that energy consumption predictions are absolutely correct, the corresponding charging strategies were assumed to be unable to ensure a reliable arrival at the destination. Moreover, it was observed that prior approaches include further simplifications, such as the assumption that the energy consumption for passing road segments is independent of time. These simplifications are primarily intended to keep computation times low. However, they are partly also an inevitable consequence of limitations from which those types of optimization problems suffer which are used in prior works to model the problem of finding optimal charging strategies.

To overcome the mentioned flaws, the problem of finding optimal charging strategies was modeled as an MDP in chapter 3. This problem formulation differs significantly from prior formulations, as the structure of MDPs allows avoiding almost any simplification other types of optimization problems are unable to avoid in the context of CSO. Unfortunately, it was concluded that the proposed MDP can hardly be treated numerically. Consequently, an alternative formulation of the problem of finding optimal charging strategies as a deterministic SPP was developed in chapters 4 and 5. The formulation as a deterministic SPP was intended to make an efficient numerical computation of charging strategies possible. However, along with the formulation as an SPP, several simplifications and restrictions had to be accepted. It was, for example, necessary to discretize the set of possible charging actions. In contrast to prior approaches, the final version of the suggested formulation as a deterministic SPP (see chapter 5) provides the possibility to compensate for prediction uncertainties. This is achieved by reserving parts of the battery capacity as an energy buffer. The more energy is reserved, the lower the probability of running out of energy becomes. On the other hand, it was stated that big energy buffers lead to conservative charging strategies and, thus, reduce the optimization potential. In order to keep the size of the energy buffers as small as possible, but, simultaneously, as big as necessary, different methods for quantifying the size of the energy buffer dynamically during the trip were proposed and compared. Another difference to prior attempts to compute charging strategies via solving SPPs is that a detailed analysis of the properties of the suggested formulation as a deterministic SPP was conducted. This analysis proved that modeling energy consumption costs as a time-dependent quantity leads to a situation in which Bellman's optimality principle does no longer hold. Based on this result, two modifications of the algorithm of Dijkstra were discussed. The first modification allows computing optimal solutions, despite the absence of Bellman's optimality principle. The second modification ignores the fact that this principle does not hold. This leads to improved computation times, but the resulting charging strategies may be suboptimal.

The development of an adequate formulation of the problem of finding optimal charging strategies represented the first part of the described research. In the second part, the ability of the developed framework to handle uncertainties was tested. In chapters 6 and 7, the testing was done via a simulation study. In this study, BEVs driving along a several hundred kilometers long route were simulated. Various scenarios, differing in terms of, for example, the available charging infrastructure or the driving range of the BEVs, were considered. The simulated BEVs followed charging strategies which were based on error-prone RTTI. Thus, the BEVs encountered traffic situations which differed from the traffic information on which the charging strategies were based. Chapter 6 was intended to prepare the simulation study, which was afterwards described in chapter 7. In chapter 6, concrete models for deriving travel times and

energy consumption values on the basis of macroscopic traffic information, such as RTTI, were proposed. Furthermore, a framework to measure the quality of RTTI was introduced.
In chapter 7, at first the simulation environment was explained in detail. Then, the influence of different types of RTTI, which showed different levels of quality, on charging strategy quality was analyzed. It was found out that this influence is significant. However, the relations between RTTI quality and charging strategy quality turned out to be complex. When comparing two types of RTTI, then the one which shows a higher quality not necessarily leads to better charging strategies than the other type. On the other hand, it can at least be stated that a sufficiently high quality of the available RTTI ensures a high quality of the resulting charging strategies. Furthermore, it could be shown that the quality of charging strategies not only depends on the available RTTI, even though RTTI represented the only source of uncertainty. If, for instance, the density of the existing charging infrastructure is very high, then already poor RTTI can be sufficient to ensure a high quality of the resulting charging strategies. Another interesting observation, which was made on the basis of the conducted simulation study, is that total travel times do not depend much on the available RTTI or on the way the size of energy buffer is quantified. Unfortunately, this does not mean that extremely big energy buffers can be used to achieve charging strategies of high quality, since big energy buffers lead to pre-trip failures. Probably the most important result of the simulation study is that the concept of energy buffers was able to keep the risk of running out of energy very low for all of the tested types of RTTI. Admittedly, not always the same method for quantifying the size of the energy buffer was applied. Instead, it depended on the considered type of RTTI, which method achieved the best results.

Finally, in chapter 8, the execution of a few field tests was described. The findings of the field tests were intended as a supplement to the results of the simulation study. A test BEV was used to cover a distance of more than 400 kilometers. The test drivers received charging strategies, which were computed on the basis of the developed framework, as an on-trip information. The gathered data and gained experiences revealed some minor issues concerning the applied models for predicting energy consumption and charging durations. Despite these issues, the developed framework appeared to be applicable in practice. The only significant problems occurred whenever charging stations failures made it impossible to conduct a recommended recharging process. In these situations, it may happen that even big energy buffers are unable to ensure a reliable arrival.

9.2 Conclusions and Outlook

At the beginning of this work, in section 1.2, several ROs were defined. In the following, it is assessed up to which degree these ROs can be achieved on the basis of the developed formulation of the problem of finding optimal charging strategies as a deterministic SPP. Furthermore, it is also discussed how some of the remaining issues may be solved in the future.

RO 1a: *The suggested problem formulation has to be able to realistically represent those aspects which are relevant for a practical application of CSO.*

The proposed deterministic SPP is formulated in a generic way. Hence, this formulation provides lots of flexibility, which again should allow taking most relevant aspects into account. Nevertheless, this formulation also leads to restrictions which are in fact not necessary to model the problem of finding optimal charging strategies. One of these restrictions is that the space of possible target states of charge is discretized. This is a consequence of the fact that SPPs are based on graphs, which are discrete objects. Second, the way graph $\vec{G}_D^{\Delta}$ is defined makes it impossible to represent arbitrary decision policies via paths. Instead, only charging strategies can be represented. Third, the concept of energy buffers does not allow taking uncertainties of travel time predictions explicitly into account. However, it was argued in sections 4.4 and 5.4 that particularly the first two of these restrictions can be assumed to be not critical. Moreover, based on the promising results of the simulation study, in which incorrect travel time predictions were caused by the imperfection of the applied types of RTTI, it can be concluded that also the third of the mentioned restrictions can be handled rather well by the developed framework. Unfortunately, the concept of energy buffers, the way it was introduced in this work, is probably unable to handle potential charging station failures effectively. From all identified limitations of the developed framework, this is the most critical one. To handle such incidents algorithmically, the author supposes that the decision graph $\vec{G}_D^{\Delta}$ has to be extended in such a way that charging policies can be represented by paths. If this was possible, then an additional constraint has to be included into the problem formulation, which ensures that computed charging policies are able to react to charging station failures. In this context, many new questions arise concerning computational effort and the existence of solutions. Alternatively, instead of extending the developed framework, it seems also reasonable to expect that the reliability of the available charging infrastructure will be improved soon. If this was the case, charging station failures would be no longer an issue.

RO 1b: *The suggested problem formulation has to ensure that charging strategies are optimized with regard to both efficiency and reliability.*

It can be stated that this RO is completely fulfilled. The optimization is done with regard to total travel times. Reliability of the resulting charging strategies is ensured by the energy security condition (recall equation 5.6) and, along with this, by the ability of the proposed framework to handle uncertainties.

RO 1c: *The suggested problem formulation has to make a practical computation of solutions possible.*

RO 1c was frequently discussed and the attempts to achieve RO 1c had a major influence on the final formulation of the problem formulation as a deterministic SPP. Still, whether it can be stated that RO 1c can be fulfilled on the basis of the proposed formulation of the problem of finding optimal charging strategies is not clear. The average computation times (between one and two seconds for the computation of a single charging strategy) that were observed during the simulation study are promising. Admittedly, these computation times resulted for a situation in which no route choices were possible. The suggested optimization algorithms are probably not able to achieve reasonable computation times for graphs representing road networks of whole countries. Prior works on CSO improve computation times by computing and storing time and energy consumption costs of paths a priori, i.e., before the first request for a charging strategy is processed (*10*) (*87*) (*137*). Unfortunately, since the proposed edge cost functions are not static, i.e., since energy consumption and time costs dependent, for instance, on arrival times, preprocessing approaches become expensive and less efficient. An alternative idea, which has been proposed in (*87*) as a supplement to the a priori computation of path costs, is to conduct the computation of charging strategies in two steps. During the first step, which is based on a given graph, a given set of charging stations, a starting node and a destination, the original graph, which can be huge, is reduced to a small subgraph. Such an approach is schematically illustrated in Figure 9.1. The idea could be to compute at first a certain number of candidate routes. These routes have to fulfill a list of properties concerning, for instance, their lengths, the charging infrastructure density along them, and their similarity to each other. It can be thought of formulations such as: „Any candidate route is allowed to be at most w percent longer than the shortest route between starting node and destination. Furthermore, there needs to be a charging station every x kilometers along any candidate route. This charging station is not allowed to be more than y kilometers away from the candidate route. Furthermore, at most z percent of the edges belonging to a new candidate route are allowed to be part of an already computed candidate route“. Variables w, x, y and z are real-valued numbers. An approach to iteratively compute a set of candidate routes which fulfill certain properties can be found, for example, in (*78*). Based on these routes, a new graph could be constructed (see also the third part of Figure 9.1), on which finally the CSO itself takes place.

Certainly, the computational effort that is necessary to conduct the computation of a charging strategy on this graph depends on the number of considered candidate routes. To gain an idea of this effort, let $n \in \mathbb{N}$ describe the number of paths leading from the starting node to the destination on the reduced graph[105]. Then, the average time for computing a charging strategy on the reduced graph should be at most n times the average computation time which is necessary to compute a charging strategy for one of the n paths. The idea behind this statement is that the simplest approach for computing an optimal charging strategy for the whole graph is to compute an optimal charging strategy for each path separately and, after this is done for

[105]The number of paths n may be higher than the number of candidate routes. This can happen whenever a candidate route crosses another one.

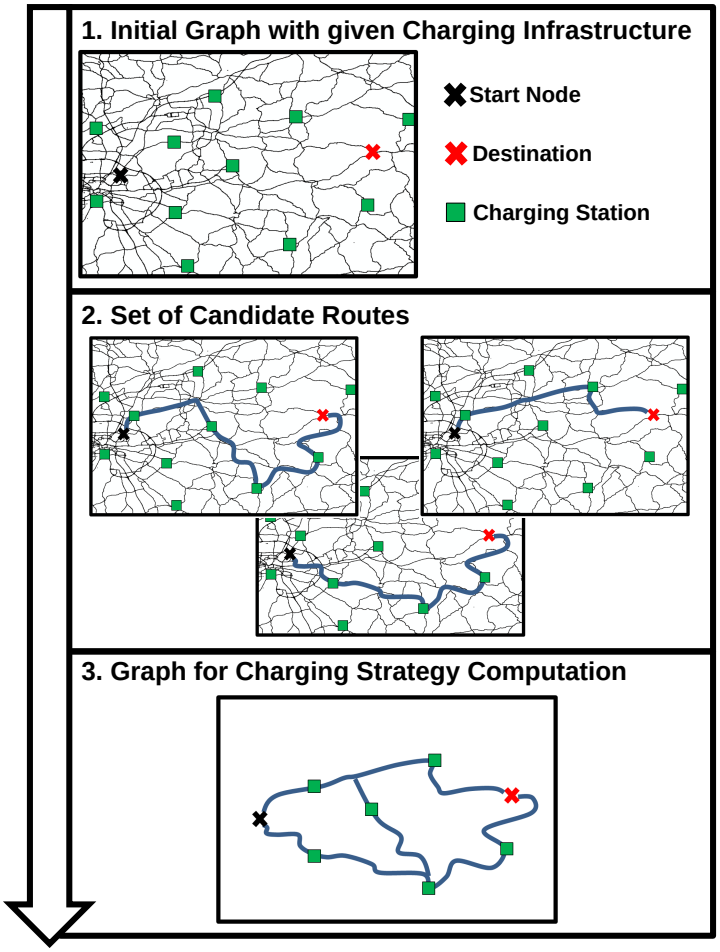

Figure 9.1: Concept for CSO on a network level.

all n paths, recommend the best of all computed charging strategies[106]. Considering that the computation of a single charging strategy for an about 360 kilometers long route took between one and two seconds during the simulation studies, it is very likely that reasonable computation times can be achieved by the described two step approach if the number of considered candidate routes is kept low. Consequently, an application on whole road networks seems to be possible. However, it has to be considered that the reduction of the graph leads to a reduction of the optimization potential. The less candidate route are used to construct the reduced graph on which the computations take place, the more significant this reduction becomes.

RO 2: *Test the suggested problem formulation under the existence of uncertainties and evaluate its ability to ensure charging strategies of practicable quality.*

[106]If the first parts of two or more candidate routes are the same, i.e., if several candidate routes start with the same sequence of edges, then optimization algorithms, such as algorithms A and B, can be expected to need even less computation time to compute an optimal charging strategy for the reduced graph. The reason for this is that the labels belonging to these starting edges are generated only once and not for each existing path separately.

It was stated that charging strategies can be said to show a „practicable“ quality if the probability of on-trip failures is close to zero and if pre-trip failures occur only rarely. Total travel times appeared to be less important. The ability of the developed framework to handle uncertainties was tested on the basis of a simulation study and by conducting a few field tests. The results of these tests were analyzed to decide whether or not the computed charging strategies can be said to show a practicable quality. The findings of the simulation study are promising. For all of the tested RTTI functions, there existed at least one combination of an energy buffer function and a reliability parameter which made it possible to keep the number of on-trip and pre-trip failures close to zero. The results of the field tests, however, are less positive. The test drives showed that the developed framework is unable to handle charging station failures. As long as such failures occur (more or less) regularly, the concept of energy buffers, the way it is described in this work, is probably not able to ensure reliable charging strategies. However, as it appears to be reasonable to expect that the number of charging station failures will fall during the next few years, this issue may loose its relevance.

In conclusion, it can be stated that the developed formulation of the problem of finding optimal charging strategies as a deterministic SPP allows achieving the introduced ROs to a great extent. Hence, a navigation system which provides charging strategy recommendations on the basis of the developed framework represents a promising tool to effectively fight range-anxiety. Nevertheless, the described research revealed many aspects which may be improved further: The ability of the concept of energy buffers to handle uncertainties resulting from, for instance, individual driving style or charging station failures could be addressed by future research. Moreover, other types of energy buffer functions could be developed or the existing approaches could be enhanced by, for instance, applying more sophisticated methods for the generation of speed bounds. The proposed optimization algorithms could be combined with speed-up techniques to enable an application of CSO on a network level. Several other topics, which may be interesting for future research, were mentioned. However, before putting a lot of effort into research, it has to be considered which of these potential research topics will be of relevance in five, ten or twenty years. More and more publicly accessible charging stations are built and the driving ranges of BEVs improve quickly. Thus, ensuring a reliable arrival will loose importance and, at some point, it will no longer be an issue. Instead, an efficient organization of trips and a reliable estimation of arrival times will become more relevant for drivers of future BEVs. Hence, future research probably should focus on topics which particularly improve the efficiency of charging strategies, such as approaches that take the coordination of charging processes of BEVs into account.

Bibliography

[1] TMC Compendium - Alert-C Coding Handbook, 1999. Retrieved 20 Jan 2015 from http://forum.pocketnavigation.de/index.php?page=Attachment&attachmentID=1020503&h=538ea165b7f14bcb4165f989ec406d15eb979118.

[2] ADAC. Selbstversuch: Im Elektro-Golf von München nach Leipzig, 2014. Retrieved 27 June 2016 from https://adacemobility.wordpress.com/2014/07/25/selbstversuch-im-elektro-golf-von-munchen-nach-leipzig/.

[3] ADAC. Entwicklung der Tankstellenanzahl seit 1965 in Deutschland, 2015. Retrieved 27 June 2016 from https://www.adac.de/infotestrat/tanken-kraftstoffe-und-antrieb/probleme-tankstelle/anzahl-tankstellen-markenverteilung/.

[4] Audi AG. A3 Sportback e-tron, 2016. Retrieved 01 Nov. 2016 from https://www.audi.de/bin/dpu-de/pdf?context=nemo-de:de&ids=default-a3sbetron.

[5] Juan Argote, Eleni Christofa, Yiguang Xuan, and Alexander Skabardonis. Estimation of measures of effectiveness based on Connected Vehicle data. In *2011 14th International IEEE Conference on Intelligent Transportation Systems (ITSC)*, pages 1767–1772. IEEE, 2011.

[6] Gunter Arnold et al. Intelligente Netzanbindung von Elektrofahrzeugen zur Erbringung von Systemdienstleistungen – INEES, 2016. Retrieved 25 June 2016 from https://lbsflibraries.blob.core.windows.net/sflibs/docs/default-source/schwarminnovationen/inees_abschlussbericht.pdf.

[7] Andreas Artmeier, Julian Haselmayr, Martin Leucker, and Martin Sachenbacher. The optimal routing problem in the context of battery-powered electric vehicles: Bologna, Italy. *Second International Workshop on Constraint Reasoning and Optimization for Computational Sustainability*, 2010.

[8] Klaus Backhaus, Bernd Erichson, Wulff Plinke, and Rolf Weiber. *Multivariate Analysemethoden*. Springer-Verlag Berlin and Heidelberg GmbH & Co. KG, Berlin, 13 edition, 2010.

[9] Sungwoo Bae and Alexis Kwasinski. Spatial and Temporal Model of Electric Vehicle Charging Demand. *IEEE Transactions on Smart Grid*, 3(1):394–403, 2012.

[10] Fouad Baouche, Rochdi Trigui, Romain Billot, and Nour Eddin El Faouzi. Electric vehicle shortest path problem with replenishment constraint. In *2014 International Conference on Connected Vehicles and Expo (ICCVE)*, pages 514–515. IEEE, 2014.

[11] John Barco, Andres Guerra, Luis Muñoz, and Nicanor Quijano. Optimal Routing and Scheduling of Charge for Electric Vehicles: Case Study, 2013. Retrieved 27 June 2016 from http://arxiv.org/abs/1310.0145.

[12] Moritz Baum, Dibbelt Julian Knoblock, Thomas Pajor, and Dorothea Wagner. Energy-optimal routes for electric vehicles. In *Proceedings of the 21st ACM SIGSPATIAL International Conference on Advances in Geographic Information Systems - SIGSPATIAL'13*, pages 54–63. ACM Press, 2013.

[13] Richard Bellman. The theory of dynamic programming. *Bull. Amer. Math. Soc.*, 60:503–515, 1954. Retrieved 27 June 2016 from http://www.ams.org/journals/bull/1954-60-06/S0002-9904-1954-09848-8/.

[14] Richard Bellman. On a routing problem. *Quaterly of Applied Mathematics*, 16:87–90, 1958.

[15] Neïla Bhouri, Maurice Aron, and Jari Kauppila. Relevance of Travel Time Reliability Indicators: A Managed Lanes Case Study. *Procedia - Social and Behavioral Sciences*, 54:450–459, 2012.

[16] Sebastian Blanco, 2016. Retrieved 25 June 2016 from http://www.autoblog.com/2016/06/20/nissan-200-mile-leaf-coming.

[17] BMW. BMW i DC Fast Charger (for BMW Centers + Partners). BMW AG, Retrieved 27 June 2016 from http://www.bmwicharging.com/BMWiDCFastCharger.

[18] BMW. BMW i3: Technische Daten. BMW AG, Retrieved 27 June 2016 from http://www.bmw.com/com/de/newvehicles/i/i3/2015/showroom/technical_data.html.

[19] Klaus Bogenberger. Qualität von Verkehrsinformationen. *Straßenverkehrstechnik*, 47:518–526, 2003.

[20] Klaus Bogenberger and Martin Hauschild. QFCD - A Microscopic Model for Measuring the Individual Quality of Traffic Information. *ITSC World Congress, Stockholm, Sweden*, 2009.

[21] Klaus Bogenberger and Simone Weikl. Quality Management Methods for Real-Time Traffic Information. *Procedia - Social and Behavioral Sciences*, 54:936–945, 2012.

[22] Susanne Breitenberger, Bernhard Grüber, Martina Neuherz, and Ronald Kates. Traffic information potential and necessary penetration rates. *Traffic Engineering & Control*, 11(45):396–401, 2004.

[23] Matthias Breitinger. Deutschland rollt ohne Strom, 2016. Die Zeit, Retrieved 01 Nov. 2016 from http://www.zeit.de/mobilitaet/2016-01/elektroauto-deutschland-leitmarkt-china.

[24] Bundesamt für Wirtschaft und Ausfuhrkontrolle, 2016. Retrieved 25 June 2016 from http://www.bafa.de/bafa/de/wirtschaftsfoerderung/elektromobilitaet/.

[25] Christos G. Cassandras, Tao Wang, and Sepideh Pourazarm. Energy-aware Vehicle Routing in Networks with Charging Nodes, 2014. Division of Systems Engineering and Center for Information and Systems Engineering, Boston University, Retrieved 21 June 2016 from http://arxiv.org/pdf/1401.6478.pdf.

[26] C. C. Chan. The State of the Art of Electric, Hybrid, and Fuel Cell Vehicles. *Proceedings of the IEEE*, 95(4):704–718, 2007.

[27] Chargemap. Statistiken über Ladestationen, 2016. Retrieved 09 June 2016 from https://de.chargemap.com/stats.

[28] Anthony Chen and Zhaowang Ji. Path finding under uncertainty. *Journal of Advanced Transportation*, 39(1):19–37, 2005.

[29] Donna Chen, Kara Kockelman, and Josiah Hanna. Operations of a Shared, Autonomous Electric Vehicle Fleet: Implications of Vehicle & Charging Infrastructure Decisions. *95th Annual Meeting of the Transportation Research Board*, 16-1840, 2016.

[30] Yanyan Chen, Michael Bell, Dongzhu Wang, and Klaus Bogenberger. Risk-Averse Time-Dependent Route Guidance by Constrained Dynamic A Search in Decentralized System Architecture. *Transportation Research Record: Journal of the Transportation Research Board*, 1944:51–57, 2006.

[31] Yusen Chen and Fan Zhang. Empirical Findings with Multi-Criteria Routing for Dynamic Traffic Management. *ITSC 2013*, pages 2218–2222, 2013.

[32] Kenneth L. Cooke and Eric Halsey. The shortest route through a network with time-dependent internodal transit times. *Journal of Mathematical Analysis and Applications*, 14(3):493–498, 1966.

[33] Brian C. Dean. Shortest Paths in FIFO Time-Dependent Networks: Theory and Algorithms. *Massachusett Institute Of Technology. Technical report*, 2004.

[34] Boris Defourny, Damien Ernst, and Louis Wehenkel. Multistage Stochastic Programming: A Scenario Tree Based Approach to Planning under Uncertainty, 2011. University of Liège, Systems and Modeling, B28, Retrieved 27 June 2016 from http://hdl.handle.net/2268/80246.

[35] Daniel Delling. *Engineering and Augmenting Route Planning Algorithms*. PhD thesis, Universität Fridericiana zu Karlsruhe, 2009.

[36] E. W. Dijkstra. A note on two problems in connexion with graphs. *Numerische Mathematik*, 1(1):269–271, 1959.

[37] Yann Disser, Matthias Müller-Hannemann, and Mathias Schnee. Multi-criteria Shortest Paths in Time-Dependent Train Networks. In Catherine C. McGeoch, editor, *Experimental Algorithms*, volume 5038 of *Lecture Notes in Computer Science*, pages 347–361. Springer Berlin Heidelberg, 2008.

[38] Stuart E. Dreyfus. An appraisal of some shortest-path algorithms. *Operations research : the journal of the Operations Research Society of America*, 17(3):395–412, 1969.

[39] Wilfried Eckl-Dorna and Nils Viktor Sorge. Was taugt Teslas elektrischer Highway?, 2013. Retrieved 12 Aug. 2015 from http://www.manager-magazin.de/finanzen/artikel/tesla-supercharger-im-test-auf-deutscher-autobahn-a-939970-3.html.

[40] ego. Bezahlbares Elektroauto durch Industrie 4.0, 2016. Retrieved 09 Nov. 2014 from http://ego-ag.com/de/presse/pressemitteilung.

[41] Matthias Ehrgott. *Multicriteria optimization*. Springer, Berlin and New York, 2 edition, 2005.

[42] Jochen Eisner, Stefan Funke, and Sabine Storandt. Optimal Route Planning for Electric Vehicles in Large Networks: San Francisco. *Proceedings of the 25th AAAI Conference on Artificial Intelligence*, pages 1108–1113, 2011.

[43] Leonid Engelson. On dynamics of traffic queues in a road network with route choice based on real time traffic information. *Transportation Research Part C: Emerging Technologies*, 11(2):161–183, 2003.

[44] Eva Ericsson. Variability in exhaust emission and fuel consumption in urban driving. *Urban Transport Systems. Proceedings from the 2nd KFB Research Conference in Lund*, pages 31–46, 2000.

[45] eridea AG. e-Routing. Retrieved 15 Aug. 2015 from http://www.erouting.net/.

[46] Robert W. Floyd. Algorithm 97: Shortest path. *Communications of the ACM*, 5(6):345, 1962.

[47] Matthew William Fontana. *Optimal routes for electric vehicles facing uncertainty, congestion, and energy constraints*. PhD thesis, Massachusetts Institute of Technology, 2013.

[48] L. R. Ford. *Network flow theory*, volume 923 of */Rand publications*. Rand Corp, Santa Monica and Calif, 1956.

[49] Abbas Fotouhi and Morteza Montazeri. An Investigation on Vehicle's Fuel consumption and Exhaust Emissions in Different Driving Conditions. *International Journal of Environmental Research*, 6:61–70, 2011.

[50] Thomas Franke and Josef F. Krems. Interacting with limited mobility resources: Psychological range levels in electric vehicle use. *Transportation Research Part A: Policy and Practice*, 48:109–122, 2013.

[51] Benjamin Frieske, Matthias Kloetzke, and Florian Mauser. Trends in vehicle concept and key technology development for hybrid and battery electric vehicles. In *2013 World Electric Vehicle Symposium and Exhibition (EVS27)*, pages 1–12. IEEE, 2013.

[52] L. Fu, D. Sun, and L.R Rilett. Heuristic shortest path algorithms for transportation applications: State of the art. *Computers & Operations Research*, 33(11):3324–3343, 2006.

[53] Song Gao and He Huang. Real-time traveler information for optimal adaptive routing in stochastic time-dependent networks. *Transportation Research Part C: Emerging Technologies*, 21(1):196–213, 2012.

[54] Kia Motors Deutschland GmbH. Kia Soul EV Broschüre, 2016. Retrieved 01 Nov. 2016 from https://www.kia.com/de/dialog/broschuere-download/download/download/?ebrochure={2171F2EC-5503-4EE7-BB13-781BD5D6BB4B}&model={BEF84C08-F692-40CB-B4BC-2915B6C951B5}.

[55] MMD Automobile GmbH. Plug-in Hybrid Outlander, 2016. Retrieved 01 Nov. 2016 from http://www.mitsubishi-motors.de/workarea/downloadasset.aspx?id=23622332115.

[56] Now GmbH. Kompendium für den interoperablen und bedarfsgerechten Aufbau von Infrastruktur für Elektrofahrzeuge, 2014. Retrieved 30 Oct. 2016 from http://sax-mobility.de/wp-content/uploads/2014/03/OEffentliche_Ladeinfrastruktur_fuer_Staedte__Kommunen_und_Versorger.pdf.

[57] Stefan Grubwinkler, Maria Kugler, and Markus Lienkamp. A system for cloud-based deviation prediction of propulsion energy consumption for EVs. In *Proceedings of*

2013 IEEE International Conference on Vehicular Electronics and Safety, pages 99–104. IEEE, 2013.

[58] Randolph W. Hall. Route choice and advanced traveler information systems on a capacitated and dynamic network. *Transportation Research Part C: Emerging Technologies*, 4(5):289–306, 1996.

[59] Horst W. Hamacher, Stefan Ruzika, and Stevanus A. Tjandra. Algorithms for time-dependent bicriteria shortest path problems: Elsevier. *Discrete Optimization*, 3(3):238–254, 2006.

[60] Cliff Hannel, Ben Hannel, Jord Hannel, and Tess Hannel. EV Trip Planner, 2013. Retrieved 18 Sep. 2015 from https://evtripplanner.com/.

[61] Pierre Hansen. Bicriterion Path Problems. In M. Beckmann, H. P. Künzi, Günter Fandel, and Tomas Gal, editors, *Multiple Criteria Decision Making Theory and Application*, volume 177 of *Lecture Notes in Economics and Mathematical Systems*, pages 109–127. Springer Berlin Heidelberg, 1980.

[62] Peter Hart, Nils Nilsson, and Bertram Raphael. A Formal Basis for the Heuristic Determination of Minimum Cost Paths. *IEEE Transactions on Systems Science and Cybernetics*, 4(2):100–107, 1968.

[63] Peter Hart, Nils Nilsson, and Bertram Raphael. Correction to A Formal Basis for the Heuristic Determination of Minimum Cost Paths. *ACM SIGART Bulletin*, 37:28–29, 1972.

[64] Nina Heitmann. *Modellierung von Investitionsentscheidungen und Kraftwerkseinsatzplanung unter Unsicherheit mittels Stochastischer Optimierung und Multi-Agenten-Ansatz am Beispiel des deutschen Strommarktes*. PhD thesis, Mathematisch-Naturwissenschafliche Fakultät der Universität Augsburg, 2012.

[65] Juan C. Herrera, Daniel B. Work, Ryan Herring, Xuegang Ban, Quinn Jacobson, and Alexandre M. Bayen. Evaluation of traffic data obtained via GPS-enabled mobile phones: The Mobile Century field experiment. *Transportation Research Part C: Emerging Technologies*, 18(4):568–583, 2010.

[66] Benjamin Hesse. Einfluss verschiedener Nebenverbraucher auf Elektrofahrzeuge. In *Zukünftige Entwicklungen in der Mobilität : betriebswirtschaftliche und technische Aspekte*, pages 91–104. Springer Gabler, 2012.

[67] Gerhard Huber. *Landmark-based Preprocessing Methods for Solving Multicriteria Shortest Path Problems: Master's Thesis*. Technical University of Munich, 2012.

[68] Gerhard Huber and Klaus Bogenberger. A Quality Evaluation Model for Real-Time-Traffic-Information. *ITSC 2013*, pages 2126–2131, 2013.

[69] Gerhard Huber and Klaus Bogenberger. Long-Trip Optimization of Charging Strategies for Battery Electric Vehicles. *Transportation Research Record: Journal of the Transportation Research Board*, 2497:45–53, 2015.

[70] Google Inc. Google maps elevation api, 2016. Die Zeit, Retrieved 27 Nov. 2016 from https://developers.google.com/maps/documentation/elevation/intro?hl=de.

[71] INRIX. Connected Driver Network: Version 4, 2014. Retrieved 18 Aug. 2015 from http://inrix.com/wp-content/uploads/2014/10/Connected-Driver-Network_4.png.

[72] Donald B. Johnson. Efficient Algorithms for Shortest Paths in Sparse Networks: New York, NY, USA. *Journal of the ACM*, 24(1):1–13, 1977.

[73] Jaeyoung Jung, Joseph Y.J Chow, R. Jayakrishnan, and Ji Young Park. Stochastic dynamic itinerary interception refueling location problem with queue delay for electric taxi charging stations. *Transportation Research Part C: Emerging Technologies*, 40:123–142, 2014.

[74] Tomas Jurik, Arben CELA, Rehda Hamouche, Abdellatif Reama, Rene Natowicz, Silviu-Iulian Niculescu, Christophe Villedieu, and Denis Pachetau. Energy Optimal Real-Time Navigation System: Application to a Hybrid Electrical Vehicle: The Hague, Netherlands. *ITSC 2013*, pages 1947–1952, 2013.

[75] Theo Kamalski. OpenLR - Introduction: Version 19-10-2009, 2009. Retrieved 08 Oct. 2014 from http://www.openlr.org/data/docs/OpenLR-Introduction.pdf.

[76] Namwoo Kang, Fred M. Feinberg, and Panos Y. Papalambros. Autonomous Electric Vehicle Sharing System Design. In *Volume 2A: 41st Design Automation Conference*, page V02AT03A034. ASME, 2015.

[77] Ioannis Kaparias. *Reliable Dynamic In-vehicle Navigation*. PhD thesis, University of London, 2008.

[78] Ioannis Kaparias, Michael Bell, Klaus Bogenberger, and Yanyan Chen. Approach to Time Dependence and Reliability in Dynamic Route Guidance. *Transportation Research Record: Journal of the Transportation Research Board*, 2039:32–41, 2007.

[79] Boris S. Kerner. *Introduction to Modern Traffic Flow Theory and Control: The Long Road to Three-Phase Traffic Theory*. Springer, Heidelberg and Dordrecht and London and New York, 2009.

[80] A. Khosravi, E. Mazloumi, S. Nahavandi, D. Creighton, and J.W.C van Lint. Prediction Intervals to Account for Uncertainties in Travel Time Prediction. *Ieee Transactions on Intelligent Transportation Systems*, 12(2):537–547, 2011.

[81] Abbas Khosravi, Ehsan Mazloumi, Saeid Nahavandi, Doug Creighton, and J.W.C van Lint. A genetic algorithm-based method for improving quality of travel time prediction intervals. *Transportation Research Part C: Emerging Technologies*, 19(6):1364–1376, 2011.

[82] Samir Khuller, Azarakhsh Malekian, and Julián Mestre. To fill or not to fill. *ACM Transactions on Algorithms*, 7(3):1–16, 2011.

[83] Kristina Kielblock. Tesla - Reichweite: Das sind die Reichweiten & Ladestationen der S-Modelle, 2015. Retrieved 01 Nov. 2016 from http://www.giga.de/extra/ratgeber/specials/tesla-reichweite-das-sind-die-reichweiten-ladestationen-der-s-modelle/.

[84] Seoungbum Kim and Benjamin Coifman. Comparing INRIX speed data against concurrent loop detector stations over several months. *Transportation Research Part C: Emerging Technologies*, 49:59–72, 2014.

[85] Maximilian Kloess. *Potentials of hybrid and electric cars to reduce energy consumption and greenhouse gas emissions in passenger car transport – Techno-economic assessment and model-based scenarios*. PhD thesis, Technische Universität Wien, 2011.

[86] S. Kluge, C. Santa, S. Dangl, S. Wild, M. Brokate, K. Reif, and F. Busch. On the computation of the energy-optimal route dependent on the traffic load in Ingolstadt: Oxford, United Kingdom, Elsevier. *Transportation Research Part C: Emerging Technologies*, 36(0):97–115, 2013.

[87] Yuichi Kobayashi, Noboru Kiyama, Hirokazu Aoshima, and Masamori Kashiyama. A route search method for electric vehicles in consideration of range and locations of charging stations. In *2011 IEEE Intelligent Vehicles Symposium (IV)*, pages 920–925. IEEE, 2011.

[88] Michael M. Kostreva and Malgorzata M. Wiecek. Time Dependency in Multiple Objective Dynamic Programming: Elsevier. *Journal of Mathematical Analysis and Applications*, 173(1):289–307, 1993.

[89] Panos Kouvelis and Gang Yu. *Robust discrete optimization and its applications*, volume 14 of *Nonconvex optimization and its applications*. Kluwer Academic Publishers, Dordrecht and Boston, ©1997.

[90] Karin Kraschl-Hirschmann. Energieorientierte Straßennetzbewertung für Routensuchverfahren. *Straßenverkehrstechnik*, 12:803–810, 2014.

[91] Terence C. Lam and Kenneth A. Small. The value of time and reliability: measurement from a value pricing experiment. *Transportation Research Part E: Logistics and Transportation Review*, 37(2-3):231–251, 2001.

[92] Michael W. Levin, Melissa Duell, and Travis S. Waller. The Effect of Road Elevation on Network Wide Vehicle Energy Consumption and Eco-Routing. *93rd annual meeting of the transportation research board*, 2014.

[93] Shieu-Hong Lin, Nate Gertsch, and Jennifer R. Russell. A linear-time algorithm for finding optimal vehicle refueling policies. *Operations Research Letters*, 35(3):290–296, 2007.

[94] Hong K. Lo and W.Y Szeto. Modeling advanced traveler information services: static versus dynamic paradigms. *Transportation Research Part B: Methodological*, 38(6):495–515, 2004.

[95] C. Lux. QBench – Evaluation of Traffic Flow Quality. In Christine Lotz and Malte Luks, editors, *Qualität von on-trip Verkehrsinformationen im Straßenverkehr*, volume 82 of *Berichte der Bundesanstalt für Strassenwesen : F, Fahrzeugtechnik*, pages 56–63. Wirtschaftsverl. NW, Verl. für Neue Wiss., 2011.

[96] G. Maggetto. Electric and electric hybrid vehicle technology: a survey. In *IEE Seminar on Electric, Hybrid and Fuel Cell Vehicles*. IEE, 2000.

[97] Hani S. Mahmassani and R. Jayakrishnan. System performance and user response under real-time information in a congested traffic corridor. *Transportation Research Part A: General*, 25(5):293–307, 1991.

[98] Gonzalo Garcia Martínez. Is the range of the second generation of electric vehicles enough, 2016. EnergyNews, Retrieved 09 June 2016 from http://www.energynews.es/english/is-the-range-of-the-second-generation-of-electric-vehicles-enough/.

[99] Ernesto Queirós Vieira Martins. On a multicriteria shortest path problem: Elsevier. *European Journal of Operational Research*, 16(2):236–245, 1984.

[100] Pierre-Emmanuel Mazarè, Olli-Pekka Tossavainen, Alexandre M. Bayen, and Daniel B. Work. Trade-offs between inductive loops and GPS probe vehicles for travel time estimation: A Mobile Century case study: 12-2746. *91st Annual Metting of the Transportation Research Board*, 2012.

[101] Sara Mehar, Sidi Mohammed Senouci, and Guillaume Remy. EV-planning: Electric vehicle itinerary planning. In *2013 International Conference on Smart Communications in Network Technologies (SaCoNeT)*, pages 1–5. IEEE, 2013.

[102] Ulrich Meyer. Average-case complexity of single-source shortest-paths algorithms: lower and upper bounds. *Journal of Algorithms*, 48(1):91–134, 2003.

[103] Edward F. Moore. The shortest path through a maze. In Harvard Univ. Press, editor, *Proc. International Symposium on Theory of Switching*, volume 2, pages 285–292, 1959.

[104] Nationale Plattform Elektromobilität (NPE). Fortschrittsbericht 2014 –Bilanz der Marktvorbereitung, 2014. Retrieved 27 June 2016 from http://www.din.de/blob/67180/c6df394edbef17083c6c845e50c82275/npe-f-bericht14-data.pdf.

[105] Bart Netten, Andreas Hegyi, Meng Wang, Wouter Schakel, Yufei Yuan, Thomas Schreiter, Bart van Arem, Coen van Leeuwen, and Tom Alkim. Improving moving jam detection performance with V2I communication. *Proceedings 20th World Congress on Intelligent Transport Systems*, 2013.

[106] Nick Nigro and Matt Frade. *Business Models for Financially Sustainable EV Charging Networks*. 2015. Center for Climate and Energy Solutions, Retrieved 09 June 2016 from http://www.c2es.org/publications/business-models-financially-sustainable-ev-charging-networks.

[107] Javier A. Oliva, Christoph Weihrauch, and Torsten Bertram. Model-based remaining driving range prediction in electric vehicles by using particle filtering and Markov chains. In *2013 World Electric Vehicle Symposium and Exhibition (EVS27)*, pages 1–10. IEEE, 2013.

[108] Ariel Orda and Raphael Rom. Shortest-path and minimum-delay algorithms in networks with time-dependent edge-length. *Journal of the ACM*, 37(3):607–625, 1990.

[109] Stefano Pallottino and MariaGrazia Scutellà. Shortest Path Algorithms In Transportation Models: Classical and Innovative Aspects. In Patrice Marcotte and Sang Nguyen, editors, *Equilibrium and Advanced Transportation Modelling*, Centre for Research on Transportation, pages 245–281. Springer US, 1998.

[110] J. Palmer, H. Rehborn, and I. Gruttadauria. Reconstruction Qualtiy of Congested Freeway Traffic Patterns Based on Kerner's Three-Phase Traffic Theory. *International Journal on Advances in Systems and Measurements 3&4*, 4, 2011.

[111] Vilfredo Pareto. *Manuel d'économie politique*. Bibliothèque internationale d'économie politique. Giard & Briére, Paris, 1909.

[112] Parichart Pattanamekar, Dongjoo Park, Laurence R. Rilett, Jeomho Lee, and Choulki Lee. Dynamic and stochastic shortest path in transportation networks with two components of travel time uncertainty. *Transportation Research Part C: Emerging Technologies*, 11(5):331–354, 2003.

[113] Igor Petrov. Tests of commercial TMC-equipped navigation systems. In Christine Lotz and Malte Luks, editors, *Qualität von on-trip Verkehrsinformationen im Straßenverkehr*, volume 82 of *Berichte der Bundesanstalt für Strassenwesen : F, Fahrzeugtechnik*, pages 38–45. Wirtschaftsverl. NW, Verl. für Neue Wiss., 2011.

[114] plugincars. Cars, 2016. Retrieved 01 Nov. 2016 from http://www.plugincars.com/cars.

[115] Portland State University. Live Traffic Speeds, 2015. Retrieved 18 Aug. 2015 from http://portal.its.pdx.edu/Portal/index.php/home/.

[116] Sepideh Pourazarm, Christos G. Cassandras, and Andreas Malikopoulos. Optimal routing of electric vehicles in networks with charging nodes: A dynamic programming approach. In *2014 IEEE International Electric Vehicle Conference (IEVC)*, pages 1–7. IEEE, 2014.

[117] Martin L. Puterman. *Markov decision processes: Discrete stochastic dynamic programming*. Wiley-Interscience paperback series. Wiley-Interscience, Hoboken, N.J [Great Britain], ©1994.

[118] Bernd Rainer. TMCplus - Improving the TMC information chain. In Christine Lotz and Malte Luks, editors, *Qualität von on-trip Verkehrsinformationen im Straßenverkehr*, volume 82 of *Berichte der Bundesanstalt für Strassenwesen : F, Fahrzeugtechnik*, pages 25–31. Wirtschaftsverl. NW, Verl. für Neue Wiss., 2011.

[119] Andrea Raith and Matthias Ehrgott. A comparison of solution strategies for biobjective shortest path problems. *Computers & Operations Research*, 36(4):1299–1331, 2009.

[120] Nadine Rauh, Thomas Franke, and Josef F. Krems. User experience with electric vehicles while driving in a critical range situation – a qualitative approach. *IET Intelligent Transport Systems*, 9(7):734–739, 2015.

[121] Will Recker, Younshik Chung, Jiyoung Park, Lesley Wang, Anthony Chen, Zhaowang Ji, Henry Liu, Matthew Horrocks, and Jun-Seok Oh. *Considering Risk-Taking Behavior in Travel Time Reliability: California PATH Research Report UCB-ITS-PRR-2005-3*. 2005. UNIVERSITY OF CALIFORNIA, BERKELEY.

[122] Hubert Rehborn, Boris S. Kerner, and Jochen Palmer. How can we determine the quality of traffic information? In Christine Lotz and Malte Luks, editors, *Qualität von on-trip Verkehrsinformationen im Straßenverkehr*, volume 82 of *Berichte der Bundesanstalt für Strassenwesen : F, Fahrzeugtechnik*, pages 46–55. Wirtschaftsverl. NW, Verl. für Neue Wiss., 2011.

[123] Hubert Rehborn, Michael Schreckenberg, Boris S. Kerner, Gerhard Hermanns, Peter Hemmerle, Igor N. Kulkov, Oliver Kannenberg, Stefan Lorkowski, Nikolaus Witte,

Heiko Böhme, Timo Finke, and Peter Maier. Eine methodische Einführung zur antriebsabhängigen Routensuche in einem Ballungsraum. *Straßenverkehrstechnik*, 58(3):151–157, 2014.

[124] Renault. Batterie und Aufladen Renault ZOE, 2016. Retrieved 01 Nov. 2016 from https://www.renault.de/modellpalette/renault-modelluebersicht/renault-zoe/batterie-und-aufladen.html.

[125] Michael Richter, Sebastian Zinser, and Herbert Kabza. Comparison of eco and time efficient routing of ICEVs, BEVs and PHEVs in inner city traffic. In *2012 IEEE Vehicle Power and Propulsion Conference*, pages 1165–1169. IEEE, 2012.

[126] Emmanouil S. Rigas, Sarvapali D. Ramchurn, Nick Bassiliades, and George Koutitas. Congestion management for urban EV charging systems. In *2013 IEEE International Conference on Smart Grid Communications (SmartGridComm)*, pages 121–126. IEEE, 2013.

[127] Amiton Dias Rodrigues and Marta Monteiro da Costa Cruz. A generic decision model of refueling policies: a case study of a Brazilian motor carrier: Brazil. *Journal of Transport Literature*, 7:8–22, 2013.

[128] Martin Sachenbacher, Martin Leucker, Andreas Artmeier, and Julian Haselmayr. Efficient Energy-Optimal Routing for Electric Vehicles. *Proceedings of the Twenty-Fifth AAAI Conference on Artificial Intelligence*, 2011. Retrieved 02 Nov. 2016 from https://www.aaai.org/ocs/index.php/AAAI/AAAI11/paper/view/3735/4092.

[129] S. Samaranayake, S. Blandin, and A. Bayen. A Tractable Class of Algorithms for Reliable Routing in Stochastic Networks. *Procedia - Social and Behavioral Sciences*, 17:341–363, 2011.

[130] Boris Schmidt. Schnurren fr den Generator, 2014. Frankfurter Allgemeine, Retrieved 20 July 2016 from http://www.faz.net/aktuell/technik-motor/auto-verkehr/bmw-i3-mit-range-extender-schnurren-fuer-den-generator-13091061.html.

[131] Michael Schneider, Andreas Stenger, and Dominik Goeke. The electric vehicle-routing problem with time windows and recharging stations. *Transportation science : the publication of the Transportation Science Section, Operation Research Society of America*, 48(4):500–520, 2014.

[132] Thomas Schreiter, Hans van Lint, Martin Treiber, and Serge Hoogendoorn. Two Fast Implementations of the Adaptive Smoothing Method Used in Highway Traffic State Estimation. *Proceedings of IEEE ITSC*, 57:1202–1208, 2010.

[133] Paolo Serafini. Some Considerations about Computational Complexity for Multi Objective Combinatorial Problems. In M. Beckmann, W. Krelle, Johannes Jahn, and Werner Krabs, editors, *Recent Advances and Historical Development of Vector Optimization*, volume 294 of *Lecture Notes in Economics and Mathematical Systems*, pages 222–232. Springer Berlin Heidelberg, 1987.

[134] A.J.V Skriver and K.A Andersen. A label correcting approach for solving bicriterion shortest-path problems. *Computers & Operations Research*, 27(6):507–524, 2000.

[135] Dark Sky. Dark sky api, 2016. Die Zeit, Retrieved 27 Nov. 2016 from https://darksky.net/dev/.

[136] Karthik K. Srinivasan, A.A Prakash, and Ravi Seshadri. Finding most reliable paths on networks with correlated and shifted log–normal travel times. *Transportation Research Part B: Methodological*, 66:110–128, 2014.

[137] Sabine Storandt. Quick and energy-efficient routes: computing constrained shortest paths for electric vehicles: Redondo Beach, CA, USA. *Proceedings of the 5th ACM SIGSPATIAL International Workshop on Computational Transportation Science - IWCTS '12*, pages 20–25, 2012.

[138] Sabine Storandt and Stefan Funke. Cruising with a Battery-Powered Vehicle and not Getting Stranded. *26th Conf. on Artificial Intelligence (AAAI)*, 2012. Retrieved 20 June 2016 from http://www.aaai.org/ocs/index.php/AAAI/AAAI12/paper/view/4794.

[139] Shivaram Subramanian. *Optimization Models and Analysis of Routing, Location, Distribution, and Design Problems on Networks*. PhD thesis, Virginia Polytechnic Institute and State University, 1999.

[140] Yoshinori Suzuki. A generic model of motor-carrier fuel optimization. *Naval Research Logistics*, 55(8):737–746, 2008.

[141] Timothy M. Sweda and Diego Klabjan. Finding minimum-cost paths for electric vehicles: Greenville, SC, USA. In *2012 IEEE International Electric Vehicle Conference*, pages 1–4. IEEE, 2012.

[142] Tesla. Performance und Sicherheit in jeder Situation, 2016. Retrieved 01 Nov. 2016 from https://www.tesla.com/de_DE/models.

[143] Tesla Motors. Trip Planner, 2015. Retrieved 18 Sep. 2016 from http://my.teslamotors.com/forum/forums/model-s-software-update-62-range-assurance-lte-valet-mode-blind-spot-and-more.

[144] TK. Model S: 60 kWh-Akkupaket wieder verfügbar, neuer Einstiegspreis bei 76.600 Euro, 2016. Retrieved 10 June 2016 from http://teslamag.de/news/model-s-kwh-akkupaket-einstiegspreis-8901.

[145] TomTom International B.V. OpenLR - White Papter, 2012. Retrieved 09 Oct. 2016 from http://www.openlr.org/data/docs/OpenLR-Whitepaper_v1.5.pdf.

[146] Martin Treiber and Dirk Helbing. Reconstructing the Spatio-Temporal Traffic Dynamics from Stationary Detector Data,. *Cooper@tive Tr@nsport@tion Dyn@mics 1*, pages 3.1 – 3.24, 2002.

[147] Martin Treiber and Arne Kesting. *Traffic Flow Dynamics: Data, Models and Simulation*. Springer, Berlin Heidelberg, 2013.

[148] Martin Treiber, Arne Kesting, and Christian Thiemann. *How Much does Traffic Congestion Increase Fuel Consumption and Emissions? Applying a Fuel Consumption Model to the NGSIM Trajectory Data*. 87th Annual Meeting of the Transportation Research Board, Presentation No. 08-2715, 2008.

[149] J.W.C van Lint. Empirical evaluation of new robust travel time estimation algorithms. *Transportation Research Record: Journal of the Transportation Research Board*, 2160:55–59, 2010.

[150] Volkswagen. Der Golf GTE, 2016. Retrieved 01 Nov. 2016 from http://www.volkswagen.de/content/medialib/vwd4/de/dialog/pdf/golf-gte/golf-gte_preisliste/_jcr_content/renditions/rendition.download_attachment.file/golf-gte-preisliste.pdf.

[151] Tao Wang, Christos G. Cassandras, and Sepideh Pourazarm. Energy-aware Vehicle Routing in Networks with Charging Nodes, 2014. Retrieved 09 Nov. 2014 from http://www.nt.ntnu.no/users/skoge/prost/proceedings/ifac2014/media/files/0814.pdf.

[152] Yan Wang, Jianmin Jiang, and Tingting Mu. Context-Aware and Energy-Driven Route Optimization for Fully Electric Vehicles via Crowdsourcing. *IEEE Transactions on Intelligent Transportation Systems*, 14(3):1331–1345, 2013.

[153] J. G. WARDROP. Road Paper. Some Theoretical Aaspects of Road Traffic Research. *Proceedings of the Institution of Civil Engineers*, 1(3):325–362, 1952.

[154] Ermer; Krause; Krieg; Kristen; Lange; Meschede; Neu; Pozybill; Rohloff; Wasmaier. *Merkblatt für die Ausstattung von Verkehrsrechnerzentralen und Unterzentralen*. Bundesanstalt für Strassenwesen, 1999.

[155] Wikipedia. List of electric cars currently available, 2016. Retrieved 09 June 2016 from https://en.wikipedia.org/wiki/List_of_electric_cars_currently_available.

[156] Thomas Wiltschko. *Sichere Information durch infrastrukturgestützte Fahrerassistenzsysteme zur Steigerung der Verkehrssicherheit an Straßenknotenpunkten*. PhD thesis, Universität Stuttgart, Stuttgart, 2004.

[157] Ho-Kwan Wong and Joseph M. Sussman. Dynamic travel time estimation on highway networks. *Transportation Research*, 7(4):355–370, 1973.

[158] Hunter Hanzhuo Wu, Aaron Gilchrist, Ky Sealy, Paul Israelsen, and Jeff Muhs. A review on inductive charging for electric vehicles. In *2011 IEEE International Electric Machines & Drives Conference (IEMDC)*, pages 143–147. IEEE, 2011.

[159] Xing Wu. Study on mean-standard deviation shortest path problem in stochastic and time-dependent networks: A stochastic dominance based approach. *Transportation Research Part B: Methodological*, 80:275–290, 2015.

[160] Baiyu Yang and Elise Miller-Hooks. Adaptive routing considering delays due to signal operations. *Transportation Research Part B: Methodological*, 38(5):385–413, 2004.

[161] Enjian Yao, Meiying Wang, Yuanyuan Song, and Yongsheng Zhang. Estimating Energy Consumption on the Basis of Microscopic Driving Parameters for Electric Vehicles. *Transportation Research Record: Journal of the Transportation Research Board*, 2454(-1):84–91, 2014.

[162] Yafeng Yin and Hai Yang. Simultaneous determination of the equilibrium market penetration and compliance rate of advanced traveler information systems. *Transportation Research Part A: Policy and Practice*, 37(2):165–181, 2003.

[163] Fangzhu Zhang and Philip Cooke. The Green Vehicle Trend: Electric, Plug-in hybrid or Hydrogen fuel cell?, 2009. Retrieved 16 Oct. 2016 from http://www.dime-eu.org/files/active/0/Cooke-09-Fang-Green-vehicle-Review.pdf.

[164] Kai Zhang, Stuart Batterman, and François Dion. Vehicle emissions in congestion: Comparison of work zone, rush hour and free-flow conditions. *Atmospheric Environment*, 45(11):1929–1939, 2011.

[165] Paweł Zieliński. The computational complexity of the relative robust shortest path problem with interval data. *European Journal of Operational Research*, 158(3):570–576, 2004.

List of Tables

List of Figures

Appendix A

Proving the Optimality of Algorithm A

In the following, a proof for Theorem 1 will be given. To reduce the length of this proof, it will only be shown that any solution computed by algorithm A is feasible and time optimal. For this purpose, it is presupposed that algorithm A terminates with finding an s-d-path. Certainly, this is a direct consequence of the finiteness of $\vec{G}$, the existence of at least one feasible s-d-path, the non-negativity of c_T, and the absence of a zero-time cycle.

Theorem 1. *Let a finite and directed graph $\vec{G} = (V, \vec{E})$, a starting node s, a destination node d, cost functions c_T and c_E (as described in section 4.1.2), and a starting state of charge SOC_S be given. Furthermore, let there be no cycle on $\vec{G}$ that leads to time costs of zero and let at least one path from s to d on $\vec{G}$ exist which is feasible under the given conditions. Then, algorithm A terminates with finding a label that encodes a time optimal and feasible s-d-path.*

Proof. Theorem 1 is proved via contradiction. For this purpose, let $\bar{L}$ be the label which is returned by algorithm A, i.e., $\bar{L}$ is the only label belonging to node d that was added by algorithm A to the set $\mathcal{L}_{perm}$ until termination. Furthermore, let $\bar{P} := [s = \bar{v}_1, \bar{v}_2, ..., \bar{v}_J = d]$ with $J \in \mathbb{N}_{>0}$ be the path which is encoded by $\bar{L}$ and let $\bar{L}_j$ denote the label that encodes sub-path $\bar{P}_{1:j}$ (for any $j \in \{1, ..., J\}$). Note that due to the feasibility condition in line 13 of algorithm A, $\bar{P}$ necessarily is feasible. To prove time optimality, a parameter $c_T^* \in \mathbb{R}_{\geq 0}$ is defined that is equal to the minimal time costs caused by an optimal solution:

$$c_T^* := \min\{c_T(P^*, t_S, SOC_S) \mid P^* \in \mathcal{P}(\vec{G}, s, d) \text{ and } P^* \text{ feasible}\}. \tag{A.1}$$

Such a value c_T^* exists due to the assumption that at least one feasible s-d-path exists (without this assumption, the set on the right-hand side of the above definition could be empty) and due to the non-negativity of c_T (otherwise, c_T^* could be equal to minus infinity). Now, let it be assumed that $\bar{P}$ is not time optimal, i.e.,

$$c_T(\bar{P}, t_S, SOC_S) > c_T^*. \tag{A.2}$$

Based on this assumption, the remainder of the proof is separated into two parts: In part A, it is proved that any label belonging to a time optimal path or a subpath of a time optimal path is lexicographically smaller than label $\bar{L}$. In part B, the statement of part A is used to demonstrate via mathematical induction that any label, which either encodes a time optimal and feasible path or a subpaths of a time optimal and feasible path, is added to the set $\mathcal{L}_{perm}$ before $\bar{L}$. As a consequence, a label which encodes an optimal s-d-path and thus belongs to the destination node d would have been added to $\mathcal{L}_{perm}$ before $\bar{L}$. Hence, algorithm A would have left the while-loop before $\bar{L}$ could have been added to $\mathcal{L}_{perm}$. This is a contradiction to the statement that algorithm A returns $\bar{L}$.

Part A: According to the non-negativity of c_T and according to condition A.2, for any time optimal path $P^* := [v_1^*, v_2^*, ..., v_M^*]$ the time costs of any of its subpaths $P_{1:m}^*$ with $m \in \{1, 2, ..., M\}$ are not higher than the time costs of $\bar{P}$:

$$c_T(\bar{P}, SOC_S, t_S) \overset{(A.2)}{>} c_T^* = c_T(P^*, t_S, SOC_S) = \tag{A.3}$$

$$= c_T(P_{1:m}^*, t_S, SOC_S) + c_T(P_{m:M}^*, t_S, SOC_S) \geq \tag{A.4}$$

$$\geq c_T(P_{1:m}^*, t_S, SOC_S) \tag{A.5}$$

This implies that all labels L_m^* which encode a subpath $P_{1:m}^*$ of a time optimal path P^* are lexicographically smaller than label $\bar{L}$:

$$\Big(c_T(\bar{L}), c_E(\bar{L})\Big) = \Big(c_T(\bar{P}, t_S, SOC_S), c_E(\bar{P}, t_S, SOC_S)\Big) \geq_{lex} \tag{A.6}$$

$$\geq_{lex} \Big(c_T(P_{1:m}^*, t_S, SOC_S), c_E(P_{1:m}^*, t_S, SOC_S)\Big) \tag{A.7}$$

$$= \Big(c_T(L_m^*), c_E(L_m^*)\Big). \tag{A.8}$$

Here, $c_T(L)$ denotes the accumulated time costs of the path which is encoded by label L and $c_E(L)$ correspondingly denotes the accumulated energy consumption costs.

Part B: Let $P^* = [v_1, v_2, ..., v_M]$ be a time optimal and feasible s-d-path on $\vec{G}$ and let L_j^* denote the label that encodes subpath $P_{1:j}^*$ for some $j \in \{1, 2, ..., M\}$. The goal of the following mathematical induction is to prove that any label, which either encodes a time optimal and feasible path or a subpaths of a time optimal and feasible path, is added to the set $\mathcal{L}_{perm}$ before $\bar{L}$. For this purpose, it is iterated over all labels which are added to the set $\mathcal{L}_{perm}$ until algorithm A terminates and it is shown that each of these labels is lexicographically smaller than label $\bar{L}$.

Start of Induction: The first label which is added to the set $\mathcal{L}_{perm}$ is the initial label:

$$L_{init} := (0, 0\%, \emptyset, 0, s, 1). \tag{A.9}$$

This label is added to $\mathcal{L}_{perm}$ during the first iteration of the while-loop in algorithm A and consequently it is added to $\mathcal{L}_{perm}$ before $\bar{L}$. It can be interpreted as a label which encodes a subpath of P^*, i.e., $L_1^* = L_{init}$.

Inductive Step: Let for some $K < M$ all labels L_m^* with $m \leq K$ be already added to $\mathcal{L}_{perm}$ and let $\bar{L} \notin \mathcal{L}_{perm}$ (induction hypothesis). As P^* is a path on $\vec{G}$, it holds that $(v_m^*, v_{m+1}^*) \in \vec{E}$. Due to this, at the time at which L_K^* was added to $\mathcal{L}_{perm}$, the label L_{K+1}^* was created in line 12 of algorithm A. Since P^* is feasible, trivially also all its subpaths are feasible and thus also $P_{1:K+1}$ needs to be feasible. Correspondingly, the label L_{K+1}^* fulfills the feasibility condition in line 13 and is added to $\mathcal{L}_{temp}$ in the same iteration of the while-loop in which L_K^* is added to $\mathcal{L}_{perm}$. Hence, $\bar{L}$ cannot be in $\mathcal{L}_{perm}$ before L_{K+1}^* is added to $\mathcal{L}_{temp}$. It can be concluded, as L_{K+1}^* is lexicographically smaller than $\bar{L}$ according to the terms in A.6 - A.8, that label L_{K+1}^* is added earlier to $\mathcal{L}_{perm}$ than $\bar{L}$. □

Appendix B

Stochastic Edge Costs and Computational Effort

Let the graph at the top of Figure B.1 be considered. It consists of four nodes and three edges. The task is to compute $\mathbb{E}[F_M]$ for path $P := [a, b, c, d]$. It is assumed that the state of charge at the beginning is equal to 29 percent. Moreover, cost distributions are the same for all edges and solely three different scenarios can occur:

$$\Big(C_T(e,t,SOC), \grave{C}_E(e,t)\Big) = \begin{cases} (8, 0.05) & \text{with a probability of } 60\% \\ (6, 0.10) & \text{with a probability of } 30\% \\ (4, 0.15) & \text{with a probability of } 10\% \end{cases} \tag{B.1}$$

It is assumed that no correlations between any edge costs exist. Furthermore, all edge cost distributions are independent of arrival times or the state of charge. Below the graph in Figure B.1, a so-called scenario tree (*34*) is placed. It shows the development of time costs and of the states of charge along path P in dependency of the scenarios that were experienced. The root of the tree is associated with starting node a, the first level of the tree with node b and so on. Due to the aforementioned stochastic independence, the displayed probabilities remain the same throughout the tree (either 60, 30 or ten percent). On the right side of Figure B.1, the overall probabilities for all possibly occuring travel times and final states of charge that result after passing path P can be found.

The value of the objective function for subpath $[a, b]$ results directly from the edge cost definition in equation B.1:

$$\mathbb{E}\left[F_M\left([a,b], t_S, SOC_S\right)\right] = 60\% \cdot 8 + 30\% \cdot 6 + 10\% \cdot 4 = 7.$$

Two additions and three multiplications are necessary for the computation. To compute the

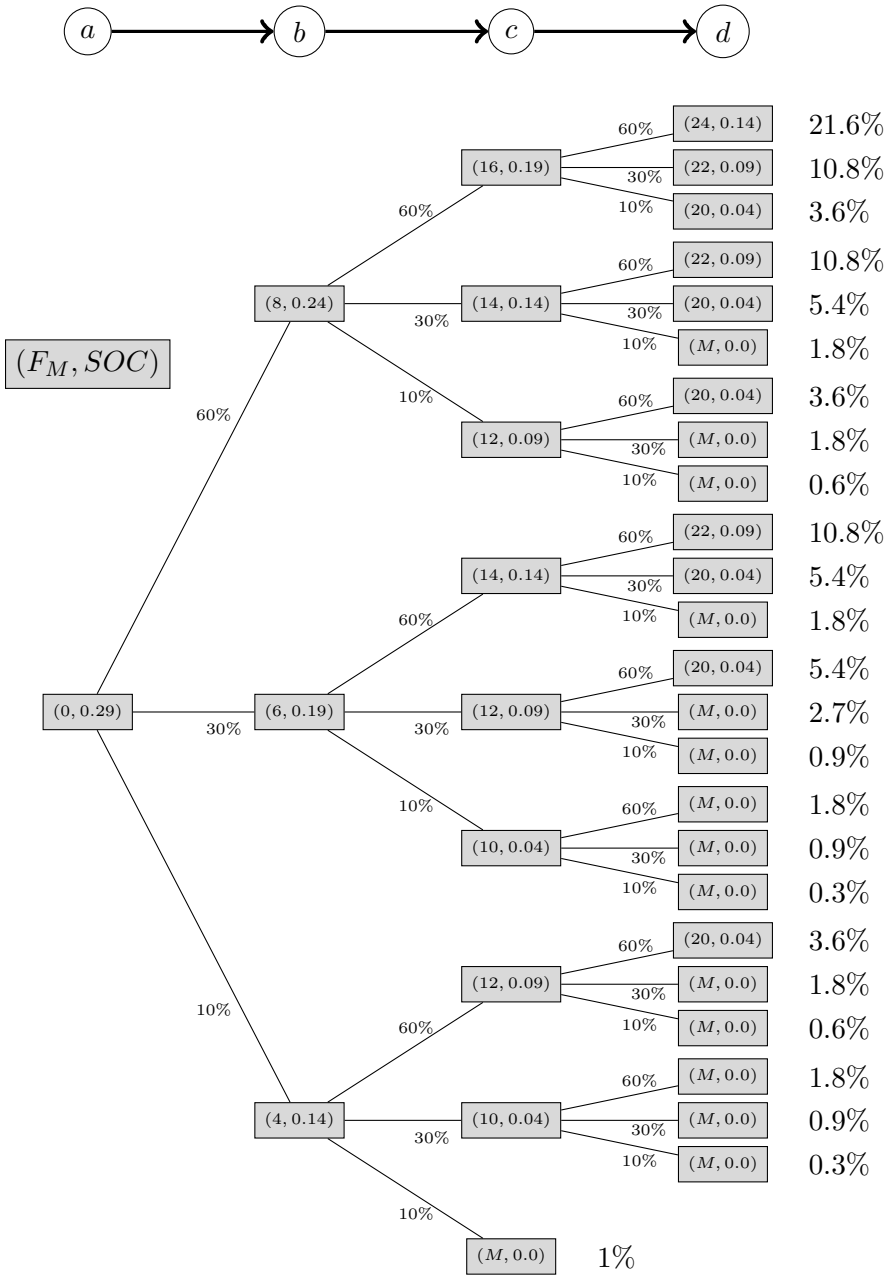

Figure B.1: Scenario tree for a single path consisting of three edges: Development of performance measure and state of charge.

costs of subpath $[a, b, c]$, conditional probabilities have to be computed. The value of the objective function can be derived as shown in the following equation:

$$\begin{aligned}\mathbb{E}\left[F_M\left([a,b,c], t_S, SOC_S\right)\right] =& 60\% \cdot (60\% \cdot 16 + 30\% \cdot 14 + 10\% \cdot 12) + \\ & 30\% \cdot (60\% \cdot 14 + 30\% \cdot 12 + 10\% \cdot 10) + \\ & 10\% \cdot (60\% \cdot 12 + 30\% \cdot 10 + 10\% \cdot M) = \\ =& 13.92 + 0.01 \cdot M\end{aligned}$$

Eight additions and 12 multiplications are necessary. Note that the probability for not reaching node c can explicitly be determined and is here equal to 1%. Finally, the rating for the whole path can be done as subsequently stated:

$$\begin{aligned}
\mathbb{E}\left[F_M\left(P, t_S, SOC_S\right)\right] =& 60\% \cdot 60\% \cdot (60\% \cdot 24 + 30\% \cdot 22 + 10\% \cdot 20) + \\
& 60\% \cdot 30\% \cdot (60\% \cdot 22 + 30\% \cdot 20 + 10\% \cdot M) + \\
& 60\% \cdot 10\% \cdot (60\% \cdot 20 + 30\% \cdot M + 10\% \cdot M) + \\
& 30\% \cdot 60\% \cdot (60\% \cdot 22 + 30\% \cdot 20 + 10\% \cdot M) + \\
& 30\% \cdot 30\% \cdot (60\% \cdot 20 + 30\% \cdot M + 10\% \cdot M) + \\
& 30\% \cdot 10\% \cdot (60\% \cdot M + 30\% \cdot M + 10\% \cdot M) + \\
& 10\% \cdot 60\% \cdot (60\% \cdot 20 + 30\% \cdot M + 10\% \cdot M) + \\
& 10\% \cdot 30\% \cdot (60\% \cdot M + 30\% \cdot M + 10\% \cdot M) + \\
& 10\% \cdot 10\% \cdot (60\% \cdot M + 30\% \cdot M + 10\% \cdot M) \\
=& 17.712 + 0.19 \cdot M
\end{aligned}$$

26 additions and 45 multiplications are necessary. It can be observed that for the case of path $[a, b, c, d]$, the number of arithmetic operations could be reduced. This is reasoned by the scenario which is represented by the lowest branch of the tree in Figure B.1, where even node c cannot be reached. Computations for edge (c, d) are thus not necessary. Certainly, such savings do not always occur when computing the value of $\mathbb{E}[F_M\left(P, t_S, SOC_S\right)]$.
Let from here on the number of possible scenarios per edge, which is assumed to be constant independently of the considered edge, be denoted by $S \in \mathbb{N}$ and the number of nodes of the considered path with $N \in \mathbb{N}$ (i.e., $S = 3$ and $N = 4$ in the example). In general, the following upper bounds for the number of arithmetic operations, which are necessary to rate a path with N nodes, can be derived:

$$\text{number of additions} \leq S^{N-1} - 1 \tag{B.2}$$

$$\text{number of multiplications} \leq S^{N-1} + S^{N-2} \cdot (N - 2) \tag{B.3}$$

A proof is not given here. It can be observed that the computational effort can grow exponentially with the length of the path. For instance, if five different scenarios per edge and a path length of ten nodes were assumed (i.e., $S = 5$ and $N = 10$), then the number of arithmetic operations for simply rating such a path exceeds five million.

It is worth mentioning that the example in Figure B.1 represents a comparably simple setting: The probability space is discretized, no correlations exist and the edge cost distributions are static, i.e., they to not depend on, for instance, arrival times. Still, again recursively defined

integrals need to be solved to assess path P[107]. At first glance, this may be surprising, since, due to the missing cost dependency and the absence of correlations, no dependencies between cost distributions of different edges seem to exist. On the other hand, the feasibility condition causes time cost distributions to depend on former realizations of energy consumption costs. In the scenario tree, this can be observed when comparing the time cost distributions for (c, d) for different branches of the displayed tree: For the topmost branch, time costs are distributed according to definition B.1, i.e., 60 percent probability for costs of eight, 30 percent probability for costs of six, and ten percent probability for costs of four. For the lowest branch (the lowest branch in which edge (c, d) is still reached is meant here), time costs are always equal to M. On the other hand, if the feasibility condition were not considered within the objective function, i.e., if $\mathbb{E}[F_M(P, t_S, SOC_S)]$ were replaced by $\mathbb{E}[C_T(P, t_S, SOC_S)]$, then the expected time costs of all edges of P could just be added up. Consequently, rating paths would not lead to a significant computational effort.

[107] No integrals can be seen in the listed calculations, since the probability space is discretized and hence all integrals are reduced to sums.

Appendix C

Parameters for Adaptive Smoothing Method

Here, the parametrization which is used in this work whenever the ASM is applied can be found. The columns of Table C.1 and the naming of the parameters are oriented towards Table 1 in (*132*).

Table C.1: Overview on applied ASM parameters

Parameter	**Value**	**Description**
Δx^{GT}	$40\ m$	spatial resolution of results
Δt^{GT}	$20\ sec$	temporal resolution of results
c^c	$-18\ km/h$	convested wave speed
c^f	$80\ km/h$	free-flow wave speed
ΔV	$10\ km/h$	length of transition region
V_{crit}	$70\ km/h$	critical speed
σ	$1100\ m$	spatial kernel length
ζ	$50\ sec$	temporal kernel length

Appendix D

Simulation Study: Further Aspects

D.1 Weighting of Pre-trip Failures

Figure D.1 shows the influence of weighting pre-trip errors less than on-trip errors exemplarily for the case of function $V_{Hist}^{t_B}$. There, three different curves based on $V_{Hist}^{t_B}$ can be found, where pre-trip errors are weighted with a factor of 1.0 (full weighting), 0.5, and 0.0 (no weighting). The black curve, showing the qualities that are achieved when presuming perfect RTTI, is just added to simplify comparison to the curves which are illustrated in Figure 7.10. The lower the weighting of pre-trip failures becomes, the more the steepness of the right branch of the parabola is reduced and, along with this, the more the vertex of the parabola is shifted to right. For a full weighting, a z-value of ten percent belongs to the setting which is represented by the vertex of the parabola of the yellow curve. If pre-trip error receive a weighting of 0.5, then a z-value of 20 percent leads to the lowest failure rate, and if pre-trip errors are not considered at all, then a relative buffer size of 30 percent leads to the lowest failure rate. Along

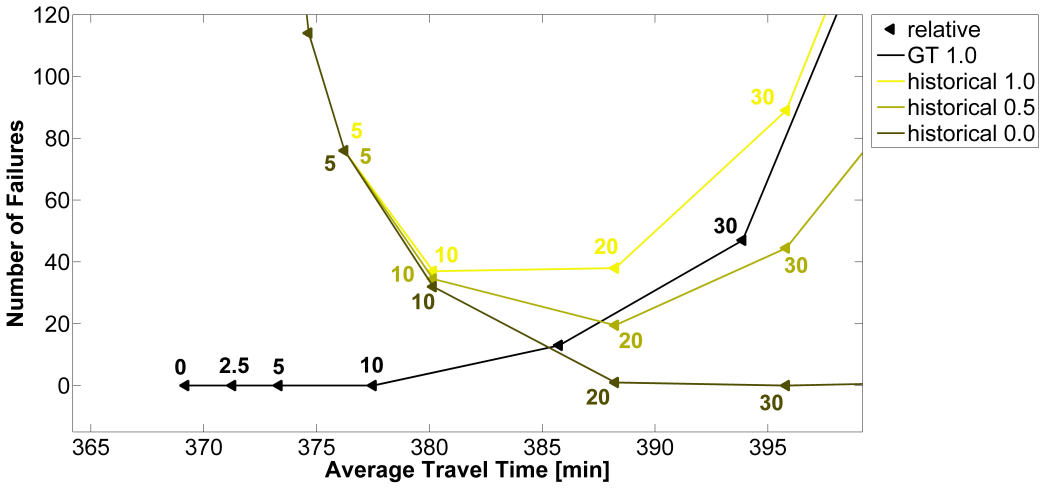

Figure D.1: Influence of assign reduced weightings to pre-trip failures for the example of traffic predictions based on historical data.

with the movement of the vertex, more and more triangles can be found on the left branches of the parabolas. Consequently, from an optimizer's point of view, higher buffer sizes become competitive. If the relation between on-trip weightings and pre-trip weightings is able to represent the preferences of the considered driver, then the described proceeding allows deriving for a given type of RTTI and a given energy buffer function a set of Pareto optimal reliability parameters. These parameters are exactly those which lead to settings which are represented by the vertex or by triangles belonging to the left branch of the corresponding parabola.

D.2 Derivation of the Primary Energy Consumption Model

Here, it will be explained how the recorded primary energy consumption data is used to derive a primary energy consumption model EC_{Prim}, which assigns realistic energy consumption values per distance traveled to given macroscopic driving speeds. For this purpose, let the set of all recorded (instantaneous) driving speeds (given in kilometers per hour) be denoted by $\{v_i\}_{i=1,...,Z}$ and the corresponding set of instantaneous energy consumption values be denoted by $\{ec_i\}_{i=1,...,Z}$ (given in watt) with $Z \in \mathbb{N}$. Based on these sets, average instantaneous primary energy consumption values $EC^{inst}_{Prim}(v^*)$ („inst“ for „instantaneous“) depending on speed v^* with $v^* \in \{1km/h, 2km/h, ..., 150km/h\}$ are computed according to the following rule:

$$Id_{[a,b[}(v_i) := \begin{cases} 1, & \text{if } a \leq v_i < b \\ 0, & \text{else} \end{cases} \tag{D.1}$$

$$EC^{inst}_{Prim}(v^*) := \frac{\sum_{i=1}^{Z} Id_{\left[v^*-0.5\frac{km}{h}, v^*+0.5\frac{km}{h}\right[}(v_i) \cdot ec_i}{\sum_{i=1}^{Z} Id_{\left[v^*-0.5\frac{km}{h}, v^*+0.5\frac{km}{h}\right[}(v_i)} \tag{D.2}$$

The energy consumption that is necessary to cover one meter while experiencing a macroscopic driving speed $v \in [0km/h, 150km/h]$ is afterwards approximated by assigning v to the closest of the values $v^* \in \{1km/h, 2km/h, ..., 150km/h\}$ and multiplying the corresponding average instantaneous consumption $EC^{inst}_{Prim}(v^*)$ with the time $t_m(v^*)$ (in seconds) that is necessary to cover one meter when driving with a speed of v^*[108]:

$$t_m(v^*) := {}^{1m}/_{\frac{v^*}{3.6\frac{km}{h}/\frac{m}{s}}} \text{ [seconds]} \tag{D.3}$$

$$EC_{Prim}(v^*) := t_m(v^*) \cdot EC^{inst}_{Prim}(v^*) \text{ [seconds} \cdot \text{watt} = \text{joule]} \tag{D.4}$$

$$EC_{Prim}(v) := \begin{cases} 0 \text{ Joule}, & \text{if } v < 0.5\frac{km}{h} \\ EC_{Prim}(v^*), & \text{if } v^* - 0.5\frac{km}{h} \leq v < v^* + 0.5\frac{km}{h} \end{cases} \tag{D.5}$$

[108] Speed v is given in kilometers per hour. The corresponding speed in meters per second is received if v is divided by 3.6.

D.3 The Impact of Near-perfect Real-time Traffic Information

The conjecture that RTTI which shows only minor differences to the ground truth leads to a high quality of the resulting charging strategies motivates Figure D.2. This figure illustrates charging strategy qualities resulting from different modifications of function $V_{Pha}^{t_B}$. These modifications are the result of linear combinations of functions $V_{Pha}^{t_B}$ and V_{GT}:

$$V_{Pha}^{t_B,\lambda}(x,t) := \lambda \cdot V_{Pha}^{t_B}(x,t) + (1-\lambda) \cdot V_{GT}(x,t) \tag{D.6}$$

This means that for $\lambda = 1$, function $V_{Pha}^{t_B,\lambda}$ is equal to $V_{Pha}^{t_B}$. For $\lambda = 0$, it is equal to $V_{Perf}^{t_B}$. In Figure D.2, the quality of charging strategies resulting from functions $V_{Pha}^{t_B,\lambda}$ for five different values of λ are visualized ($\lambda \in \{0, 0.1, 0.25, 0.8, 1.0\}$). It can be observed that with increasing

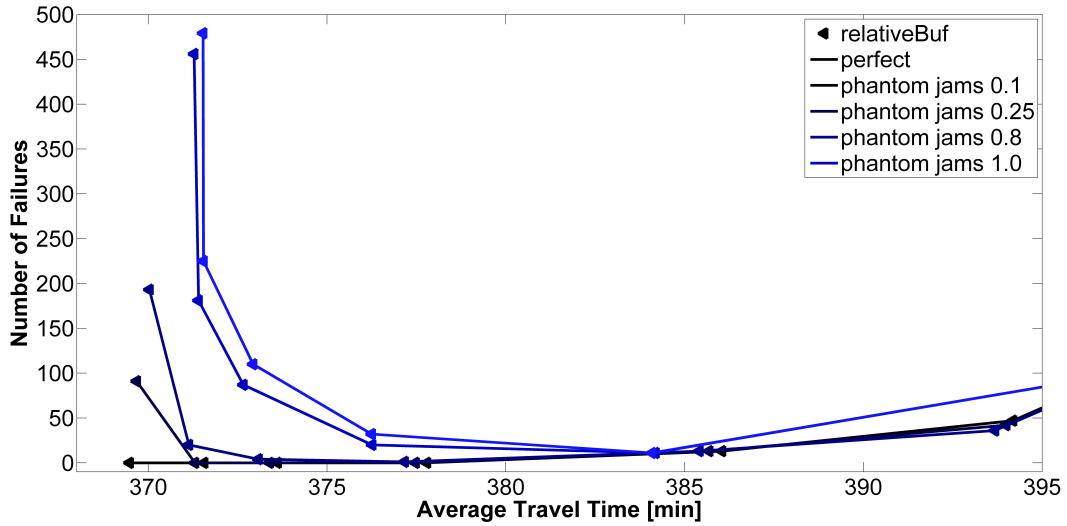

Figure D.2: Charging strategy qualities resulting from function $V_{Pha}^{t_B,\lambda}$ for different values of λ.

similarity between the applied RTTI and the ground truth, charging strategy qualities tend to improve until the same results are achieved as for function $V_{Perf}^{t_B}$.

D.4 Real-time Traffic Information Errors and Explanatory Variables

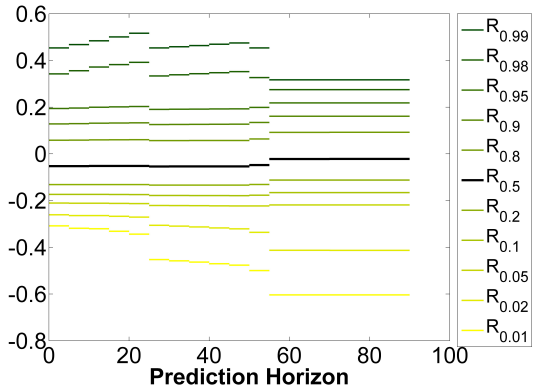

(a) Plots of step functions $R_\alpha(e_1)$.

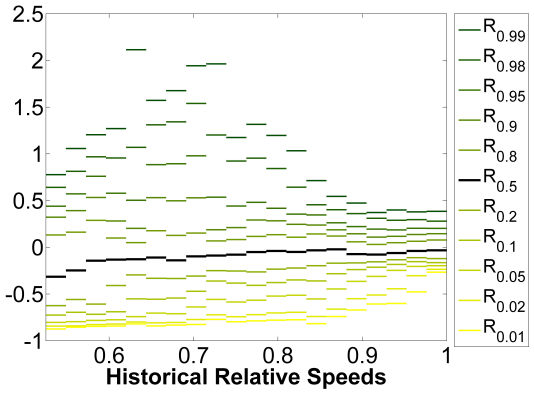

(b) Plots of step functions $R_\alpha(e_2)$.

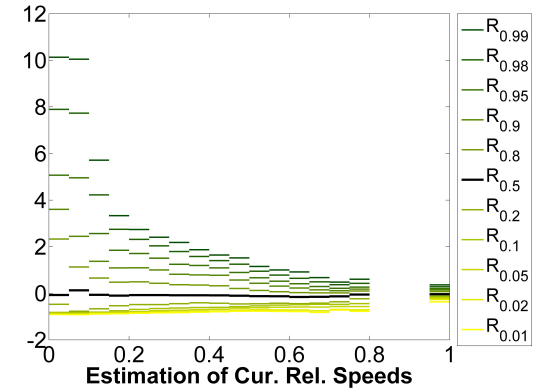

(c) Plots of step functions $R_\alpha(e_3)$.

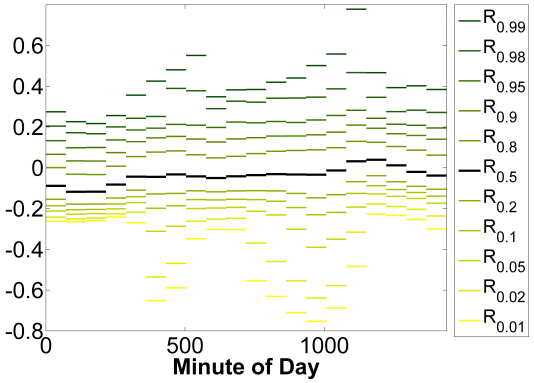

(d) Plots of step functions $R_\alpha(e_4)$.

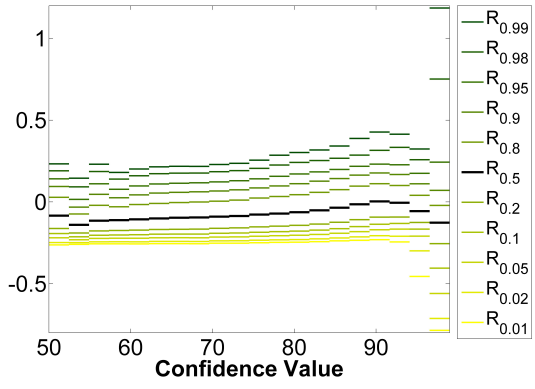

(e) Plots of step functions $R_\alpha(e_5)$.

Figure D.3: Relation of quantile functions on the suggested predictors for the case of commercial RTTI.

D.5 Speed Bounds Quality Depending on Selected Predictors

The following figures show the quality of adaptive speed bounds resulting from all possible combinations of considering one, two and three explanatory variables. The curves from Figure 7.17 are additionally displayed in each of these figures to give some orientation and to simplify comparison. It can be observed are that adaptive bounds perform in generally better than static bounds if high success rates have to be achieved (see right upper corners of the figures). Furthermore, it can be seen that including three explanatory variables leads to the best results, even though the differences between the curves are rather small.

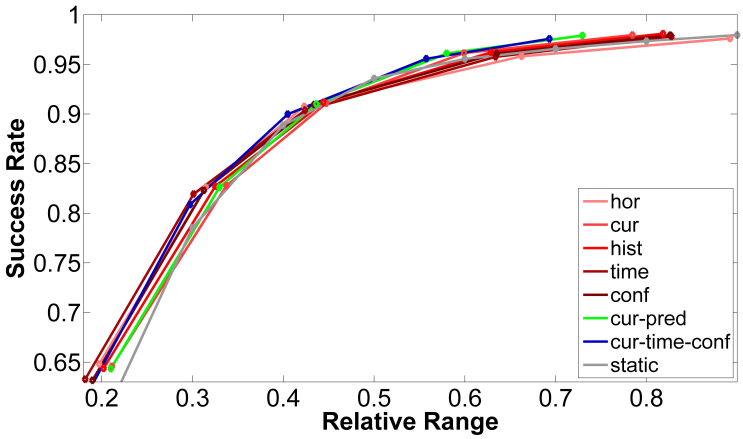

(a) Considering only one predictor.

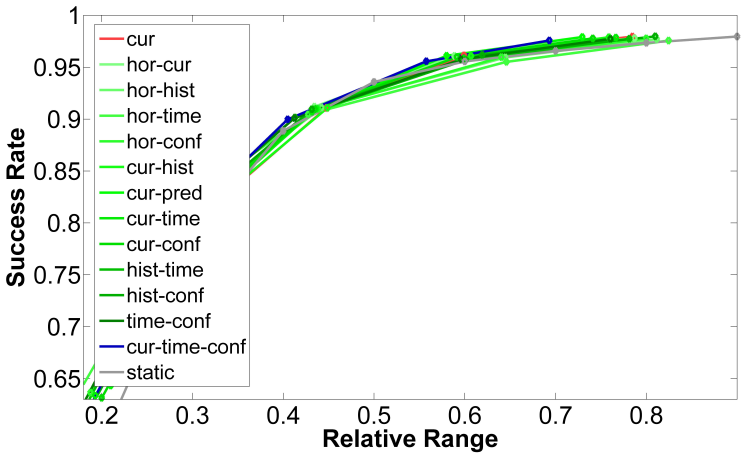

(b) Considering two predictors.

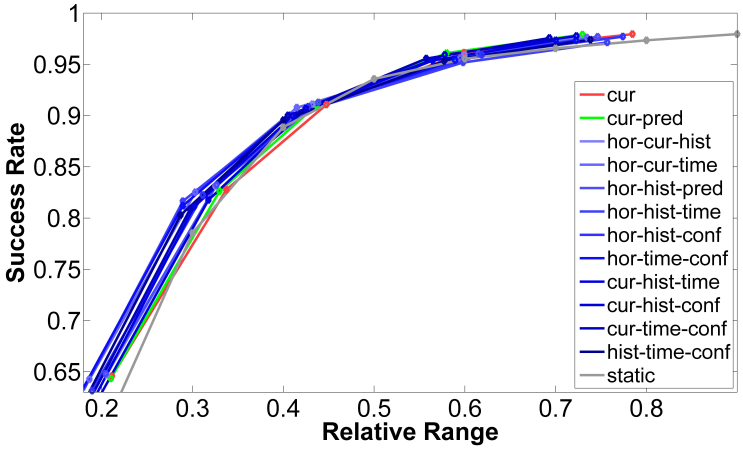

(c) Considering three predictors.

Figure D.4: Relation between considered predictors and the quality of the resulting adaptive speed bounds for the case of traffic information $V_{Com}^{t_0}$.

D.6 Comparing Combinations of Explanatory Variables

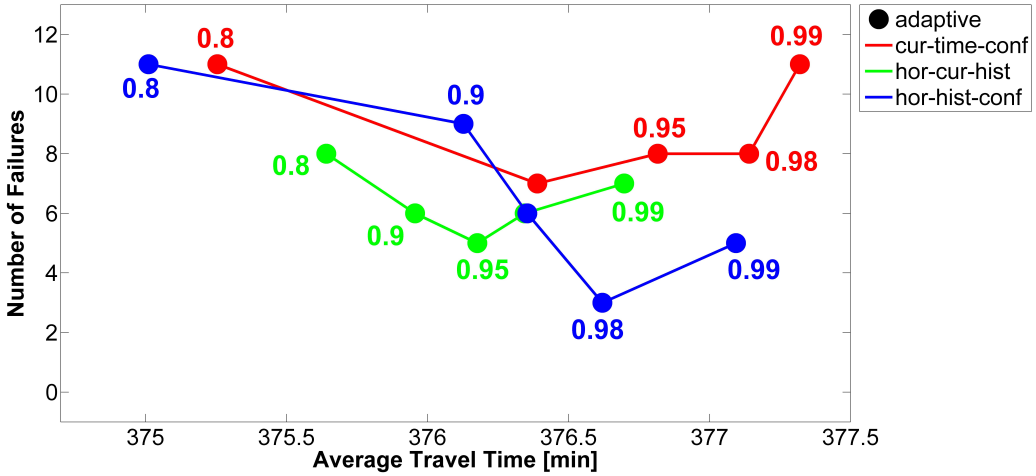

Figure D.5: Charging strategy qualities resulting from applying function $V_{Com}^{t_B}$ and adaptive trajectory buffers, which are based on different combinations of explanatory variables.

The curves in Figure 7.19 which belong to energy buffer functions $SOC_{min}^{ad,\alpha}$ (the circles) can solely be understood as examples. Different combinations of explanatory variables could be taken into account for the generation of speed bounds $V_{low}^{t_B,\alpha}$ and $V_{up}^{t_B,\alpha}$. However, further tests indicate that this has only a minor influence on the resulting charging strategy qualities. Figure D.5 supports this statement for the case of using function $V_{Com}^{t_B}$ as basis for the charging strategy computation. The charging strategy qualities resulting from applying three different combinations of explanatory variables for the generation of energy buffer function $SOC_{min}^{ad,\alpha}$ can be found. When comparing different circles belonging to the same value of α, then it can be observed that only very little differences occur.

Appendix E

Overview of Conducted Test Drives

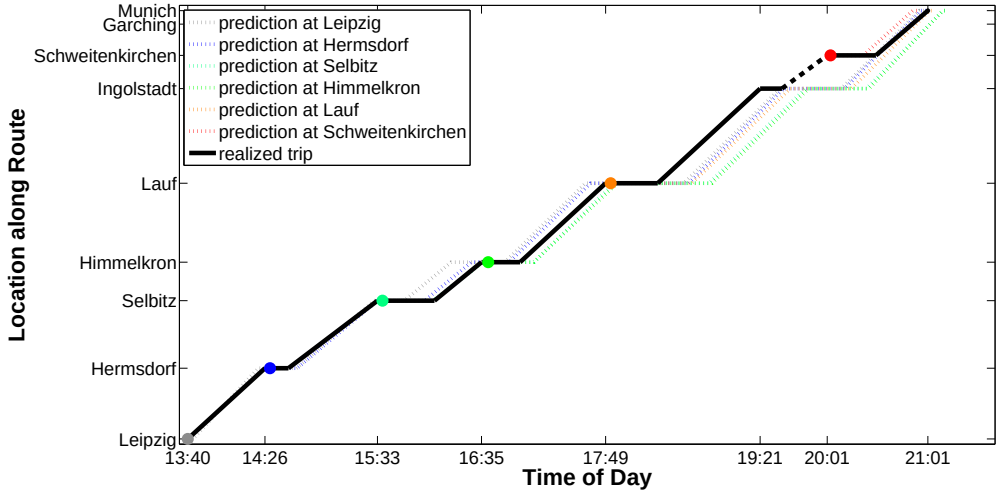

(a) Overview of arrival times at charging stations and charging durations.

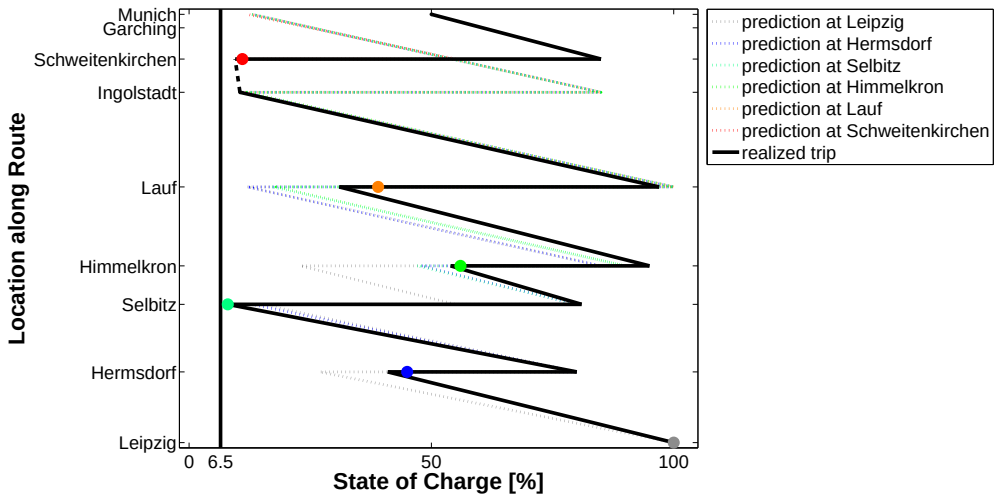

(b) Overview of the states of charge at charging stations.

Figure E.1: Development of arrival times and states of charge for the test drive from Leipzig to Munich (southbound) on the 12th of May, 2016.

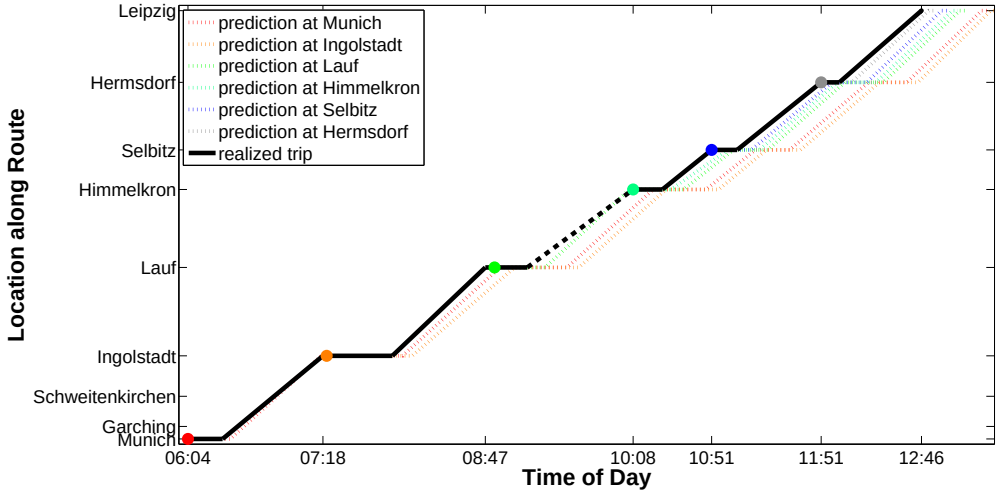

(a) Overview of arrival times at charging stations and charging durations.

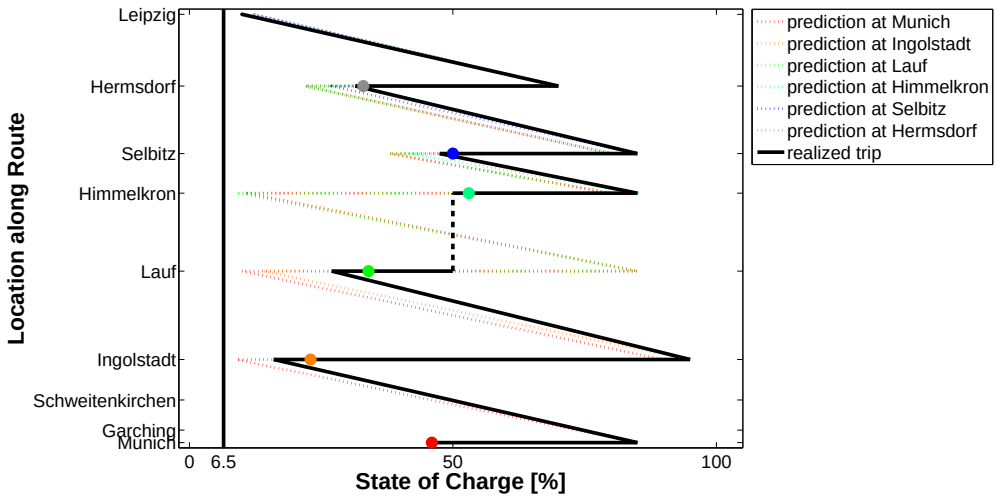

(b) Overview of the states of charge at charging stations.

Figure E.2: Development of arrival times and states of charge for the test drive from Munich to Leipzig (northbound) on the 6th of May, 2016.

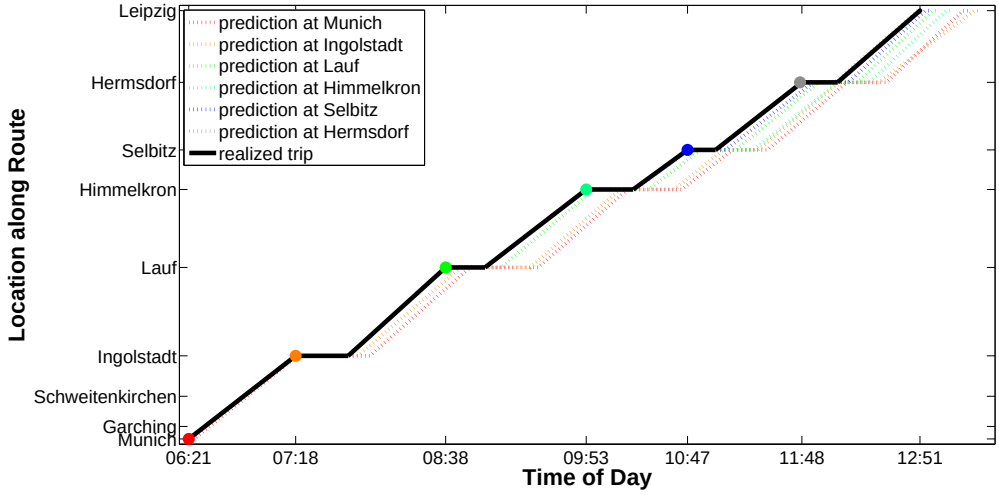

(a) Overview of arrival times at charging stations and charging durations.

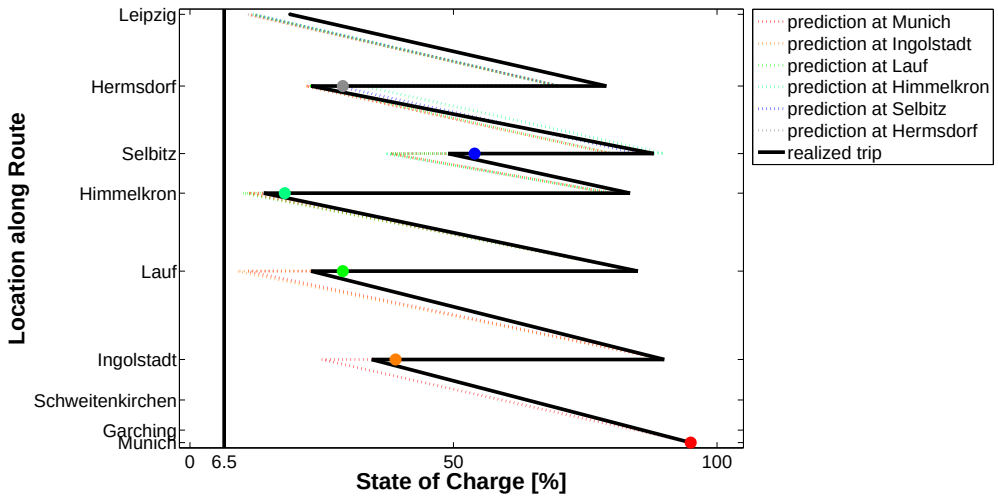

(b) Overview of the states of charge at charging stations.

Figure E.3: Development of arrival times and states of charge for the test drive from Munich to Leipzig (northbound) on the 12th of May, 2016.

Notation

The main abbreviations and the most important symbols that are used in this thesis can be found below:

Abbreviations:

BEV	battery electric vehicle
ICEV	internal combustion engine vehicle
SOC	state of charge
CSO	charging strategy optimization
HEV	hybrid electric vehicle
PHEV	plug-in hybrid electric vehicle
CHAdeMO	charge de move
CCS	combined charging system
NEDC	new European driving cycle
RTTI	real-time traffic information
SPP	shortest path problem
GPS	global positioning system
MDP	multistage decision problem
FIFO	first-in first-out
ASM	adaptive smoothing method
GT	ground truth
TGT	technical ground truth
APE	absolute percentage error
PE	percentage error

Symbols in the context of graphs:

$\vec{G} = (V, \vec{E})$	a graph consisting of nodes V and edges $\vec{E}$
P	a path on a graph
$[v_1, v_2, ..., v_Q]$	a path described by the sequence of nodes v_1 to v_Q
$P_{i:j}$	a subpath of a path P, starting with the i-th node and ending with j-th node of P
$\mathcal{P}(\vec{G}, v_1, v_2)$	the set of all paths on graph $\vec{G}$ which lead from node v_1 to node v_2

Symbols in the context of decision problems:

t_k	decision stage k (with $k \in \{1, 2, ..., K\}$)
$\mathcal{U}_k$	decision space at decision stage k
u_k	one single decision in $\mathcal{U}_k$
ξ_k	random variables representing the considered system's development until decision stage t_k
f	performance measure
$\pi = (\pi_1, ..., \pi_K)$	a decision policy consisting of decision rules π_k
$\mathcal{F}$	space of possible decision rules
$\vec{G}_D = (V_D, \vec{E}_D)$	decision graph
V_D^{cs}	the set of all nodes of the decision graph that represent locations of charging possibilities
t_k^A	random variable describing the arrival time at node k
SOC	random variable describing the state of charge when arriving at node k
$\xi_{\leq K+1}$	vector consisting of all random variables ξ_k, where t_k denotes a decision stage that is visited until destination node v_{K+1} is reached
c_T	random variable assigning travel times to edges
U_t	modified decision space

Symbols in the context of deterministic SPP:

Δ	step length for target states of charge
$\mathcal{U}_k^{\Delta}$	decision space at node v_k resulting from parameter Δ
$\vec{G}_D^{\Delta} = (V_D^{\Delta}, \vec{E}_D^{\Delta})$	graph which is used for defining the suggested SPP
$\vec{E}_{cs}^{\Delta}$	set of all edges in $\vec{E}_D^{\Delta}$ which represent parts of a charging process
ω_T	abstract object containing all kinds of information which may be used to estimate travel times
ω_E	abstract object containing all kinds of information which may be used to estimate the energy consumption of BEVs
$\grave{c}_E(e,t)$	deterministic energy costs for traversing at time t an edge e which represents a road segment
$c_T(e,t)$	deterministic time costs for traversing at time t an edge e which represents a road segment
$c_E(e,t,SOC)$	deterministic energy costs for passing an edge e, which represents a road segment, when arriving at time t with a state of charge SOC; adjusted version of $\grave{c}_E$ which ensures reasonable states of charge

Symbols in the context of SPPs under uncertainty:

c_T^W	waiting time due to occupied charging stations
c_T^A	additional time consumption during charging processes
$c_T^C(e, SOC)$	time for charging
S	function describing the charging behavior of a BEV
$c_E^C(e, SOC)$	negative energy costs due to charging
$c_T(e, t, SOC)$	deterministic time costs for passing an edge $e \in \vec{E}_{cs}^{\Delta}$ when arriving at time t with a state of charge SOC
$\mathcal{L}_{temp}$	set of temporary labels
$\mathcal{L}_{perm}$	set of permanent labels
$g_T(e, t, \omega_T)$	probability density function of the travel time that is necessary for passing edge e at time t while facing conditions described by ω_T
$\grave{g}_E(e, t, \omega_E)$	probability density function of the energy consumption that is necessary for passing edge e at time t while facing conditions described by ω_E
$\grave{C}_E(e, t)$	random variable describing the energy consumption that is necessary for passing edge e at time t
$C_T(e, t, SOC)$	random variable describing the travel time that is necessary for passing edge e at time t
$C_E(e, t, SOC)$	random variable describing the energy consumption that is necessary for passing edge e at time t; adjusted version of $\grave{C}_E(e, t)$ which ensures reasonable states of charge
$SOC_{min}(\omega)$	energy buffer function; returns minimal energy buffers depending on parameter set ω
$SOC_{min}^{r,z}(\omega)$	energy buffer function for relative energy buffers
$SOC_{min}^{q,\alpha}(\omega)$	energy buffer function for quantile-based energy buffers
$SOC_{min}^{t,NT}(\omega)$	energy buffer function for trajectory based energy buffers
$T(e, t)$	driving trajectory for passing edge e at time t
$T^{nt}(e, t)$	auxiliary trajectory for passing edge e at time t; used for computing trajectory buffers

Symbols in context of error-prone traffic information:

$V_{RTTI}^{t_B}$	spatio-temporal speed function representing RTTI (traffic state estimations and traffic predictions); the function is provided at time t_B
$T(e, t_S, V)$	driving trajectory for passing edge e at time t_S; the spatio-temporal speed function V describes the prevailing traffic conditions
$V_{Real}(x, t)$	random variable describing macroscopic average driving speeds for location x and time t
V_{RTTI}	spatio-temporal speed function representing RTTI (traffic state estimations only)
$\underline{X}, \overline{X}$	start/end of interval X
S_i^{RTTI}	road segment describing the spatial resolution of the considered RTTI
T_j^{RTTI}	time interval describing the temporal resolution of the considered RTTI
$t_B(t)$	the last time before (or until) time t, at which RTTI has been broadcasted
$V_{low}^{t_B,\alpha}$	spatio-temporal speed function describing lower speed bounds; these bounds are supposed to be lower than real future driving speeds with a probability of α
$V_{up}^{t_B,\alpha}$	the same as $V_{low}^{t_B,\alpha}$, but now for upper bounds
V_{GT}	spatio-temporal speed function resulting from a traffic state reconstruction; this function is used as representation of the real traffic situation
V_{TGT}	resulting from V_{GT}, but here the spatial and the temporal resolution is artificially reduced to represent provision limitations of RTTI
d	a distance measure
$D(V_1, V_2, X \times T, d)$	Value describing the differences between spatio-temporal speed functions V_1 and V_2 on $X \times T$ according to distance measure d
S_i^{GT}	road segment describing the spatial resolution of the numerical representation of the ground truth
T_j^{GT}	time interval describing the temporal resolution of the numerical representation of the ground truth

Symbols in context of error-probe traffic information:

S_i^U	road segment describing the spatial resolution of the grid that results when combining the RTTI grid and the ground truth grid
T_j^U	time interval describing the temporal resolution of the grid that results when combining the RTTI grid and the ground truth grid
Y	dependent variable describing the deviation between ground truth and RTTI
E_q	independent/explanatory variable or predictor, respectively
y^m	realization of the dependent variable Y
e_q^m	realization of explanatory variable E_q
$e_q(t_B, S_i^{RTTI}, T_j^{RTTI})$	function assigning realization of explanatory variable E_q to triple $(t_B, S_i^{RTTI}, T_j^{RTTI})$
Cf^{t_B}	function (broadcasted at time t_B) returning so-called confidence values in dependency of location
$V_{ff}(S_i^{RTTI})$	speed function returning free-flow driving speeds depending on location
$V_{Hist}(S_i^{RTTI}, T_j^{RTTI})$	spatio-temporal speed function returning average historical driving speeds
R	function describing the relation between explanatory variables and the dependent variable
R_α	function returning the α-quantile of the dependent variable in dependency of the realizations of the available explanatory variables
v_p	the preferred driving speed

Symbols used for the description of the executed simulation:

v_{Est}	estimated current driving speed (applied for predicting minutes 0 to 10); part of the recorded commercial RTTI
v_{sho}	short-term speed prediction (future period from minutes 11 to 25); part of the recorded commercial RTTI
v_{mid}	mid-term speed prediction (future period from minutes 26 to 40); part of the recorded commercial RTTI
v_{lon}	long-term speed prediction (future period from minutes 41 to 55); part of the recorded commercial RTTI
Tp	outdoor temperature
$\tilde{c}_{Prim}$	primary energy consumption
$\tilde{c}_{Sec}$	secondary energy consumption
SP	speed profile; function assigning speeds to locations given a driving trajectory
EC^{inst}_{Prim}	average instantaneous primary energy consumption
EC^{inst}_{Sec}	average instantaneous secondary energy consumption
$V^{t_B}_{Perf}$	spatio-temporal speed function representing perfect RTTI
$V^{t_B}_{ff}$	spatio-temporal speed function representing RTTI which presumes free-flow traffic conditions
$V^{t_B}_{Hist}$	spatio-temporal speed function representing RTTI that are based on historical average driving speeds
$V^{t_B}_{Inst}$	spatio-temporal speed function representing RTTI that results from making use of instantaneous travel time predictions
$V^{t_B}_{Com}$	spatio-temporal speed function based on recorded commercial RTTI
$V^{t_B}_{Pha}$	spatio-temporal speed function representing RTTI which frequently reports non existing congestion
t_h	prediction horizon
V_{RTTI,t_h}	function representing RTTI based on traffic predictions for a prediction horizon of t_h
$V^{t_B,f}_{low}$, $V^{t_B,f}_{up}$	lower and upper speed bounds resulting from multiplying RTTI with a constant factor
$V^{t_B,\alpha}_{low}$, $V^{t_B,\alpha}_{up}$	adaptive lower and upper speed bounds
$SOC^{con,f}_{min}$	trajectory energy buffer function using constant speed bounds for auxiliary trajectory generation
$SOC^{ad,\alpha}_{min}$	trajectory energy buffer function using adaptive speed bounds for auxiliary trajectory generation
$V^{t_B,m}_{RTTI}$	function representing RTTI where systematic prediction errors are compensated